Aus dem Institut für Virologie
Geschäftsführender Direktor: Prof. Dr. Stephan Becker
Des Fachbereichs Medizin der Philipps-Universität Marburg

In Zusammenarbeit mit dem Paul-Ehrlich-Institut, deutsches
Bundesinstitut für Impfstoffe und biomedizinische Arzneimittel

Titel der Dissertation:

Targeting Subtype-Independent Immune Responses Against Influenza A Virus

Inaugural-Dissertation zur Erlangung des Doktorgrades der Naturwissenschaften

dem Fachbereich Medizin der Philipps-Universität Marburg

vorgelegt von

Kevin Wittwer aus Siegen

Marburg, 2022

Angenommen vom Fachbereich Medizin der Philipps-Universität Marburg am:

Gedruckt mit Genehmigung des Fachbereichs Medizin

Dekan/in:	Prof. Dr. Denise Hilfiker-Kleiner
Referent/in:	Prof. Dr. Eva Friebertshäuser/Dr. Christian K. Pfaller
1. Korreferent:	Prof. Dr. Stefan Bauer

Content

ABBREVIATIONS

(-)ssRNA	single-stranded RNA with negative polarity
(+)ssRNA	single-stranded RNA with positive polarity
A	adenosine
ADAR1	adenosine deaminase acting on RNA 1
ADCC	antibody-dependent cell-mediated cytotoxicity
ADCP	antibody-dependent cell-mediated phagocytosis
AEC	3-amino-9-ethylcarbazole
ANOVA	analysis of variance
AP	alkaline phosphatase
APS	ammonium persulfate
ARDS	acute respiratory distress syndrome
AUC	area under the curve
BCIP/NBT	5-bromo-4-chloro-3-indolyl-phosphate/nitro blue tetrazolium
BHK	baby hamster kidney
BSA	bovine serum albumin
ca	cold-adapted
Cas9	CRISPR-associated protein 9
CDC	Center for Disease Control
cDNA	copy DNA
CEC	chicken embryo cells
CMV	Cytomegalovirus
ConA	concanavalin A
CPE	cytopathic effect
CRISPR	clustered regularly interspaced short palindromic repeats
cRNA	Copy RNA
DAPI	4′,6-Diamidino-2-phenylindoldihydrochlorid
DC	dendritic cell
ddH_2O	double-distilled H_20
DIA	diascopic
DMEM	Dulbecco's modified Eagle medium
DMSO	dimethyl sulfoxide
DNA	desoxyribonucleic acid
dNTP	desoxy-nucleotide triphosphate
dsRNA	double-stranded RNA
DTT	dithiothreitol
E. coli	*Escherichia coli*
ECDC	European center for disease control
EDTA	ethylenediaminetetraacetic acid
eGFP	enhanced GFP
ELISA	enzyme-linked immunosorbent assay
ELISpot	enzyme-linked immune absorbent spot
EMA	European Medicines Agency
EtOH	ethanol
FACS	flourescence-activated cell sorting
FBS	fetal bovine serum

FcγR	Fc-gamma receptor
FDA	Food and Drug Administration
ffu	focus-forming units
FITC	fluorescein isothiocyanate
fwd	forward
g	gravity
G	glycine
GAPDH	glyceraldehyde 3-phosphate dehydrogenase
GFP	green fluorescence protein
GISRS	Global Influenza Surveillance and Response System
gRNA	guide RNA
$H3_{stem}$	stem region of H3 Influenza HA
HA	hemagglutinin
HA_{head}	head region of Influenza HA
HAI	hemagglutinin inhibition
HA_{stem}	stem region of Influenza HA
HAU	hemagglutination units
HRP	horseradish-peroxidase
I	inosine
IAV	influenza A virus
IBV	influenza B virus
IFN	interferon
IFNγ	interferon γ
IgA	immunoglobulin A
IgG	immunoglobulin G
IgM	immunoglobulin M
IIV	inactivated influenza vaccine
IL-4	interleukin 4
iNOS	induced Nitric oxide synthase
IPMA	immuno-peroxidase monolayer assay
IRF3	interferon regulatory factor 3
IVI	Institute for Virology and Immunology
kb	kilobase
kDa	kilodalton
LAIV	live attenuated influenza vaccine
LB	lysogeny broth
LD_{50}	lethal dose 50%
LDL	low-density lipoprotein
M1	matrix protein 1
M2	matrix protein 2
M2e	ectodomain of M2
MDA-5	melanoma differentiation-associated protein 5
MDCK	Madin-Darby Canine Kidney
MEM	Minimum Essential Medium
MeOH	methanol
mFcγR	Murine Fcγ receptor
MHC	major histocompatibility complex
MOI	multiplicity of infection
mono	monocyte

mRNA	messenger RNA
MTT	3-(4,5-dimethylthiazol-2-yl)-2,5-diphenyltetrazolium bromide
MVA	modified vaccinia Ankara
MVA-T7	modified vaccinia Ankara expressing T7 polymerase
MΦ	macrophage
NA	neuraminidase
NFκB	nuclear factor kappa-light-chain-enhancer of activated B cells
NK cell	natural killer cell
NLRP3	NOD-, LRR-, and pyrin-domain containing 3
NLS	nuclear localization signal
NP	nucleoprotein
OD	optical density
PA	polymerase acidic protein
PAMP	pathogen-associated molecular pattern
PB1	polymerase basic protein 1
PB2	polymerase basic protein 2
PBS	phosphate-buffered saline
pIRF3	phosphorylated Interferon regulatory factor 3
PKR	proteinkinase R
PMSF	phenylmethylsulfonylfluorid
pPKR	phosphorylated proteinkinase R
PR8	A/Puerto Rico/8/1934(H1N1)
PRR	pattern recognition receptors
PVDF	polyvinylidendifluorid
RBC lysis	red blood cell lysis
rev	reverse
RIG-I	retinoic acid inducible gene-1
RNA	ribonucleic acid
RNP	ribonucleoprotein
rpm	rounds per minute
rSC35M	recombinant SC35M
S.O.C.	Super Optimal broth with Catabolite Repression
SA	sialic acid
SARS-CoV-2	severe acute respiratory syndrome coronavirus 2
SC35M	A/Seal/Massachusetts/1-SC35M/1980(H7N7)
SD	standard deviation
SDS	sodium-Dodecyl sulfate
SDS-PAGE	sodium-Dodecyl solfate-polyacryl amide gel electrophoresis
SEM	standard error of the mean
SNP	single nucleotide polymorphism
SPC	spot-forming cell
TAE	TRIS-acetate-EDTA
TBS	tris-buffered saline
TBS-T	tris-buffered saline-Tween20
$TCID_{50}$	tissue culture infectious dose 50%
TEMED	N, N, N′, N′-Tetramethylethylendiamin
TGF-β	transforming-growth factor-β

TLR	toll-like receptors
TNF-α	tumor necrosis factor-α
TPCK-trypsin	tosylsulfonyl phenylalanyl chloromethyl ketone-treated trypsin
TRAIL	TNF-related apoptosis-inducing ligand
TxRed	TexasRed
U	uracil
u	units
US	United States
UV light	ultraviolet light
vRNA	viral RNA
VSV	vesicular stomatitis virus
VSV-G	vesicular stomatitis virus glycoprotein
VSV-L	vesicular stomatitis virus large protein
VSV-N	vesicular stomatitis virus nucleoprotein
VSV-P	vesicular stomatitis virus phosphoprotein
WB	western blot
WHO	World Health Organization
ZBP1	Z-DNA binding protein 1

LISTS OF FIGURES AND TABLES

Figures

Tables

1 INTRODUCTION

1.1 Influenza Virus

Influenza viruses belong to the family of *Orthomyxoviridae* and are further divided into four different species A, B, C, and D, based on their antigenic and biological properties (ICTV 2021). While influenza viruses A, B, and C are known to cause pathologies in humans, no infection with influenza D virus has been detected so far (Su et al. 2017). Influenza B and C viruses usually cause mild symptoms in humans, making influenza A virus (IAV) the major threat to public health among all influenza viruses (Taubenberger and Morens 2008). IAVs are further divided into different subtypes based on the antigenicity of their surface proteins hemagglutinin (HA) and neuraminidase (NA). So far, 18 different hemagglutinin- and eleven different neuraminidase-subtypes have been characterized. While H17, H18, N10, and N11 are only found in bats and differ significantly in their structure and function (Tong et al. 2012; Tong et al. 2013), viruses of H1-16 and N1-9 subtypes are found in wild water fowl, which is the natural reservoir of IAV. Aside from this, IAV is a zoonotic pathogen and can spread among many different hosts, including domestic poultry, seals, dogs, horses, and humans (Mostafa et al. 2018). This broad host range and the enormous diversity of IAV have led to many zoonotic spillovers and make it a major candidate for future outbreaks and pandemics.

The designation of IAV includes type of the virus, the species of which the virus was isolated (if other than human), the number and location of isolation, as well as the subtype of the surface proteins HA and NA. The influenza virus A/Seal/Massachusetts/1/80(H7N7) is thus the first isolate from 1980 of a seal IAV in Massachusetts and has the subtype H7N7.

1.2 Influenza Virus Particle and Composition

The influenza virus particle typically has a spherical (80-120 nm in diameter) or filamentous (several hundred nm in length) shape (Figure 1) (Noda 2011; Li et al. 2021a). It consists of a host-derived lipid bilayer, incorporating the two major surface proteins hemagglutinin (HA) and neuraminidase (NA), and an ion channel membrane protein 2 (M2). HA serves as the viral attachment protein by binding terminal sialic acid (SA), linked to galactose of glycoproteins on the host cell

membrane and can induce fusion of the viral and cellular membrane (Pabis et al. 2020). M2 is important for acidification of the inner of the virus particle once it has reached the endosome during infection. NA cleaves terminal SA from the galactose of the cellular glycoprotein, thereby playing an important role in the release of progeny virus as well as inhibiting binding of virus particles to each other or mucins in the host respiratory system (Palese et al. 1974; Liu et al. 1995). The inner of the virus particle contains the viral ribonucleoprotein (RNPs) complexes. Each of the eight single-stranded RNA segments with negative polarity is associated with the nucleoprotein (NP), which is an important factor for transcription and replication of the viral genome. The viral RNA-dependent RNA polymerase is a complex consisting of polymerase basic protein 1 (PB1), polymerase basic protein 2 (PB2), and polymerase acidic protein (PA). It is associated with the panhandle-structured end of the RNA and mediates transcription and replication of the viral genome during the replication cycle. The matrix protein 1 (M1) is the mediator between the lipid bilayer and the RNPs by interacting with both of them. It further has important functions in the assembly of newly generated virus (Palese and Shaw 2007). In this respect, the viral proteins can be categorized in surface proteins that are found on the virus particle (HA, NA, M2) and internal proteins in the inner of the virion (NP, M1, PB1, PB2, PA).

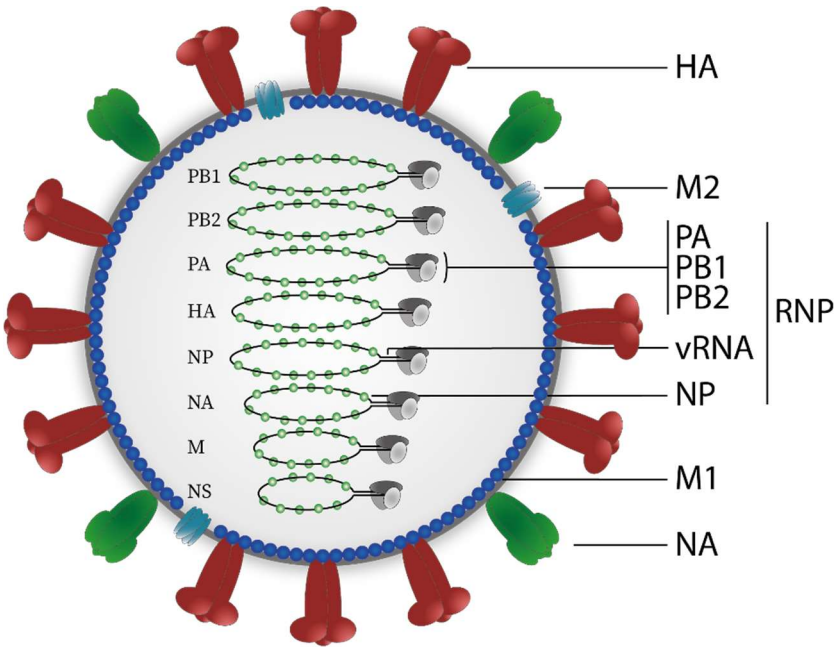

Figure 1: Schematic structure of an influenza A virus particle.

The surface proteins hemagglutinin (HA; red), neuraminidase (NA; dark green), and membrane protein 2 (M2; light blue) are incorporated into the host cell membrane-derived lipid bilayer (gray). Underneath the viral membrane, the membrane protein 1 (M1; dark blue) coats the inner of the viral

particle and regulates the interaction with the eight ribonucleoprotein complexes (RNPs). The RNPs consist of the viral RNA (vRNA; black line), associated nucleoprotein (NP; light green), and the polymerase complex, a heterotrimer of polymerase basic protein 1 (PB1), polymerase basic protein 2 (PB2), and polymerase acidic protein (PA) (grey tones), respectively. The eight segments of the viral genome form a panhandle structure, important for viral replication and transcription and encode for eight structural and at least two non-structural proteins. Adapted from (Horimoto and Kawaoka 2005).

1.3 Influenza Virus Replication Cycle

Initially, the virus particle attaches to the cell via the globular head domain of its HA protein by binding the cellular receptor SA on the surface (Figure 2, upper left). After attachment, the cells internalize the virus particles via clathrin-mediated endocytosis (Rust et al. 2004; Roy et al. 2000) or clathrin-independent mechanisms (Sieczkarski and Whittaker 2002). The subsequent acidification of the endosomal lumen results in a conformational change of the HA protein, bringing the internal fusion peptide in close proximity to the endosomal membrane of the host cell (Bullough et al. 1994). The hydrophobic fusion peptide is inserted into the endosomal membrane, which induces the fusion process with the virus particle. In parallel, the M2 protein serves as an ion channel in the viral membrane (Pinto et al. 1992), allowing protons to enter the particle and thereby weakening the interaction between M1 and NP (Bui et al. 1996). These two events enable the viral RNPs to enter the cytoplasm from where they are transported into the nucleus via nuclear localization signals (NLS) located in the NP (Figure 2 lower left). The panhandle-structure of the RNPs is warranted by complementary 5' and 3' ends of the viral genome, which are identical in all segments and serve as promoters for transcription of the RNA genome into viral mRNA. During this, a mechanism called "cap-snatching" is used to ensure subsequent translation by host ribosomes. The PB2 protein binds to the 5'-cap structure of cellular mRNA and attaches it to the 3'-end of the viral genome. The intrinsic nuclease activity of PB2 subsequently results in the cleavage of the cellular mRNA, resulting in a free 3'-OH group, serving as a primer for viral mRNA production. The polymerase complex can then produce the primary transcripts, which are subsequently polyadenylated at their 3' end. Some transcripts, including the M- and NS-segments, can undergo splicing by the cellular spliceosome and the mature mRNAs are transported to the cytoplasm, where translation via the cellular machinery takes place (Figure 2 center). Membrane-associated proteins, like HA, NA, and M2, are produced at the rough endoplasmic reticulum and transported to the plasma membrane via the Golgi network, where they are glycosylated and form

trimers (HA) or tetramers (NA). Viral proteins that are not membrane-associated have a NLS and are therefore transported into the nucleus. The enrichment of soluble NP affects the polymerase activity of PB1, PB2, and PA and results in a switch from transcription to production of full-length anti-genomes. Associated with NP, PB1, PB2, and PA, these anti-genomes serve as a template for replication and for the production of new viral genomes (Dou et al. 2018). The new viral RNPs are then transported into the cytoplasm and cluster at areas in close proximity to the membrane, where HA, NA and M2 are accumulated. Via a specific sorting mechanism (Fujii et al. 2003; Gog et al. 2007) it is ensured that the correct number and identity of segments are incorporated into the newly budding virions (Figure 2 upper right) (Moreira et al. 2016).

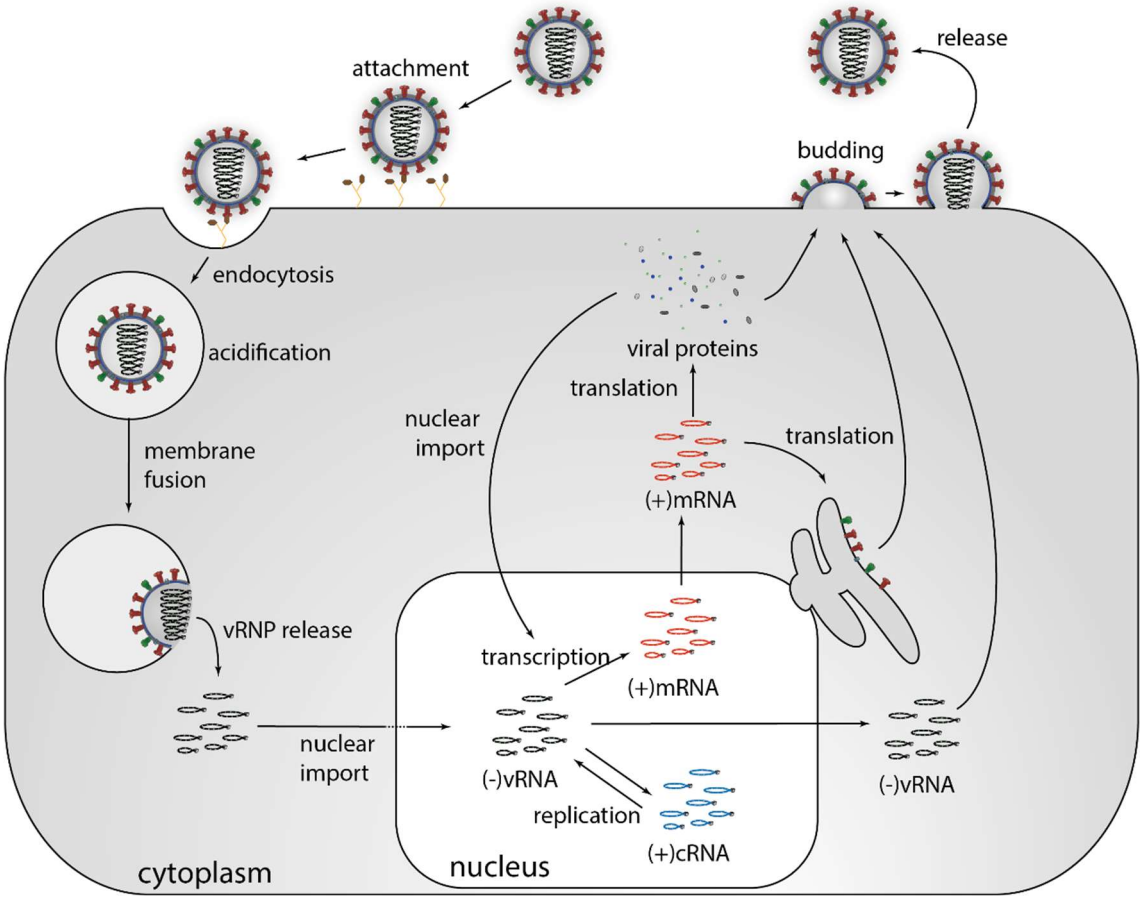

Figure 2: Schematic illustration of the IAV replication cycle.

IAV attaches to the host cell via binding of HA to terminal sialic acids (illustrated in brown color) on the cell membrane. The virus particle is then taken up into the endosome, where acidification leads to HA-mediated fusion of the viral and the endosome membrane. After release of vRNPs into the cytoplasm, import of vRNPs into the nucleus is mediated via nuclear localization signals (NLS) in NP. Transcription, splicing, and replication takes place in the nucleus, from where the processed mRNAs are exported into the cytoplasm and translated at free ribosomes (internal IAV proteins) or at ribosomes associated with the endoplasmic reticulum (membrane-bound IAV proteins). Free viral proteins are translocated back into the nucleus to support and regulate the replication of the viral genome into copy RNAs (cRNA) serving as a template for new viral genomes. Viral proteins and

newly synthesized viral genomes bud at the plasma membrane of the infected host cell. Release of progeny virus particles is supported by NA cleavage of terminal sialic acids, which would otherwise result in clumping of progeny virus to the host cell membrane and other virus particles. Adapted from (Sandbulte et al. 2015).

The NA protein can cleave terminal neuraminic acid on the cellular and viral membrane to prevent newly budding virus particles from clumping. To obtain infectivity, the HA protein has to be cleaved, which enables the fusion protein to be exposed upon acidification in the endosomal lumen during the subsequent infection cycle. The cleavage is performed by proteases which can be located in the endosomal membrane itself, on the surface of host cells or in extracellular matrix (Klenk et al. 1975; Lazarowitz and Choppin 1975; Dou et al. 2018).

1.4 Influenza Pathology

1.4.1 Seasonal Influenza

Currently circulating IAV strains of the subtypes H1N1 and H3N2, together with influenza B virus (IBV) strains, result in annual epidemics in the human population during cold seasons. Human infections with seasonal influenza viruses cause three to five million cases of severe disease including 290.000 – 650.000 deaths worldwide per year (WHO 2017). Infection leads to respiratory signs, like sore throat, runny nose, and cough, but can also result in systemic symptoms including fever, headache, muscle and joint pain, and severe malaise (Wright et al. 2007). In most cases, human infection with seasonal IAV is self-limiting and clinical signs vanish after one to two weeks. However, IAV infection can also lead to life-threatening disease of the lower respiratory tract with primary, viral or secondary, bacterial pneumonia, and acute respiratory distress syndrome (ARDS) (Kalil and Thomas 2019). People at higher risk for these lethal outcomes are those with chronic medical or immunosuppressive conditions, children, and the elderly. Given the high number of annual infections during IAV seasons, this is a substantial burden for public health.

1.4.2 Avian and Pandemic Influenza

In addition to the seasonal influenza, IAVs can spillover from animals like avian species or pigs to humans (Joseph et al. 2017; Kim et al. 2016). These subtypes typically harbor different antigenic features and are usually poorly adapted to the human host. However, since the human population does not possess immunity against the IAVs, these viruses may spread very fast and lead to global pandemics if

a sustainable human-to-human transmissibility was present. In contrast to seasonal influenza virus, IAVs of direct avian origin replicate in the lung of infected patients (see 1.5) and disease outcomes are far more devastating with death rates reaching up to 60% for highly pathogenic H5N1 viruses. However, no efficient human-to-human transmission of these avian viruses has been reported so far.

Nevertheless, adaptation of zoonotic IAV to the human host can lead to fast spread of the virus in the population. In the past, four major pandemics have occurred (Table 1). Although it is difficult to recapitulate exact death rates for past pandemics, in 1918/1919, the Spanish flu led to the death of approximately 27 – 50 million people worldwide (Johnson and Mueller 2002; Spreeuwenberg et al. 2018; Taubenberger and Morens 2006). In this case, an avian influenza virus crossed the species-barrier and adapted to the human host by antigenic drift (1.5), leading to human-to-human transmissibility. The latter three pandemics were caused by a newly reassorted virus containing either human and avian gene segments (Asian and Hong Kong flu) (Jackson 2009; Belshe 2005) or human, avian, and swine influenza virus gene segments (swine flu) (Guo et al. 2020).

Table 1: Past influenza A virus pandemics

Virus(Subtype)	*Year*	*Deaths*	*Lethality*	*Source*
Spanish flu (H1N1)	1918/1919	27 – 50 million	5 – 10%	(Taubenberger and Morens 2006)
Asian flu (H2N2)	1957/1958	>1 million	~ 0.5 %	(Wright et al. 2007)
Hong Kong flu (H3N2)	1968	approx. 1 million	~ 0.5 %	(CDC 2019a)
Swine flu (H1N1)	2009	150,000 - 575,000	~ 0.1 %	(CDC 2019b)

1.5 Antigenic Shift and Drift

Since the influenza virus polymerase complex does not have any proofreading activity, single-nucleotide polymorphisms (SNPs) occur during the replication of the viral genome with a frequency of approximately one mutation per replication cycle (~12.000 nucleotides) (Drake 1993). Upon selective pressure, for example when

humoral immunity against influenza virus exists in the host, progeny virus containing SNPs at the antibody-binding sites in HA or even NA can be positively selected (Both et al. 1983). This mechanism, called *antigenic drift* (Figure 3 A), leads to the annual emergence of new influenza serotypes and is the reason why the seasonal influenza vaccine has to be updated every year (Carrat and Flahault 2007). Antigenic drift can also occur, when an influenza virus spreads to a new host, for example from an avian species to humans. In this case, mutants that support the efficient production of progeny virus in the new host are positively selected (Klenk et al. 2011). In this manner, avian influenza viruses can acquire the capability of human-to-human transmission as described above. One major determinant of the IAV host range is the binding specificity and affinity of the viral HA for distinct SA-host receptors. Avian influenza viruses predominantly bind to α-2,3-linked SAs, found in the intestinal tract of many aquatic birds, but they have a sub-optimal binding affinity to the α-2,6-linked SAs in the human upper respiratory tract. This results in a species barrier for avian influenza viruses between birds and humans. However, adaptation of avian IAVs trough accumulation of mutations in the HA can lead to altered receptor specificity and human-to-human transmission of IAVs of avian origin (Cox and Subbarao 2000).

Another mechanism, by which new types of influenza viruses can emerge, is the so-called *antigenic shift* (Figure 3 B). It is based on the segmented nature of the viral genome and can occur when a cell is co-infected by different influenza viruses. Here, the RNPs of the different parental viruses mix during the assembly process and are thereby reassorted into the budding progeny virus. The newly emerging virus is thus a genetic mixture of the parental viruses. Although it is known that not all subtypes of influenza viruses can reassort with each other, several influenza pandemics of the past have proven that antigenic shift can indeed lead to novel virus reassortants, especially, when the surface proteins originate from an animal host and the human population does not have serological protection (Sandbulte et al. 2015). In the past, many properties important for IAVs crossing the species barriers between different hosts have been elucidated, in order to predict zoonotic and pandemic potential of those viruses (Subbarao 2019). A major aspect of antigenic shift are intermediate hosts of different IAV strains. The above mentioned different specificity of human and avian IAV for α-2,6- and α-2,3-linked SA, respectively, builds a natural barrier for spillover events between those species that is crossed only in rare cases where

individuals had close contact to infected poultry. However, pigs do express both forms of terminal SA in their respiratory system, making them susceptible for human and avian viruses. In this respect, pigs are thought to act as a kind of "mixing vessel" for IAVs of different hosts by harboring high probability of co-infection and subsequent reassortment, as this was the case for the 2009 swine flu (Ma et al. 2008; Cox and Subbarao 2000). Although many other aspects of inter-host transmission of IAV have been observed, this aspect is a major concern regarding mixed animal farming of poultry and pigs.

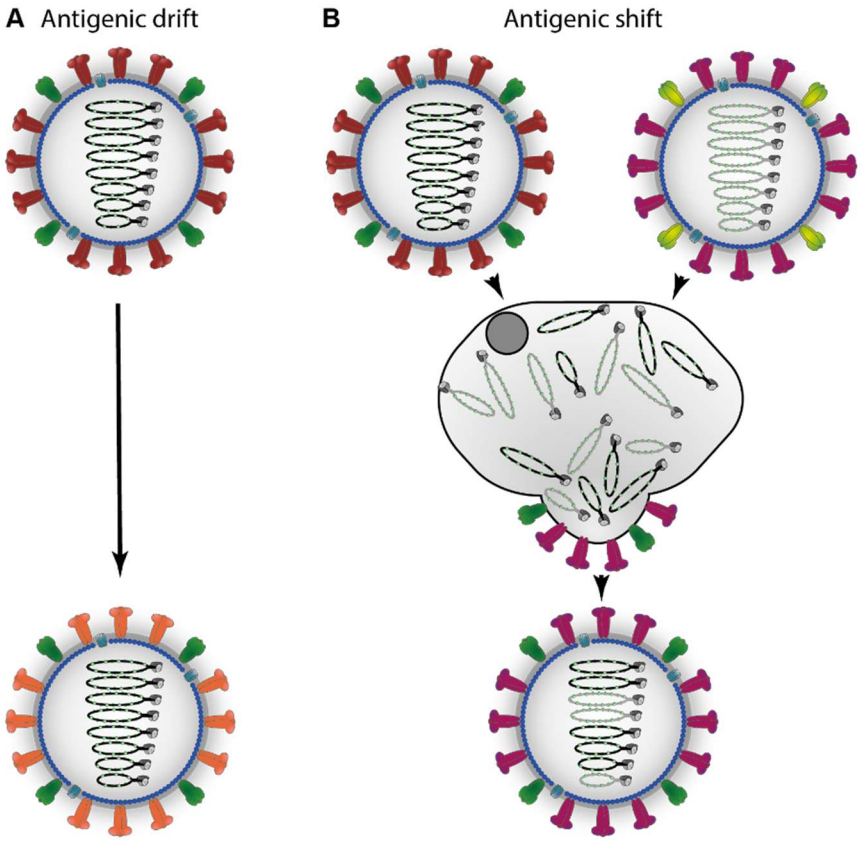

Figure 3: Schematic illustration of antigenic drift and antigenic shift.

(A) Accumulation of point mutations in the viral proteins (here HA) leads to altered properties and/or antigenicity, rendering immunity previously directed against the source virus inefficient against the drifted virus. Furthermore, antigenic drift can play a major role in adapting to a new host of IAV after crossing the species barrier from other IAV hosts to establish efficient viral replication and a human-to-human transmissibility. (B) Antigenic shift occurs when two different IAVs infect the same host cells and vRNPs reassort during the assembly process of progeny virus. Antigenic shift can give rise to novel IAVs, harboring fundamentally different properties in terms of transmission, pathogenicity, host range, etc. Note that antigenically drifted viruses can subsequently also undergo antigenic drift. Adapted from (Krammer et al. 2018).

1.6 Murine Influenza A Models

Murine animal models are the gold-standard to assess pathogenicity of IAV infection and vaccine efficacy (Matsuoka et al. 2009). However, certain biological differences

between the murine model and humans have to be considered when interpreting the results. A major difference between mice and humans is the distribution of α-2,3- and α-2,6-linked SA in the respiratory tract, and the susceptibility of the expressing cells for IAV (Long et al. 2019). In mice, ciliated, α-2,3-linked SA-expressing airway and type II alveolar epithelial cells are found to be infected in *in vitro* models (Ibricevic et al. 2006), modelling a human infection with avian IAVs. After intranasal inoculation, IAV replicates in the murine model in the nasopharyngeal passage and in the lung as demonstrated by a luciferase expressing reporter IAV (Pan et al. 2013). In contrast to humans, murine cells do not express α-2,6-linked SAs on the surface, explaining the inability of many human IAV isolates to infect mice without further adaptation (Ibricevic et al. 2006; Matsuoka et al. 2009). Therefore, in order to use murine models for IAV experiments, either avian IAVs, to which mice are naturally susceptible, or mouse-adapted IAVs of human isolates have to be used. Besides receptor specificity, many other factors play important roles in the pathology and clinical outcome of IAV infections in mice.

The most widely used mouse-adapted IAV originates from the virus H1N1 A/Puerto Rico/8/34 (PR8) (Francis 1937). Initially, a human isolate of H1N1 IAV isolated in Puerto Rico was used to infect ferrets (Smith et al. 1933) and was further propagated in mice (Francis 1937). The original PR8 virus gave rise to many variants over the following decades, which induce different levels of pathology and mortality in different mouse strains (Blazejewska et al. 2011).

Another widely used mouse-adapted IAV strain originates from an IAV isolated from seals (H7N7 A/Seal/Massachusetts/1/80), during a pandemic in these animals in 1979-1980 (Geraci et al. 1982). While the original isolate induced no pathology in a great variety of experimentally infected animals, serial passage in chicken embryo cells (CECs) led to the isolation of a chicken-adapted virus with high pathology in these avian species (SC35) (Webster et al. 1981; Li et al. 1990). Although SC35 does not result in high mortality in the murine model, serial passage of SC35 in mice gave rise to host adaptations, ultimately leading to the a highly-virulent SC35 in mice (SC35M) (Scheiblauer et al. 1995).

1.7 Immune Responses

1.7.1 Cell-intrinsic Innate Immune Response

When foreign pathogens enter the body of the host, they are sensed by a variety of receptors, called pattern recognition receptors (PRRs). These PRRs are either present in the cytoplasm or membrane-anchored and bind pathogen-associated molecular patterns (PAMPs). As a consequence, they activate signal transduction cascades resulting in the expression of a plethora of different proteins to fight infection. PAMPs are molecular structures that are part of a pathogen or generated during replication, and the produced double stranded RNA (dsRNA)-intermediates, as well as the panhandle-structured ends of IAV, are prominent ligands for different PRRs (Murphy and Weaver 2018).

1.7.1.1 DsRNA-mediated Innate Immunity

Many different PPRs that sense dsRNA during IAV replication have been identified in the past. This includes soluble proteins like retinoic acid inducible gene-I (RIG-I), melanoma differentiation-associated protein 5 (MDA-5), protein kinase R (PKR), NOD-, LRR-, and pyrin-domain containing 3 (NLRP3), 2'-5'-oligoadenylat-sythetase (OAS), RNase L, as well as Z-DNA binding protein 1 (ZBP1). Furthermore, the membrane-associated PRRs Toll-like receptors 3 and 7 (TLR3/7), located in the endosome, are known to bind viral RNA (Murphy and Weaver 2018). RIG-I binds double-stranded, 5'-triphosphorylated RNA and is expressed in the cytoplasm, therefore providing sensing of intracellular viral RNAs. Activation of RIG-I via binding to its ligand results in conformational change, exposing its caspase activating and recruiting domain (CARD). The mitochondria antiviral-signaling (MAVS; also, IFN-β promotor stimulator 1 (IPS-1)) protein is located at the mitochondrial membrane and also possesses a CARD, that interacts with activated RIG-I. Interaction leads to an activation of MAVS and starts a subsequent signaling cascade, resulting in translocation of interferon-regulation factor (IRF) 3, IRF7 and nuclear factor kappa-light-chain-enhancer of activated B cells (NFκB) into the nucleus. While IRF3 and IRF7 mainly induce expression of type I interferons (IFN) and other IFN-stimulated genes (ISGs), NFκB activation additionally leads to production of pro-interleukin (IL)-1β, pro-IL-18 and other pro-inflammatory cytokines. Besides type I IFN, type III IFN (IFN-λ) is produced upon influenza A

virus infection, predominantly by epithelial cells (Killip et al. 2015). For MDA-5, different and redundant roles have been demonstrated when compared to RIG-I signaling during viral infection. However, for IAV, prominent interferon-stimulated genes (ISGs) are strictly dependent on RIG-I, which suggests a subordinate role for MDA-5 during IAV-RNA sensing (Loo et al. 2008).

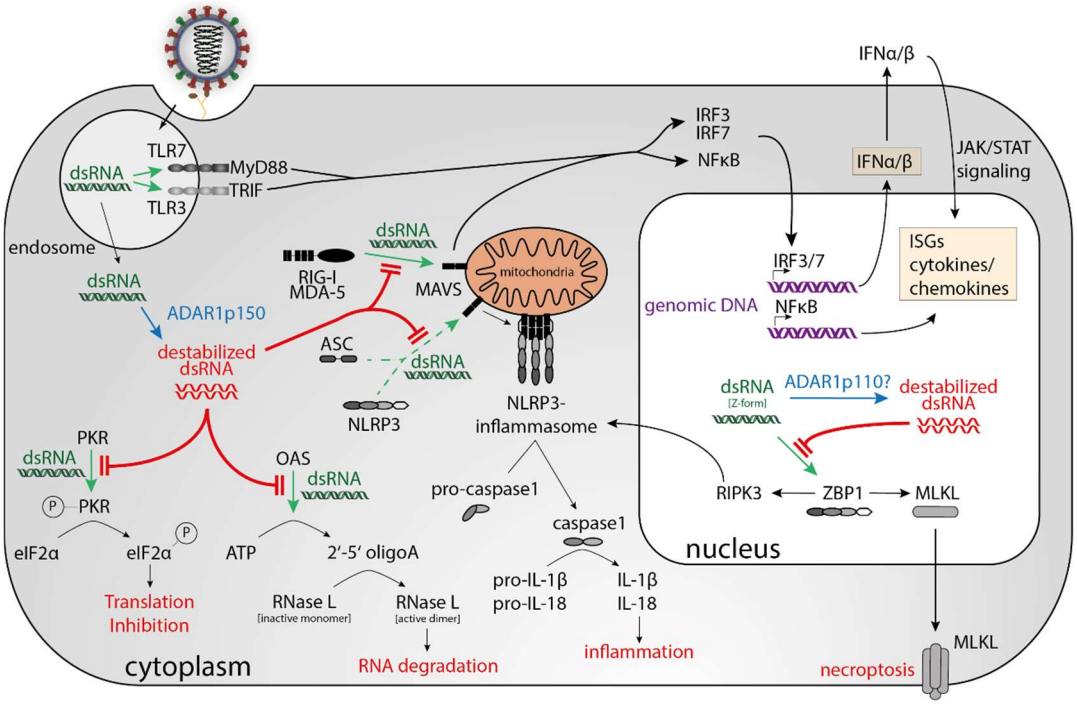

Figure 4: Schematic illustration of dsRNA-mediated innate immune pathways
Soluble, as well as endosomal membrane-associated, PRRs sense dsRNA (green) generated during the infection cycle of RNA viruses. TLR3 and TLR7 (upper left) sense dsRNA which leads to the signal transduction trough the adapter molecules TRIF and MyD88, respectively. RIG-I, and to a lesser extent MDA-5 (center), bind dsRNA in the cytoplasm and co-localize with the MAVS protein at the mitochondria. Both pathways activate IRF3/7 and NFκB which then re-locate into the nucleus and drive the expression of type I IFNs and interferon-stimulated genes, including pro-inflammatory cytokines and chemokines (right). On the other hand, dsRNA is bound by PKR und ultimately results in the phosphorylation and thereby inhibition of eIF2α (lower left). As eIF2α is a critical factor for translation, this leads to a translation stop in the cell. OAS (lower left) binds dsRNA and produces 2'-5' oligoA, acting as a second messenger for RNase L. RNase L then dimerizes and digests cytoplasmic RNA. In the presence of dsRNA, the adapter molecule ASC bind to NLRP3 and MAVS, leading to the assembling of the mitochondria-associated inflammasome (center). However, direct binding of dsRNA by NLRP3 is under investigation (dotted line). Building of the inflammasome results in the cleavage of pro-caspase1 into its active form caspase 1 and a subsequent cleavage of pro-IL-1β and pro-IL-18, two prominent pro-inflammatory cytokines (lower center). dsRNA in Z-conformation is produced during die IAV replication cycle and can be sensed by ZBP1 (right). ZBP1 can drive activation of the NLRP3-inflammasome as well as assembly of MLKL. MLKL then builds pores in the plasma membrane and leads to necroptosis of the respective cell (lower right). The isoform p150 of ADAR1 can destabilize dsRNA structures by deamination of adenosine and therefore inhibit the mentioned pathways, as imperfectly matched dsRNA strands cannot activate the respective PRRs. Furthermore, ADAR1p110 in the nucleus is supposed to act on dsRNA structures and immune activation pathways, but the exact impact remains elusive (indicated by `?`). Adapted from (Pfaller et al. 2021; Herold et al. 2015; Zhang et al. 2020).

PKR is a cytosolic protein kinase that dimerizes upon binding of dsRNA to get activated. It phosphorylates the eukaryotic translation initiation factor 2α (eIF2α)

thereby blocking translation of cellular, as well as viral, mRNA (Hovanessian 1989). As efficient viral replication is strongly alleviated when PKR is active, IAV has developed two major mechanisms to counteract this. Firstly, IAV recruits P58IPK, a chaperone known to suppress PKR activity (Melville et al. 1999). Secondly, the viral non-structural protein 1 (NS1) was shown to inhibit PKR, although different mechanisms of action have been proposed, including a direct binding to PKR or a binding and thereby shielding the viral dsRNA (Bergmann et al. 2000)

The third important PRR in the context of IAV dsRNA is the NLRP3-receptor, which is also expressed in the cytoplasm. In contrast to TLRs and RIG-I, NLRP3 activation directly leads to the formation of a NLRP3-inflammasome. Activated NLRP3 binds pro-caspase 1 via the adapter molecule ASC and leads to cleavage of the active caspase 1. Caspase 1 itself can cleave and thereby activate pro-IL-1β and pro-IL-18, which are expressed upon NFκB activation. The active cytokines IL-1β and IL-18 are subsequently released from the cell.

OAS senses dsRNA of cellular and viral origin in the cytoplasm, which triggers the production of the second messenger 2'-5'-oligoadenylate. 2'-5'-oligoadenylate itself binds to RNase L and activates its RNA-specific cleaving activity, which results in translation stop through degradation of mRNAs and apoptosis (Siddiqui et al. 2015).

ZBP1 is located in the nucleus and binds via its Zα domain to RNA in Z-conformation, a left-handed double helix, which was found to be produced during IAV replication (Zhang et al. 2020). Upon binding, ZBP1 activates a signaling cascade leading to disruption of the nuclear membrane and necroptosis via mixed lineage kinase domain-like pseudokinase (MLKL) (Jiao et al. 2020). Importantly, necroptosis is a major driver of immunopathology and knock-out of MLKL in the mouse model resulted in decreased pathogenic neutrophil recruitment in the lung and a beneficial outcome of IAV disease (Zhang et al. 2020). The Zα domains of ZBP1 is structurally similar to that of adenosine deaminase acting on RNA 1 (ADAR1) (Schwartz et al. 2001), and previous studies demonstrate that ADAR1 indeed can bind Z-RNA (Placido et al. 2007), suggesting that editing or binding of IAV-derived Z-RNA prevents ZBP1-induced necrosis.

TLR-3 and TLR-7 are expressed in the endosome and sense viral dsRNA and ssRNA, respectively. Upon TLRs binding to their respective ligand, TLR-adapter molecules TIR-domain-containing adapter-inducing interferon-β (TRIF) in case of

TLR-3, or myeloid-differentiation primary response 88 (MyD88) in case of TLR7, are phosphorylated. While TLR-3 is the predominant TLR in macrophages, taking up infected cell debris, TLR-7 is important for the signaling cascade in plasmacytoid dendritic cells (pDCs) (Iwasaki and Pillai 2014). Activation of these TLRs leads to a signaling cascade ultimately resulting in the activation and translocation of transcription IRF3 and IRF7 and NFκB.

1.7.1.2 Negative Regulation by Adenosine Deaminases Acting on RNA

ADAR1 is an enzyme catalyzing the deamination of adenosine (A) to inosine (I) in dsRNA. Two isoforms of ADAR1 exist, namely an IFN-inducible 150 kDa isoform (ADAR1p150), and a constitutively expressed 110 kDa isoform (ADAR1p110). Since only ADAR1p150 possesses a nuclear export signal (Figure 5; NES; illustrated in brown), it is mainly located in the cytoplasm, while ADAR1p110 is present in the nucleus. Both isoforms contain an enzymatically active deaminase domain at the C-terminus, as well as three consecutive dsRNA-binding domains. At the N-terminal end, ADAR1p150 possesses one active Z-DNA/RNA binding domain (Zα) and a structurally homologous Z-DNA binding-like domain (Zβ) without binding affinity (illustrated in green). In contrast to this, ADAR1p110 does only contain the inactive Zβ domain (Samuel 2011a).

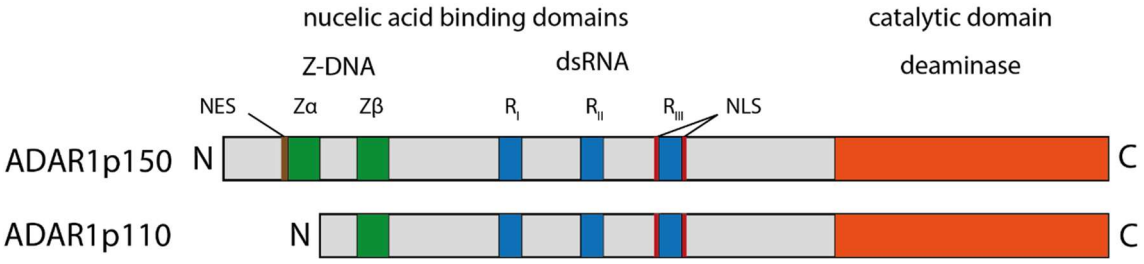

Figure 5: Schematic depiction of the ADAR1 isoforms p150 and p110.
Both isoforms consist of a C-terminal enzymatic domain that catalyzes the deamination of adenosine to inosine. Two kinds of nucleic acid binding regions can be distinguished for Z-DNARNA and A-form dsRNA. While dsRNA binding domains consist of three repetitive domains (R_I-R_{III}) in both isoforms, ADAR1p150 possesses two (Zα, Zβ) and ADAR1 one (Zβ) Z-DNA binding domains. The bipartite nuclear localization signal (NLS; red) leads to the transport of both isoforms into the nucleus, whereas only ADAR1p150 has a nuclear export signal (NES; brown) that results in accumulation of ADAR1p150 in the cytoplasm.

When ADAR1 binds to dsRNA and deaminates A to I, these dsRNA structures are disrupted, as no strong base-pairing occurs between I and the opposing uracil (U). Imperfect dsRNAs are not efficiently bound by PRRs like RIG-I or MDA-5, so that activation of innate immune responses are impaired (Figure 4). The importance of disrupting intrinsic dsRNA structures is demonstrated by the fact, that mice

harboring a functional *Adar* gene knockout succumb during the embryonic stage, and that additional knockout of the gene for MDA-5 (*Ifih1*) can largely rescue this phenotype (Liddicoat et al. 2015). Also in humans, findings of enzymatic ADAR1 inactivity based on mutations in the Zα domain of ADAR1p150 highlight the major role in cellular homeostasis, as patients suffer from severe disease though intrinsic inflammatory responses (Rice et al. 2012; Livingston et al. 2014).

In the context of viral infection, ADAR1 can be a proviral factor, as it has been shown for many viruses (Pfaller et al. 2021). One striking example for this is measles virus. It was demonstrated that ADAR1p150 edits, besides cellular dsRNA, viral defective-interfering RNA genomes. These are accidently generated via flawed genome replication and possess the ability to form dsRNA structures (Pfaller et al. 2018). Knock-out of ADAR1 results in increased innate immune activation, particularly shown by phosphorylation of PKR and IRF3, and significantly impaired viral growth. As re-introduction of ADAR1p150 into knock-out cells restored this phenotype, it can be concluded that ADAR1p150 has a proviral role by disrupting dsRNA-intermediates generated during viral replication and that this disruption lessens innate immune activation.

IAV is well-known to produce dsRNA during its replication cycle, and previous experiments, published while this thesis was in process, have shown that ADAR1p150 is essential for effective viral replication by interfering with the activation of innate immune responses through dsRNA disruption (Vogel et al. 2020). As IAV, unlike many other RNA viruses, replicates in the nucleus of infected cells, ADAR1p110 may also have a great impact on replication. Indeed, it was shown that sole reduction of the ADAR1p110 resulted in increased IAV replication, suggesting an antiviral impact and thereby a contrary effect of the two isoforms. One hypothesis is that ADAR1p110 edits viral RNA in the nucleus and impairs viral growth, whereas ADAR1p150 disrupts viral dsRNA in the cytoplasm and negatively influences innate immunity. (Cao et al. 2018).

Taken together, ADAR1 reduces the outcome of multiple antiviral innate immune response pathways, thereby enhancing viral replication. Consequently, ADAR1 may serve as a promising therapeutic target to enhance early innate immunity by blocking ADAR1 function. However, opposing functions of ADAR1p110 in the context of influenza A virus highlight the necessity for a more detailed mechanistic

understanding to exploit possible beneficial effects of potential drugs targeting ADAR1.

1.7.2 Adaptive Immune Response

In parallel to cell intrinsic immunity of the primarily infected epithelial cells, activation and stimulation of leukocytes results in additional innate immune responses and activation of specific adaptive immunity. The first cells to react to the viral infection are tissue-resident macrophages, which can clear virus-infected cells by phagocytosis and release many different cytokines, especially type I IFN, and chemokines. Type I IFNs provide a pro-inflammatory environment and chemokines lead to the influx of monocytes from the blood stream. In the before-mentioned pro-inflammatory milieu, these further differentiate to monocyte-derived macrophages and monocyte-derived dendritic cells (DCs). The former ones are a major driver of tissue damage, as they are a source of TNF-α, IL-1β, -6, -18, and type I IFN, all known to play crucial roles in apoptosis and necrosis of epithelial cells and the decay of its barrier function. DCs on the other hand primarily take up IAV virions or debris of infected and dying epithelial cells and migrate to the draining lymph nodes, where they present the foreign antigens to T- and B cells and thereby activate adaptive immunity (Herold et al. 2015).

1.7.2.1 T cell Responses

Naïve T cells reside in the lymph node and are activated when three different stimuli are present. Firstly, this includes the presentation of peptide fragments from DCs. Two different major histocompatibility complexes (MHCs) are used to present antigens to lymphocytes (MHC-I and MHC-II), and which one is necessary depends on the subtype of T cells to be activated. The MHC of DCs binds peptides of the absorbed antigens and is subsequently transported to the plasma membrane, where it can interact with the T cell receptor (TCR). A crucial requirement for the activation is the correct affinity between the loaded MHC and the TCR, which regulates the activation of only "matching" T cells to the intruding pathogen (Smith-Garvin et al. 2009). In addition, a costimulatory signal from the DC has to be provided. In terms of T cells, the surface marker B7 on DCs is upregulated during its activation in the lung and interacts with CD28 on the T cell. Thirdly, cytokines released from the DC

are important for the activation of the T cells and drive, for $CD4^+$ T cells, their polarization (Murphy and Weaver 2018).

$CD4^+$ T cells, also called T helper cells (T_H), are important for the activation of humoral immunity (1.7.2.2) by providing necessary signals to B cells. The TCR of T_H cells interacts with MHC-II, which is also present on B cells and can thereby stimulate those to expand and produce antibodies. They furthermore leave the lymph node and home to the infected tissue, attracted by chemokines, to establish a cytokine milieu based on their polarization (T_H1, T_H2, T_H9, T_H17, and multi-/polyfunctional T cells) (Thakur et al. 2012). Although cytotoxic activity of T_H cells have gained increasing interest in the recent past, the current understanding of those cells mainly focuses on the activation of other immune cells.

$CD8^+$ T cells are known to confer cytotoxic effects, mainly the lysis of infected cells. They carry a TCR on their surface that interacts with MHC-I, which is not only expressed on the activating DCs, but also on almost every cell type. This makes them capable of interacting with these cells by MHC-I-TCR interaction and is a requirement to lyse different kinds of infected cells. Upon their activation in the lymph node, they home into the infected tissue, screen the tissue for cells presenting the respective peptides on MHC-I molecules and release cytotoxic mediators, like granzyme B and perforin, upon binding (Martin and Badovinac 2018).

1.7.2.2 Humoral Responses

Plasma cells produce antibodies and are thereby the origin of humoral immunity. They express the B cell receptor (BCR) complex on their surface, consisting of a surface immunoglobulin (Ig), and two invariant proteins, called Igα and Igβ, important for signal transduction. The surface Ig corresponds to the soluble Ig of the respective B cell, which is released after activation, concerning the specificity of its recognition site. Igs consist of two light chains and two heavy chains, both containing a variable and a constant part (Figure 6). During the maturation of the B cell, genes for those chains re-arrange, a mechanism called somatic recombination, to form Igs with individual specificity on each B cell clone. This ensures diversity of recognizable antigens within one individual. For the light chain, the two gene segments V and J build the variable region, while the C gene segment builds the constant region. For the heavy chain, the variable region is generated by recombination of three different

gene segments (V, J, and D) while the constant region consists of three C gene segments (Figure 6; illustrated by different colors).

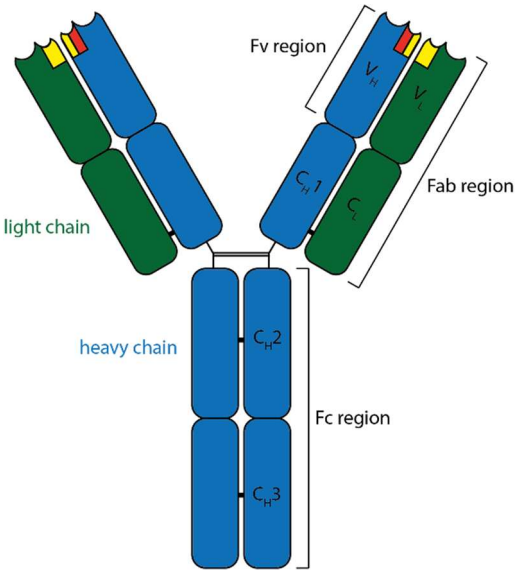

Figure 6: Schematic illustration of IgG as an example for the antibody structure

The antibody molecule has a Y-shape and is built by a heavy chain (blue) and a light chain (green). While the light chain consists of a variable (V_L) and a constant (C_L) segment, the heavy chain contains one variable (V_H) and three constant (C_H1-C_H3) segments of which C_H2 and C_H3 determine the IgG subclass and properties of the Fc region. The Fv region is responsible for the binding of the antigen and somatic recombination of V,(D),J gene segments during the maturation of the B cell results in the composition of different antigen-binding sites in each B cell clone (D and J gene segments indicated by red and yellow color). Black lines illustrate disulfide bonds.

It is important to note that each B cell contains many different alleles for the respective regions and that random recombination of those results in different binding domains on the Ig. In addition, when the gene segments are rearranged, several nucleotides can be inserted or deleted at the junction site, further increasing heterogeneity between B cell clones (junctional diversity). While the V,(D),J joining determines the binding specificity of the antibody, the constant region defines the isotype of the antibody. Five isotypes exist in humans, namely IgM, IgD, IgG, IgE, and IgA and naïve B cells express IgM and IgD as surface Igs. Upon activation through antigen recognition, they switch to the expression of other isotypes, first as membrane-associated Igs, and later as soluble Igs. Besides the interaction of the BCR with an antigen, B cells need, in many cases, stimulatory signals by T_H cells. Therefore, they express the MHC-II molecule. Importantly, the exact isotype to be produced depends on multiple different factors, including the co-stimulus during antigen-recognition and the provided cytokine milieu during activation by T_H cells. IgG is the most abundant isotype and plays important roles for the protection against IAV (Murphy and Weaver 2018).

IgGs can fight IAV infection in many ways. The most prominent functions is neutralization. Here, antibodies bind to the surface proteins of IAV, especially HA, and block essential functions, for example receptor binding or conformational change after uptake. Other mechanisms, like blocking the cleavage site of HA or inactivating NA are under investigation. Notably, apart from HA and to some extent NA, antibodies cannot neutralize the functions of other viral proteins, as these are not accessible. However, non-neutralizing antibodies directed against internal proteins have been described, and they can confer protection via their Fc part. Many immune cells express specific Fc-receptors (FcR) on their surface and interaction of these with an antibody bound to antigen can trigger effective immune responses. For example, the Fc-gamma receptor (FcγR) interacts with IgG. However, as several different FcγRs exist with different effector functions, the elicited immune response depends on the exact type of receptor, the cell that expresses it, and the antibody subclass bound (Krammer 2019).

Murine IgG antibodies can be differentiated into four different subclasses IgG1, IgG2b, IgG3, and IgG2a/c. In mice, IgG2a and IgG2c are strain-specific. For example, the strain C57BL/6 expresses IgG2c, while BALB/c mice express IgG2a. Although some similarities between human and murine IgG subclasses exist, it is of great importance to stress the differences as experimental findings in mice cannot be adopted to human without further consideration. In the current understanding of human IgG subclass development, B cells sequentially switch from IgG3 to IgG1, IgG2, and IgG4 (Collins and Jackson 2013). This model is based on the increasing appearance and accumulation of hypermutations throughout the subclasses. However, this phenomenon was not detected in mice (Collins et al. 2015). This suggests that murine B cell do not sequentially switch from subclass to subclass, but rather undergo a subtype-switch from IgA to any distinct IgG subclass directly, and this depends on the cytokine environment to which the cells are exposed to during education (Figure 7).

In contrast to humans, mice express all subclasses of IgG upon vaccination with different antigens or bacterial/viral infection, while the proportion greatly varies. Distinct cytokine profiles are considered to drive class-switching from IgM to the respective IgG subclasses in B cell follicles of lymph nodes. Transforming-growth factor-β (TGF-β), interleukin-4 (IL-4), and interferon-γ (IFNγ) promote IgG2b, IgG1

and IgG2a/c expression, respectively (Figure 7) (Deenick et al. 1999; Snapper and Mond 1993). Furthermore, IgG3 and IgG2b are referred to as early antibody subclasses, as class-switching is independent of $CD4^+$ T helper cell activity, whereas IgG1 and IgG2a/c require $CD4^+$ T cell engagement (Collins 2016).

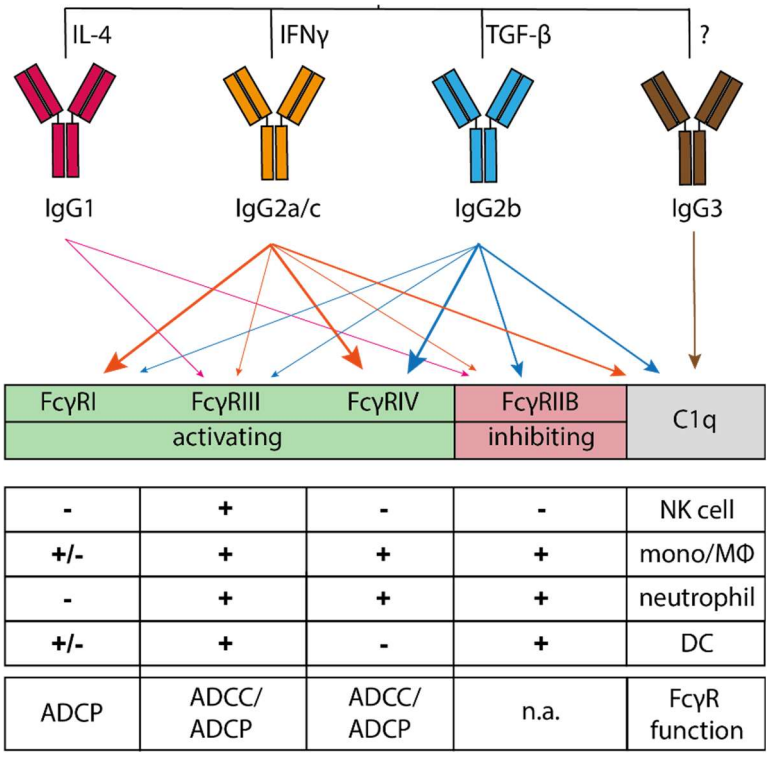

Figure 7: IgG subclass responses and their binding to FcγRs
Depending on the cytokine milieu during antibody-subtype switch, B cells produce different IgG subclasses. They bind to the activating/inhibitory FcγRs and complement activating factor C1q with different affinities (indicated by thickness of arrows). While IgG1 cannot be bound by C1q but FcγRIII and –IV, the opposite is true for IgG3. Strikingly, IgG2a/c and b subclasses both bind to the FcγRIV with high affinity, but differ in their ability to activate FcγRI, IIB, or –III. Based on the expression of the different FcγRs on selected immune cells, different effector functions can be expected. NK cells known to mediate antibody-dependent cell-mediated cytotoxicity (ADCC) are the only cells on which the FcγRIII is expressed, making this subclass a potential mediator for ADCC. Monocytes, macrophages, and neutrophils take up opsonized pathogens and infected cells thereby mediating antibody-dependent cell-mediated phagocytosis (ADCP) but can also mediate ADCC. However, it has to be taken into consideration that multiple studies suggest different, partly opposing, effector functions of IgG subclasses and further research is needed to doubtlessly elucidate the exact mechanisms conferred by each subclass. NK cell: natural killer cell; mono: monocyte; MΦ: macrophage; DC: dendritic cell. Adapted from (Collins 2016; Bruhns and Jönsson 2015)

When binding to an antigen, IgG antibodies can mediate various effector functions, and this depends on FcγR expression on the effector cells. These functions include antibody-dependent cell-mediated cytotoxicity (ADCC), antibody-dependent cell-mediated phagocytosis (ADCP), and complement activation (Krammer 2019). The various IgG subclasses have different affinities for specific FcγRs and thereby predominantly modulate certain immune cells expressing the specific FcγRs (Figure

7). In mice, IgG1 is not able to facilitate activation of antibody-mediated complement activation as it is not bound by the C1q complement factor but can efficiently bind different FcγRs, especially of the inhibitory type FcγRIIb. IgG2a/c and IgG2b particularly bind FcγRI, -III, and -IV resulting in ADCP and ADCC. In addition, IgG2 subclasses also induce complement fixation on the surface of infected cells. IgG3 on the other hand exclusively leads to complement activation through C1q fixation but does not engage with any FcγRs. Taken together, the exact immune stimulus during vaccination or infection greatly influences the generated subclass profiles, which then in turn have major impacts on the effect of non-neutralizing antibodies in fighting infection and disease. Understanding the shape of the IgG subclass profile and the resulting FcγR effector and complement functions can therefore help to build a reasonable basis for the rational design for long lasting, universal influenza vaccines in the future.

1.8 Influenza Virus Vaccines

Vaccines are the most effective way to prevent people from being infected with influenza virus, and to reduce the potentially severe complications followed by infection. To date, different types of influenza vaccines are commonly in use, for example inactivated influenza vaccines (IIV), and live attenuated influenza vaccines (LAIV). Since the development of the first approved influenza virus vaccine over 80 years ago (Plotkin 2014), it is still the major antiviral strategy against IAV. Currently, IAV vaccines exist in a trivalent or quadrivalent form, containing a mixture of the two IAV subtypes H1N1 and H3N2, and IBV lineages Yamagata and Victoria. As seasonal influenza viruses undergo a permanent antigenic drift in the human population (see section 1.5), a reformulated vaccine has to be produced annually to match the antigenic properties. For this, the World Health Organization (WHO) gathers data from the Global Influenza Surveillance and Response System (GISRS) based on analyses of influenza samples in many different collaboration centers (Global Influenza Surveillance and Response System (GISRS) 2021). With these data, the WHO tries to predict the upcoming antigenicity of the next seasonal influenza virus. However, since vaccine production takes several months, the antigenic composition of the annual vaccine has to be determined in February, while the influenza season usually starts during fall or winter of the respective year. This may result in antigenic mismatches of the vaccine and the circulating virus. While

the efficacy, measured as the protection in vaccinees under controlled conditions, is generally very high, the effectiveness, measured as the extent to which infections can be avoided in the field, varies (Fedson 1998). Overall, the vaccine effectiveness between the different seasons is usually assessed in retrospect and assumed to reach 20 to 60% (Zimmerman et al. 2016; Jackson et al. 2017; Doyle et al. 2019). Consequently, influenza virus vaccines only elicit partial protection against the respective strains, reducing disease symptoms. However, as subliminal viral replication under humoral selective pressure is still possible, circulating strains may undergo antigenic-drift and further expand immunologic escape. Because of the annual re-vaccination, leading to a low patient compliance and financial burden, the risk of an antigenic mismatch through substantial antigenic drift and the missing protection against potential upcoming pandemic influenza viruses, novel vaccine approaches are urgently needed.

1.8.1 Inactivated Influenza Vaccines (IIV)

Most of the currently licensed vaccines are IIVs that are applied intramuscularly. They are manufactured by reassorting an egg-adapted master strain virus, usually H1N1 PR8, providing efficient growth to high viral titers, with WHO-determined strains. For this, the same eggs are inoculated with a mixture of these viruses, giving rise to many possible, different reassortant viruses. During the manufacturing process, those viruses harboring gene segments encoding the virus-internal proteins of H1N1 PR8, providing efficient growth, and the HA/NA gene segments of the circulating strain are isolated and used as a *master seed virus*, with which millions of new eggs are infected (Gerdil 2003; Kilbourne et al. 1971). Alternatively to this egg-based approach, as a reaction to existing allergic reactions towards traces of egg proteins in the final product, new cell culture-based approaches have been developed and were first approved in 2012 (FDA 2012). After harvesting the grown viruses, they are inactivated by either formalin or β-propiolactone and purified via an ultra-centrifugation step. Virus particles are disrupted by detergents, the HA content is quantified by single-radial immune-diffusion assay, and standardized to 15 µg per HA component (Gerdil 2003). Furthermore, for each vaccine production, clinical trials for safety and immunogenicity have to be undertaken in order to provide clinical data for the licensing procedure (Wood and Levandowski 2003). Since production and testing are time-consuming processes, they have to be initiated early

ahead of the start of the influenza season, and therefore do not allow rapid adaption to newly emerging IAV strains.

Vaccination with IIVs induces the generation of hemagglutinin-binding antibodies, which can neutralize HA activity and therefore inhibit infection. As the titer of these antibodies correlates with the protection against antigenically similar strains, hemagglutination inhibition (HAI) titers are measured to assess vaccine efficacy (Potter and Oxford 1979; Couch et al. 2012). In parallel, as these vaccines contain all viral proteins derived from the egg-grown virus, humoral and cellular immune response directed against other components can be observed, especially targeting NA. However, standardization protocols for IIV vaccine only contain quantification of the HA content, but not NA or internal proteins. As the stability and integrity of viral proteins highly depend on the exact mechanism used to inactivate and especially to split the virus particles through detergent incubation, the containment and conformation of other viral proteins substantially varies between individual vaccine products. Although antibodies reactive against other viral proteins can be found in some vaccinees, especially against NA, NP, and M1, the overall immune response induced by IIVs is quite HA specific (Boer et al. 1990; Krammer 2019; Monto et al. 2015; Cox and Brokstad 1999). This is further illustrated by the fact that a vast majority of IIV induced plasmablasts are HA specific (Chen et al. 2018). The disadvantage of massively varying humoral immune response towards internal proteins between licensed IIVs due to divergent inactivation procedures can be circumvented by using live virus that contains naturally folded viral proteins.

1.8.2 Live Attenuated Influenza Vaccines (LAIV)

Live attenuated influenza vaccines contain replication competent virus and are applied intranasally. They are currently licensed for people between 2 and 49 years in the United States and 2 and 17 years in the European Union (EMA 2021; CDC 2021). As for IIV vaccines, they contain a reassortant virus, that only includes the surface proteins HA and NA of the circulating target strain (Subbarao and Joseph 2007). However, besides the requirement for efficient high-titer growth during the manufacturing process the intranasal application of replication-competent virus makes it mandatory to maintain an attenuated phenotype. This is achieved by using a *master donor virus* for recombination with WHO-determined strains. The master donor virus is a cold-adapted and temperature-sensitive strain originating from the

isolate A/Ann Arbor/6/60(H2N2) via serial passages at decreasing temperature (Maassab 1967; Maassab et al. 1972; Kendal et al. 1982). The cold-adapted phenotype results in attenuation in preclinical ferret experiments and clinical trials (Maassab et al. 1982; Davenport et al. 1977; Murphy et al. 1979). Subsequent analysis of the genetic background of attenuation revealed 24 mutations distributed in all of the internal proteins of the ca A/Ann Arbor/6/60 virus (Cox et al. 1988). Molecular characterization of the mutations revealed that the attenuated phenotype is predominantly linked to those found in the M2 protein and the polymerase complex proteins PA, PB1, and PB2 (Cox et al. 1988). Importantly, phenotypic characterization of this live-attenuated virus re-isolated from hundreds of vaccinated humans revealed no reversion of mutations, confirming genetic stability of the attenuated phenotype *in vivo* (Murphy et al. 1980; Wright et al. 1982).

The immune response after LAIV differs to IIV in many ways, as the vaccine is administered intranasally and induces seroconversion in adults less frequently. Consequently, HAI titers cannot be established as a correlate of protection and vaccine efficacy is therefore measured on the basis of clinical trials. However, compared to IIVs, mucosal immunity is a major component of LAIV induced immunity and is known to play a critical role in protection against subsequent infection (Krammer 2019). In contrast to adults, clinical studies in children demonstrate that humoral immunity is more long-lived as after IIV vaccination and in general broader against drifted strains (Johnson et al. 1985). LAIVs induce moderate or weak HA- and NA-specific immune responses, respectively, while antibody titers targeting internal proteins remain to be determined. On the other hand, strong $CD4^+$ and $CD8^+$ T cell responses were found to be induced in children, although not in adults, pointing to a protection supported by cellular immunity (He et al. 2006).

1.8.3 Future Vaccine Development

Since currently licensed influenza vaccines have many drawbacks, like annual re-formulation, a long production time, which makes it hard to react to spontaneous changes in the antigenic-properties of circulating strains, and almost no protection against pandemic influenza viruses, there is a huge interest for novel vaccines. In this respect, future vaccines aim to induce a protection not only against the vaccine virus,

but also against different strains (*heterologous*) and subtypes (*heterosubtypic*). The long-term goal is to create a universal influenza A virus vaccine.

To achieve a broader protection, different approaches have been undertaken, which can be categorized into two strategies. The first one is to induce humoral immunity against conserved epitopes, especially the stem region of HA (HA_{stem}), NA, as being less variable in its antigenicity than HA, or the ectodomain of M2 (M2e). The second strategy is based on cellular immunity targeting highly conserved internal proteins NP, M1, and polymerase complex proteins. These immune responses provide at least partial protection and can therefore be a promising approach for heterosubtypic vaccine candidates (Wei et al. 2020; Jazayeri and Poh 2019).

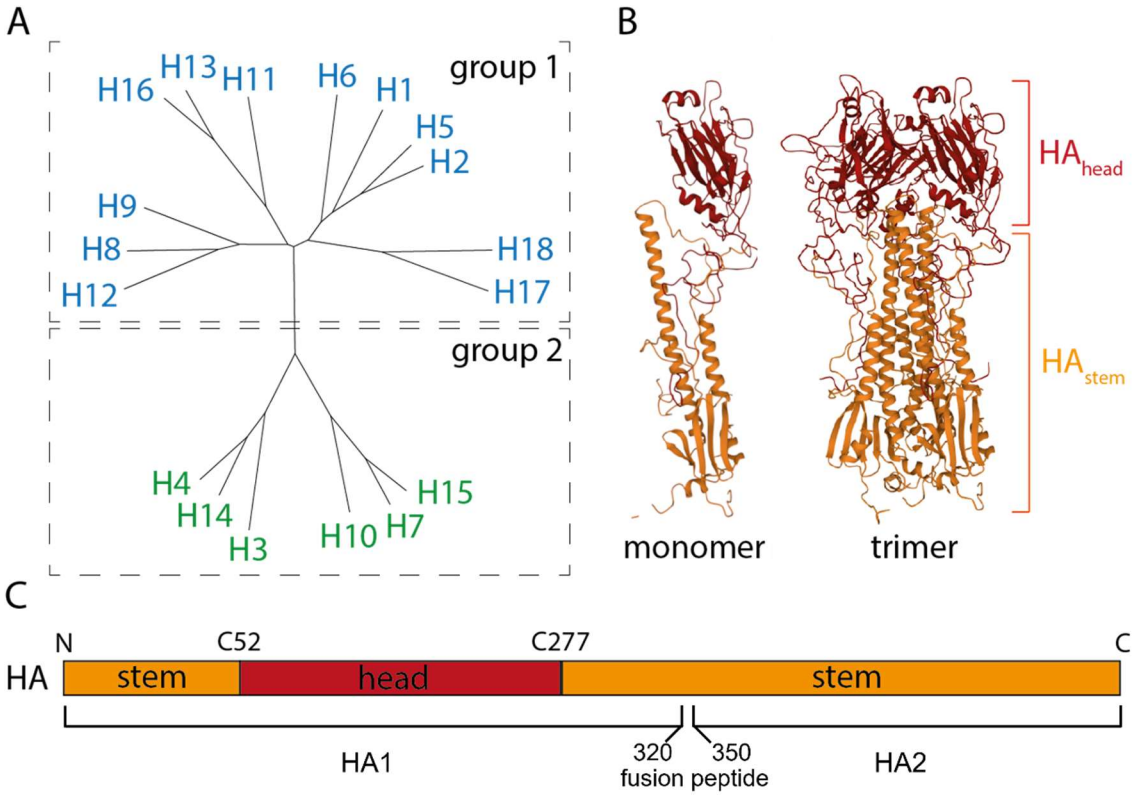

Figure 8: Classification and structure of influenza A virus hemagglutinin

(A) Phylogenetic tree to classify IAV HAs. While H1, H2, H5, H6, H8, H9, H11, H12, H13, H16, H17, H18 cluster together as group 1 (blue), H3, H4, H7, H10, H14, H15 build group 2 (green). (B) HA protein structure of a monomer (left) and an assembled trimer (right). The HA_{head} domain (red) attaches to the SA receptor on the host cell, is the prominent target of neutralizing antibodies and shows a low homology between different strains. The HA_{stem} domain (orange) is more conserved and show high amino acid similarity within the respective groups of HA. (C) Schematic representation of the unfolded HA protein where die cysteine residues flanking the head domain (red) are indicated as C52 and C277. The fusion peptide located in the stem region divides HA in the HA1 and HA2 subunit. Adapted from (Sauter et al. 1992; Hashem 2015).

HA_{stem} based vaccines target the stem region of HA and are being developed since 1983 (Graves et al. 1983). IAV HAs can be divided into two groups based on their

phylogenetic similarity (Figure 8 A) and the stem regions within each group are highly conserved (Sutton et al. 2017; Hashem 2015). The stem-region consists of the N- and C-terminal domain of HA1 and the N-terminal domain of the HA2 subunit and is defined by two cysteines (C52 and C277) creating a stabilizing disulfide bridge (Figure 8 B, C) (Hai et al. 2012; Steel et al. 2010).

Influenza vaccination using currently licensed vaccines does not induce considerable HA_{stem}-directed antibodies, mainly because of the immunodominant head domain and sterical hindrance (Moody et al. 2011; Margine et al. 2013; Corti et al. 2010). However, finding HA_{stem}-reactive antibodies in naturally infected individuals indicates that humoral immune responses towards this antigen exist and may play a significant role in protection (Wrammert et al. 2011; Pica et al. 2012). The presumed mechanisms behind this is that people are sequentially infected with drifted influenza A viruses that harbor an antigenically different HA_{head} domain and a conserved HA_{stem}, thereby boosting HA_{stem}-directed responses (Krammer and Palese 2013). This proposed mechanism is exploited in current vaccine development approaches by using chimeric HAs. These consist of the same stem region and variable head domains for consecutive vaccinations (Hai et al. 2012). Other approaches are using "headless" constructs to avoid humoral responses reactive against the head domain at all by substituting it with different forms of linkers, or by just expressing the prominent alpha-helix of the HA_2 subunit known to harbor strong B-cell epitopes (Steel et al. 2010; Wang et al. 2010). Humoral immune responses directed against HA_{stem} can act in many ways, by either blocking conformational change during viral entry or obstructing the cleavage site necessary for HA maturation (Ekiert et al. 2009; Dreyfus et al. 2012). Furthermore, FcγR-effector functions like ADCC and complement-driven cell lysis have been observed (Figure 9) (Terajima et al. 2011; Jegaskanda et al. 2013).

Apart from HA_{stem}-based vaccine approaches, the M2 protein is an attractive target for universal influenza vaccines. It is incorporated into the host cell-derived plasma membrane and is highly conserved among different IAVs, making it another promising target for broadly protecting vaccine candidates. It involves an extracellular ectodomain of 23 amino acids in length (M2e) against which antibodies in naturally infected humans and experimentally infected mice can be detected (Zhong et al. 2014; Wolf et al. 2011). Since first protective effects were found in 1988

conferred by a monoclonal M2-targeting antibody against influenza infection in mice (Zebedee and Lamb 1988), many studies have been conducted to further understand the mode of action and have found FcγR effector functions, by which those antibodies can provide protection (Deng et al. 2015; Saelens 2019). These include ADCC, complement-activation, and ADCP. Macrophages and dendritic cells play important roles in M2-mediated ADCP (Figure 9) (Guilliams et al. 2014). Additionally, M2-directed T cell responses can be elicited by experimental vaccination in mice and were shown to have protective potential (Hashemi et al. 2012; Schotsaert et al. 2013).

The NP protein is the main antigen inducing cytotoxic T cell responses after infection. Therefore, it is considered an attractive target for vaccine approaches (Zheng et al. 2014; Grant et al. 2013). Experiments using vaccination with recombinant NP following influenza A virus challenge in mice provided first evidence that the induced immune responses can protect mice, and that this effect is provided by T cell-mediated immunity (Wraith et al. 1987; Taylor and Askonas 1986). As cellular immunity relies on infected cells that can present T cell epitopes of internal proteins via MHC-I presentation, vaccination with NP cannot avoid initial infection, but contributes to the clearance of infected cells, thereby decreasing clinical burden and accelerating recovery (Del Campo et al. 2019; Wang et al. 2014; Wang et al. 2015). In addition, patients can have high levels of NP-specific antibodies after IAV infection (Jegaskanda et al. 2017). Although experiments in mice confirmed at least partial protective immunity via NP-directed antibodies, the exact proportion and mechanisms are not fully understood (Carragher et al. 2008; LaMere et al. 2011). Immunization with recombinant NP and a NP-M2e fusion peptide (NM2e) show that the magnitude of humoral immune responses, as well the exact IgG subclass profile may play an important role in conferring protection against IAV challenge in mice (Wang et al. 2012; Wang et al. 2014). Antibody-forming plasma cells generating anti-NP IgGs show a substantially extended existence in the bone-marrow when compared to anti-HA generating plasma cells. (Sealy et al. 2003). This further weighs on the potential benefits of humoral immune responses towards NP. However, other studies failed to show protective capacity of NP-directed humoral responses (Bodewes et al. 2013; Vanderven et al. 2016), and the underlying reason remains unknown.

M1 is another internal protein that has received a lot of attention because of its high degree of conservation. Indeed, M1-directed immune responses have some protective potential (Xie et al. 2009). As seroconversion in experimentally infected individuals appears in only a minor fraction (6%) of study participants, anti-M1 antibodies probably play a negligible role during human IAV infections (Cretescu et al. 1978). However, immunization with M1 can provide some protection against heterologous IAV challenge in the murine model, suggesting a T cell based immunity (Sui et al. 2010; Moon et al. 2019). In heterologous vaccine approaches, M1 is frequently combined with other IAV proteins, as it is expected to provide supporting cellular immunity, but no autologous protection.

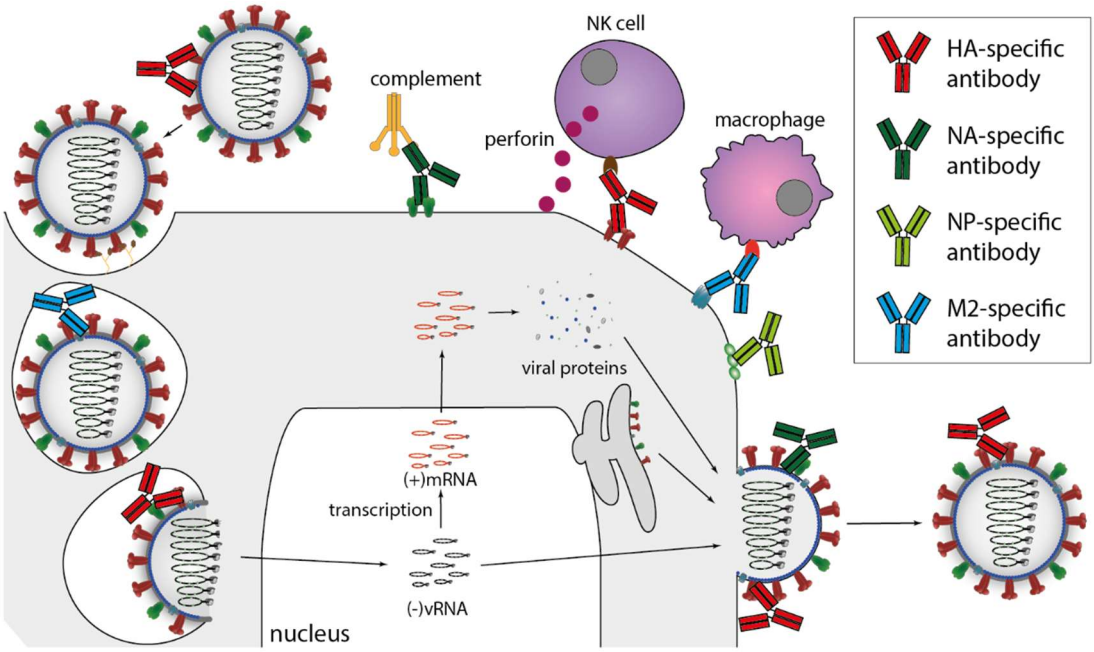

Figure 9: Antibody responses elicited against different IAV antigens

IAV-directed antibodies can impede viral infection and replication in different ways. While HA-specific antibodies can neutralize the virus by either blocking receptor binding or by fusion of viral and host cell membrane, non-neutralizing antibodies can activate NK cell-mediated cell death of infected cells. Furthermore, HA specific antibodies can hinder viral release and HA maturation by blocking proteolytic cleavage of the pre-mature HA_0 into HA_1 and HA_2. Also for NA, many different ways in which humoral immune responses can interfere with viral replication are known. Antibodies can block enzymatic activity of NA, thereby decreasing cleavage of mucins and effective release of progeny virus. Additionally, non-neutralizing antibodies can induce complement-activated cell lysis. M2-directed antibodies can block ion-influx during viral uptake and thereby release of viral RNPs into the host cell. Furthermore, these antibodies can induce antibody-dependent cell-mediated phagocytosis (ADCP). In contrast, NP has been found on the surface of infected cells and antibodies directed against these NP-plaques were reported. However, exact mechanisms by which these antibodies contribute to viral clearance remain elusive. Adapted from (Rajão and Pérez 2018; Krammer 2019)

All these efforts have not yet resulted in a broadly protective universal IAV vaccine that could protect from influenza disease by generating broadly reactive and long-lasting humoral and T cell responses. To accomplish this, further research is needed

in order to specifically characterize the capability of different antigens to induce humoral and cellular immunity. While extensive research was performed to characterize T cell mediated immunity towards internal proteins, further investigation is needed in terms of humoral responses, as previous studies clearly suggest a substantial role in conferring protective immunity. As demonstrated for HA, NA, NP and M2-directed antibodies, non-neutralizing antibodies can have a substantial impact on disease progression and outcome (Figure 9).

1.8.4 Vesicular-stomatitis Virus-based Vaccines

Vesicular-stomatitis virus (VSV) belongs to the family of *Rhabdoviridae.* The viral particles are bullet-shaped and measure approximately 200 nm in length and 70 nm in width (Cureton et al. 2010).

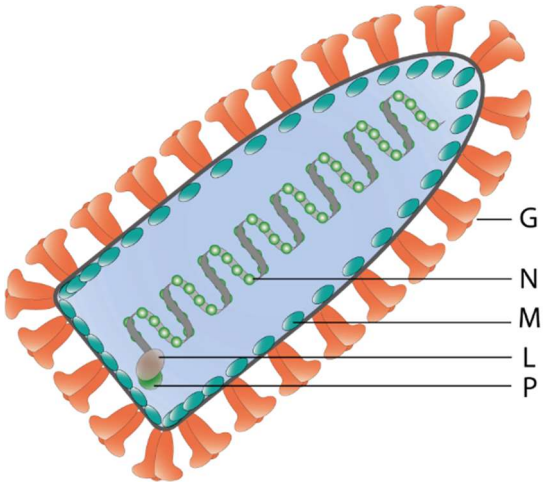

Figure 10: Schematic illustration of a vesicular-stomatitis virus (VSV) particle.

Viral particles are bullet-shaped and measure approximately 200 x 70 nm. They consist of a host-derived lipid bilayer in which the viral receptor, VSV glycoprotein (G), is embedded in. The inner surface is coated by the matrix protein (M), which is attached to the viral ribonucleoprotein complex (vRNP), consisting of the single-stranded RNA genome, the large polymerase (L) and the phosphoprotein (P). Adapted from (Dricu 2012).

VSV carries a single-stranded RNA genome with negative polarity. It has a simple genomic structure consisting of approximately 11,000 nucleotides. The five viral genes are present in the order 3'-nucleoprotein (N)-phosphoprotein (P)- matrix protein (M)-glycoprotein (G)- large polymerase (L)-5'. Its genomic and structural composition make it a well-suited candidate as a viral vector (Munis et al. 2020). VSV is an animal pathogen, usually infecting cattle, horses, or pigs, but can also rarely lead to flu-like illness in humans. Since human cases of VSV infection are very uncommon, no considerable sero-prevalence is found in the human population

(Brody et al. 1967). The VSV G protein is the only surface protein and mediates attachment and entry into the host cell (Fields et al. 2015). VSV can infect a great variety of cells via attachment to the low density lipoprotein (LDL)-receptor family (Finkelshtein et al. 2013), which is expressed on a many tissues *in vivo*.

VSV was first rescued from cDNA in 1995 (Lawson et al. 1995), laying the foundation for subsequent manipulation and usage of VSV as a viral vector by reverse genetics. Initial experiments using a VSV-vector expressing full length IAV HA demonstrated the proof-of-concept to exploit VSV as a vaccine platform by providing full protection against subsequent homologous challenge. However, these experiments also revealed severe pathogenicity of VSV replication in mice, making further attenuation of VSV necessary (Roberts et al. 1998). Cytotoxicity and pathogenicity of VSV predominantly depend on a functional viral glycoprotein (VSV-G). Therefore, different approaches were performed, like deleting parts of VSV-G, or even replacing it. These vectors still proved to be effective in protecting mice from a lethal IAV challenge, while not showing any pathogenicity in the animals (Roberts et al. 1998; Roberts et al. 1999). If the transgene cannot complement VSV G, deletion of VSV G from the viral genome results in single-round replicons (VSVΔG) with a beneficial safety profile (Zimmer 2010). Although they are not able the efficiently replicate, they are capable of inducing humoral as well as cellular immune responses and have been suggested as a vaccine platform for example for SARS-CoV (Kapadia et al. 2008). These experiments paved the way for further optimization of VSV as a vaccine platform and resulted in the development of the first approved Ebola vaccine in 2019 (Ervebo) (Marzi et al. 2015; Banadyga and Marzi 2017). Furthermore, different approaches using replication competent, or single-round replicons as a vaccination strategy against influenza virus were examined. For example, it was demonstrated that recombinant VSV encoding IAV NP can induce strong influenza-specific CD8 T cell responses and protect mice from severe pathology (Barefoot et al. 2009). Other approaches examined protective efficacy against humoral targets, mainly HA, and found that immunization with VSV vectors expressing full-length, or chimeric HAs provide efficient protection against infection and disease (Halbherr et al. 2013; Furuyama et al. 2020; Ryder et al. 2015). Taken together, the VSV platform, especially VSVΔG, is a favorable approach for the development of universal influenza vaccines. Furthermore, as strong cellular and humoral immune responses can be elicited via VSV vector immunization, it is also a promising tool for

the detailed characterization of immune responses targeting individual antigens of IAV and other pathogens.

1.9 Aims

This study aims to provide further insights into innate and adaptive immune responses against IAV infections. The primary focus is to investigate, which immune responses can elicit protection against IAV independent of the virus subtype. For this, two different projects were investigated.

In the first project, the adaptive immune responses directed against individual antigens of the licensed LAIV Fluenz® Tetra were characterized using the VSV replicon system as a viral vaccine vector platform in a mouse model of IAV infection. The goal was to investigate the magnitude and shape of immune responses directed against internal, highly-conserved antigens, in order to understand, how these immune responses contribute to protection against the two different subtypes PR8 and rSC35M. A major focus was the characterization of humoral immune responses induced by the different vectors. For this, we determined IgG subclass profiles induced by the different vaccine vectors and correlated these with the effectiveness to protect against heterologous IAV infection. In addition, to understand how protection can be achieved, we investigated FcγR effector functions mediated by certain subclasses. Finally, we investigated whether partially protective humoral responses against individual antigens can exert synergistic effects when combined, and thus have a greater potential of protection.

In a second project, the role of ADAR1 on the replication of IAV was investigated. ADAR1 is known as a negative regulator of dsRNA-mediated innate immune responses and its proviral activity has been demonstrated for a variety of other viruses. Since antiviral innate immune responses are not pathogen-specific, enhancing them by targeting ADAR1 may be a strategy to develop broadly acting antiviral therapies. However, a detailed understanding of this mechanism, especially in case of IAV infection, is still missing. This project therefore aimed to address whether ADAR1 has a proviral activity for IAV, whether this activity was equally observed for two different IAV subtypes, and what the underlying mechanism of the proviral activity may be.

2 OWN CONTRIBUTION

The present PhD thesis consists of two individual projects. If not stated otherwise, I planned, performed, and analyzed the described experiments and the respective data with the help of my supervisor Dr. Christian K. Pfaller. In parallel, I repeatedly presented the progress of my projects to Prof. Dr. Eva Friebertshäuser, Prof. Dr. Veronika von Messling, and Dr. Ralf Wagner, discussed the obtained data and planned further experiments. A detailed description of my own contribution is listed below.

2.1 Humoral Immune Responses Against Internal Influenza A Virus Antigens Correlate With Protection Against Heterologous Challenge

For cloning the NP, M1, and M2 genes I used the Fluenz® Tetra Vaccine virus and previously published primer pairs, both kindly provided by Prof. Dr. Veronika von Messling. The generation of the $H3_{stem}$ constructs and the subsequent cloning of the VSV expression plasmids were performed under supervision of PD Dr. Gert Zimmer at the Institute of Virology and Immunology (Mittelhäusern, Switzerland). For time constrains, generation of VSV replicons was performed by PD Dr. Gert Zimmer and rescued replicons were provided for further experiments. VSV*ΔG and VSV*ΔG(HA PR8) were available from previous studies of Dr. Lisa Walz. I produced new replicon stocks and purification was performed under supervision by Dr. Bevan Sawatsky. Titration of VSV replicons, as well as characterization via immunoblot analysis, single-round character confirmation, and immunofluorescence analysis was conducted by me, with technical assistance of Sylvia Panitz for microscopy. Animal experiments were planned together with Dr. Bevan Sawatsky and experimental help was provided by Dr. Bevan Sawatsky, Yvonne Krebs, Dr. Svetlana Rezincuic, Marcel Rommel, and Franziska Schenk for LD_{50} titration, immunization, and infection. The rSC35M virus was provided by Dr. Hannah Seidiri and Prof. Dr. Eva Friebertshäuser. Viral stock production in embryonated chicken eggs was supervised by Dr. Hannah Seidiri. Total antibody titration, neutralizing antibody titration, IgG subtype titration, IFNγ ELISpot and IL-4 ELISA were planned and executed by me with help during initial troubleshooting from Dr. Bevan Sawatsky. FcγR effector assays were performed by me with technical assistance from Dr. Nina Hein-Fuchs

for the usage and setup of the luminometer. A manuscript containing the obtained data is currently in preparation.

Wittwer K, Zimmer G, Sawatsky B, Rezincuic S, Rommel MGE, von Messling V, Pfaller CK. Non-Neutralizing Antibody Responses after Vesicular stomatitis virus-vectored Influenza A Virus Vaccine Correlate With Protection. In preparation

2.2 ADAR1 Has Proviral Activity for Influenza A Virus

HeLa wildtype, HeLa-ADAR1p150^{KO} and HeLa-ADAR1^{KO} cells were provided by Dr. Christian Pfaller. Infection and immunoblot analysis were performed by me. Cas9n- and gRNA-encoding plasmids were designed by Dr. Christian Pfaller and subsequent generation of MDCK-ADAR1^{KO} variants conducted by me, while Marcel Rommel helped with the GFP^{+} sorting procedure and post-sorting analysis. MTT-based assays for cell growth and cell death assays were planned independently by me, while Dr. Bevan Sawatsky helped with initial troubleshooting during the viral growth analysis in MDCK cells.

2.3 Further Contributions

Additionally, I participated in other research projects during my PhD time at the Paul-Ehrlich-Institute.

I performed RNA isolation of squirrel monkey organ samples obtained during my master's thesis, which were subsequently quantified for viral RNA in cooperation with Richard Plemper's research group from the Atlanta State University. Furthermore, I analyzed histology slides under supervision of Dr. Roland Plesker and performed viral neutralizing antibody titrations. In this project, we treated squirrel monkeys with different treatment regimens of the experimental compound ERDRP-0519 and followed course of infection and several virological and immunological parameters. As a first author, I planned and executed animal experiments with the help of Prof. Dr. Veronika von Messling, Dr. Danielle Anderson, Dr. Lisa Walz, Dr. Kristin Pfeffermann, and Dr. Mareike Dörr. I wrote the first draft of the manuscript, was responsible for figure design and in charge of subsequent corrections. We published this study in Nature Communications.

Wittwer K, Anderson DE, Pfeffermann K, Cox RM, Wolf JD, Santibanez S, Mankertz A, Plesker R, Sticher ZM, Kolkykhalov AA, Natchus MG, Pfaller CK, Plemper RK, von Messling V. Small-molecule polymerase inhibitor protects non-human primates from measles and reduces shedding.

Nat Commun. 2021 Sep 2;12(1):5233. doi: 10.1038/s41467-021-25497-4. PMID: 34475387; PMCID: PMC8413292.

In a further project, VSV replicon particles expressing a fusion protein of rabies virus G and SARS-CoV-2 spike protein (VSV*ΔG-miniS) were designed by our collaboration partner Prof. Dr. Conzelmann. Together with Dr. Bevan Sawatsky and Dr. Christian Pfaller, I performed immunization and challenge experiments in the murine model and helped analyzing the obtained data. The described study resulted in a co-authorship and was published in PLOS Pathogens.

Hennrich AA, Sawatsky B, Santos-Mandujano R, Banda DH, Oberhuber M, Schopf A, Pfaffinger V, **Wittwer K**, Riedel C, Pfaller CK, Conzelmann KK. Safe and effective two-in-one replicon-and-VLP minispike vaccine for COVID-19: Protection of mice after a single immunization. *PLoS Pathog*. 2021 Apr 21;17(4):e1009064. doi: 10.1371/journal.ppat.1009064. PMID: 33882114; PMCID: PMC8092985.

In another study, we supported the laboratory of Prof. Dr. Dr. Ute Modlich in our department, who investigated the effect of IAV infection in mice on the hematopoietic stem cell compartment in the bone marrow. We analyzed the development of different cell populations and showed that inflammatory cytokines induced by non-systemic influenza A virus infection triggers emergency megakaryopoiesis. During this study I helped performing the animal experiments and was involved in internal re-vision and correction of the manuscript.

Rommel MGE, Walz L, Kohlscheen S, Schenk F, Miskey C, Botezatu L, **Wittwer K**, Krebs Y, Ivics Z, Pfaller CK, von Messling V, Modlich U. Influenza A Virus Infection Instructs Hematopoiesis to Megakaryocyte-lineage Output. *Under review in Cell Reports*

In a consortium of different research institutions (Freie Universität Berlin, Friedrich-Schiller-Universität Jena, Julius-Maximillians-Universität Würzburg, Paul-Ehrlich-Institut) I participated in the "ProMatLeben Polymere" project "NextPEG", in which several alternative conjugates to polyethylene glycol were generated, linked to recombinant interferon, and subsequently analyzed in the murine model concerning pharmacokinetic properties. I performed the *in vivo* analysis of these conjugates with the help of Marcel Rommel and Franziska Schenk, by planning the experimental setup, applying the respective interferon, and collecting serum samples. Two separate manuscripts listing me as a co-author were prepared and are currently under review.

Hauptstein N, Pouyan P, **Wittwer K**, Dirauf M, Cinar G, Raschig M, Licha K, Scherf-Clavel O, Lühmann T, Nischang I, Schubert US, Pfaller CK, Haag R, Meinel L. Polymer selection impacts

the pharmaceutical profile of site-specifically conjugated Interferon-α2a. ChemRxiv. 2022; doi: 10.26434/chemrxiv-2022-j85br; *Under review in Journal of Controlled Release.*

Hauptstein N, Dirauf M, **Wittwer K**, Cinar G, Siering O, Raschig M, Lühmann T, Scherf-Clavel O, Sawatsky B, Nischang I, Schubert US, Pfaller CK, Meinel L. PEtOxylated Interferon- α2a bioconjugates addressing H1N1 influenza A virus infection. *Under review in Biomacromolecules.*

I further participated in a study investigating the adaptation of canine distemper virus to the ferret host. First, different virus preparations either recombinant or originating from natural isolation were characterized regarding their genetic diversity. After serial passage in ferrets, the ability of the respective preparations to replicate in the host and induce severe disease were assessed. Furthermore, RNAseq was used to investigate the underling genetic adaptation during each passage. I helped performing the serial passage experiments by handling, anesthetizing, infecting, and sacrificing the animals. I further supported isolation of virus from ferret organs and subsequent processing for next serial infection.

Siering O, Doerr M, Herrmann M, **Wittwer K**, von Messling V, Sawatsky B, Pfaller CK. Natural canine distemper virus diversity confers rapid adaptation to new carnivore host. *Under review in mBio*

3 MATERIALS AND METHODS

3.1 MATERIALS

3.1.1 Chemical and Reagents

Product	**Notes**	**Source**
1kb DNA ladder		Thermo Fisher Scientific, Karlsruhe
6X DNA Loading Dye		Thermo Fisher Scientific, Karlsruhe
70% Ethanol	In H_2O	Paul-Ehrlich-Institute, Langen
Ammonium persulfate (APS)	10% working dilution	Carl Roth, Karlsruhe
Ampicillin	>97%	Carl Roth, Karlsruhe
Bovine serum albumin (BSA)		Sigma-Aldrich, München
Concanavalin A	Isolated from *Canavalia ensiformis*	Sigma-Aldrich, München
DAPI	100 ng/ml working dilution	Sigma-Aldrich, München
Dimethyl sulfoxide (DMSO)		Sigma-Aldrich, München
DMEM w/o phenolred		Thermo Fisher Scientific, Karlsruhe
dNTPs	10 mM	Agilent Technologies, Waldbronn
Dulbecco's modified Eagle medium (DMEM)	High glucose (4.5 g/L)	Sigma-Aldrich, München
Earles's Minimum Essential Medium (MEM)		Sigma-Aldrich, München
Ethylenediaminetetraacetic acid (EDTA)		Paul-Ehrlich-Institute, Langen
Fetal bovine serum (FBS)		Invitrogen, Karlsruhe
GelRed	10.000x	Biotium, Fremont, CA
H_2O		Paul-Ehrlich-Institute, Langen
HL-1 medium		Biozym Scientific GmbH, Hessisch Oldendorf

Hydrogen peroxide solution (H_2O_2)	30% (v/v) in H_2O	Sigma-Aldrich, München
Hygromycin B	Isolated from *Streptomyces hygroscopius*	Sigma-Aldrich, München
Isopropanol		Paul-Ehrlich-Institute, Langen
Ketamin		Bela-Pharm, Vechta
L-glutamine	200 mM	Biochrom AG, Berlin
Lysogeny broth (LB) Agar plates		IVI, Mittelhäusern/Paul-Ehrlich-Institute, Langen
Lysogeny broth (LB) medium		IVI, Mittelhäusern/Paul-Ehrlich-Institute, Langen
MeOH (methanol)		Paul-Ehrlich-Institute, Langen
Mifepristone	Working dilution 10^{-9} M in EtOH	Sigma-Aldrich, München
Mitomycin C		Sigma-Aldrich, München
N,N-dimethylformamide (DMF)		Sigma-Aldrich, München
Opti-MEM		Thermo Fisher Scientific, Karlsruhe
Penicillin/Streptomycin	10.000 units penicillin/10 mg streptomycin per 1 ml	Paul-Ehrlich-Institute, Langen/ Sigma-Aldrich, München
Phosphate-buffered saline (PBS)		Paul-Ehrlich-Institute, Langen
ProLong Diamond Antifade Mountant		Invitrogen, Karlsruhe
Protein Ladder PageRuler Plus Prestained		Thermo Fisher Scientific, Karlsruhe
RNAse OUT		Invitrogen, Karlsruhe
Rotigarose (agarose)		Carl Roth, Karlsruhe
Rotiphorese acrylamide	30% working dilution	Carl Roth, Karlsruhe
RPMI1640		Sigma-Aldrich, München
Skim milk powder		Carl Roth, Karlsruhe
Sodium pyruvate		Thermo Fisher Scientific, Karlsruhe
Sodium-dodecyl sulfate (SDS)	10% working solution	Paul-Ehrlich-Institute, Langen

Sucrose		Sigma-Aldrich, München
TEMED	≥ 98.5% working dilution	Carl Roth, Karlsruhe
Tolyl-sulfonyl phenylalanyl chloromethyl keton (TPCK)-trypsin		Sigma-Aldrich, München
Tryphan blue		Sigma-Aldrich, München
Trypsin-EDTA	0.05% (w/v) trypsin/0.002% (w/v) EDTA	Paul-Ehrlich-Institute, Langen
Tween20		Sigma-Aldrich, München
Xylavet	100 mg/ml	cp-pharma, Burgdorf
Zeocin		Sigma-Aldrich, München
β-mercapthoethanol		Sigma-Aldrich, München

3.1.2 Buffers and Solutions

Buffer	**Details**
10% running gel (SDS-PAGE) (volume 10 ml)	2.5 ml 1.5 M Tris-HCl, pH 8.8 3.3 ml 30% Rotiphorese acrylamide 100 µl 10% (v/v) SDS solution 10 µl ≥98.5% TEMED 100 µl 10% APS 4.1 ml H_2O
10X SDS running buffer (Paul-Ehrlich-Institute, Langen)	250 mM Tris 192.1 mM glycine 1% (w/v) SDS In H_2O
10X TAE-buffer (Paul-Ehrlich-Institute, Langen)	2 M Tris 1 M acetic acid 50 mM EDTA-Na In H_2O, pH 8.5
10X TBS (Paul-Ehrlich-Institute, Langen)	50 mM Tris base 150 mM NaCl, In H_2O pH 7.4
12% running gel (SDS-PAGE) (volume 10 ml)	2.5 ml 1.5 M Tris-HCl, pH 8.8 4 ml 30% Rotiphorese acrylamide 100 µl 10% (v/v) SDS solution 10 µl ≥98.5% TEMED 100 µl 10% APS 3.4 ml H_2O
2X Urea sample buffer	200 mM Tris, pH 6.8 8 M Urea 5% (w/v) SDS

	0.1 mM EDTA 0.03% (w/v) bromophenol blue 1.5% (w/v) β-mercapthoethanol In H_2O
4% stacking gel (SDS-PAGE) (volume 5 ml)	1.25 ml Tris-HCl, pH 6.8 650 µl 30% Rotiphorese acrylamide 50 µl 10% (v/v) SDS solution 5 µl ≥98.5% TEMED 50 µl 10% APS 3.05 ml H_2O
5% blocking buffer (Western Blot)	5% (w/v) BSA In PBS
AEC substrate	5 ml 0.05 M $C_2H_3NaO_2$ (sodium acetate buffer) 300 µl 3-amino-9-ethylcarbazole in DMF 2.5 µl 30% H_2O_2
ELISpot antibody buffer	1% (w/v) BSA 0.0025% (w/v) Tween 20 In PBS
ELISpot blocking buffer	1% (w/v) BSA In PBS
ELISpot washing buffer	0.0025% (w/v) Tween20 In PBS
FACS buffer	5 mM EDTA In PBS
Fixation buffer	3% (w/v) Paraformaldehyde In PBS
Lysogeny broth medium (Paul-Ehrlich-Institute, Langen)	1% (w/v) Trypton from casein 0.5% (w/v) yeast extract 1% (w/v) NaCl In H_20, pH 7.0
Permeabilization buffer	0.5% (v/v) Triton X-100 In PBS
Protein lysis buffer	10 mM HEPES, pH7.9 200 mM NaCl 5 mM KCl 10% (v/v) glycerol 0.5% (v/v) NP-40 1 mM EDTA 1 mM Na_3VO_4 5 mM NaF 1 mM PMSF 1 mM DTT 1% (v/v) protease inhibitor cocktail 1% (v/v) phosphatase inhibitor cocktail In H_2O
Quenching buffer	50 mM NH_4Cl

	In PBS
RBC lysis buffer (Paul-Ehrlich-Institute, Langen)	0.8 M NH_4CL 50 mM Tris-HCl In H_2O, pH 7.5
S.O.C. medium	2 % (w/v) Trypton from Casein 0,5 % (w/v) yeast extract 10 mM MgCl2 10 mM MgSO4 10 mM NaCl 2,5 mM KCl 20 mM D(+)-Glucose in H_2O, pH 7.0
TBS-T	0.1% (v/v) Tween20 In 1X TBS
Transfer buffer	10% (v/v) MeOH 10% (v/v) Tris/glycine buffer In H_2O
Tris-HCl 1.5 M pH 6.8	1.5 M Tris base In H_2O, pH 6.8
Tris-HCl 1.5 M pH 8.8	1.5 M Tris base In H_2O, pH 8.8

3.1.3 Equipment and Technical Devices

Product	**Source**
A.EL.VIS ELISPOT Scanner	stefan badur electronic GmbH & Co. KG, Hannover
ABI Prism 3100 Genetic Analyzer	Thermo Fisher Scientific, Karlsruhe
Accu-jet pro (pipetter)	Brand, Wertheim
Agarose gel chamber (40-1214)	PEQLAB Biotechnologie GMBH, Erlangen
Avanti J-26 XPI (highspeed-centrifuge) rotor: JA-25.50	Beckman Coulter, Krefeld
Axio Observer.Z1	Carl Zeiss AG, Oberkochen
Bacterial incubator Heraeus Instruments	Thermo Fisher Scientific, Karlsruhe
Bacterial incubator/shaker innova42	New Brunswick Scientific, Edison (NJ)
Bio-Rad Gel Chamber MINI-Protean	Bio-Rad Laboratories GmbH, Puchheim
Centrifuge 5810R (rotor A-4-81)	Eppendorf, Hamburg
Centrifuge ST 8FR	Thermo Fisher Scientific, Karlsruhe

ChemiDoc MP Imaging System	Bio-Rad Laboratories GmbH, Puchheim
DITABIS HLC Heating Thermo Shaker MHR 13	DITABIS Digital Biomedical Imaging Systems AG, Pforzheim
Drying cabinet: WTC	Binder, Tuttlingen
Eppendorf centrifuge 5418	Eppendorf, Hamburg
Erlenmeyer flask	VWR International GmbH, Darmstadt
FACSAria Fusion	BD biosciences, Heidelberg
Finnpipette F2 (multichannel pipette)	Thermo Fisher Scientific, Karlsruhe
Freezer (-150°C) VIP+	Panasonic, Hamburg
Freezer (-20°C) GG4010-20	Liebherr, Biberach an der Riss
Freezer (-80°C) HERAFreeze Top	Thermo Fisher Scientific, Karlsruhe
Fridge (4 - 8°C) FKS 1800-20	Liebherr, Biberach an der Riss
Heatblock (Thriller)	PEQLAB Biotechnologie GMBH, Erlangen
Heracell 150i (Cell culture incubator)	Thermo Fisher Scientific, Karlsruhe
Microwave (7809)	Severin, Sundern
Mr. Frosty Freezing container	Thermo Fisher Scientific, Karlsruhe
MSC-Advantage 1.2 (tissue culture hood)	Thermo Fisher Scientific, Karlsruhe
NanoDrop 2000c	Thermo Fisher Scientific, Karlsruhe
Neubauer chamber: Neubauer Brightlight	LO-Laboroptik, Friedrichsdorf
Nikon Eclipse T*i*-S (Fluorescence microscope)	Nikon GmbH, Düsseldorf
Nikon Eclipse TS100-F (light microscope)	Nikon GmbH, Düsseldorf
Optima L-80 XP (ultra-centrifuge), Swinging bucket rotor: SW32 Ti	Beckman Coulter, Krefeld
PerfectBlot hybridization chamber	PEQLAB Biotechnologie GMBH, Erlangen
PHERAstar FSX luminescence reader	BMG Labtech, Ortenberg
Pipettes: Reference 2 (0.1–0.5 µl, 0.5–10 µl, 10–100 µl, 20–200 µl, 100–1000 µl)	Eppendorf, Hamburg
PowerPac 300 (power supply)	Bio-Rad Laboratories GmbH, Puchheim

Sartorius (scale)	VWR International GmbH, Darmstadt
Shaker RockingShaker	OHAUS Europe GmbH, Nänikon
Shaker SSL4	Stuart, Villepinte
Tecan SUNRISE microplate absorbance reader	Tecan Group Ltd., Männedorf
Tecan SUNRISE microplate absorbance reader	Tecan Group Ltd., Männedorf
TProfessional TRIO (PCR Cycler)	Biometra/Analytik Jena, Göttingen
Trans-Blot Turbo Transfer System	Bio-Rad Laboratories GmbH, Puchheim
UV-illuminator	Syngene, Schwerte
Vacuum pump TopStream 3000	Fastbiotech, Frankfurt
Water bath	GFL, Burgwedel
Water bath (Julabo TW8)	Julabo GmbH, Seelbach

3.1.4 Consumables

Product	**Source**
0.2 ml PCR reaction tubes	Thermo Fisher Scientific, Karlsruhe
1.1 ml Z-Clot Serum Tubes	Sarstedt, Nürnbrecht
1.5 ml Eppendorf reaction tubes	Eppendorf, Hamburg
15 ml and 50 ml Falcon tubes	Greiner bio-one, Frickenhausen
8 Chamber Polystyrene Vessel Tissue Culture Treated Glass Slide	Corning, Kaiserslautern
Cannula (26GX ½ 0.45x12mm) for cardiac puncture	Henke-Sass, Wolf, Tuttlingen
Cell strainer (70 µm)	Corning, Kaiserslautern
Cover slip 24x32 mm	Thermo Fisher Scientific, Karlsruhe
Cryo tubes (Cryo S)	Greiner bio-one, Frickenhausen
Culture dish	Thermo Fisher Scientific, Karlsruhe
Disposable scalpel	B.Braun, Melsungen
ELISpot 96-well plates	Merck Millipore, Darmstadt
FACS tubes with 70 µm cell strainer	BD biosciences, Heidelberg
MaxiSorp polystyrene 96-well plate	Thermo Fisher Scientific, Karlsruhe
Multiwell plates (black) 96-well plates	Nunc, Rochester
Multiwell-plates (6-, 12-, 24- and 96-well plates)	Nunc, Rochester

Omnican syringes (1, 3, 5, 10, 20 ml)	B.Braun, Melsungen
Omnican-F 0.01 – 1 ml syringes with attached cannula	B.Braun, Melsungen
Pipette filter tips (10, 100, 300, 1000 µl)	Sarstedt, Nürnbrecht
Polycarbonate ultracentrifugation tube	Beckman Coulter, Krefeld
Polyvinylidendifluorid (PVDF) membrane (Immobilon-P)	Merck Millipore, Darmstadt
Serological pipettes (5, 10 and 25 ml)	Greiner bio-one, Frickenhausen
Tissue culture treated cell culture flasks (T25, T75, T175)	Greiner bio-one, Frickenhausen
Whatman filter paper	GE Healthcare, Backinghamshire

3.1.5 Kits, Enzymes, Substrates

Product	**Source**
10X FastAP-buffer	Thermo Fisher Scientific, Karlsruhe
10X FastDigest buffer	Thermo Fisher Scientific, Karlsruhe
3-amino-9-ethylcarbazole (AEC) substrate	Sigma-Aldrich, München
Amersham ECL Western Blot Detection Reagent	GE Healthcare, Backinghamshire
BCIP/NBT-Purple Liquid Substrate	Sigma-Aldrich, München
BigDye Terminator V3.1 Cycle Sequencing Kit	Applied Biosystems, Foster City, CA
CellTiter 96 Non-Radioactive Cell Proliferation Assay	Promega, Mannheim
FastAP	Thermo Fisher Scientific, Karlsruhe
FastDigest Eco911	Thermo Fisher Scientific, Karlsruhe
FastDigest MluI	Thermo Fisher Scientific, Karlsruhe
IL-4 Mouse Uncoated ELISA Kit	Thermo Fisher Scientific, Karlsruhe
Lipofectamine 3000	Thermo Fisher Scientific, Karlsruhe
Mouse FcγRIV ADCC Bioassay	Promega, Mannheim
NucleoSEQ Column Kit	Macherey-Nagel, Düren
NucleoSpin Gel and PCR clean-up Kit	Macherey-Nagel, Düren
PfuUltra II Fusion High-Fidelity DNA polymerase	Agilent Technologies, Waldbronn
Phusion Hot Start II High-Fidelity DNA Polymerase Kit, F-549S	Thermo Fisher Scientific, Karlsruhe

Plasmid Midi Kit	Qiagen, Hilden
Protein Assay Dye Reagent Concentrate (pre-diluted 1:5 in H_2O)	Bio-Rad Laboratories GmbH, Puchheim
Qiagen Gel Extraction Kit	Qiagen, Hilden
QIAmp Viral RNA Mini Kit	Qiagen, Hilden
QIAprep Spin Miniprep Kit	Qiagen, Hilden
SuperScript III Reverse Transcriptase (200 units/µl)	Thermo Fisher Scientific, Karlsruhe
T4 DNA ligase	Thermo Fisher Scientific, Karlsruhe
Taq DNA Polymerase (5 units/µl)	
Zero Blunt™ TOPO™ PCR cloning kit	Thermo Fisher Scientific, Karlsruhe

3.1.6 Bacteria

Bacteria	**Notes**	**Source**
OneShot TOP10 *E. coli*	Chemically competent *E.coli*	Thermo Fisher Scientific, Karlsruhe

3.1.7 Primer & Oligonucleotides

Oligonucleotide	**Sequence [5‘ → 3‘]**
Uni12 primer	AGCAAAAGCAGG
VSV-1S	AGCCTCTCGAACAACTAATATCC
pEGFP NS1-rev	GTCCAGCTCGACCAGGATG
MluI-NP fwd	TTCCTTACGCGTATGGCGTCCCAAGGCACCAAACGG
Eco91I-NP rev	TTCCTTGGTAACCTTAATTGTCGTACTCCTCTGCATTG
MluI-HA fwd	TTCCTTACGCGTATGAAGGCAATACTAGTAGTTCTGC
Eco91I-HA rev	TTCCTTGGTAACCTTAAATACATATTCTACACTGTAGA GACCC
MluI-M1 fwd	TTCCTTACGCGTATGAGTCTTCTAACCGAGGTCG
Eco91I-M1 rev	TTCCTTGGTAACCTCACTTGAATCGTTGCATCTG
MluI-M2 fwd:	TTCCTTACGCGTATGAGTCTTCTAACCGAGGTCGAAA CGCCTATCAGAAACGAATGGG
Eco91I-M2 rev	TTCCTTGGTAACCTTACTCCAGCTCTATGCTGACAAA
MluI-HA_{stem} generation fwd I	AAAAAAACGCGTAAAATGAAGACTATCATTGCTTTG AGCTA
HA_{stem} generation rev I	GACTTGCATCCACCACCTCCGCATATTTCACCTATTG AGGAATTCTGAAC
HA_{stem} generation fwd II	AAATATGCGGAGGTGGTGGATGCAAGTCTGAATGCA TCACTCCAAATGGA

Eco91I-HA_{stem} generation rev I	AAAAAAGGTAACCTCAAATGCAAATGTTGCACCTAATGT
Bm-HA-1 fwd	TATTCGTCTCAGGGAGCAAAAGCAGGGG
Bm-NP-1	TATTCGTCTCAGGGAGCAAAAGCAGGGTA
Bm-M-1	TATTCGTCTCAGGGAGCAAAAGCAGGTAG
Bm-NS-890R	ATATCGTCTCGTATTAGTAGAAACAAGGGTGTTTT
Bm-NP-1565R	ATATCGTCTCGTATTAGTAGAAACAAGGGTATTTTT
Bm-M1027R	ATATCGTCTCGTATTAGTAGAAACAAGGTAGTTTTT

3.1.8 Plasmids

Plasmid	**Description**	**Source**
pCRII-Influenza NP(Fluenz® Tetra)	pCR™-Blunt II-TOPO® plasmid with inserted IAV NP from cold-adapted A/Ann Arbor/6/1960 (H2N2)	This thesis
pCRII-Influenza M1(Fluenz® Tetra)	pCR™-Blunt II-TOPO® plasmid with inserted IAV M1 from cold-adapted A/Ann Arbor/6/1960 (H2N2)	This thesis
pCRII-Influenza M2(Fluenz® Tetra)	pCR™-Blunt II-TOPO® plasmid with inserted IAV M2 from cold-adapted A/Ann Arbor/6/1960 (H2N2)	This thesis
pCRII-Influenza HA(Fluenz® Tetra)	pCR™-Blunt II-TOPO® plasmid with inserted IAV HA from cold-adapted A/Hong Kong/4801/2014 (H3N2)-like	This thesis
pSpCas9n(cADAR1_B.1)-2A-GFP	Encoding for Cas9 nickase and guide RNA targeting *adar1* gene	Dr. Christian Pfaller, Paul-Ehrlich-Institute
pSpCas9n(cADAR1_B.2)-2A-GFP	Encoding for Cas9 nickase and guide RNA targeting *adar1* gene	Dr. Christian Pfaller, Paul-Ehrlich-Institute

pSpCas9n(cADAR1_D.1)-2A-GFP	Encoding for Cas9 nickase and guide RNA targeting *adar1* gene	Dr. Christian Pfaller, Paul-Ehrlich-Institute
pSpCas9n(cADAR1_D.2)-2A-GFP	Encoding for Cas9 nickase and guide RNA targeting *adar1* gene	Dr. Christian Pfaller, Paul-Ehrlich-Institute
pVSV*ΔG	Genomic plasmid pVSV*ΔG containing VSV-N, -P, -M, -L and eGFP transcription units (N-P-M-eGFP-L)	Dr. Gert Zimmer, IVI, Mittelhäusern
pVSV*ΔG(NP)	Genomic plasmid pVSV*ΔG containing VSV-N, -P, -M, -L and eGFP transcription units. An additional NP from IAV cold-adapted A/Ann Arbor/6/1960 (H2N2) was inserted (N-P-M-NP-eGFP-L)	this thesis
pVSV*ΔG(M1)	Genomic plasmid pVSV*ΔG containing VSV-N, -P, -M, -L and eGFP transcription units. An additional M1 from IAV cold-adapted A/Ann Arbor/6/1960 (H2N2) was inserted (N-P-M-M1-eGFP-L)	this thesis
pVSV*ΔG(M2)	Genomic plasmid pVSV*ΔG containing VSV-N, -P, -M, -L and eGFP transcription units. An additional M2 from IAV cold-adapted A/Ann Arbor/6/1960 (H2N2) was inserted (N-P-M-M2-eGFP-L)	this thesis
pVSV*ΔG($H3_{stem}$)	Genomic plasmid pVSV*ΔG containing VSV-N, -P, -M, -L and eGFP transcription units. An additional $H3_{stem}$ from IAV A/Hong Kong/4801/2014 (H3N2)-like was inserted (N-P-M-$H3_{stem}$-eGFP-L)	this thesis

pVSV*ΔG(HA PR8)	Genomic plasmid pVSV*ΔG containing VSV-N, -P, -M, -L and eGFP transcription units. An additional HA from IAV A/Puerto Rico/8/1934(H1N1) was inserted (N-P-M-HA-eGFP-L)	Dr. Gert Zimmer, IVI, Mittelhäusern
pVSV-N	Helper plasmid used for rescue of VSV replicons encoding for VSV-N	Dr. Gert Zimmer, IVI, Mittelhäusern
pVSV-P	Helper plasmid used for rescue of VSV replicons encoding for VSV-P	Dr. Gert Zimmer, IVI, Mittelhäusern
pVSV-L	Helper plasmid used for rescue of VSV replicons encoding for VSV-L	Dr. Gert Zimmer, IVI, Mittelhäusern

3.1.9 VSV Vectors

Vector	**Description**
VSV*ΔG	Vesicular stomatitis virus(VSV)-based replicon; VSV-G protein deleted, eGFP gene added
VSV*ΔG(NP)	VSV-based replicon; VSV-G protein deleted, eGFP and influenza A virus (IAV) NP from cold-adapted A/Ann Arbor/6/1960 (H2N2) added
VSV*ΔG(M1)	VSV-based replicon; VSV-G protein deleted, eGFP and IAV M1 from cold-adapted A/Ann Arbor/6/1960 (H2N2) added
VSV*ΔG(M2)	VSV-based replicon; VSV-G protein deleted, eGFP and IAV M2 from cold-adapted A/Ann Arbor/6/1960 (H2N2) added
VSV*ΔG($H3_{stem}$)	VSV-based replicon; VSV-G protein deleted, eGFP and IAV $H3_{stem}$ construct from A/Hong Kong/4801/2014 (H3N2)-like added
VSV*ΔG(HA PR8)	VSV-based replicon; VSV-G protein deleted, eGFP and IAV HA construct from A/Puerto Rico/8/1934(H1N1) added

3.1.10 Antibodies and Sera

Antibody	**Dilution (Application)**	**Source**
biotin rat α-mouse IFNγ	1:250 ($IFN\gamma^+$ ELISpot)	BD biosciences (clone: XMG1.2; #554410)
bovine α-goat IgG-HRP	1:20000 (WB)	Santa Cruz Biotechnology (sc-2384)

ferret α-IAV (H3N2 Victoria) serum	1:1000 (Immunofluorescence)	Paul-Ehrlich-Institute
ferret α-IAV (PR8) serum	1:500 (IPMA) 1:1000 (Immunofluorescence)	Paul-Ehrlich-Institute
goat α-biotin peroxidase conjugated	1:2000 (IFNγ$^+$ ELISpot)	Vector Laboratories (SP-30-20-1)
goat α-ferret IgG h+l HRP conjugated	1:750 (IPMA)	Bethyl Laboratories (A140-108P)
goat α-ferret IgG, IgA, IgM h+l TexasRed	1:1000 (Immunofluorescence)	Sigma-Aldrich (SAB3700804)
goat α-IAV serum	1:200 (WB)	Paul-Ehrlich-Institute
goat α-mouse IgG HRP conjugated	1:750 (IPMA + antibody titration) 1:20000 (WB)	Jackson Immunoresearch (115-035-003)
goat α-mouse IgG1 HRP conjugated	1:750 (antibody titration)	Jackson Immunoresearch (115-035-205)
goat α-mouse IgG2b HRP conjugated	1:750 (antibody titration)	Jackson Immunoresearch (115-035-207)
goat α-mouse IgG2c HRP conjugated	1:750 (antibody titration)	Jackson Immunoresearch (115-035-208)
goat α-mouse IgG3 HRP conjugated	1:750 (antibody titration)	Jackson Immunoresearch (115-035-209)
goat α-rabbit IgG Fc-HRP conjugated	1:20000 (WB)	Abcam plc.
mouse α-GAPDH	1:1000 (WB)	Cell Biolabs Inc. (AKR-001)
mouse α-IAV M1	1:1000 (WB)	Invitrogen (clone: GA2B; MA1-80736)
mouse α-IAV M2	1:1000 (WB)	Invitrogen (clone: 14C2; MA1-082)
mouse α-IAV NP	1:5000 (WB) 1:2000 (IPMA)	Invitrogen (MA5-29926)
rabbit α-ADAR1	1:1000 (WB)	Cell Signaling (D7E2M)
rabbit α-IAV (H1N1 HA)	1:1000 (WB)	Invitrogen (PA5-81670)
rabbit α-IRF3	1:1000 (WB)	Cell Signaling (D83B9)
rabbit α-pIRF3	1:1000 (WB)	Abcam (ab32036)
rabbit α-PKR	1:1000 (WB)	Cell Signaling (D7F7)
rabbit α-pPKR	1:1000 (WB)	Cell Signaling (D1I6C)

rabbit α-VSV serum	1:5000 (WB)	Prof. Dr. Conzelmann, Gene Center, Munich
rat α-mouse IFNγ	1:500 (IFNγ^{+} ELISpot)	BD biosciences (clone: R4-6A2; #551216)

3.1.11 Cell Lines

Cells	**Description**	**Source**
BHK-21	Baby hamster kidney cells	ATCC: CCL-10
BHK-G43	BHK-21 cells expressing VSV-G after mifepristone induction	(Kalhoro et al. 2009)
VeroE6	*Cercopithecus aethiops* kidney cells	ATCC: CRL-1586
MDCK	Madin-Darby Canine Kidney cells	ATCC: CCL-34
MDCK-ADAR1p150^{KO}	MDCK cells harboring a knock-out of the p150 isoform of the *adar1* gene	This thesis
MDCK-ADAR1^{KO}	MDCK cells harboring a knock-out of the *adar1* gene	This thesis
HeLa	Human epithelial cells originating from a cervical cancer	ATCC: CCL-2
HeLa-ADAR1p150^{KO}	HeLa cells harboring a knock-out of the p150 isoform of the *adar1* gene	(Pfaller et al. 2018)
HeLa-ADAR1^{KO}	HeLa cells harboring a knock-out of the *adar1* gene	(Pfaller et al. 2018)

3.1.12 Animals and Products of Animal Origin

Animal/Product	**Source**
C57BL/6J mice	Janvier Labs; Le Genest-Saint-Isle, France/Charles River; Wilmington, MA, USA
Turkey-erythrocytes	Paul-Ehrlich-Institute, Langen
Eleven days-old embryonated chicken eggs	Paul-Ehrlich-Institute, Langen

3.1.13 Viruses

Virus	**Source**
A/Puerto Rico/8/1934(H1N1)	Prof. Dr. Veronika von Messling,

	Paul-Ehrlich-Institute, Langen
Recombinant, mouse adapted rSC35M derived from A/Seal/Massachusetts/1/1980(H7N7)	(Scheiblauer et al. 1995) Provided by: Prof. Dr. Eva Friebertshäuser, Philipps-University, Marburg
Fluenz® Tetra 2016/2017 A/California/7/2009 (H1N1)pdm09-like (A/Bolivia/559/2013) A/Hong Kong/4801/2014 (H3N2)-like (A/New Caledonia/71/2014) B/Brisbane/60/2008-like (B/Brisbane/60/2008) B/Phuket/3073/2013-like (B/Phuket/3073/2013)	MedImmune, LLC, Nijmegen, Netherlands
MVA-T7	Prof. Dr. Gerd Sutter, Ludwig-Maximilians-University, Munich

3.1.14 Accession Numbers of Viruses Used For Amino Acid Homology Analysis

Viral protein	**Accession number**
A/Seal/Massachusetts/1-SC35M/1980(H7N7) HA	ABB90267.1
A/Seal/Massachusetts/1-SC35M/1980(H7N7) NP	ABB90269.1
A/Seal/Massachusetts/1-SC35M/1980(H7N7) M1	ABB90273.1
A/Seal/Massachusetts/1-SC35M/1980(H7N7) M2	ABB90274.1
A/HongKong/4801/2014(H3N2)-like (A/Massachusetts/3791/2014(H3N2)) HA	AIC73815.1
A/Puerto Rico/8/1934(H1N1) HA	ABO21709.1
A/Puerto Rico/8/1934(H1N1) NP	ABO21710.1
A/Puerto Rico/8/1934(H1N1) M1	ABO21712.1
A/Puerto Rico/8/1934(H1N1) M2	ABO21713.1
A/Ann Arbor/6/1960(H2N2) NP	AAA43451.1
A/Ann Arbor/6/1960(H2N2) M1	AAA43256.1
A/Ann Arbor/6/1960(H2N2) M2	AAA43255.1

3.1.15 Software

Software	**Source**

A.EL.VIS ELISPOT Analysis Software	stefan badur electronic GmbH & Co. KG, Hannover
AAT Bioquest LD_{50} calculator	AAT Bioquest Inc., Sunnyvale, CA
Adobe Illustrator 24.4.1	Adobe Inc., Mountain View, CA
BioRender	www.biorender.com (accessed 08.02.2022)
Clone Manager Professional 9	Sci-Ed Software, Westminster, CO
GenBank	NCBI
Genome Compiler	Genome Compiler Corporation, Los Altos, CA
GraphPad Prism 9 Version 9.2.0	GraphPad Software, Inc. La Jolla, CA
Image Lab 6.0.1	Bio-Rad Laboratories GmbH, Puchheim
Magellan V7.3	Tecan Group Ltd., Männedorf
MARS Data analysis software	BMG Labtech
NCBI Protein BLAST	NCBI
Nis-Elements 4.20.00 LO	Nikon GmbH, Düsseldorf
PHERAstar FSX software	BMG Labtech
Sequencher 5.3	Gene Code Corporation, Ann Arbor, MI
ZENblue 3.3	Carl Zeiss AG, Oberkochen

3.2 METHODS

3.2.1 Molecular Biology Methods

3.2.1.1 Viral RNA-Isolation

For isolation of viral RNA from the Fluenz® Tetra vaccine, the QIAamp Viral RNA Mini Kit was used. All steps were performed following the manufacturer's instructions. In brief, one full dose (200 µl) of Fluenz® Tetra vaccine was mixed with 800 µl buffer AVL containing 8 µl carrier-RNA and viral RNA was isolated, washed on QIAamp Mini columns and eluted in 40 µl of buffer AVE.

3.2.1.2 Reverse Transcription

For reverse transcription of viral RNA into cDNA, 4 µl of RNA were mixed with 1 µl of 25 mM Uni12 primers (Hoffmann et al. 2001), 1 µl of 10 mM dNTP Mix, and 4 µl H_2O. After incubation for 5 min at 65°C, the mixture was put at 4°C for 1 min and 4 µl 5X First Strand Buffer, 1 µl 0.1 M DTT, 1 µl RNase OUT and 1 µl SuperScript III (200 units/µl) were added. The reaction was incubated sequentially for 5 min at 25°C, 60 min at 50°C and 15 min at 70°C. cDNA was either frozen until further use at -20°C or directly subjected to polymerase-chain-reaction.

3.2.1.3 Polymerase-Chain-Reaction (PCR)

PfuUltra II Fusion High-Fidelity polymerase was used to specifically amplify the respective influenza genes of interest. Therefore, the following reagents were mixed.

Table 2: Segment-specific PCR reagents for IAV cDNA amplification

Reagent	*Volume*
PfuUltra II Fusion High-Fidelity DNA Polymerase	1 µl
10X PfU Ultra II Buffer	5 µl
dNTPs (10 mM)	1.25 µl
cDNA	1 µl
Primer sense (10 mM)	1 µl
Primer antisense (10 mM)	1 µl
H_2O	39.75 µl

PCR was performed using the following temperature-cycle program. In the initial denaturation step, cDNA strands were detached, so that the specific sense and antisense primer could bind to the DNA during the annealing phase. In the elongation step, the DNA polymerase Pfu Ultra II can build a complementary strand

using the dNTPs thereby completing the dsDNA, which is then in the next cycle denatured and amplified again.

Table 3: PCR program for segment-specific IAV cDNA amplification

Step	*Temperature*	*Time*	
Initial Denaturation	98°C	1 min	
Denaturation	98°C	10 sec	30x
Annealing	55°C	20 sec	
Elongation	72°C	4 min	
Final Elongation	72°C	10 min	
Cooldown	4°C	infinite	

PCR samples were either directly used for gel electrophoresis or stored at -20°C until further use.

To generate restriction enzyme sites for the directed ligation of the influenza genes into the VSV-plasmid, a PCR was performed as described above. Specific primers containing the restriction enzyme sites of either MluI or Eco91I were used. After PCR, the DNA product was purified from remaining buffer and enzymes using reagents from the NucleoSpin Gel and PCR clean-up Kit and eluted in 30 µl elution buffer.

3.2.1.4 Agarose Gel Electrophoresis

To purify the PCR fragments of the respective influenza genes, agarose gel electrophoresis was performed and respective DNA fragments were extracted from the gel. For this, 1 g agarose was diluted in 100 ml 1X TRIS-acetate-EDTA (TAE)-buffer) and supplemented with 10 µl of GelRed (1:10,000). PCR samples and 1kb DNA ladder were prepared by adding 1 µl of 6X Loading Dye to 5 µl of the sample or 5 µl of 1 kb DNA ladder diluted 1:4 with H_2O, respectively. Gel electrophoresis was run at 120 V for 30-60 min and results were visualized using an UV-illuminator. Bands with the size of the fragment of interest were cut out and DNA was extracted using the QIAquick Gel Extraction Kit following the manufacturer's instructions. DNA was eluted in 30 µl of elution buffer. Concentration of purified PCR products was measured using the NanoDrop 2000c spectrophotometer and subsequently used for TOPO cloning.

3.2.1.5 TOPO Cloning

For TOPO Cloning of the different IAV gene segments, the Zero Blunt TOPO PCR Cloning Kit was used. 2 µl of PCR product were mixed with 4 µl of H_2O, 1 µl of manufacturer's salt solution and 1 µl TOPO vector. The cloning reaction was then incubated for 5 min at room temperature. The generated TOPO plasmid containing IAV ORFs (pCRII-Influenza X(Fluenz® Tetra)) were then amplified in *E. coli*.

3.2.1.6 Plasmid Transformation

45 µl of chemically-competent OneShot TOP10 *E. coli* were thawed on ice and 1 µl of respective TOPO plasmid-DNA was added. After an incubation period of 20 min on ice, bacteria were heat-shocked for 30 sec at 42°C using a water bath and immediately transferred on ice. 250 µl S.O.C. medium was added and the bacteria were incubated on a shaker at 37°C for 1 h with 200 rpm. 100 µl of bacterial solution were equally distributed on a pre-warmed selective plate containing 100 µg/ml Ampicillin or Kanamycin. The plates were then incubated overnight at 37°C in a bacteria incubator.

The next day, 5 ml of Lysogeny broth (LB) medium containing 100 µg/ml Ampicillin or Kanamycin was prepared in a bacteria culture flask and a picked colony from the selective plate was added. Bacterial grow flasks were put in an incubator (innova 42) at 37°C and 200 rpm overnight. Alternatively, to obtain more plasmid-DNA, 100 ml of LB medium with 100 µg/ml Ampicillin or Kanamycin were filled in a 500 ml conical flask and incubated at 37°C and 200 rpm overnight.

3.2.1.7 Plasmid Preparation

For preparation of the plasmid-DNA from the 5 ml bacteria culture, the QIAprep Spin Miniprep Kit was used and all steps were performed following the manufacturer's instructions. Plasmid-DNA was eluted in 30 µl elution buffer.

For preparation of the plasmid-DNA from the 100 ml bacteria culture, the Plasmid Midi Kit was used. Eluted plasmid-DNA was then further purified by adding 3.5 ml Isopropanol and centrifugation at 12,000 rpm for 30 min at 4°C (Avanti J-26 XPI; Beckman Coulter; JA-25.50 rotor) was performed. The isopropanol was discarded and 2 ml of 70% ethanol were added. After centrifugation at 12,000 rpm for 10 min

at 4°C, ethanol was discarded, the pellet was dried and the plasmid-DNA dissolved in 250 µl elution buffer.

Concentration of plasmid preparations was measured using the NanoDrop 2000c spectrophotometer.

3.2.1.8 DNA Sequencing

5 µl of plasmid-DNA samples were mixed with 5 µl of the respective sequencing primer (10 mM) and sent to GATC Biotech AG for sequencing. Retrieved sequence files were aligned against the target sequences and analyzed using Sequencher 5.3 and Genome Compiler software.

3.2.1.9 $H3_{stem}$ Generation

To obtain the stem region of influenza hemagglutinin protein, the head domain was replaced by four glycines using a two-step PCR. Firstly, the two different regions flanking the head domain were amplified by mixing the following PCR reactions:

Table 4: PCR regents for HA_{stem} generation

Reagent	*Volume*	
	region I	*region II*
Phusion Hot Start II High-Fidelity DNA Polymerase	0.5 µl	0.5 µl
5X Phusion Buffer	10 µl	10 µl
dNTPs (10 mM)	1 µl	1 µl
DNA	2 µl	2 µl
Primer sense (20 µM)	1.25 µl (Sense Primer I (MluI))	1.25 µl (Sense Primer II)
Primer antisense (20 µM)	1.25 µl (Antisense Primer I)	1.25 µl (Antisense Primer (Eco91I)
H_2O	34 µl	34 µl

The PCR was run with the following conditions:

Table 5: PCR program for HA_{stem} generation

Step	*Temperature*	*Time*	
Initial Denaturation	98°C	1 min	
Denaturation	98°C	10 sec	20x
Annealing	50°C	20 sec	
Elongation	72°C	2 min	
Final Elongation	72°C	10 min	
Cooldown	4°C	infinite	

The PCR products of the two regions were purified via an agarose gel electrophoresis (3.2.1.4) and were subsequently joined using a second PCR. For this, the two DNA fragments were mixed equimolarly as outlined in Table 6 and after two initial annealing cycles, 1.25 µl of Sense Primer I (MluI) and Antisense Primer II (Eco91I) were added. The PCR was then performed as described in Table 5.

Table 6: PCR reagents for HA_{stem} joining PCR

Reagent	*Volume*
Phusion Hot Start II High-Fidelity DNA Polymerase	1 µl
5X Phusion Buffer	10 µl
dNTPs (10 mM)	1 µl
DNA (region I)	1 µl
DNA (region II)	2 µl
H_2O	33 µl

3.2.1.10 DNA Restriction and Vector Dephosphorylation

For DNA restriction of the PCR products, 1 µl of both restriction enzymes FastDigest MluI and FastDigest Eco91I, 5 µl 10X FastDigest Buffer and 33 µl H_2O were added to 10 µl of the DNA and incubated at 37°C overnight in the incubator.

The VSV*ΔG-plasmid, kindly provided by Dr. Gert Zimmer (IVI, Mittelhäusern, Switzerland), was digested by using 4 µl of plasmid DNA, 1 µl of both restriction enzymes FastDigest MluI and FastDigest Eco91I, respectively, 5 µl 10X FastDigest Buffer and 39 µl H_2O. Restriction reaction was performed for overnight at 37°C in the incubator.

For purification of digested PCR products and the VSV*ΔG-plasmid, 1% agarose gels were casted in 1X TBE-buffer and ethidium bromide (1:20,000; 10 mg/ml stock) was added. Bands with the correct band size were cut out and DNA was extracted using the NucleoSpin Gel and PCR clean-up Kit. DNA was eluted in 30 µl elution buffer.

After gel extraction, the vector was dephosphorylated to avoid self-religation in the following ligation step. To achieve this, 1 µl of FastAP, 4 µl of 10X FastAP-buffer and 5 µl H_2O were added to the extracted VSV*ΔG-plasmid. After an incubation period of 1 h at 37°C, PCR clean-up was performed using the NucleoSpin Gel and PCR clean-up Kit.

3.2.1.11 Ligation of DNA

In order to ligate the gene of interest into the VSV*ΔG-plasmid, both DNA fragments were added in a ration insert:vector 5:1. Overall, 5 µl vector and 1 µl T4 DNA ligase were used, and the appropriate volume of insert and H_2O was added to obtain a total reaction volume of 20 µl. Ligated plasmid was transformed as described in 3.2.1.6 and colonies on the agar were used for colony PCR.

3.2.1.12 Colony PCR

Using a colony PCR, five clones of each ligation reaction were screened. For this, a primer pair flanking the vector's insertion region is used. If the size of the product matches the size of the added insert, the ligation may have been successful and the respective colony of bacteria can be grown for plasmid stock production. The colony PCRs were prepared as described in the following table:

Table 7: Colony PCR reagents

Reagent	*Volume*
TaqPol (5U/µl)	0.1 µl
10X Taq PCR-Puffer with KCl	2 µl
dNTPs (10 mM)	0.4 µl
$MgCl_2$ (25 mM)	1.2 µl
Primer sense (20 µM) VSV-1S	0.4 µl
Primer antisense (20 µM) pEGFP NS1-rev	0.4 µl
H_2O	15.5 µl

A 10-100 µl pipet-tip was used to transfer bacteria from the plate into the reaction mix. The rest of the colony was then suspended in 250 µl LB medium (0,1% Ampicillin) and stored in the fridge for further cultivation if the colony PCR shows correct results.

Table 8: Colony PCR program

Step	*Temperature*	*Time*	
Initial Denaturation	95°C	1 min	
Denaturation	95°C	15 sec	20x
Annealing	55°C	30 sec	
Elongation	72°C	1 min 30 sec	
Final Elongation	72°C	5 min	
Cooldown	4°C	infinite	

PCR fragments were controlled using an agarose gel electrophoresis (3.2.1.4) and positive clones were transformed (3.2.1.6) and prepared for sequencing (3.2.1.7).

3.2.1.13 Sequencing

Sequencing of the clones were performed using the BigDye V3.1 Cycle Sequencing Kit. 2 µl DNA and 2 µM of the respective primer (either VSV-1S or pEGFP NS1-rev) were mixed with 1 µl AB-buffer, 2 µl termin rxn 2.5x and 3.4 µl H_2O. The sequencing reactions were performed as follows:

Table 9: Sequencing PCR program

Step	*Temperature*	*Time*	
Initial Denaturation	96°C	1 min	
Denaturation	96°C	10 sec	25x
Annealing	50°C	5 sec	
Elongation	60°C	4 min	
Cooldown	4°C	infinite	

PCR constructs were subsequently purified using the NucleoSeq Column Kit following the manufacturer's instructions. 10 µl of the purified product were mixed with 10 µl HIDI Formamid and analyzed via the ABI Prism 3100 Genetic Analyzer.

3.2.2 Cell Culture and Virological Methods

3.2.2.1 Cell Culture

Madin-Darby Canine Kidney (MDCK) cells were maintained in Dulbecco's modified Eagle medium (DMEM) with 5% fetal bovine serum (FBS) and 200 mM L-glutamine. Baby Hamster Kidney cells (BHK-21) (German Collection of Microorganisms and Cell Culture Braunschweig) were cultivated in Eagle's Minimal Essential Medium (MEM) with 10% FBS and 200 mM L-glutamine. BHK-G43 cells, which are BHK-21 cells inducibly expressing the VSV-G protein, were handled equally. Additionally, 0.5 mg/ml Zeocin and 125 µg/ml Hygromycin B were added every third to fourth passage. HeLa cells were maintained in DMEM with 10% FBS, 200 mM L-glutamine and 1% penicillin/streptomycin. All cells were grown in a humidified incubator at 37°C and 5% CO_2.

For passaging cells, medium was removed and the cells were washed with 10 ml of phosphate-buffered saline (PBS) to remove residual FBS and dead cells. 3 ml of trypsin/EDTA were added and cells were incubated at 37°C until fully detached and re-suspended in pre-warmed cell culture medium. Cells were then either seeded in cell culture dishes for further use or split accordingly.

For seeding cells, 10 µl of singe-cell suspension were mixed 1:10 with trypan blue solution. 10 µl of this dilution were pipetted into a Neubauer chamber and counted using a light microscope (Nikon Eclipse TS100-F). The following formula was used to determine the cell numbers:

$$concentration\ \left[\frac{cells}{ml}\right] = \frac{total\ number\ of\ cells}{4} \times \frac{10^4}{ml} \times 10\ (dilution\ factor)$$

Intended cell concentration was reached by adding the respective growth medium and cells were then seeded in the cell culture dish.

3.2.2.2 Knock-out of ADAR1 in MDCK Cells Using CRISPR

$5x10^5$ MDCK cells were seeded in 6-well plates to reach 90% confluence. The following day, 6 µl of Lipofectamine 3000 were diluted in 200 µl Opti-MEM per well, respectively. In parallel, 4 µg of pSpCas9n plasmid (2 µg for each gRNAs) were mixed in 200 µl Opti-MEM and supplemented with 8 µl P3000. The Lipofectamine 3000 mix was then added to the DNA solution, incubated for 30 min at room temperature, transferred to the cells and incubated for 2 days at 37°C.

GFP-activated cell sorting was performed to enrich for transfected cells. For this, cells were detached using trypsin/EDTA, harvested and re-suspended in FACS buffer (PBS + 5 mM EDTA) with 2% FBS and 1% penicillin/streptomycin on ice. Directly prior sorting, cells were filtered through strainer caps of FACS tubes to prevent cell clumping. GFP^+ cells were sorted using the BD FACSAria Fusion with 70 µm nozzle purity mode into pre-cooled 1.5 Eppendorf tubes containing DMEM (5% FBS, 200 mM L-glutamine, 2% penicillin/streptomycin). Positively sorted cells were subsequently subjected to post-sorting analysis to confirm successful cell-sorting process, seeded in 6-well plates in 2 ml DMEM (5% FBS, 200 mM L-glutamine) and incubated until reaching confluence. As soon as cells grew to a contiguous monolayer, they were trypsinized using trypsin/EDTA and a 1:4 dilution row in cell growth medium was performed in a 96-well plate to obtain single-cell solutions. Cells were then incubated at 37°C and observed daily for presence of a single, living cell. Cell clones from positive wells were transferred to a 24-well plate and incubated at 37°C until reaching confluence. Subsequently they were grown in a 6-well plate, to establish a cell stock, and a 12-well plate for confirmation of ADAR1 knock-out via immunoblot analysis as described in 3.2.4.1 and 3.2.4.3.

3.2.2.3 Freezing and Thawing of Cells

Cells were detached using trypsin/EDTA and cell culture medium was added. Cells were either centrifuged at 300 g for 10 min at 4°C, medium was discarded and FBS added or directly transferred into a 50 ml falcon tube on ice and gently swirled while adding Dimethyl sulfoxide (DMSO) to reach a final concentration of 8%. Cell suspension was aliquoted in cryo tubes and frozen at -80°C in a Mr. Frosty Freezing Container filled with isopropanol. After 24 hours, aliquots were transferred to -150°C for long-term storage. To thaw cells, cryo tubes were put in a pre-warmed water bath (37°C) until completely thawed and cells were transferred into a T25 cell culture flask containing pre-warmed cell culture medium and incubated at 37°C and 5% CO_2.

3.2.2.4 Cell Growth and Survival of MDCK Cell Lines

To test for differences in cell growth, triplicates of MDCK wildtype, MDCK-ADAR1p150^{KO} and MDCK-ADAR1^{KO} cells were seeded sub-confluently in 96-well plates in DMEM without phenol red, supplemented with 5% FBS, 200 mM L-glutamine, 1% penicillin/streptomycin and cell number was quantified at different time points using the CellTiter 96 Non-Radioactive Cell Proliferation Assay following manufacturer's instructions. In brief, 15 µl of dye solution were added to each well and incubated for 4 h at room temperature or at 37°C to allow formazan crystal formation. Subsequently, 100 µl of solubilization/stop mix were added and plates were incubated at room temperature in a wet chamber overnight. The next day, all wells were mixed using a multichannel pipette and absorbance was read out at 570 nm using 700 nm as a reference in the Tecan SUNRISE microplate absorbance reader.

To test if the used cell lines show differences in survival, they were seeded in triplicates in 96-well plates and 24 hours later medium was changed to DMEM without phenol red supplemented with 1% Sodium-Pyruvat and Tolyl-sulfonyl phenylalanyl chloromethyl ketone-treated trypsin (TPCK-trypsin) with a concentration of 0.75 µg/ml. To test survival under IAV infection, additionally virus with an MOI=0.01 - 5 was added. To measure the amount of living cells at the time of medium change or infection and after 24, 48, and 72 hours, the above-mentioned MTT-based assay protocol was performed.

3.2.2.5 Virus Stock Production

Mouse-adapted influenza virus A/Puerto Rico/8/1934(H1N1) (PR8) and recombinant mouse-adapted A/Seal/Massachusetts/1-SC35M/1980(H7N7) (rSC35M) were grown in eleven days old embryonated chicken eggs. For this, virus was inoculated into the allantoic fluid and incubated for 1-2 days at 37°C and 60% humidity in an egg incubator. Allantoic fluid was harvested and centrifuged for 2000 rpm at 4°C for 5 min. Hemagglutination titers of the supernatant were determined as follows: Supernatants were two-fold diluted in a V-shaped 96-well plate and 50 µl of 1% turkey-erythrocyte-suspension was added. After 30 min at 4°C, hemagglutination titers were determined according to standard protocols (WHO manual on animal influenza diagnosis and surveillance 2002) and supernatants with comparable titers where pooled. Stocks were aliquoted and frozen at -80°C until further use.

For cell culture-grown virus stocks, MDCK cells were infected with either PR8 or rSC35M in serum-free DMEM, for PR8 additionally supplemented with TPCK-trypsin. Cells were observed daily and supernatant was cleared from cell debris by centrifugation at 3.000 g for 15 min at 4°C as soon as cytopathic effect was widespread. Virus stocks were stored at -80°C until further use.

3.2.2.6 Virus Titration

For titration of virus, $2x10^6$ MDCK cells were seeded in a flat-bottom 96-well plate and incubated for one day at 37°C. After incubation, 10-fold dilutions of virus in DMEM (5% FBS, 200 mM L-glutamine) were added in quadruplicates and incubated for additional two days at 37°C. Plates were washed with 1:3 PBS: double-distilled H_2O (ddH_2O) and air-dried for 20 minutes prior to heat fixation at 65°C for 8 hours. Plates were then incubated with 50 µl of ferret anti-PR8 serum at a dilution of 1:500 or mouse anti-Influenza NP of 1:2000 in PBS for 2 hours at room temperature. Plates were washed for 20 min with 100 µl PBS and subsequently incubated with either goat anti-ferret IgG-h+l horseradish peroxidase (HRP)-conjugated antibody (1:750) or goat anti-mouse HRP-conjugated antibody (1: 750) for 1 hour. After incubation, plates were again washed for 20 min with PBS and 3-amino-9-ethyl-carbazol (AEC) substrate diluted in N,N-Dimethylformamide (DMF) was added. Positive wells were visualized by red staining of infected cells and expressed as the 50% tissue culture infectious dose per milliliter ($TCID_{50}$/ml). For

calculation of the $TCID_{50}$, the following formula was used (Spearman 1908; Kärber 1931).

$$\log(TCID_{50}) = -(x_0 - \frac{d}{2} + d \times (1 + \sum \frac{r_i}{n_i})$$

$x_0 = reciprocal\ of\ the\ decadic\ logarithm\ of\ the\ highest\ dilution\ in\ which\ all\ wells\ show\ a\ CPE$

$d = decadic\ logarithm\ of\ the\ dilution\ factor$

$r_i = amount\ of\ wells\ showing\ a\ CPE\ in\ higher\ dilutions\ than\ x_k\ (out\ of\ n_i)$

$n_i = amount\ of\ wells\ \ in\ higher\ dilutions\ than\ x_k$

3.2.2.7 Influenza A Virus Infection

To analyze the effect of ADAR1 on viral replication in MDCK cells, the different cell lines were seeded in 6-well plates to reach 90% confluence. The following day, cell medium was discarded, cells were washed with DMEM and MOI=0.01 of PR8 virus was added in DMEM supplemented with TPCK-trypsin. 24 and 48 hours post-infection, supernatant was harvested and frozen in cryotubes until titration (3.2.2.6).

To investigate the effect of ADAR1 on IAV replication in HeLa cells, HeLa wildtype, HeLa-ADAR1p150^{KO}, and HeLa-ADAR1^{KO} cells from previous studies were used (Pfaller et al. 2018). Cells were seeded in 6-well plates and the next day were washed with PBS. Subsequently, MOI=1 of rSC35M in 500 µl of DMEM was added for 1 h at 37°C to allow attachment of the virus particles to the cell. After incubation, infectious medium was discarded and substituted with fresh DMEM medium. After 24 hours, cells were scraped off using a blue pipette tip and centrifuged for 5 min at 350 g and 4°C. Supernatant was discarded and cells were lysed and subjected to SDS-PAGE and immunoblot analysis as described in 3.2.4.1 and 3.2.4.3, respectively.

3.2.2.8 VSV Replicon Generation

Respective plasmids encoding for VSV*ΔG including the transgene (VSV*ΔG(X)) were handed over to Dr. Gert Zimmer (IVI, Mittelhäusern) to generate VSV*ΔG(X) replicons as described in (Berger Rentsch and Zimmer 2011).

3.2.2.9 VSV Replicon Production and Purification

To produce purified VSV replicon stocks, BHK-G43 cells were seeded in a T175 flask and incubated at 37°C for two days. After incubation, the medium was discarded and

fresh cell culture medium containing 10^{-9} M mifepristone was added to induce VSV-G protein expression. Six hours after medium change, cells were infected with the respective VSV*ΔG(X) replicon and incubated at 37°C overnight. The supernatant was centrifuged at 1000 g for 15 min at 4°C the next day and purified trough a 20% sucrose cushion using high-speed centrifugation (100.000 g, 1 h, 4°C) (Avanti Centrifuge; SW32 Ti rotor). The pellet was re-suspended in PBS, aliquoted and stored at -80°C.

3.2.2.10 VSV Replicon Titration

To titrate VSV*ΔG(X) replicons, $2x10^4$ BHK-21 cells were seeded in a 96-well plate and incubated at 37°C overnight. The next day, cells were infected with 40 µl of 10-fold dilutions of the VSV*ΔG(X) replicons in duplicates and 60 µl of fresh MEM were added after 90 min. After 12 h at 37°C, GFP-expressing cells in the last well showing appropriate GFP^+ cell numbers were counted using a fluorescence microscope (Nikon Eclipse T*i*-S), titer was calculated using the following formula and expressed as fluorescence forming units (ffu) per milliliter:

$$\frac{ffu}{ml} = GFP^+ \, cells \times dilution \, factor \times 25$$

3.2.2.11 VSV Replicon Transduction of BHK-21 Cells

To transduce BHK-21 cells with the different VSV replicons, cells were seeded and incubated at 37°C to reach 90% confluence the next day. Medium was then substituted with not-supplemented, or 10^{-9} M mifepristone-supplemented, MEM and VSV replicons were added after an incubation time of 6 h. The next day, cells were either lysed and subjected to SDS-PAGE and immunoblot analysis as described in 3.2.4.1 and 3.2.4.3, respectively, or the Nikon Eclipse T*i*-S light microscope was used to take pictures of the cell monolayer and GFP expression. For confirmation of the single-round character, 5 µl of supernatant were transferred to a fresh, untreated monolayer of BHK-G43 cells and incubated at 37°C and 5% CO_2 for another 24 hours. The following day, pictures were taken as described above.

3.2.3 Animal Experiments

All animal experiments were conducted in compliance with the German animal protection laws and authorized by the responsible state authority (approval number F 107/1058).

3.2.3.1 Immunization

Six- to eight-weeks-old female C57BL/6J mice (Janvier Labs; Le Genest-Saint-Isle, France/Charles River; Wilmington, MA, USA) were immunized intramuscularly with a total of $1.0x10^6$ fluorescence-forming units (ffu) of the respective VSV replicons (or mixtures) diluted in 30 µl sterile PBS. After four weeks, animals were immunized using the same dose as a booster vaccination. To confirm injected VSV replicon doses, first doses of a new stock of replicons were back-titrated as described in 3.2.2.10. All back-titrations confirmed intended doses.

3.2.3.2 Infection

Animals were weighed to determine initial weight. All mice were anesthetized by intraperitoneal injection of ketamine (100 mg/kg body weight) and xylazine (5 mg/kg body weight) and inoculated with $6.0x10^2$ $TCID_{50}$ of PR8 or $1.2x10^3$ $TCID_{50}$ of rSC35M in 30 µl PBS intranasally, respectively. To confirm correct IAV infection, first doses of a new stock of virus were back-titrated as described in 3.2.2.6. All back-titrations confirmed intended doses. During the following 14 days, animals were monitored daily by measuring body weight and evaluation of clinical signs of infection (Table 10) (Ullman-Culleré and Foltz 1999).

Table 10: Score sheet for evaluating IAV disease in mice

Score	0	1	2	3	4
Weight loss	<5%	5-15%	15-20%	20-25%	>25% (humane endpoint)
Behavior	Normal activity, normal eating behavior, no problems at climbing	Reduced activity, slightly decreased eating behavior, no problems at climbing	Low activity, decreased eating behavior, slightly impaired at climbing	Freezing in place, hardly reacting to external stimuli, highly decreased eating behavior, problems at climbing (humane endpoint)	Not defined
Appearance	Robust appearance, groomed fur	Robust appearance, shineless fur	Gaunt appearance, fuzzy or scruffy fur	Emaciated, scruffy fur, kyphotic (humane endpoint)	Not defined

As soon as pre-defined humane endpoints were reached, mice were euthanized using ketamine (100 mg/kg body weight) and xylazine (10 mg/kg body weight) anesthesia and exsanguination through cardiac puncture. Humane endpoints were defined as a score of three in one category of either behavior or appearance, a score of four in the category weight loss, or alternatively the sum of all categories reaching ten or higher.

3.2.3.3 Serum Preparation

Serum was purified from whole blood collected through cardiac puncture at euthanasia. For this, blood was filled into a 1.1 ml Z-Clot Serum Tube, centrifuged for 10 min at 14,000 g and 4°C and purified serum was transferred into 1.5 ml Eppendorf tubes. Aliquots of serum were frozen at -20°C until further analysis.

3.2.3.4 Splenocyte Preparation

Spleens were dissected from euthanized mice and stored in PBS in ice. To isolate single cells, spleens were transferred onto a 70 µm cell strainer and pushed through using a syringe plunger. The cell strainer was flushed with sterile PBS and cells pelleted by centrifugation for 8 min at 300 g and 4°C. After discarding the supernatant, cells were re-suspended in 5 ml Red Blood Cell lysis buffer (RBC lysis buffer) and incubated for 5 min at room temperature to allow lysis of erythrocytes. 25 ml of PBS were added to neutralize RBC lysis buffer followed by centrifugation for 10 min at 300 g and 4°C. The supernatant was discarded and cells resuspended in PBS or RPMI for further use in IFNγ$^+$ ELISpot and IL-4 ELISA assays (3.2.4.5 and 3.2.4.6).

3.2.4 Immunological Methods

3.2.4.1 Immunofluorescence Analysis

$3x10^4$ VeroE6 cells were seeded in microscopic slide chambers and incubated for 24 hours. The next day, cells were transduced in MEM with either VSV*ΔG, VSV*ΔG($H3_{stem}$), or VSV*ΔG(HA PR8) at an MOI=1 for 12 hours. After washing with PBS, cells were fixed with fixation buffer (3% paraformaldehyde in PBS) for 20 minutes, quenched (50 mM NH_4Cl in PBS) for 10 minutes and permeabilized in 0.5% Triton X-100 for 5 minutes. To block unspecific binding, 2.5% milk powder (w/v) with 0.1% Triton X-100 in PBS were added and incubated for 20 minutes on the shaker. Cells were washed with PBS and stained with 1:1000 dilution of ferret α-

H1N1 or ferret α-H3N2 serum in 0.1% Triton X-100 in PBS for 2 hours in the dark. Subsequently, cells were washed again and secondary antibody dilution (goat α-ferret TxRed-conjugated; 1:1000 in 0.1% Triton X-100/PBS) was added for 1.5 hours in the dark. Cells were washed three times with PBS and stained with DAPI (100 ng/ml in water) to visualize cell nuclei. Finally, cells were washed three times with water, mounted in ProLong Diamond Antifade Mountant, covered with a 24x32 mm cover slip, and stored in the dark at 4°C. Pictures were taken at the Axio Observer.Z1 and analyzed using the ZENblue 3.3 software.

3.2.4.2 Sodium Dodecyl Sulfate-Polyacrylamide Gel Electrophoresis (SDS-PAGE)

For lysing cells, protein lysis buffer (3.1.2) was used. For this, cells were washed once with PBS and 100 µl of freshly prepared, cold lysis buffer was added on dry cell monolayer. Cells were scraped off, transferred into a fresh 1.5 ml Eppendorf tube, and incubated on ice for 15 min. Afterwards, lysates were clarified from cell debris by centrifugation at 4°C and 14.000 g for 30 min and supernatant was stored at -20°C. Protein content was determined using the Protein Assay Dye Reagent Concentrate in a 1:5 dilution at the NanoDrop 2000c spectrophotometer. 15-25 µg protein sample were mixed with 15 µl 2X Urea sample buffer (3.1.2) containing 5% β-mercapthoethanol and the total volume was adjusted to 30 µl with protein lysis buffer. To fully denature proteins, samples were heated to 95°C for 5 min before loading onto a SDS-PAGE.

To obtain SDS gels, the preparation for the 10-12% running gel solution (3.1.2) was mixed in a 15 ml falcon tube and approximately 8 ml were filled between the glass plates. To obtain a plain surface on the gel, 500 µl isopropanol were added carefully and running gel was polymerized for 45 min. After incubation, isopropanol was discarded and approximately 3 ml of stacking gel solution (3.1.2) were added on top, in which a comb was inserted to form out gel pockets. The stacking gel solution was polymerized for 20 minutes.

Proteins were separated by SDS-PAGE with 10-12% running- and 4% stacking gel (1.5 mm thick) for 60-90 min at 120 V in the Bio-Rad Mini-PROTEAN Tetra Gel Chamber system following manufacturer's instructions.

3.2.4.3 Immunoblot Analysis

After the run, gel was placed in pure water and transferred to transfer buffer for 10 min on the shaker. The polyvinylidendifluorid (PVDF)-membrane was activated in pure methanol and together with Whatman paper incubated on a shaker in transfer buffer. The TransBlot Turbo system was used to transfer the proteins from the SDS-PAGE onto the PVDF-membrane by applying 12 V for 30 min. For this, two layers of Whatman paper were placed in the transfer cassette and the PVDF-membrane was added on top. Then the gel was placed upon, followed by two more layer of Whatman paper. After transfer, unspecific binding of primary antibodies was prevented by incubation of the PVDF-membrane with 5% bovine serum albumin (BSA) in PBS for 1 h at room temperature (5% blocking buffer). Primary antibody incubation was performed over night at 4°C on a shaker with antibodies diluted 1:200-1:1000 in Tris-buffered saline (TBS) with 0.05% Tween20 and 2.5%. The next day, PVDF-membranes were washed three times with 10 ml of TBS with 0.1% Tween20 (TBS-T) for 5 min each and subsequently incubated for 1 h at room temperature with the respective secondary antibody at a dilution of 1:10.000-20.000 in TBS-T. Finally, the membrane was washed again three times with TBS-T as described above, dapped onto paper tissue and 2 ml of ECL Western Blot substrate were added on top of the membrane. For visualization, the ChemiDoc Imaging System was used.

3.2.4.4 Antibody Titration

3.2.4.4.1 Total IgG and IgG subclass Antibody Titration

For titration of total IgG or IgG antibody subclasses in mouse serum, $2x10^6$ MDCK cells were seeded in a 96-well plate and incubated overnight at 37°C. The next day, cells were infected with 10^2 $TCID_{50}$ of either PR8 or rSC35M and further incubated for two days. Plates were washed with 1:3 PBS: double-distilled H_2O (ddH_2O) and air-dried for 20 minutes prior to heat fixation at 65°C for 8 hours. The next day, serum to be tested was 2-fold diluted in PBS (starting at 1:50 dilution) using a U-bottom 96-well plate and transferred in duplicates onto the cell monolayer for 2 hours at room temperature. After a 20 min washing step with 100 µl PBS, 50 µl of secondary goat α-mouse HRP conjugated antibody (1:750), specific for all murine IgG or the respective subclasses, was added for 1 h. Finally, cells were washed again for 20 min in 100 µl PBS and positive reactivity of serum antibodies against PR8 or rSC35M was

visualized as described in 3.2.2.6. The last dilution showing positive wells was considered positive and expressed as the reciprocal of the dilution factor [1/X].

3.2.4.4.2 Virus-Neutralizing Antibody Titration

For virus-neutralizing antibody titration, 50 µl of 2-fold dilutions (starting with 1:10 dilution) of serum were prepared in DMEM (5% FBS, 200 mM L-glutamine) and co-incubated with 10^2 $TCID_{50}$ of either PR8 or rSC35M virus in 50 µl for 20 min at room temperature. Furthermore, a back-titration of virus was performed ranging from 10^3-10^{-1} $TCID_{50}$/ml to confirm intended viral dose through serial dilutions. In parallel, MDCK cells were trypsinized and adjusted to $2x10^6$ cells/plate. After incubation time, 50 µl of cell suspension were added to all wells and plates were stored in the incubator for 3 days. To visualize infected cells as a measure of absence of neutralization, IPMA staining as described in 3.2.2.6 for total murine IgG was performed. The last wells in the dilution rows showing no infected cells were considered as containing neutralizing activity against 10^2 $TCID_{50}$ of virus and expressed as the reciprocal of the dilution factor [1/X].

3.2.4.5 IFNγ$^+$ ELISpot

To investigate cellular immunity induced by VSV replicon vaccination, splenocytes (3.2.3.4) of immunized animals were tested for their capability to release IFNγ upon IAV antigen stimulation. Therefore, 96-well ELISpot plates were coated with 20 µl of rat α-mouse IFNγ antibody diluted 1:500 in PBS and incubated overnight in a wet chamber at 4°C. The following day, plates were washed three times with 200 µl of sterile PBS and subsequently blocked with ELISpot blocking buffer (sterile filtered 1% BSA in PBS) to avoid unspecific binding of secondary antibodies. After incubation for 1-1.5 h at room temperature, ELISpot blocking buffer was discarded and plates were washed again three times with 200 µl sterile PBS. Splenocytes of immunized animals (responder cells) were counted using trypan blue solution, diluted accordingly to obtain $1x10^7$ cells/ml in RPMI supplemented with 10% FBS, 200 mM L-glutamine, 1% penicillin/streptomycin or HL-1 medium, and stored at 37°C until further use. Splenocytes from naïve mice (stimulator cells) were used to ensure proper antigen presentation to responder cells. To achieve this, they were centrifuged after separation for 8 min at 300 g and 4°C and re-suspended in 1 ml of sterile PBS. 0.5 mg/ml mitomycin C was added for 20 min at 37°C to suppress unspecific cytokine release originating from responder cells. Stimulator cells were

then washed three times by sequential centrifugation at 300 g for 5 min and re-suspension with 15 ml each time. After the last centrifugation, responder cells were taken up in 10 ml RPMI supplemented with 10% FBS, 200 mM L-glutamine, 1% penicillin/streptomycin or HL-1 medium and stored at 37°C until further use. As a positive control, 10 µg/ml concanavalin A (ConA)-solution was prepared in cell culture medium. ConA is a lectin binding to, and thereby activating, CD3 co-receptor of T cells, leading to unspecific activation and IFNγ release. To test IAV specific IFNγ release, PR8 and rSC35M were diluted in RPMI to comprise 10 hemagglutination units (HAU) per well. Finally, 50 µl of responder cell-solution, together with 50 µl of stimulator cell-solution and 100 µl of the respective stimulus were added to the 96-well ELISpot plate and incubated for 24-36 h at 37°C. After incubation period, supernatant was transferred to a fresh 96-well plate for IL-4 ELISA (3.2.4.6) and plates washed four times with PBS and afterwards four times with ELISpot washing buffer (PBS + 0.0025% Tween20). 100 µl of biotin rat α-mouse IFNγ secondary antibody, diluted 1:250 in ELISpot antibody buffer (PBS + 0.0025% Tween 20 + 1% BSA), were added and plates incubated overnight in a wet chamber at 4°C. The next day, plates were again washed four times with ELISpot washing buffer and 100 µl of α-biotin-alkaline phosphatase was added in a 1:2000 dilution in ELISpot washing buffer and incubated for 1.5 h at room temperature. To visualize spots, all wells were washed four times with PBS and 100 µl of BCIP/NBT-Purple Liquid Substrate was added per well. After spots formation, the reaction was stopped by washing the wells four times with ddH_2O. After carefully removing the plastic bottom of the ELISpot plates, they were dried in the dark overnight and subjected to spot counting using the A.EL.VIS ELISPOT Scanner.

3.2.4.6 IL-4 ELISA

To assess the capability of splenocytes from immunized animals to release IL-4 after stimulation with IAV, an IL-4 ELISA with supernatant originating from the ELISpot plates (3.2.4.5) was performed. Therefore, the IL-4 Mouse Uncoated ELISA Kit was used, following the manufacturer's instructions. To stop the reaction, 1 M H_2SO_4 was used and the optical density (OD) was read out at the Tecan SUNRISE microplate absorbance reader at 450 nm wavelength using 570 nm as a reference.

3.2.4.7 FcγRIV Effector Assay

To investigate the capacity of post-immunization antibodies to activate mFcγRIV, the Mouse FcγRIV ADCC Bioassay (Promega) was used. All steps were performed following the manufacturer's instructions, if not stated otherwise. In brief, MDCK cells were seeded to reach confluence in a 96-well plate overnight. The next day, PR8 or SC35M virus was added with an MOI=1 in DMEM without supplements and plates were incubated at 37°C for PR8 and 32° for rSC35M. 24 hours post-infection, low IgG serum was thawed in the water bath and 1.5 ml were mixed with 36 ml RPMI1640 to obtain 4% assay buffer. Sera to be tested were 2-fold diluted (starting dilution 1:10) in an U-bottom plate in 4% assay buffer. After washing the cells with PBS, 25 µl of 4% assay buffer and 25 µl of the respective serum dilution was transferred in duplicates onto the cells. mFcγRIV effector cells were thawed in the water bath and 650 µl of stock were added into 7.2 ml of pre-warmed 4% assay buffer. After mixing, 25 µl of cell suspension were added into the cells containing the serum dilutions and plates were incubates at 37°C for 6 h. After incubation, cells and Bio-Glo Reagent were put at ambient temperature for 15 minutes and 75 µl of prepared Bio-Glo Reagent were added to the cells and incubated for 20-30 minutes in the dark at room temperature. 140 µl were then transferred into a black 96-well plate without creating bubbles and luminescence was measured using the PHERAStar FSX luminescence reader.

4 RESULTS

4.1 Humoral Immune Responses Against Internal Influenza A Virus Antigens Correlate With Protection Against Heterologous Challenge

4.1.1 Generation of Single-round VSV Replicons Expressing Internal Influenza A Virus Proteins

To examine the protective efficacy of different highly conserved influenza A virus (IAV) proteins, single-round VSV replicons expressing IAV-NP, -M1, -M2, and -HA_{stem} were used as a vaccine vector. Since these proteins show high amino acid conservation between different influenza virus strains, they are promising targets for eliciting heterologous protection (Table 11). The commercially available live attenuated influenza vaccine (LAIV) Fluenz® Tetra (season 2016/2017) served as a source for these antigens, while VSV replicons expressing either no IAV antigen (VSV*ΔG) or the full-length HA of PR8 virus (VSV*ΔG(HA PR8)) were already available from previous studies (Walz et al. 2018). To obtain the different IAV genes, RNA was isolated from the vaccine virus, reverse transcribed into cDNA by using universal primers for all IAV gene segments (Uni12) and subsequently amplified by segment-specific PCR (Figure 11 A) (Hoffmann et al. 2001). The HA_{stem} construct was generated from the HA of the Fluenz® Tetra vaccine virus. Although primers suitable for the H1 and H3 gene were used in the specific PCR, we only successfully amplified the H3 gene segment which was subsequently used to generate the HA_{stem} construct ($H3_{stem}$) by two sequential joining PCRs (Figure 11 B).

Table 11: Amino acid homology of LAIV antigens compared to mouse-adapted IAV PR8 (H1N1) and rSC35M (H7N7)

Amino acid homology of…	PR8	rSC35M
NP (ca A/Ann Arbor/6/1960 (H2N2) backbone)	94.2%	92.8%
M1 (ca A/Ann Arbor/6/1960 (H2N2) backbone)	97.6%	96.4%
M2 (ca A/Ann Arbor/6/1960 (H2N2) backbone)	87.6%	88.7%
HA (A/Hong Kong/4801/2014 (H3N2)-like)	41.1%	48.5%
$H3_{stem}$ (A/Hong Kong/4801/2014 (H3N2)-like)	46.8%	59.4%

All constructs were cloned into a VSV-rescue plasmid coding for the full-length VSV genome lacking VSV-G but containing an eGFP transcription cassette (VSV*ΔG(X)) (Figure 11 C).

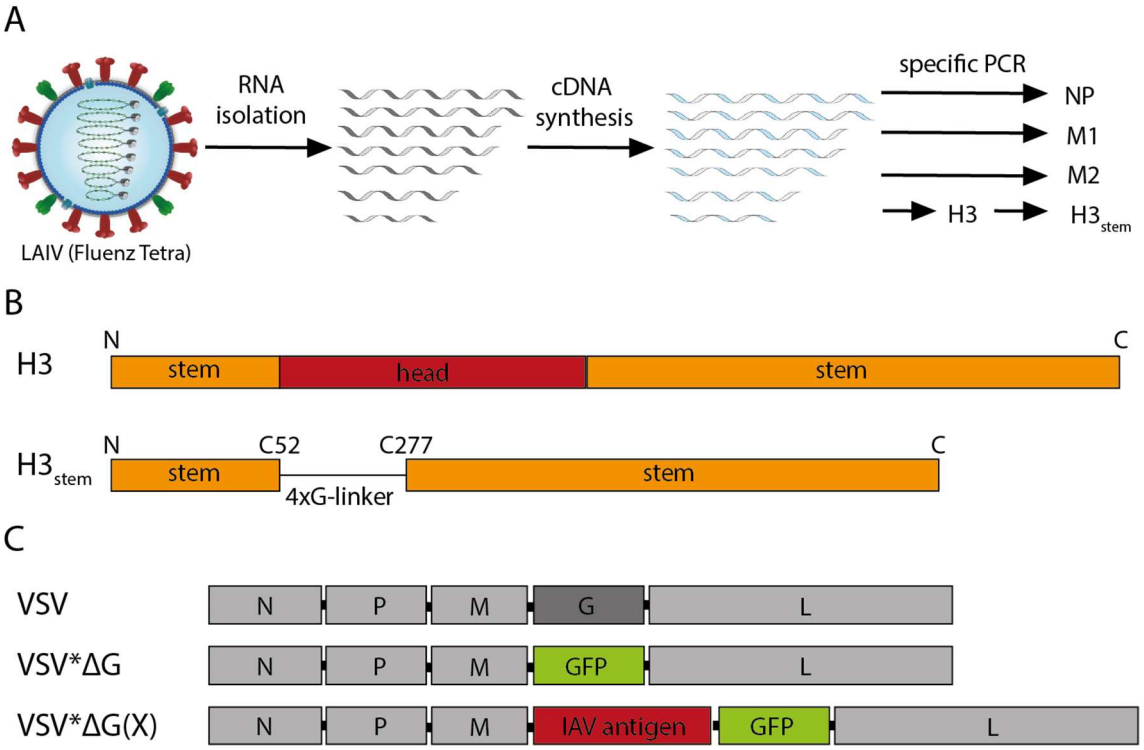

Figure 11: Generation of IAV antigen-expressing VSV replicons

(A) The LAIV Fluenz® Tetra was used as a source of IAV-NP, -M1, -M2, and -$H3_{stem}$ antigens. Viral RNA was isolated and subsequently reverse transcribed into cDNA. Via segment-specific PCR, genes of interest were amplified and used for cloning into a VSV-rescue plasmid. (B) Schematic illustration of the original full length H3 and the $H3_{stem}$ construct obtained by sequential joining PCRs. The stem-region at the N- and C-terminus is illustrated in orange, the head in red. $H3_{stem}$ lacks the head domain, which is substituted by a 4xG-linker (black line). C52 and C277 illustrate the start and end of the HA head domain, respectively. (C) Depiction of the genomic structure of VSV (top), VSV*ΔG (middle) and VSV*ΔG(X) (bottom).

To generate VSV replicons, the helper cell line BHK-G43, expressing VSV-G after mifepristone induction, was infected with modified vaccinia Ankara (MVA) virus expressing a T7 phage RNA polymerase (MVA-T7) (Sutter et al. 1995). Subsequently, the respective VSV*ΔG(X) plasmid, in combination with VSV helper plasmids encoding for VSV-N, VSV-P, and VSV-L, was transfected as described previously (Halbherr et al. 2013). The provided T7 phage RNA polymerase leads to the generation of (+)ssRNA, complementary to the VSV*ΔG(X) plasmid sequence, and production of helper proteins, which are all expressed under a T7 promotor. Translated helper proteins then associate with the (+)ssRNA to form the RNP complex which is subsequently replicated into viral genomes ((-)ssRNA). Viral genomes serve as a template for transcription of mRNAs, which are then translated

into more viral proteins including the matrix protein required for particle assembly and budding (Figure 12). Rescued VSV*ΔG(X) replicons were grown via further passage on BHK-G43 cells, purified and titrated for further experiments.

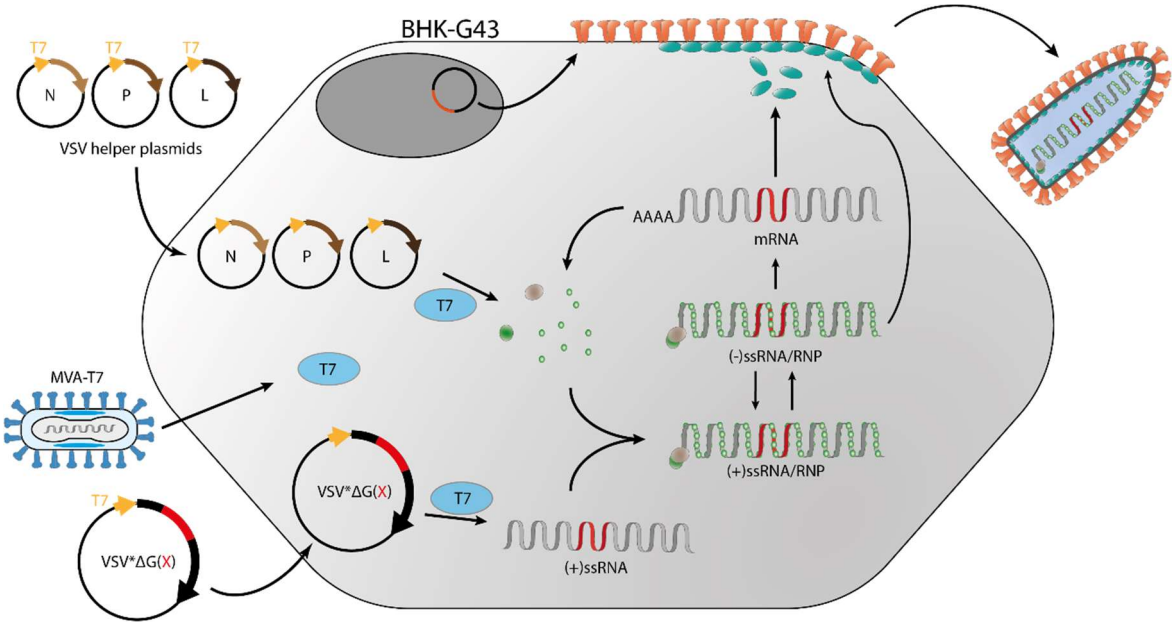

Figure 12: Schematic illustration of VSV replicon generation

BHK-G43 cells were infected with MVA-T7 to obtain the T7 phage RNA polymerase in the cytoplasm, which leads to transcription and translation of transfected VSV*ΔG(X) and VSV helper plasmids. VSV-N, -P, and –L associate with the antigenomic (+)ssRNA of the replicons, building RNPs and initiating transcription into viral genomes ((-)ssRNA/RNP). These viral genomes give rise to mRNA following expression of VSV proteins, which support further viral replication. Ultimately, the recombinant VSV*ΔG(X) genomes bud at the plasma membrane with produced viral proteins. Adapted from (Zimmer 2010).

To validate expression of IAV antigens by the respective VSV replicons, immunoblot analysis was performed. For this, confluent monolayers of BHK-21 cells were transduced with the respective replicon and lysed 24 hours post infection. Protein lysates were subjected to immunoblot analysis and stained with monoclonal α-GAPDH antibody, polyclonal α-VSV serum, polyclonal α-IAV serum, or antibodies against specific IAV proteins (Figure 13). While uninfected cells show no bands at the expected size of viral proteins, VSV-specific bands corresponding to VSV N, P, and M proteins were detected in cells transduced with the various VSV replicons, indicating comparable transduction rates and similar protein expression levels. Transduction of BHK-21 cells with the respective replicons further resulted in bands at the expected sizes of encoded proteins for IAV-NP (55 kDa), IAV-M1 (25 kDa), and IAV-M2 (15 kDa). Whereas full length HA was readily detected in its premature HA_0 conformation as well as the proteolytically cleaved HA_1 and HA_2 subunits, we

were unable to detect any specific band for the $H3_{stem}$ construct (predicted molecular weight of ~39 kDa).

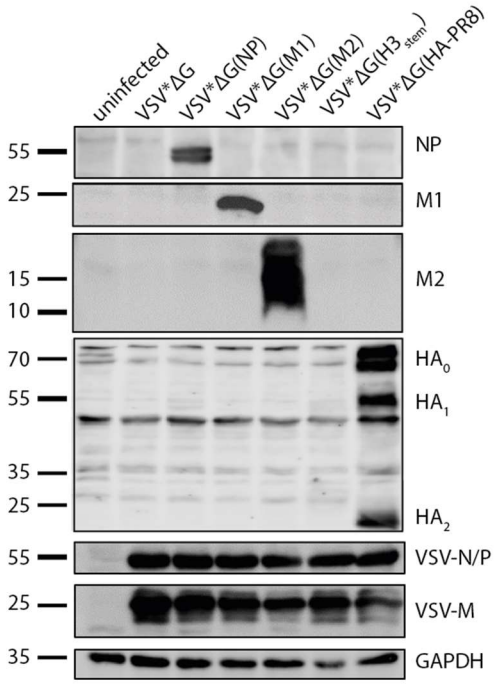

Figure 13: *In vitro* validation of IAV protein expression

Confluent BHK-21 cells were transduced with the respective replicon and lysed after 24 hours for protein extraction and immunoblot analysis. α-GAPDH staining serves as a loading control and confirms comparable loading of protein lysates for analysis. While VSV*ΔG infected cells only show specific bands for VSV-N/P (~50 kDa) and VSV-M (~30 kDa), demonstrating efficient transduction and expression of virally encoded genes, IAV protein expression is shown for NP (55 kDa), M1 (25 kDa), M2 (15 kDa), and HA (HA_0: 70 kDa, HA_1: 55 kDa, HA_2: 20 kDa). No specific band for VSV*ΔG($H3_{stem}$) was detected.

As we were not able to detect a specific band for the $H3_{stem}$ construct via immunoblot analysis, immunofluorescence was performed (Figure 14). For this, VeroE6 cells were transduced with either VSV*ΔG, VSV*ΔG($H3_{stem}$), or VSV*ΔG(HA PR8) and subsequently stained with ferret serum directed against H1 IAV (Figure 14 A) or H3 IAV (Figure 14 B) and a TxRed-conjugated secondary antibody. Dominant eGFP expression in all samples confirms successful transduction of VeroE6 cells, while specific TxRed signal was not found in VSV*ΔG samples. Interestingly, H1 as well as H3 serum show reactivity with the $H3_{stem}$ construct and staining occurs on the cell surface of $eGFP^+$ cells, demonstrating efficient expression and presentation. While H1 serum is reactive against VSV*ΔG(HA PR8) infected cells, this was not the case for the H3 serum. Overall, our immunofluorescence analysis confirmed $H3_{stem}$ surface expression on transduced cells.

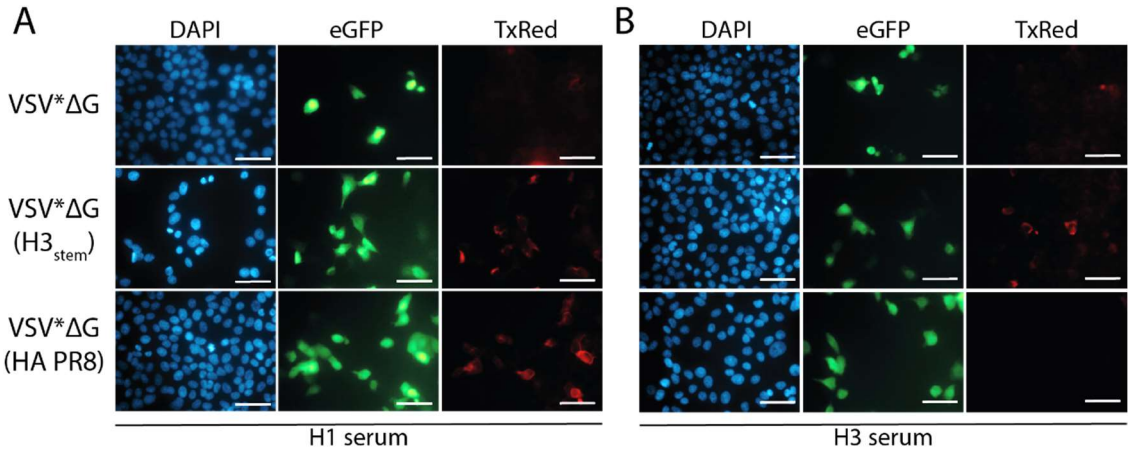

Figure 14: Immunofluorescence analysis to confirm $H3_{stem}$ expression and presentation
Confluent monolayers of VeroE6 cells were transduced with an MOI=1 of the respective VSV replicons and 12 hours post-infection fixed and permeabilized. Staining was performed using DAPI and with either H1 serum (A) or H3 serum (B) and TxRed-conjugated secondary antibody. Expression of eGFP demonstrated successful transduction of VeroE6 cells and TxRed signal in $eGFP^+$ cells indicates expression of $H3_{stem}$ or HA PR8. Pictures were taken at the Axio Observer.Z1 microscope (Carl Zeiss). Scale bar in white represents 50 µm.

4.1.2 Validation of the Single-round Character of VSV Replicons

It is known that some viral receptor proteins, for example Ebola glycoprotein (Jones et al. 2005), can complement VSV-G-deficiency and lead to efficient replication of VSV replicons even without VSV-G. In our hands, the VSV replicon expressing full length IAV HA protein (VSV*ΔG(HA PR8)) represents the replicon with the highest probability of complementing lack of VSV-G. Therefore, we tested the ability of this replicon to form infectious particles in the absence of VSV-G. To assess the single-round character of VSV replicons lacking VSV-G (Roberts et al. 1999; Zimmer et al. 2014; Walz et al. 2018), BHK-G43 cells were transduced with VSV*ΔG(HA PR8) and treated with mifepristone to induce VSV-G expression, or left untreated (Figure 15). While non-transduced cells show no GFP signal 24 hours post-infection (left column), GFP expression was detected in VSV*ΔG(HA PR8) transduced cells (middle/right column). When mifepristone was additionally present in the medium, GFP signal was markedly increased as compared to the untreated well. This illustrates efficient replication and propagation of VSV replicons when VSV-G is provided *in trans*. Importantly, only supernatants from cells expressing VSV-G contained infectious progeny replicons, which led to GFP expression after transfer to fresh cells not treated with mifepristone (Figure 15, right column). This indicates that in the absence of VSV-G expression, no infectious VSV replicons were generated (Figure 15, middle column). The single-round character adds an important safety factor to the VSV replicon platform.

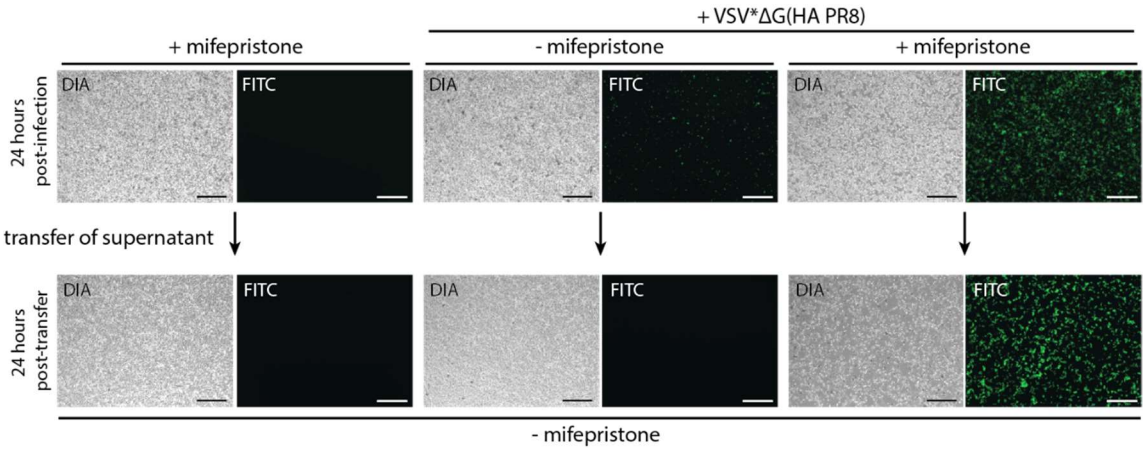

Figure 15: Validation of the single-round character of VSV*ΔG(HA PR8)

BHK-G43 cells were seeded in 6-well plates, transduced with MOI=1 of VSV*ΔG(HA PR8) and either treated with mifepristone (right panel) or left untreated (middle panel). Diascopic brightfield pictures (DIA) are shown on the left and fluorescence pictures using FITC filter on the right (GFP), respectively. Increased GFP expression in treated cells indicated efficient replication of VSV replicons in contrast to untreated cells. 24 hpi supernatant was transferred to fresh, untreated BHK-G43 cells and GFP was visualized after another 24 h. Scale bars represent 500 µm.

4.1.3 Determination of the Lethal Dose 50 (LD_{50}) of PR8 and rSC35M in C57BL/6J mice

With the goal to investigate the protective efficacy of the generated VSV replicons in C57BL/6J mice, we first established an IAV challenge model for two mouse-adapted IAV strains, PR8 and rSC35M. To estimate a challenge dose resembling severe pathology, we titrated the PR8 and rSC35M viruses by infecting naïve mice intranasally with increasing doses of each virus. Per group, three animals were infected intranasally with 10^2, 10^3, 10^4, 10^5, or 10^6 $TCID_{50}$ in 30 µl PBS. To investigate the severity of disease, animals were monitored daily for weight loss and clinical signs (see score sheet Table 10) and euthanized as soon as they reached pre-defined humane endpoints (either losing 25% of initial weight or exceeding clinical scores for behavior or appearance). All groups of PR8 challenged mice showed a severe pathology, and infection dose positively correlated with onset of weight loss (Figure 16 A) and time point of death (Figure 16 B). Ultimately, all animals inoculated with 10^2 $TCID_{50}$ survived PR8 challenge, and doses of $\geq 10^3$ $TCID_{50}$ led to death within one week. In contrast to this, rSC35M infected mice showed a slower disease progression. Infected animals lost up to 20% of initial weight in mean, but the variability in each group was higher than in the groups infected with PR8 (Figure 16 C). However, even doses of 10^2 $TCID_{50}$ led to the death of two animals, respectively, whereas no survival was observed in groups infected with 10^4 $TCID_{50}$ or higher (Figure 16 D). Finally, we used AAT Bioquest calculator to estimate 50% lethal dose

(LD_{50}) and chose $6.0x10^2$ $TCID_{50}$ and $1.2x10^3$ $TCID_{50}$ of PR8 and rSC35M, respectively (approximately $3xLD_{50}$) for further experiments to induce high severity of IAV infection in mice.

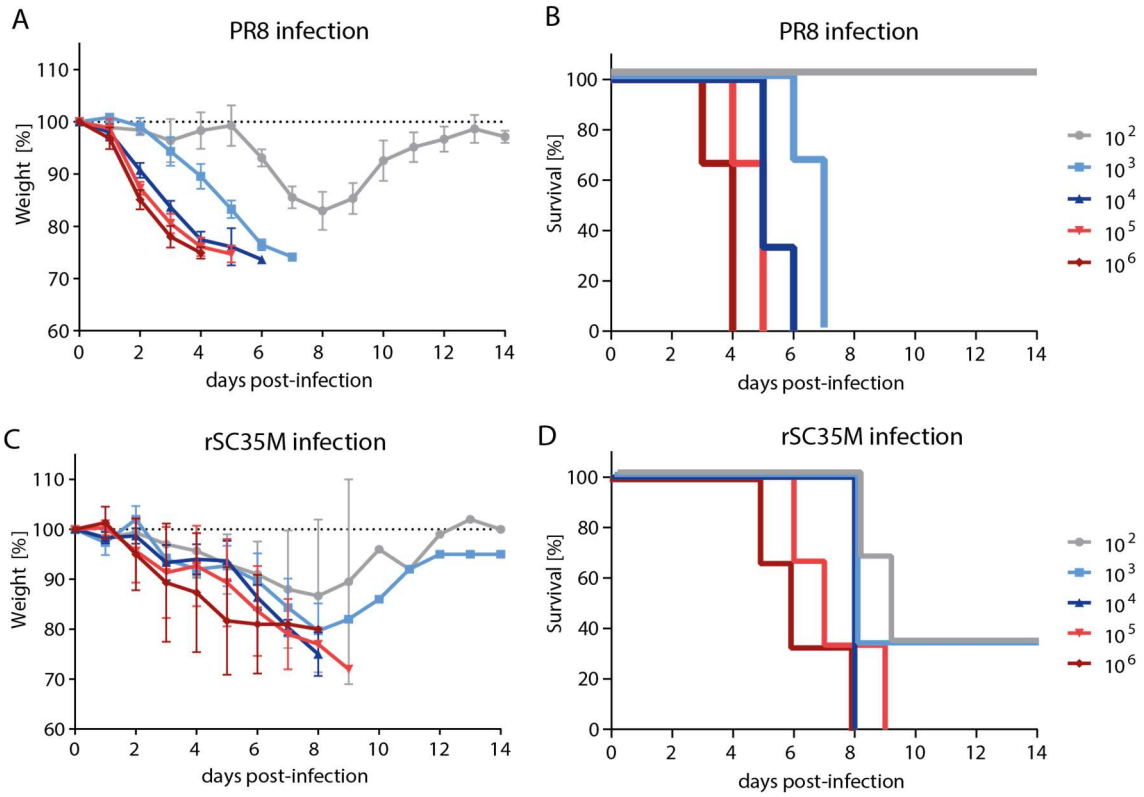

Figure 16: 50% lethal dose (LD_{50}) titration of PR8 and rSC35M in C57BL/6J mice

N=3 mice were anesthetized using intraperitoneal Ketamin/Xylazine anesthesia, infected with ascending doses of PR8 or rSC35M and monitored daily over a period of 14 days. When reaching 25% weight loss or clinical score of ≥8 (see score sheet), animals were euthanized. (A) Weight loss of PR8 infected mice expressed as percentage of initial weight, dotted line indicates bodyweight on day of infection. (B) Survival rate of PR8 infected mice. (C) Weight loss of rSC35M infected mice expressed as percentage of initial weight, dotted line indicates bodyweight on day of infection. (D) Survival rate of rSC35M infected mice. Data points in A and C illustrate mean and error bars represent standard deviations.

4.1.4 VSV Replicons Provide (Partial) Protection Against IAV Pathogenicity

To investigate the protective effect of the generated VSV replicons against the high pathology of IAV in our murine model, we immunized C57BL/6J mice in a prime-boost regimen. For this, 10^6 fluorescence-forming units (ffu) were injected intramuscularly in the hind leg in 30 µl PBS at day 56 and 28 prior to infection (Figure 17 A). On the day of infection, mice were weighed, anesthetized, and infected intranasally with $6.0x10^2$ $TCID_{50}$ of PR8. After challenge, mice were monitored for 14 days for weight loss (Figure 17 B) and disease score (Figure 17 C). To compare the disease development between the different groups, we calculated the area under

the curve (AUC) of each group (Figure 17 D). Finally, we documented the survival of animals in each group by Kaplan-Meier-analysis (Figure 17 E).

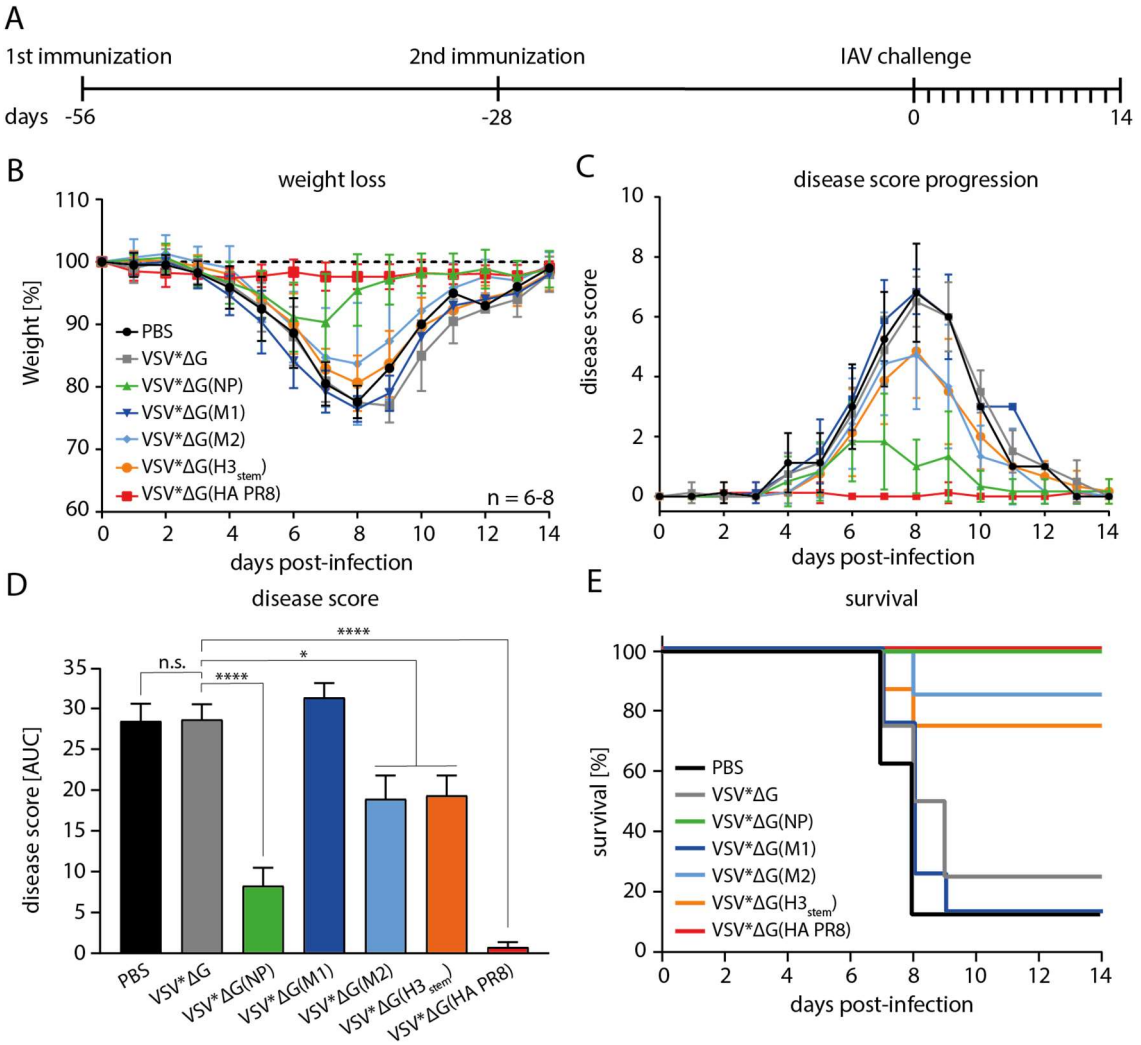

Figure 17: Protection of C57BL/6J mice against PR8 after prime-boost immunization with VSV replicons

To assess the protective effect of the respective VSV*ΔG replicons, C57BL/6J mice were immunized twice and subsequently challenged with $6.0x10^2$ $TCID_{50}$ of PR8. (A) Schematic illustration of the prime-boost regimen 56 and 28 days before infection and the observation period of 14 days after challenge. (B) Weight loss of PR8 infected mice immunized with VSV replicons. All data points represent the mean and error bars are standard deviations (SD). Dotted line indicates initial weight. (C) Clinical scores of infected mice, based on weight, behavior, and appearance. All data points represent the mean and error bars are SD. (D) Disease scores expressed as area under curve (AUC). Height of bars represent the mean and error bars are standard error of the mean (SEM). For statistical analysis, one-way analysis of variance (ANOVA) with Tukey's multiple comparison post-hoc-test using the VSV*ΔG as a reference was performed. *p<0.05; ****p<0.0001. (E) Survival rates of animals until day 14 of infection.

PBS and VSV*ΔG groups showed severe weight loss of up to 25% after eight days (Figure 17 B), high disease scores (Figure 17 C,D), and most animals succumbed within 8 days post-infection (Figure 17 E). In contrast to this, VSV*ΔG(HA PR8) immunized mice did not show any weight loss (Figure 17 B) or signs of disease

throughout the observation period (Figure 17 C, D). Furthermore, none of these animals reached humane end points (Figure 17 E). This underlines the strong protection against HA-matched viruses after vaccination. Mice immunized with VSV*ΔG(NP) lost up 10 % of initial weight on average until day 7 post-infection and showed a fast recovery thereafter (Figure 17 B). Initial weight was reached approximately 9 days post-infection. Disease scores during the study did not exceed 2 in mean and AUC calculation of disease progression was significantly decreased ($p<0.0001$) compared to VSV*ΔG (Figure 17 C, D). Furthermore, none of these animals reached humane endpoints during the study period (Figure 17 E). VSV*ΔG(M1) immunized mice showed a similar disease progression to unvaccinated animals, indicating that the vaccine did not confer any benefit. We observed severe weight loss up to 25% in mean (Figure 17 B), high clinical scores that did not differ from those observed in VSV*ΔG immunized mice (Figure 17 C, D) and low survival rates (Figure 17 E). We therefore concluded, that M1 as an antigen does not elicit protective immune responses in our VSV replicon platform. Although profound weight loss and high peak disease scores were not prevented by VSV*ΔG(M2) or VSV*ΔG($H3_{stem}$) immunization (Figure 17 B, C), AUC calculation of disease progression revealed a significant, beneficial overall effect ($p<0.05$) regarding severity of pathology (Figure 17 D). A minority of animals succumbed to infection, underlining some degree of protection after VSV*ΔG(M2) or VSV*ΔG($H3_{stem}$) vaccination (Figure 17 E).

To assess the protective efficacy of our VSV replicons against rSC35M, we used the same prime-boost regimen and challenged mice with $1.2x10^3$ $TCID_{50}$ of rSC35M. Infected mice immunized with either PBS or VSV*ΔG showed comparable disease progression to PR8, including severe weight drop until day 8 post-infection and slow recovery (Figure 18 A), high disease scores (Figure 18 B, C) and low survival rates (Figure 18 D). For VSV*ΔG(HA PR8) immunized mice, no significantly protective effect was observed regarding any parameter. This highlights the inefficient protection conferred in challenges after mismatched immunizations. Interestingly, while VSV*ΔG(NP) vaccination did not avert weight loss of infected animals (Figure 18 A), disease score progression and overall AUC calculation revealed a beneficial effect that was significant ($p<0.05$) when compared to the VSV*ΔG group (Figure 18

B, C). Furthermore, VSV*ΔG(NP) immunized animals showed high survival rates, underlining the protection of IAV-NP directed immunity (Figure 18 D).

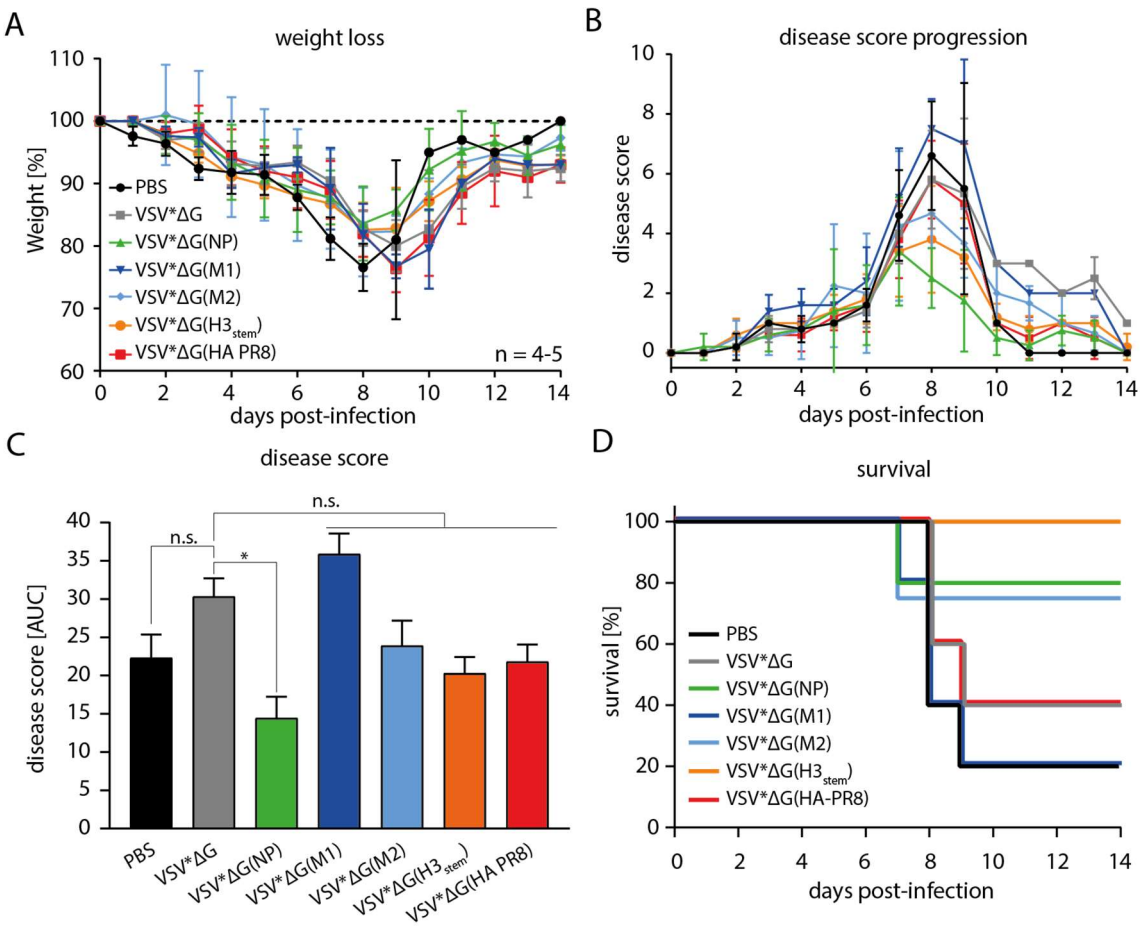

Figure 18: Protection of C57BL/6J mice against rSC35M after prime-boost immunization with VSV*ΔG replicons

To assess the protective effect of the respective VSV*ΔG replicons, C57BL/6J mice were immunized twice and subsequently challenged with $1.2x10^3$ $TCID_{50}$ of rSC35M. (A) Weight loss of rSC35M infected mice immunized with VSV replicons. All data points represent the mean and error bars are standard deviations. Dotted line indicates initial weight. (B) Clinical scores of infected mice, based on weight, behavior, and appearance. All data points represent the mean and error bars are SD. (C) Disease scores expressed as area under curve (AUC). Height of bars represent the mean and error bars are standard error of the mean (SEM). For statistical analysis, one-way analysis of variance (ANOVA) with Tukey's multiple comparison post-hoc-test using the VSV*ΔG as a reference was performed. *$p<0.05$. (D) Survival rates of animals until day 14 of infection.

As for PR8, rSC35M-induced pathology was not alleviated after VSV*ΔG(M1) immunization in terms of weight loss (Figure 18 A), disease score (Figure 18 B, C) or overall survival (Figure 18 D). While VSV*ΔG(M2) and VSV*ΔG($H3_{stem}$) immunization did also not prevent weight loss (Figure 18 A), a decreasing trend, although not significant, was observed regarding disease scores (Figure 18 B, C) and the majority of challenged mice survived the infection (Figure 18 D).

In conclusion, we demonstrated that the NP, M2 and $H3_{stem}$ proteins of the LAIV alone can confer protection against heterologous IAV infection. While NP vaccine clearly reduced disease progression of both IAV strains and led to improved survival rates in both cases, the M1 vaccine had no beneficial effect on either. The M2 and $H3_{stem}$ vaccines reduced disease progression only to a limited degree and worked better in case of PR8 than rSC35M. However, even this limited reduction of pathology had a positive effect on the survival rate after challenge with either virus.

4.1.5 VSV Replicons Do Not Induce Detectable Cellular, But Humoral Immunity

To examine the underlying immune response that led to the different outcomes in our murine IAV-challenge model, we investigated cellular and humoral immune responses towards IAV after VSV replicon immunization. Since it is known for the applied VSV vaccine platform to induce antigen specific T cells against IAV (Asthagiri Arunkumar et al. 2019), we performed IFNγ$^+$ ELISpot and IL-4 ELISA assays to investigate whether prominent T_H1 and T_H2-mediated cellular immune responses were activated, respectively (Figure 19). As stimulation is a critical step in ELISpot analysis, we validated efficient stimulation of IAV-specific splenocytes through infection by testing cells of PR8 infected mice (Figure 19 A), and found high spot numbers after homologous stimulation with PR8 virus particles, and limited stimulation by the heterologous rSC35M. Cells were co-incubated with splenocytes from a naïve mouse pretreated with mitomycin C (stimulator cells) and stimulated with Concanavalin A (ConA) or infected with either PR8 or rSC35M virus. Concanavalin A is a lectin that unspecifically binds the T cell receptor, thereby leading to activation and cytokine release from all splenocytes, serving as a positive control. This confirms the general feasibility of our IFNγ$^+$ ELISpot stimulation approach. For measuring cellular immune responses after VSV replicon vaccination, mice were immunized in a prime-boost regimen four weeks apart as described above, and splenocytes were harvested seven days after boost immunization (Figure 19 B). As expected, none of the animals showed significant IFNγ$^+$ response when left untreated, but ConA stimulation in some cases resulted in more than 300 spot-forming cells (SPCs) per 10^6 seeded cells (Figure 19 C). However, neither PR8 nor rSC35M stimulation led to IFNγ$^+$ release in any of the tested groups. We therefore tested supernatant of the same splenocytes for IL-4 release (Figure 19 D).

Interestingly, even unstimulated cells showed some release of IL-4 in the VSV*ΔG(NP), VSV*ΔG(M1), VSV*ΔG($H3_{stem}$), and VSV*ΔG(HA PR8) groups. These groups revealed similar levels of IL-4 after either PR8 or rSC35M stimulation, demonstrating no alleviated cytokine release. In fact, none of the groups was tested significantly different from unstimulated groups and we therefore concluded that the implemented VSV replicon immunization procedure did not lead to generation of T_H1 or T_H2 T cells that could directly respond to PR8 or rSC35M viruses.

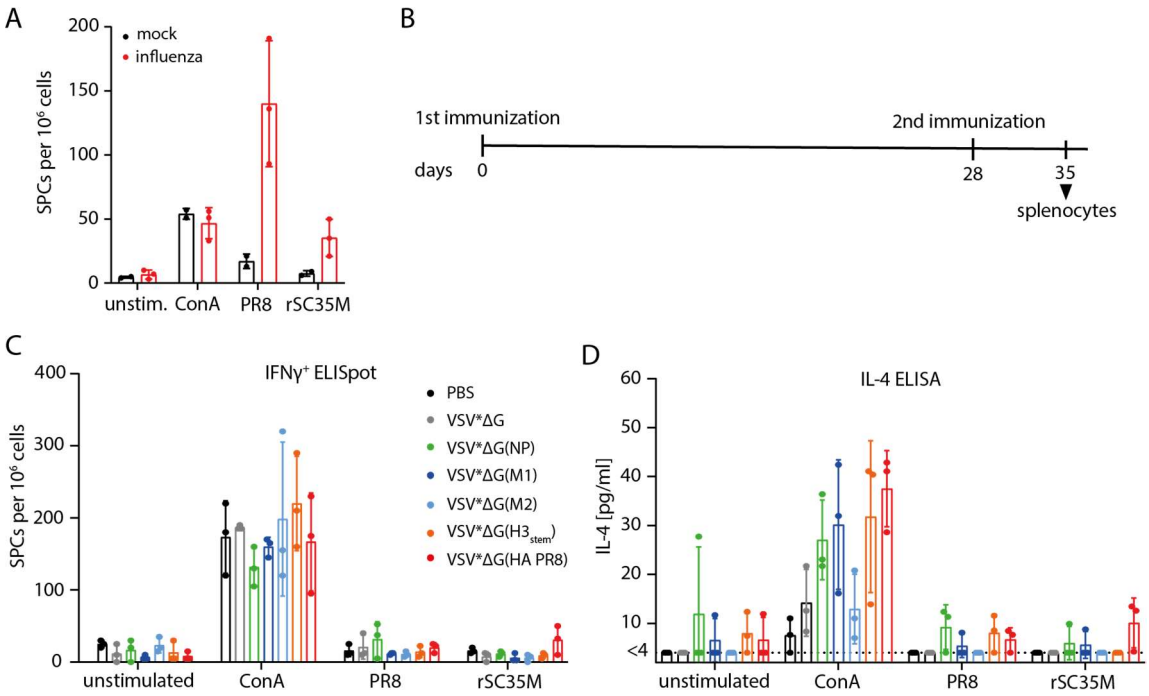

Figure 19: Cellular immune responses after VSV replicon vaccination

(A) Stimulation control subjecting splenocytes of PR8-infected mice to ELISpot analysis using PR8 or rSC35M virus particles as stimulation or concanavalin A (ConA) as a positive stimulation control. unstim.: unstimulated. (B) N=3 mice were intramuscularly immunized with 10^6 ffu/animal on day 0 and day 28. 7 days after boost immunization, animals were sacrificed and splenocytes were harvested for IFNγ⁺ and IL-4 response analysis. (C) IFNγ⁺ cells expressed as spot-forming cells (SPCs) per 10^6 seeded cells, either left untreated or treated with Concanavalin A (ConA), PR8, or rSC35M virus. (D) Supernatants of B were used for IL-4 ELISA and cytokine levels were plotted as pg/ml. The dotted line indicates the lower detection limit of the ELISA assay. Statistical analysis using two-way ANOVA with Dunnett's multiple comparison post-hoc test showed no significant differences for IFNγ⁺ ELISpot or IL-4 ELISA between unstimulated and stimulated cell in one group.

To assess the humoral immune responses after VSV replicon immunization, we immunized mice as described before and isolated serum from blood withdrawn 28 days after prime and 28 days after boost (Figure 20 A). We then determined total IgG antibodies in the sera reactive against PR8 or rSC35M virus, respectively, using immuno-peroxidase monolayer assay (IPMA). In this assay, infected MDCK cells are incubated with 2-fold dilution series of serum and afterwards stained via HRP-conjugated α-mouse IgG antibody. The last dilution showing specific staining is

considered positive and expressed as the dilution factor [1/X]. In line with our expectations, analysis of serum from mock-immunized groups (PBS and VSV*ΔG) revealed no reactivity towards either PR8 (Figure 20 B) or rSC35M virus (Figure 20 C). Animals immunized with VSV*ΔG(NP) developed high antibody titers reactive with both viruses after prime immunization, which were even further elevated after boost vaccination. In strong contrast to this, mice immunized with VSV*ΔG(M1) showed significantly less ($p<0.0001$) antibodies, as no antibodies reactive against PR8 (Figure 20 B) and negligible amounts against rSC35M (Figure 20 C) were detected.

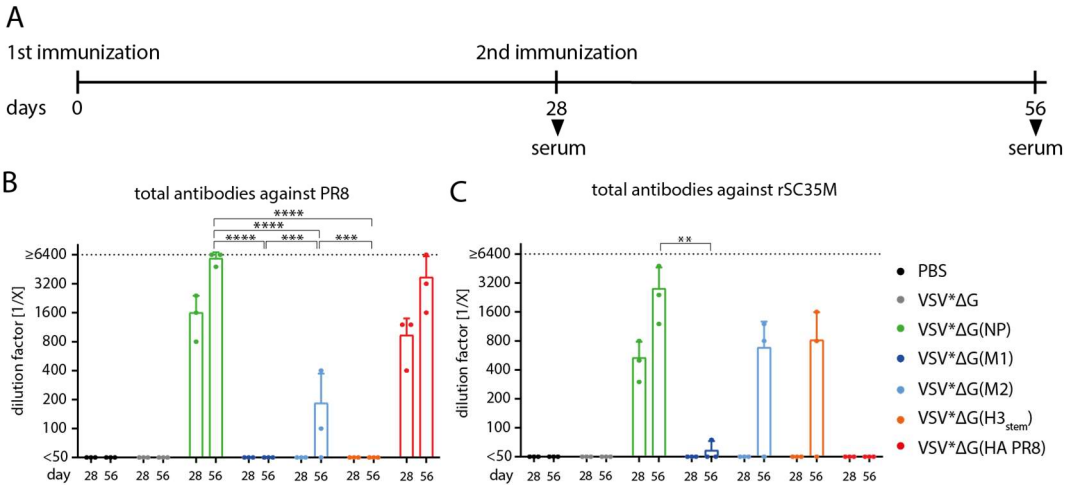

Figure 20: Total antibody response of VSV replicon-immunized animals reactive against PR8 and rSC35M

Humoral immune responses were evaluated via immuno-peroxidase monolayer assay (IPMA). (A) Timeline illustrating prime (1st immunization), boost (2nd immunization), and days of blood sampling (black triangle). (B and C) Total antibodies directed against PR8 (B) and rSC35M (C) virus, respectively. Upper dotted line indicates upper limit of detection. Height of bars represents mean and all error bars are standard deviations. For statistical analysis, two-way analysis of variance (ANOVA) with Dunnett's multiple comparison post-hoc test was performed on log2-transformed titers. **p<0.01; ***p<0.001; ****p<0.0001. Significance levels compared to VSV*ΔG(HA PR8) are not stated. Only significance levels between boost groups of VSV*ΔG(NP), VSV*ΔG(M1) , VSV*ΔG(M2), and VSV*ΔG($H3_{stem}$) are indicated.

No antibody responses were observed after prime immunization with VSV*ΔG(M2), but 28 days post-boost, antibodies reactive against both PR8 and rSC35M were detectable at intermediate levels (Figure 20 B, C). Interestingly, VSV*ΔG($H3_{stem}$) immunization did not induce antibodies recognizing PR8 (Figure 20 B), but rSC35M (Figure 20 C). After VSV*ΔG(HA PR8) immunization, high antibody levels reactive against PR8 (Figure 20 B) but without specificity for rSC35M (Figure 20 C) were detectable after prime and boost immunization.

Since antibodies differ in their mode of action, we investigated via virus neutralization assay (VNA) if induced antibodies after VSV replicon prime/boost-immunization were capable of neutralizing PR8 or rSC35M virus (Figure 21). Here, virus was pre-incubated with 2-fold serial dilutions of serum and transferred onto a MDCK cell monolayer. Infected cells were stained via virus-specific antibodies afterwards and neutralizing titers are the last dilution, in which pre-incubation led to neutralization of virus and therefore absence of infection. Of the different groups that showed prominent total antibody levels, only VSV*ΔG(HA PR8) induced antibodies that were capable of neutralizing PR8 but not rSC35M (Figure 21). This result confirms the strong protective effect in HA-matched immunization-challenge experiments (Figure 21). Importantly, antibodies developed against NP, M2, and $H3_{stem}$ had no neutralizing activity at all, indicating that they may have different functions in alleviating IAV pathology.

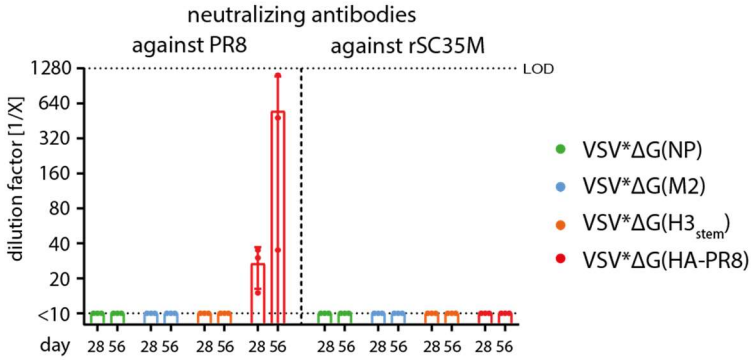

Figure 21: Virus neutralizing antibodies after VSV vaccination.

Neutralizing antibodies against PR8 (left) and rSC35M (right) were determined. Only serum from VSV*ΔG(HA PR8) group was capable of neutralizing PR8 virus but not rSC35M. Lower dotted line indicates lower limit of detection; upper dotted line indicates upper limit of detection. Height of bars indicates mean and error bars are standard deviations.

As antibodies of different IgG subclasses have various capabilities of activating FcγR effector functions, we analyzed the IgG subclass-profiles after the prime/boost-immunization using an IPMA with secondary α-mouse antibodies specific for the subclasses IgG1, IgG2b, IgG2c, IgG3 (Figure 22).

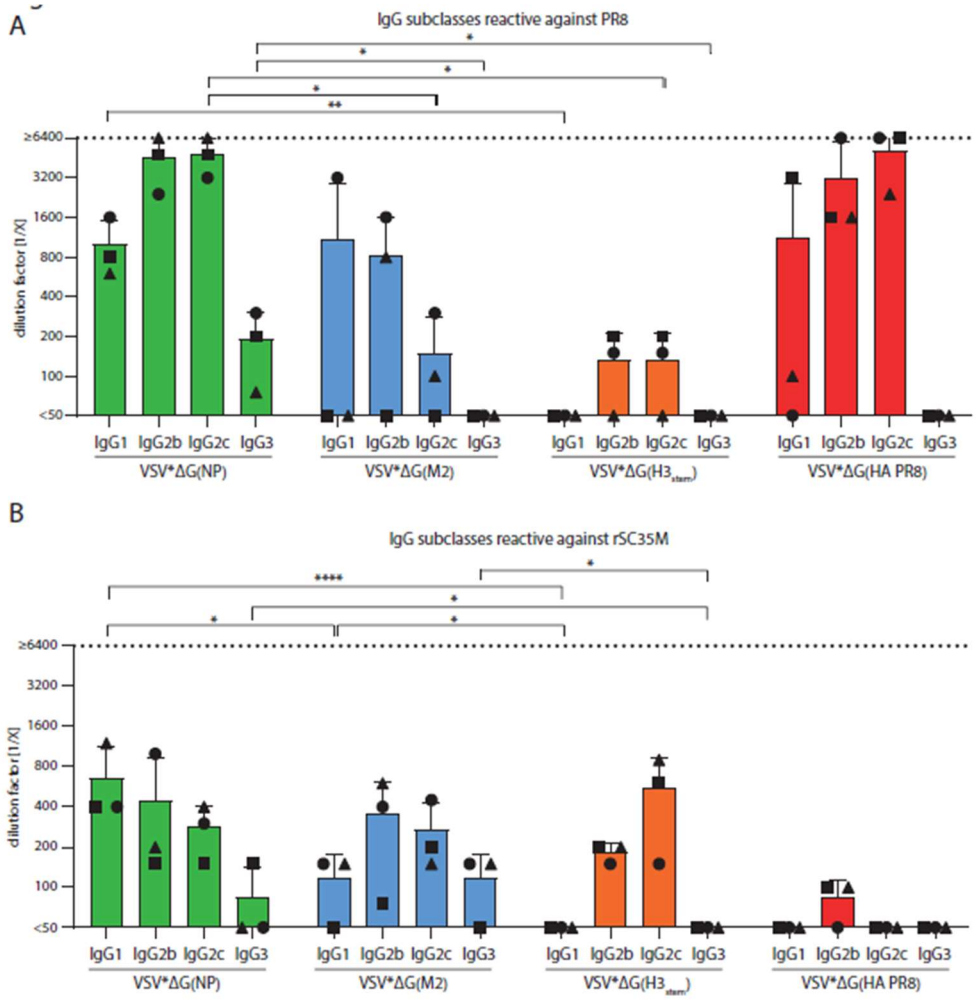

Figure 22: IgG subclass-analysis of VSV immunized mice after boost

28 days after booster immunization, serum of mice was isolated and tested for IgG subtypes in an adapted IPMA, utilizing secondary α-mouse antibodies specific for either subtype. (A) IgG subclasses reactive towards PR8 virus in mice immunized with VSV replicons. (B) IgG subclasses reactive towards rSC35M virus in mice immunized with VSV replicons. For statistical analysis, two-way analysis of variance (ANOVA) with Tukey's multiple comparison test on log2-transformed titers was used. Statistical significance is indicated by *p<0.05; **p<0.01; ****p<0.0001, and significance levels compared to VSV*ΔG(HA PR8) are not stated. Upper dotted line indicates upper limit of detection. Each animal is indicated by an individual symbol.

Animals immunized twice with VSV*ΔG(NP) developed antibodies of all four subclasses reactive against PR8, while antibodies against M2 were of the IgG1, IgG2b, and IgG2c subclasses (Figure 22 A). Antibodies generated against $H3_{stem}$ were IgG2b an IgG2c. In all cases, the PR8-reactive antibody titers of each subclass were higher after NP vaccine than after M2 or $H3_{stem}$ vaccine. Titers of IgG2c were significantly higher when compared to VSV*ΔG(M2) ($p<0.05$) or VSV*ΔG($H3_{stem}$) ($p<0.05$). Furthermore, IgG3 titration revealed higher titers against PR8 after VSV*ΔG(NP) immunization when compared to other groups (VSV*ΔG(M2) $p>0.05$; VSV*ΔG($H3_{stem}$) $p<0.05$). For VSV*ΔG(M2) immunized mice, antibody

responses were less consistent among individual animals and reached lower levels on average, as one animal (rectangle) was observed failing to produce any detectable titers of IgG subclasses. In the VSV*ΔG($H3_{stem}$) group no antibodies of the IgG1 or IgG3 subclass, and just intermediate levels of IgG2b/IgG2c were measured. In serum of VSV*ΔG(HA PR8) immunized animals, high levels of PR8-specific IgG2b and IgG2c were detected, but just low and inconsistent levels of IgG3 and IgG1, respectively.

In comparison to this, overall IgG subtype levels against rSC35M were lower (Figure 22 B), although different appearance of infected and stained cells needs to be taken into consideration. However, interestingly, VSV*ΔG(NP) immunization led to significantly higher IgG1 titers against rSC35M than VSV*ΔG(M2) ($p<0.05$) and VSV*ΔG($H3_{stem}$) ($p<0.0001$). Furthermore, antibodies elicited through VSV*ΔG(HA PR8) vaccination were found not to be reactive towards rSC35M, with exception of antibodies of the IgG2b subclass. This is in line with our expectations from total antibody titrations (Figure 20) and confirms the poor reactivity of PR8-directed humoral immune responses against rSC35M.

4.1.5.1 Antibodies Directed Against NP Can Cause Antibody-dependent Cell-mediated Cytotoxicity (ADCC)

As antibodies directed against internal proteins had no neutralizing activity (Figure 21), we investigated potential effector functions elicited by these antibodies. Specifically, we tested whether they had FcγRIV (mFcγRIV) effector functions (Figure 23), which are known to mediate for example ADCC. Activation of this function through antibodies against internal proteins would provide evidence that these non-neutralizing antibodies contribute to the protection against IAV infection. For this, IAV-infected MDCK cells were co-incubated with effector cells, which are genetically engineered Jurkat T cells expressing the mFcγRIV, and a luciferase reporter driven by an nuclear factor of activated T cell (NFAT)-response element. When mFcγRIV-activating antibodies targeting IAV antigens are present in the sample, they bind the viral epitopes on the MDCK cells and activate the signaling cascade in the effector cells leading to luciferase expression. Thereby, luciferase signal can directly be linked to the potential of the present antibodies to bind IAV-antigen and activate mFcγRIV. While no mFcγRIV activity was detected for serum of VSV*ΔG immunized mice, an activation was observed in all the vaccinated groups.

Especially serum from VSV*ΔG(M2) immunized animals strongly activated mFcγRIV in the presence of either PR8 or rSC35M infected cells. Also, for VSV*ΔG(NP) and VSV*ΔG($H3_{stem}$) groups, similar reactivity was observed, indicating that this immune reaction was efficiently induced independent of the IAV subtype. In contrast, antibodies after VSV*ΔG(HA PR8) immunization activated mFcγRIV after incubation with PR8 infected cells more efficiently than after incubation with rSC35M infected cells. Strikingly, antisera from animals infected with either virus only activated mFcγRIV when incubated with cells infected with the homologous virus but not with the other virus. Taken together, our results provide evidence that non-neutralizing antibodies directed against NP and M2 activating antibody-mediated effector functions exist and could contribute to protection after heterologous challenge. This mechanism adds another layer of protection to the action of neutralizing antibodies against surface antigens, and cytotoxic T cell responses against internal proteins.

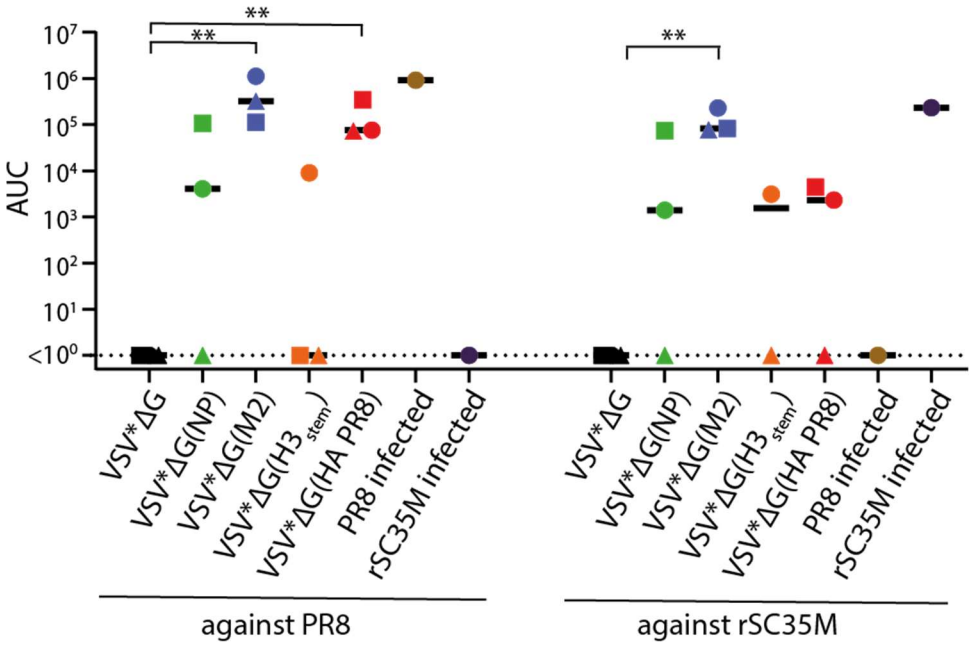

Figure 23: mFcγRIV assay of VSV immunized mice after boost

21 days after boost vaccination, sera of immunized mice was collected and tested for the capacity to activate mFcγRIV in a mouse FcγRIV ADCC bioassay. For this, PR8- (left) or rSC35M (right)-infected MDCK cells were incubated with 2-fold dilutions of the respective serum and mFcγRIV-expressing reporter cells were added. Luminescence of the different dilutions was measured and area under curve (AUC) was calculated using serum of a naïve mouse + 3x its standard deviation as baseline, black bar illustrates mean. For statistical analysis, two-way analysis of variance (ANOVA) with Sidák's multiple comparison test on log2-transformed titers was used. Statistical significance is indicated by **p<0.01 and significance levels compared to infected animals are not stated. Lower dotted line indicates lower limit of detection. Each animal is indicated by an individual symbol. N=2 for VSV*ΔG($H3_{stem}$) immunized animals tested against rSC35M for limitation of available serum.

4.1.6 Cocktail Immunization Can Provide Full Protection Against PR8, But Not rSC35M Challenge

Since VSV*ΔG(NP), VSV*ΔG(M2), and VSV*ΔG($H3_{stem}$) vaccines induced some degree of protection, we hypothesized that these effects may be synergistic by generating antibodies with different effector functions. To test this, we immunized mice with a double-cocktail containing $5.0x10^5$ ffu of VSV*ΔG(NP) + VSV*ΔG(M2), respectively to reach a total dose of 10^6 ffu per immunization (VSV*ΔG(NP)+(M2)). As it can be hypothesized that a reduction of the amount of the single replicons in this cocktail approach may lead to decreased immune responses by diluting the antigen, we further included single immunizations with either $5.0x10^5$ ffu of VSV*ΔG(NP) (0.5 x VSV*ΔG(NP)) or $5.0x10^5$ ffu of VSV*ΔG(M2) (0.5 x VSV*ΔG(M2)). All animals were boosted on day 28 prior to infection and subsequently challenged and monitored as described above (Figure 17 A). Mock-immunized mice developed severe disease including profound weight loss of up to 20% in mean (Figure 24 A), high clinical scores (Figure 24 B, C) and low survival rates (Figure 24 D). In contrast, the VSV*ΔG(HA PR8) immunized group showed no signs of infection, confirming infectious dose and immunization protocol as intended. Interestingly, animals immunized with the double-cocktail did not show strong signs of pathology, with negligible weight loss (Figure 24 A), low disease score progression (Figure 24 B), a significantly decreased ($p<0.0001$) overall pathogenicity (Figure 24 C), and 100% survival (Figure 24 D). In contrast to this, 0.5 x immunizations with either VSV*ΔG(NP) or VSV*ΔG(M2) led to intermediate weight loss of up 10-15% in mean (Figure 24 A) and a high disease score progression, especially for the 0.5 x VSV*ΔG(M2) group (Figure 24 B). However, overall pathogenicity differed (Figure 24 C). While for the 0.5 x VSV*ΔG(NP) immunized mice, intermediate pathogenicity was observed, for 0.5 x VSV*ΔG(M2) it was indistinguishable to VSV*ΔG and significantly increased ($p<0.001$) when compared to the double-cocktail. Furthermore, while all 0.5 x VSV*ΔG(NP) immunized animals survived the challenge, 40% of 0.5 VSV*ΔG(M2) reached humane endpoints (Figure 24 D). We therefore concluded that NP and M2 antigens have synergistic effects in terms of protection and lead to superior efficacy when compared with single VSV vaccinations. This is certainly the case when compared to 0.5 x single immunizations, but also in comparison to 10^6 ffu of a single VSV*ΔG(X) replicon (Figure 17).

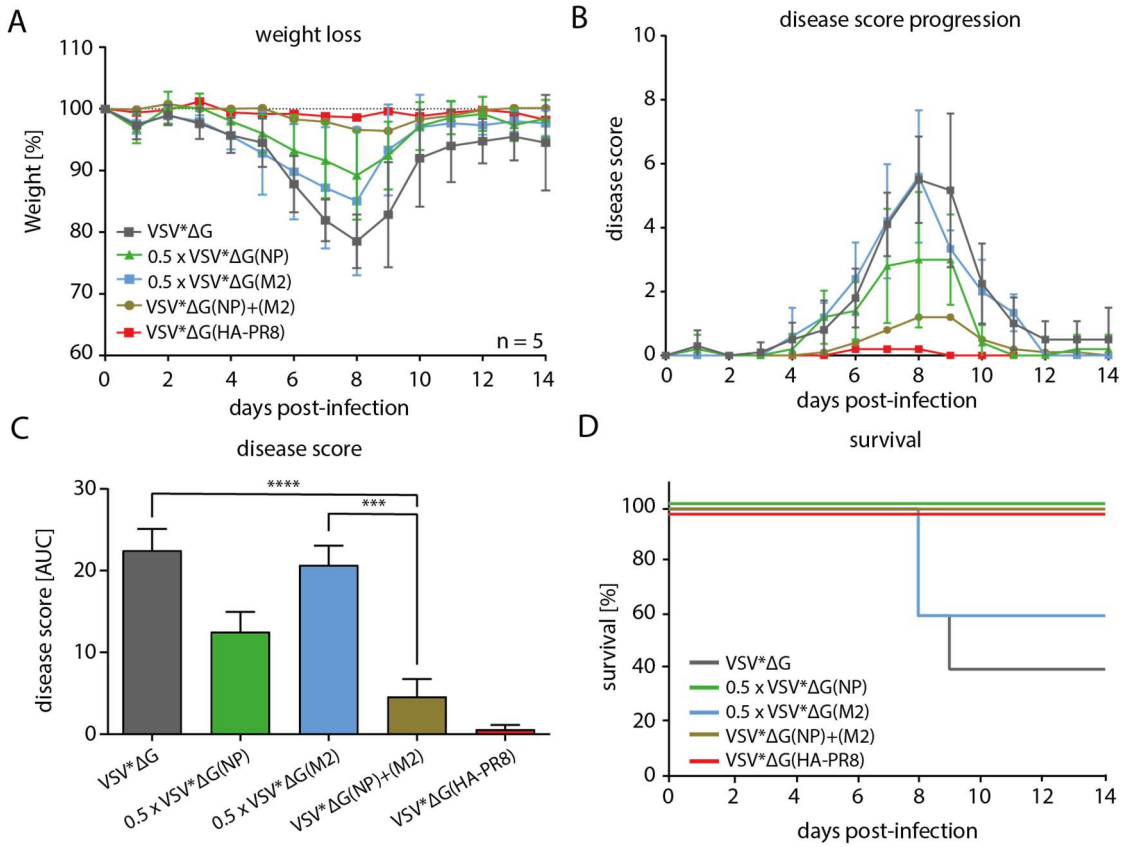

Figure 24: Protection of C57BL/6J mice against PR8 after prime-boost immunization with a double-cocktail immunization

To investigate the capability of compensation of the respective VSV replicons, C57BL/6J mice were immunized twice with a double-cocktail of $5.0x10^5$ ffu of VSV*ΔG(NP) + VSV*ΔG(M2) (VSV*ΔG(NP)+(M2)), or either $5x10^5$ ffu of VSV*ΔG(NP) or $5x10^5$ ffu of VSV*ΔG(M2) alone, and subsequently challenged with $6.0x10^2$ $TCID_{50}$ PR8. Notably, for single VSV replicon vaccination, $5x10^5$ of VSV*ΔG expressing no antigen was added respectively to reach an equal amount of administered replicon particles in all groups. (A) Weight loss of PR8 infected mice immunized with VSV replicons. All data points represent the mean and error bars are standard deviations. Dotted line indicates initial weight at the time of infection. (B) Clinical scores of infected mice, based on weight, behavior, and appearance. All data points represent the mean and error bars are SD. (C) Disease scores expressed as area under curve (AUC). Height of bars represent the mean and error bars are standard error of the mean (SEM). For statistical analysis, one-way analysis of variance (ANOVA) with Tukey's multiple comparison post-hoc-test using the VSV as a reference was performed. ***$p<0.001$; ****$p<0.0001$. (D) Survival rates of animals until day 14 of infection.

As low pathogenicity was still observed for animals challenged with PR8 after double-cocktail immunization, we hypothesized that a triple-cocktail containing the most promising antigens determined during single vaccinations (Figure 17) may further dampen the signs of infection and lead to a complete protection comparable to VSV*ΔG(HA-PR8). For this, we combined $0.3x10^6$ ffu of VSV*ΔG(NP) + VSV*ΔG(M2) + VSV*ΔG($H3_{stem}$), respectively to reach a total dose of 10^6 ffu per immunization (VSV*ΔG(NP)+(M2)+($H3_{stem}$)) (Figure 25). As described for the double-cocktail, we further used control groups to determine possible dilutions effects due to decreased amounts of single VSV*ΔG(X) replicons. When immunized with

the triple-cocktail, a profound weight loss was detected after challenge (Figure 25 A), however, this finding was not as prominent as in mock-immunized animals, reaching ~15% on average. In line with this, we found that this group recovered faster and reached initial weight at around 10 days post-infection. Clinical score progression was also decreased when compared to mock-immunized animals and resolved faster (Figure 25 B), which was confirmed by AUC calculation, revealing significantly decreased ($p<0.05$) pathology (Figure 25 C). Furthermore, we found a high survival rate (Figure 25 D).

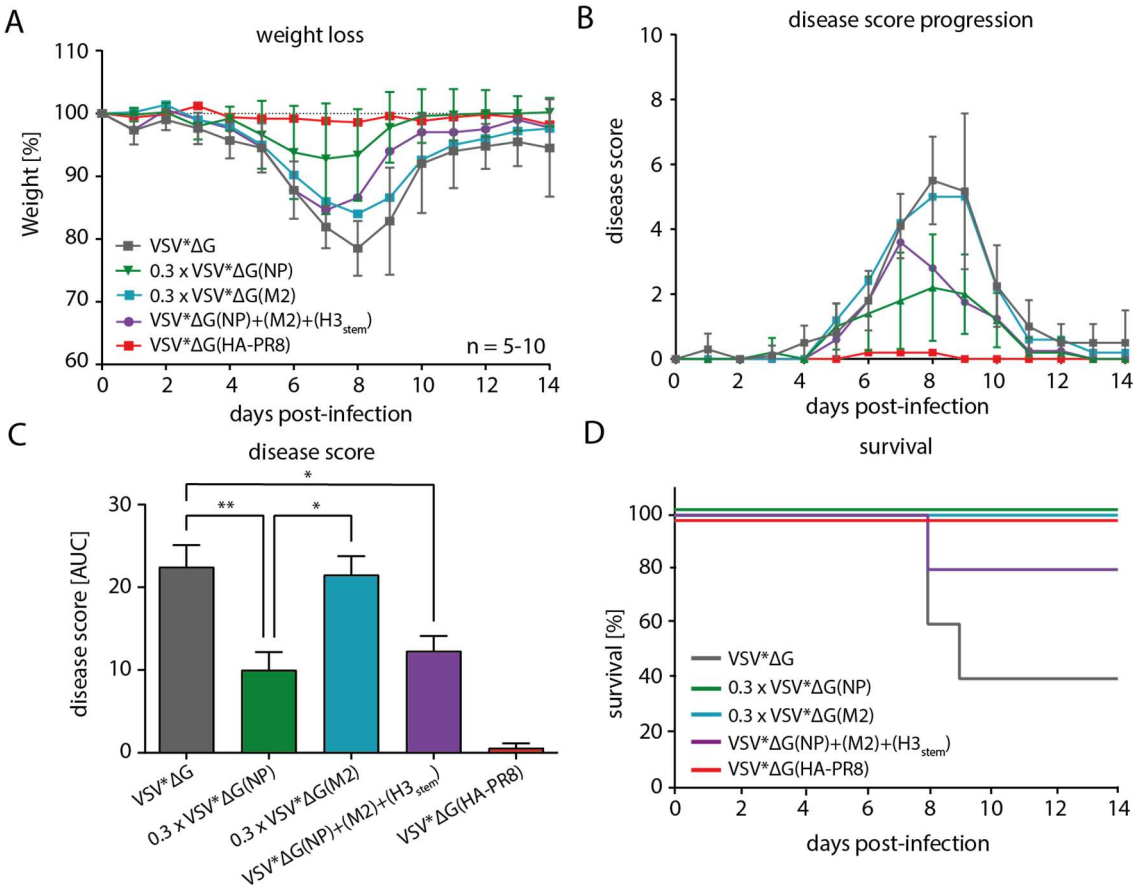

Figure 25: Protection of C57BL/6J mice against PR8 after prime-boost immunization with a triple-cocktail immunization

To investigate the capability of compensation of the respective VSV replicons, C57BL/6J mice were immunized twice with a triple-cocktail of $0.3x10^6$ ffu of VSV*ΔG(NP) + VSV*ΔG(M2) + VSV*ΔG($H3_{stem}$), respectively, or either $0.3x10^6$ ffu of VSV*ΔG(NP) or $0.3x10^6$ ffu of VSV*ΔG(M2) alone, and subsequently challenged with $6.0x10^2$ $TCID_{50}$ PR8. (A) Weight loss of PR8 infected mice immunized with VSV replicon cocktails. All data points represent the mean and error bars are standard deviations. Dotted line indicates initial weight. (B) Clinical scores of infected mice, based on weight, behavior, and appearance. All data points represent the mean and error bars are SD. (D) Disease scores expressed as area under curve (AUC). Height of bars represent the mean and error bars are standard error of the mean (SEM). For statistical analysis, one-way analysis of variance (ANOVA) with Tukey's multiple comparison post-hoc-test using the VSV as a reference was performed. *$p<0.05$; **$p<0.01$. (D) Survival rates of animals until day 14 of infection.

However, when compared to single VSV*ΔG(NP) (Figure 17) or double-cocktail vaccination (Figure 24), the triple-cocktail led to inferior protection, suggesting that the lower dose of each replicon used for immunization could be responsible for limited immune responses, which in turn reduced the overall protection. Interestingly, while groups immunized with either 0.3 x VSV*ΔG(NP) or 0.3 x VSV*ΔG(M2) showed prominent weight loss (Figure 25 A) and disease score progression (Figure 25 B), statistical analysis of disease scores (Figure 25 C) were highly comparable to those of 0.5 x VSV*ΔG(NP) and 0.5 x VSV*ΔG(M2) (Figure 24). Even more, animals immunized with 0.3 x VSV*ΔG(NP) had a significantly decreased overall disease score when compared to VSV*ΔG ($p<0.01$) and VSV*ΔG(M2) ($p<0.05$). Also, survival rates of both $0.3x10^5$ ffu single immunizations were 100% (Figure 25 D), which indicates that in fact protective responses are not vanishing through dilution of VSV*ΔG(X) replicon amounts.

In conclusion, we demonstrated that the double-cocktail immunization was superior to single VSV replicon vaccination (Figure 17) or triple-cocktail immunization (Figure 25) against PR8, as animals were completely protected from weight loss, pathogenicity, and death (Figure 24).

4.1.7 Cocktail Immunizations Induces Comparable Humoral Immune Responses Against PR8

To investigate the extent of humoral immune responses during cocktail-immunization, we determined total virus-reactive IgG titers against PR8 via IPMA 28 days after prime and boost, respectively (Figure 26). As demonstrated before, none of the mock-immunized animals developed antibodies reactive against PR8, while serum from the VSV*ΔG(HA PR8) groups showed a very strong reactivity. Interestingly, we observed highest antibody titers against PR8 after double-cocktail immunization, when compared to 0.5/0.3 x single or triple-cocktail immunization (Figure 26), correlating with protection efficacy during challenge experiments (Figure 24). Overall, although a trend of decreased antibody production reactive against PR8 appears when the dose of the respective replicon is diluted, this effect was not significant between any groups and is therefore in line with challenge experiments demonstrating comparable protection after 0.5 and 0.3 doses (Figure 24, Figure 25).

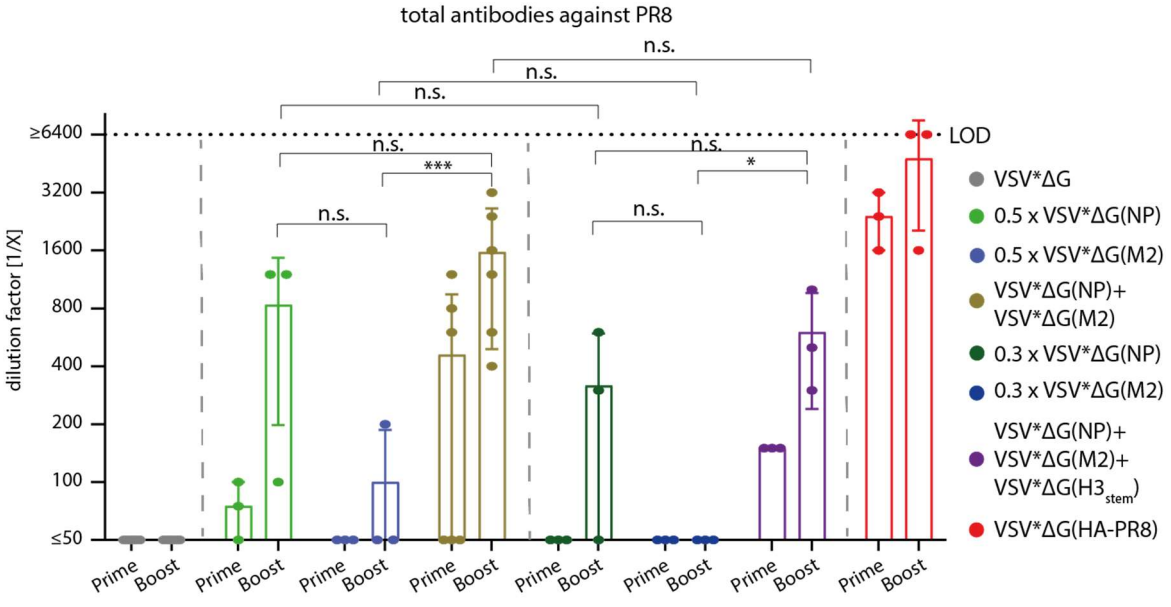

Figure 26: Total IgG antibody response of cocktail immunized animals against PR8

Total antibodies reactive against PR8 were evaluated via (IPMA). Upper dotted line indicates upper limit of detection. Height of bars represents mean and all error bars are standard deviations. For statistical analysis, two-way analysis of variance (ANOVA) with Dunnett's multiple comparison post-hoc test on log2-transformed titers was performed. *p<0.05; ***p<0.001. Significance levels for all prime immunizations and VSV*ΔG and VSV*ΔG(HA PR8) boost immunizations are not stated.

As it was observed that the double-cocktail immunization massively improves disease outcome, when compared to a triple-cocktail immunization, without significantly altering total antibody production, we hypothesized that the underlying IgG subclass profile determines reactive potential of humoral responses.

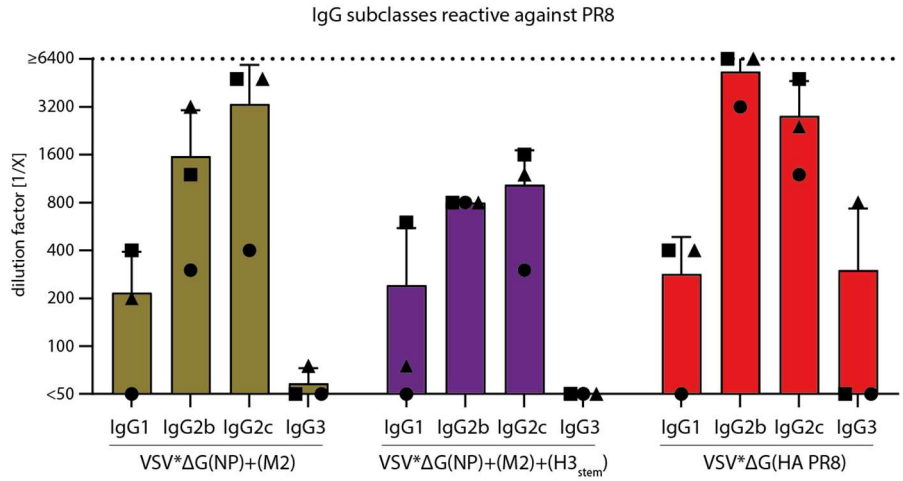

Figure 27: IgG-subclass analysis of cocktail immunized mice after boosting reactive against PR8

28 days after booster immunization, serum of mice was isolated and tested for IgG subtypes reactive against PR8 in an adapted IPMA, utilizing secondary α-mouse antibodies specific for either subtype. For statistical analysis, two-way analysis of variance (ANOVA) with Tukey's multiple comparison test on log2-transformed titers was used and significance levels compared to VSV*ΔG(HA PR8) are not stated. Upper dotted line indicates upper limit of detection. Each animal is indicated by an individual symbol.

We performed the before-mentioned modified IPMA, utilizing secondary α-mouse IgG antibodies against the respective IgG subtypes with serum we obtained 28 days after boost (Figure 27). We found IgG1, IgG2b, and IgG2c induced by both cocktail immunizations against PR8 to comparable levels, although a similar trend as for total IgG antibodies was observed (Figure 26).

4.1.8 Cocktail Immunizations Have Lower Effect Against rSC35M Challenge

To test the protective effect of the different cocktail immunizations against rSC35M infection, we immunized mice as described above, challenged with $1.2x10^3$ $TCID_{50}$ rSC35M 28 days after boost and monitored development of weight loss, clinical signs, and survival over 14 days (Figure 28). We observed severe weight loss of mock-immunized animals exceeding 25% in mean (Figure 28 A) and high clinical scores (Figure 28 B). Quantification of overall disease scores for VSV*ΔG cannot be calculated because all animals reached humane endpoints (Figure 28 D). Therefore VSV*ΔG(HA PR8) immunized mice were used as a reference for statistical analysis, as previous infection demonstrated similar disease progression between VSV*ΔG and VSV*ΔG(HA PR8) mice infected with rSC35M (Figure 18). In line with our expectations based on previous experiments, VSV*ΔG(HA PR8) immunizations did not lead to any degree of protection against heterologous challenge. Neither double-cocktail, nor triple-cocktail immunized groups were remarkably protected against the high pathology of viral infection as both groups lost up to ~20% of initial weight (Figure 28 A). However, assessment of clinical scores revealed, that triple-cocktail immunization resulted in significantly decreased ($p<0.05$) overall severity of infection, when compared to VSV*ΔG(HA PR8) (Figure 28 C). Furthermore, both cocktail immunizations led to the survival of 40% of animals (Figure 28 D). Based on former experiments (Figure 24 and Figure 25), resulting protection of single immunization with reduced doses can be considered to be inferior when compared to the combined cocktail vaccinations.

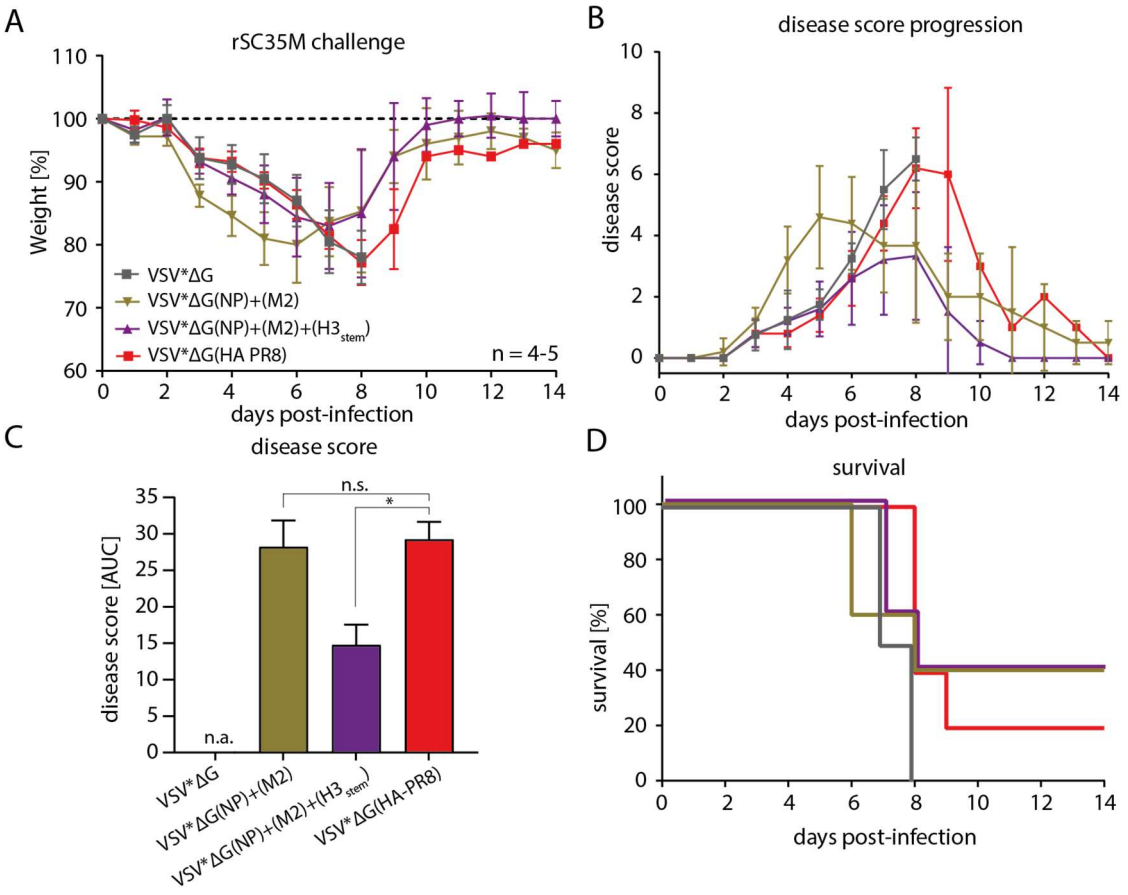

Figure 28: Protection of C57BL/6J mice against rSC35M after prime-boost immunization with different cocktail immunizations

To investigate the capability of compensation of the respective VSV replicons, C57BL/6J mice were immunized twice with a double-cocktail of $5.0x10^5$ ffu of VSV*ΔG(NP) + VSV*ΔG(M2), respectively, or a triple-cocktail with $3.3x10^5$ ffu of VSV*ΔG(NP) + VSV*ΔG(M2) + VSV*ΔG($H3_{stem}$), respectively, and subsequently challenged with $1.2x10^3$ $TCID_{50}$ rSC35M. (A) Weight loss of rSC35M infected mice immunized with VSV replicon cocktails. All data points represent the mean and error bars are standard deviations. Dotted line indicates initial weight. (B) Clinical scores of infected mice, based on weight, behavior, and appearance. All data points represent the mean and error bars are SD. (D) Disease scores expressed as area under curve (AUC). Height of bars represent the mean and error bars are standard error of the mean (SEM). For statistical analysis, one-way analysis of variance (ANOVA) with Tukey's multiple comparison post-hoc-test using the VSV as a reference was performed. *$p<0.05$. (D) Survival rates of animals until day 14 of infection.

To investigate the humoral immune responses elicited after cocktail immunization and reactive towards rSC35M, we again performed total IgG and IgG subclass titration utilizing IPMAs (Figure 29 and Figure 30). As expected, neither serum of VSV*ΔG or VSV*ΔG(HA PR8) group showed any reactivity with rSC35M serum (Figure 29). Although total IgG titers were significantly ($p<0.0001$) decreased in serum from triple-cocktail immunized animals when compared to double-cocktail immunized animals after prime vaccination, this effect was not present after boost. We therefore concluded that total amount of IgG present in the serum is not necessarily predictive for protection against challenge.

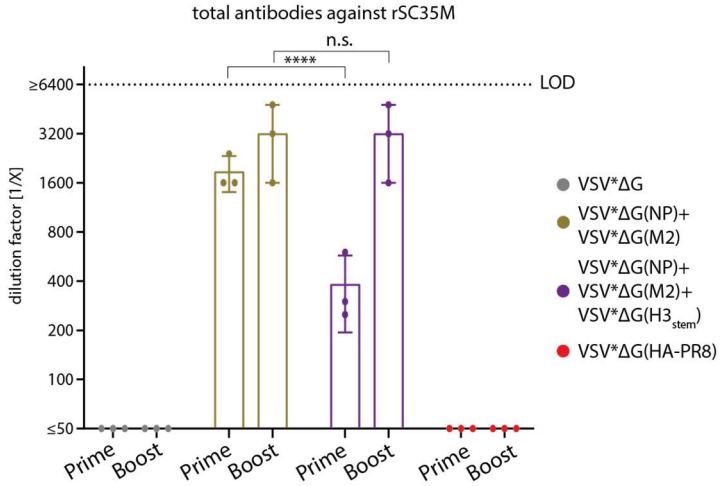

Figure 29: Total IgG antibody response of cocktail immunized animals against rSC35M

Total antibodies reactive against rSC35M were evaluated via (IPMA). Upper dotted line indicates upper limit of detection. Height of bars represents mean and all error bars are standard deviations. For statistical analysis, two-way analysis of variance (ANOVA) with Dunnett's multiple comparison post-hoc test on log2-transformed titers was performed. ****p<0.0001. Significance levels for VSV*ΔG and VSV*ΔG(HA PR8) immunizations are not stated.

When comparing IgG subclass profiles after different cocktail-immunizations, we did not detect striking differences (Figure 30). Although IgG3 levels after double-cocktail vaccination were slightly elevated when compared to triple cocktail groups ($p<0.05$), IgG1, as well as IgG2b/c titers were highly similar. From this IgG subclass profile, we concluded that IgG subclasses alone are not predictive for disease progress in the environment of multiple antigens using mixed VSV replicon vaccinations.

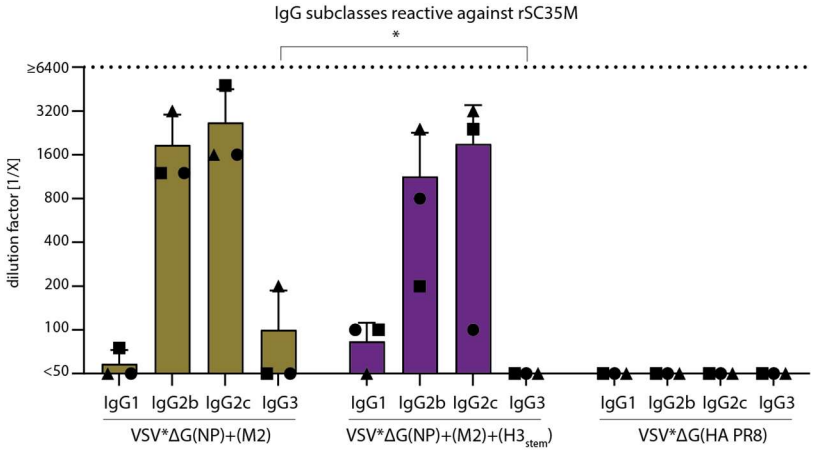

Figure 30: IgG-subclass analysis of cocktail immunized mice after boosting reactive against rSC35M

28 days after booster immunization, serum of mice was isolated and tested for IgG subtypes reactive against rSC35M in an adapted IPMA, utilizing secondary α-mouse antibodies specific for either subtype. For statistical analysis, two-way analysis of variance (ANOVA) with Tukey's multiple comparison test on log2-transformed titers was used and significance levels compared to VSV*ΔG(HA PR8) are not stated. *p<0.05. Upper dotted line indicates upper limit of detection. Each animal is indicated by an individual symbol.

Taken together, our results demonstrate that the internal proteins of IAV can be targeted by strong humoral immune responses and that these antibodies are able to confer protection in the absence of neutralization. In contrast, ADCP and ADCC are mediated by FcγR activation and lead to beneficial outcome after heterologous IAV challenge in terms of disease severity and overall survival. This underlines the protective potential of non-neutralizing antibodies and can serve as a basis for the rational design of heterologous IAV vaccines.

4.2 ADAR1 Has Proviral Activity for Influenza A Virus

4.2.1 ADAR1p150 is a Proviral Factor in HeLa Cells

It is known that the ADAR1p150 isoform can have a proviral impact on growth of several viruses by preventing innate immune activation through dsRNA intermediates (Pfaller et al. 2021). Cellular factors, known to be proviral for a great variety of viruses, represent a promising target for broadly acting antivirals, as development of one inhibitor can be used as a drug against multiple viruses. We therefore wanted to examine the role of ADAR1 during IAV infection. For this, we used the HeLa cell model, where the respective ADAR1p150^{KO} and ADAR1^{KO} (knockout of both ADAR1p150 and ADAR1p110 isoforms) cell lines were already available from previous studies (Pfaller et al. 2018). To investigate its effect on viral replication, the rSC35M virus was used, as initial experiments revealed that PR8 did not induce any visible cytopathic effect (CPE) in infected HeLa cells, whereas CPE was widespread after rSC35M inoculation (data not shown). We infected HeLa wild type, HeLa-ADAR1p150^{KO}, and HeLa-ADAR1^{KO} cells with an MOI of 1 and investigated viral protein expression via immunoblot analysis (Figure 31). While both isoforms of ADAR1 are clearly visible in HeLa wild type cells, ADARp150^{KO} and ADAR1^{KO} was confirmed by absence of specific bands (Figure 31 A). Interestingly, while absence of ADAR1p150 led to a pronounced reduction of the level of expressed IAV NP, this effect was less pronounced when both isoforms were lacking. To quantify this finding, we analyzed band intensity normalized to GAPDH staining (Figure 31 B). We demonstrated a significant difference ($p<0.05$) of IAV NP expression between HeLa-ADAR1p150^{KO} and HeLa wild type cells, whereas the difference between wild type and HeLa-ADAR1^{KO} cells was not significant. Remarkably, in contrast to previous observations regarding IAV proviral mechanisms of ADAR1p150 (Vogel et al. 2020), we did not find characteristic innate immunity pathways involved, as phosphorylation of the dsRNA-sensor PKR and the transcription factor IRF3 was not observed (Figure 31 A). To examine the generation of progeny virus during the absence of ADAR1p150 and ADAR1 in HeLa cells, we performed a growth curve analysis. However, after 24, as well as 48 hours, no infectious virus was detected in the supernatants of infected cells (data not shown). This circumstance made a different cell system necessary for further investigation.

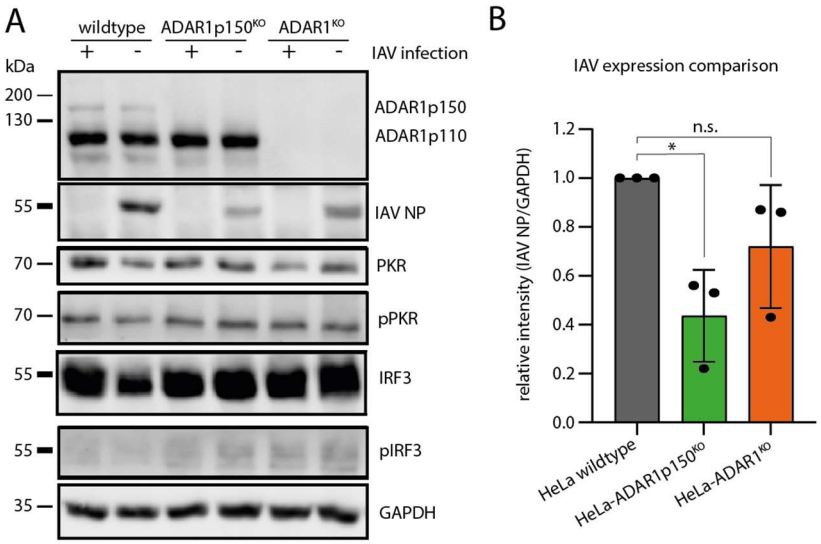

Figure 31: Proviral effect of ADAR1p150 in rSC35M infected HeLa cells

Wild type, ADAR1p150^{KO}, and ADAR1^{KO} HeLa cells were infected with rSC35M (MOI=1) and 24 hpi, cell lysates were produced and subjected to immunoblot analysis. (A) Representative blot showing ADAR1p150 and ADAR1p110 absence in knock-out cell lines. While IAV-NP expression was strongly decreased in HeLa ADAR1p150^{KO} cells, this was not as pronounced in the absence of both ADAR1 isoforms. No activation of characteristic innate immunity pathways was observed, regarding phosphorylated PKR (pPKR) and IRF3 (pIRF3). (B) Quantification (n=3) of IAV NP expression levels in the different cell lines. Height of bars represent the mean and error bars are standard deviations. For statistical analysis, one-way analysis of variance (ANOVA) with Tukey's multiple comparison post-test was used; *p<0.05.

4.2.2 Knock-out of ADAR1 in MDCK Cells Using the CRISPR/Cas9n System

To investigate if the absence of ADAR1p150 also reduces the amount of progeny infectious IAV particles, the MDCK cell line was used in which IAV can grow to high titers. We generated MDCK cells harboring either a knock-out of the ADAR1p150 isoform or both ADAR1 isoforms using the CRISPR/Cas9n system. For this we used expression plasmids expressing a Cas9n-2A-GFP fusion construct under control of the CMV promoter (Figure 32 A). The expressed protein is cleaved at the internal 2A autocleavage site, into the Cas9n enzyme and GFP as an expression marker. The plasmid further contains a U6-promotor driven cassette into which a guide RNA (gRNA) sequence can be inserted. The Cas9n endonuclease is a nickase, since it is only capable of inserting a single-strand break (Ran et al. 2013). We therefore used two plasmids with gRNA sequences in close proximity (gRNA1/2) to the target site and on the opposite strands of the DNA to induce a double-strand break resulting in functional gene knock-out.

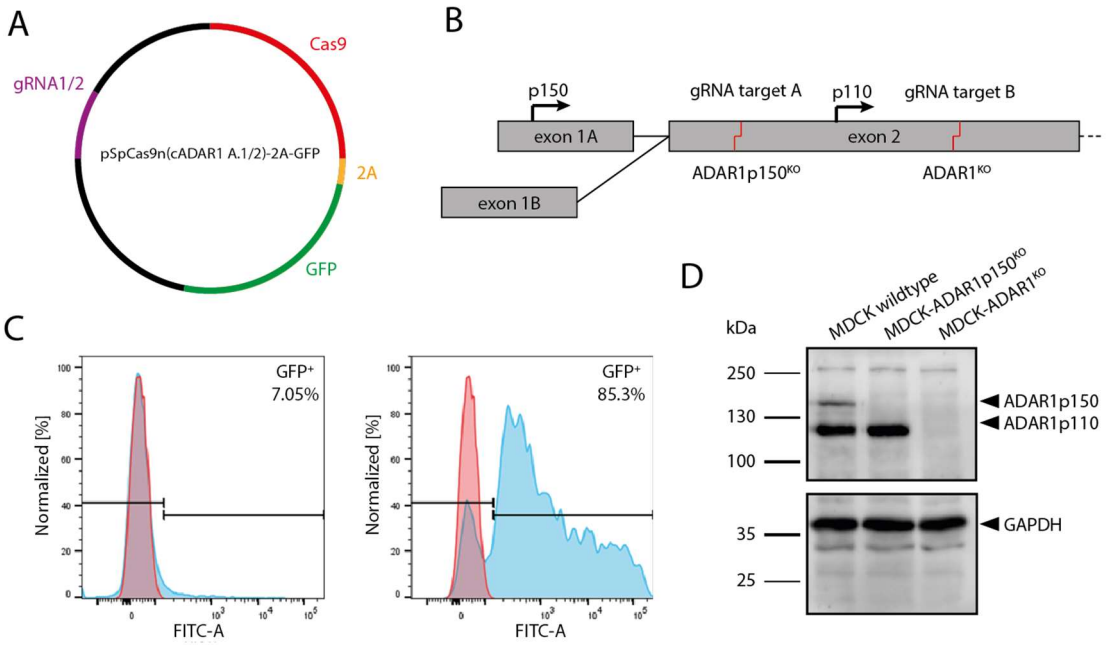

Figure 32: Knock-out of ADAR1 isoforms in MDCK wild type cells using CRISPR/Cas9n

(A) pSpCas9n(cADAR1 A.1/2)-2A-GFP expression plasmid used for ADAR1 knock-out in MDCK cells encoding for Cas9n endonuclease, a 2A internal-cleavage site, GFP, and one of two different guide RNAs (gRNA). (B) Genomic orientation of the *ADAR* gene. During maturation of pre-mRNAs, alternative promotor usage gives rise to ADAR1p150- or ADAR1p110-mRNA. While exon 1A contains a start codon that leads to the expression of ADAR1p150, exon 1B does not contain a start codon. This results in the translation initiation further downstream and by that expression of the shorter ADAR1p110 isoform. gRNA target sites A and B are indicated above, with the approximate site of cleavage indicated by a red, nicked line and the resulting knock-out underneath. (C) GFP expression of transfected MDCK cells pre-sorting (left) and post-sorting (right). (D) Immunoblot analysis of MDCK cell lysates, stained with α-ADAR1 antibody to confirm knock-out of ADAR1p150 or complete ADAR1. As a loading control α-GAPDH staining was used.

During the expression of the *ADAR* gene, alternative promoter usage results in expression of primary transcripts containing either exon 1A or exon 1B, from which the respective isoforms ADAR1p150 and ADAR1p110 are eventually expressed (Figure 32 B) (Pfaller et al. 2021). In case of gRNA pair A (gRNA A.1 + gRNA A.2), the Cas9n endonuclease cuts upstream of the ADAR1p110-start codon. This affects only the ADAR1p150 open reading frame, but not that of ADAR1p110. When gRNA pair B is present in the cell, Cas9n cleaves downstream of the ADAR1p110-start codon, thereby affecting both isoforms (Figure 32 B). Transfected GFP-expressing MDCK cells were sorted by flow cytometry to enrich transfected cells (Figure 32 C). While the average transfection efficiency was low (7.05% GFP^+ of all cells), their proportion was greatly enhanced (85.3%) after sorting. Individual cell clones were grown and screened for ADAR1 expression by immunoblot analysis. Several clones showed absence of ADAR1p150 or both ADAR1 isoforms (Figure 32 D) and representative clones were used in the subsequent experiments.

4.2.3 ADAR1 Knock-out Does Not Lead to Phenotypic Effects in MDCK Cells

In certain cell lines, loss of ADAR1 can induce cell death programs (Li et al. 2017), while in others it does not (Chung et al. 2018; Pfaller et al. 2018). To test whether the knock-out of ADAR1 affected the viability of MDCK cells, we monitored the appearance of the different cell line monolayers to investigate if cell shape or growth was altered (Figure 33). No obvious differences in growth, survival or appearance were detected when cells were seeded in cell-culture plates and examined through a light-microscope 24 hours later.

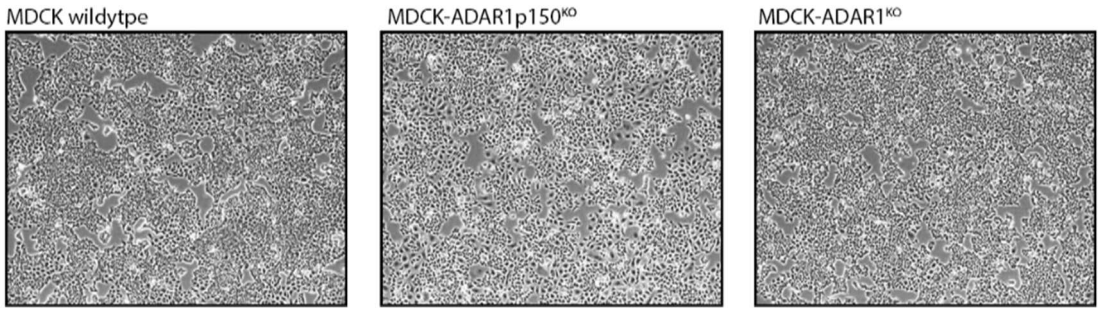

Figure 33: Appearance of MDCK wildtype, MDCK-ADAR1p150^{KO}, and MDCK-ADAR1^{KO} cells

Cells of the respective cell line were seeded in 6-well plates and incubated for 24 h at 37°C. Pictures were taken through a light microscope and do not show any noticeable differences in growth, survival, or appearance.

To examine the growth and survival kinetics of the different cell lines, we used a 3-(4,5-dimethylthiazol-2-yl)-2,5-diphenyltetrazolium bromide (MTT)-based assay, in which the yellow tetrazolium dye MTT is metabolized by the mitochondrial dehydrogenase to form purple formazan crystals (Figure 34 A). Since only living cells exhibit dehydrogenase activity, purple staining intensity after solubilization of formazan crystals positively correlates with cell number and can be used to assess cell growth and survival. By seeding cells sub-confluently and measuring the amount of produced formazan at different time points, we confirmed that cell growth is not severely altered between MDCK wildtype, MDCK-ADAR1p150^{KO}, and MDCK-ADAR1^{KO} cells during the first 48 hours after seeding (Figure 34 B). To evaluate if the different composition of serum-free medium used for upcoming infection experiments (DMEM^{-}) can have an impact on survival of confluent cell monolayers, were conducted a cell survival assay, were the amount of cells after medium exchange was measured. No significant differences were observed for any of the examined cell lines. Taken together, these results further illustrate that the knockout of

ADAR1p150 alone or in combination with ADAR1p110 did not result in phenotypical differences when compared to MDCK wild type cells.

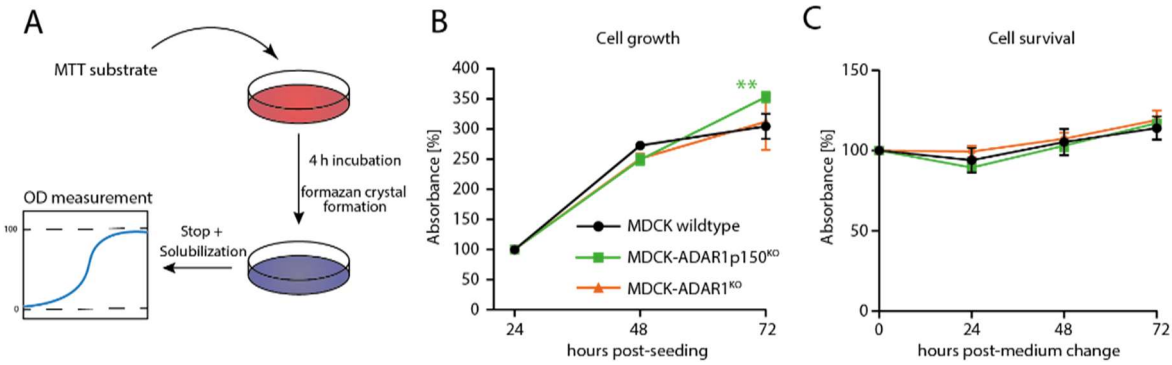

Figure 34: Cell growth and survival of different cell lines via MTT-based assay

(A) Schematic illustration of an MTT-based assay to determine the cell viability. The tetrazolium dye MTT (3-(4,5-dimethylthiazol-2-yl)-2,5-diphenyltetrazolium bromide) is added and metabolized by living cells to build formazan crystals. Solubilization of formazan crystals results in homogenous staining of supernatant and can be measured via absorbance at 570 nm. (B) MTT-based cell growth assay. After seeding the different cell lines sub-confluently, the amount of produced formazan was determined after 24, 48, and 72 hours-post seeding and normalized to absorbance 24 hours post-seeding for the respective cell line. (C) MTT-based cell survival assay to determine the influence of serum-free medium used for subsequent infections (DMEM$^-$) on the used cell lines. 24 hours after seeding, medium was changed and amount of cells was determined after 24, 48, and 72 hours. All values are normalized to the absorbance at the time of medium change for the respective cell line. Two-way ANOVA with Dunnett's multiple-comparison post-test was used for statistical analysis and **p<0.01.

4.2.4 ADAR1 Has a Proviral Activity in MDCK Cells

To investigate the effect of the different ADAR1 isoforms on IAV replication *in vitro*, we infected MDCK wild type, MDCK-ADAR1p150^{KO}, and MDCK-ADAR1^{KO} with PR8 and determined the viral titers in the supernatant at 24 and 48 hours post-infection via IPMA (Figure 35).

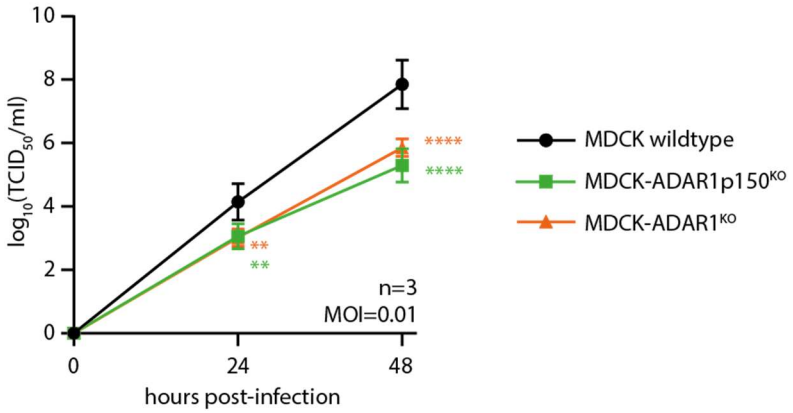

Figure 35: Viral replication of PR8 on different ADAR1 knock-out cell lines

Cell monolayers of MDCK wildtype (black), MDCK-ADAR1p150^{KO} (green), and MDCK-ADAR1^{KO} (orange) cells were infected with PR8 (MOI=0.01) and supernatant was titrated after 24 and 48 hours

via IPMA. Viral titers are expressed as $\log_{10}(TCID_{50}/ml)$. Two-way ANOVA with Dunnett's multiple comparison post-test was used to test for statistical significance with **p<0.01; ****p<0.0001.

We found that viral replication was significantly decreased in both cell lines lacking ADAR1 isoforms 24 hours post infection (p<0.01) and that this effect was even higher 48 hours post-infection (p<0.0001), demonstrating a proviral effect of ADAR1 also in the MDCK cell model. Finding viral replication impaired in both of the investigated cell lines leads to the conclusion that ADAR1p150 alone is responsible for the proviral effect, as additional knock-out of ADAR1p110 did not further lead to altered viral growth when comparing MDCK-ADAR1p150^{KO} and MDCK-ADAR1^{KO} cells.

4.2.5 ADAR1 Knock-out Results in Increased Resistance Against IAV-Induced Cell Death

It is well established that IAV infection induces several cell death pathways as a result of dsRNA-sensing by innate immune receptors (Laghlali et al. 2020; Jiao et al. 2020; Zhang et al. 2020).

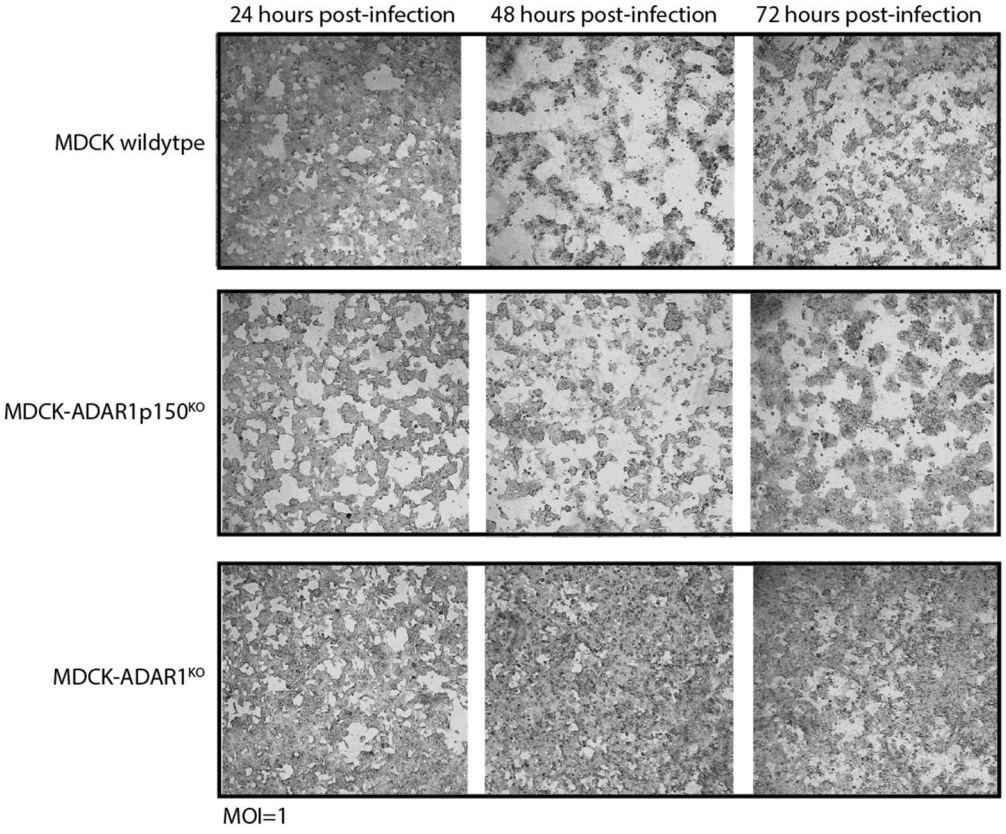

Figure 36: Evaluation of cell monolayer disruption after PR8 infection

Cells were seeded in 24-well plates and confluent monolayers were infected with MOI=1 of PR8. 24, 48, and 72 hpi, IPMA staining was performed to better visualize the infected monolayer and increase

contrast of cells. Representative pictures of MDCK wildtype (upper lane), MDCK-ADAR1p150^{KO} (middle lane) and MDCK-ADAR1^{KO} (lower lane) cells were taken using a light microscope.

Therefore, we further investigated if lack of ADAR1 isoforms affected cell survival in response to IAV infection. We infected the different MDCK cell clones with PR8 at an MOI of 1 and examined the occurrence of cytopathic effect for up to 72 hours (Figure 36). In addition, we performed IPMA staining to visualize infected cells. High MOI was chosen to ensure equal infection in the majority of cells. Surprisingly, neither MDCK-ADAR1p150^{KO}, nor MDCK-ADAR1^{KO} cells were found to induce increased cell death upon infection. In contrast to our initial expectations, while ADAR1p150^{KO} did not have any striking effect when compared to MDCK wildtype cells (middle lane), ADAR1^{KO} seemingly conferred protection against infection-induced cell death (lower lane).

A MTT-based survival assay was used to further examine and measure the magnitude of cell death after PR8 infection. For this, we seeded and incubated the different cell lines for 24 hours before we infected them with different MOIs reaching from 0.01 to 5. 24, 48, and 72 hours post-infection, we measured the cell viability as described above (Figure 37 A).

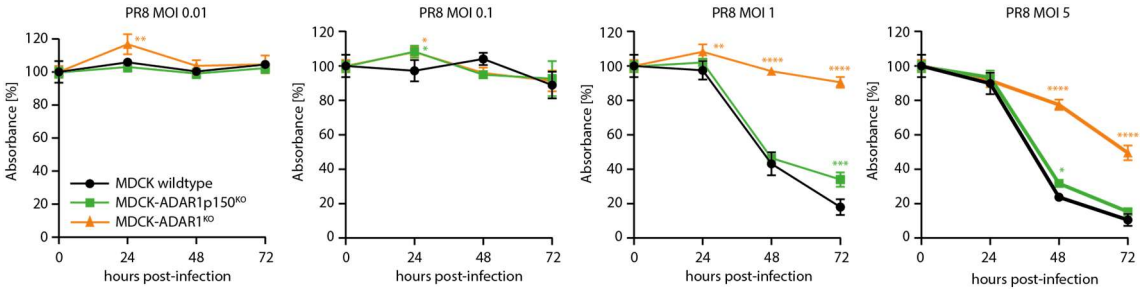

Figure 37: MTT-based survival assay to investigate IAV-induced cell death in absence of ADAR1

Cells were seeded and 24 hours later infected with different MOIs of PR8 virus ranging from MOI=0.01 to MOI=5. At 0, 24, 48, and 72 hpi, MTT substrate was added to determine the amount of living cells after infection. Absorbance was normalized to the initial value representing cell numbers before infection, respectively. Two-way ANOVA with Dunnett's multiple-comparison post-test was used for statistical analysis and *p<0.05; **p<0.01; ***p<0.001; ****p<0.0001

Infection with low MOIs of 0.01 and 0.1 had no profound effect on cell viability in any of the cell lines. However, when cells were infected with MOI=1 or MOI=5, a strong induction of cell death was observed between 24 and 48 hours post-infection in MDCK wild type and MDCK-ADAR1p150^{KO} cells. This is in line with our observations from previous experiments (Figure 36). In contrast to this, MDCK-ADAR1^{KO} cells resisted to cell death and maintained cell numbers throughout the 3

days for MOI of 1, revealing significant differences already 24 hours post-infection ($p<0.01$). This effect was even stronger after 48 and 72 hours. The same trend was seen for an infectious dose of MOI of 5, as significant differences ($p<0.0001$) were observed from 48 hours on. These results are in line with our observations from previous experiments (Figure 36) and confirm the inherent protection against IAV-mediated cell death in our MDCK cell model when both isoforms of ADAR1 are knocked out.

In summary, we confirmed our hypothesis of a proviral activity of ADAR1 for different IAVs and in different cell types. While we observed impaired IAV NP levels in the absence of ADAR1p150 in HeLa cells, our MDCK cell model harboring different KOs of ADAR1 isoforms revealed that this also affects virus replication. The presented results, in combination with previous reports about proviral effect of ADAR1 on other viruses, support the assumption that ADAR1 can be used as a promising target for broadly-acting antivirals.

5 DISCUSSION

Since IAV is a major burden for the human population, many countermeasures have been developed in the past to fight disease and mortality associated with infection. These can either be vaccines, acting prophylactically, or antivirals, acting therapeutically. However, genetic variability between different IAV strains can render these countermeasures inefficient, so that currently licensed vaccines provide sub-optimal protection against infection and drive antigenic drift of seasonal influenza virus (Hensley et al. 2009). Furthermore, emergence of different avian IAVs that crossed the species-barrier in the past fuel the fear for potential pandemics of new reassortants (Fouchier et al. 2004; Yuen et al. 1998; Peiris et al. 1999). Although antiviral reagents have been developed to treat severe cases of IAV when vaccine protection fails, evolving resistance highlights the need for development of additional countermeasures which efficiently inhibit IAV mutants as well. Here, we investigated protective adaptive immune responses towards conserved antigens of LAIV against heterologous strains of flu in a mouse model and characterized mechanisms by which these responses can drive protection. Furthermore, we examined the influence of the host factor ADAR1 on IAV replication, which is known to be proviral for several viruses and thus a potential target for broadly acting antivirals.

5.1 Humoral Immune Responses Against Internal Influenza A Virus Proteins

We demonstrated that VSV-vectored immunization against different proteins of IAV can result in protective immunity against challenge and that this protection is not based on cellular, but humoral immunity. It has to be highlighted that we utilized a heterologous immunization-challenge model, as the antigens used for immunization were derived from the LAIV Fluenz®. We further showed that vaccination with VSV-vectors expressing M2, $H3_{stem}$, or the internal protein NP, in contrast to M1, led to activation of FcγR, which is a strong indicator for antibody-dependent cell-mediated cytotoxicity (ADCC) and antibody-dependent cell-mediated phagocytosis (ADCP). Combination of the most promising antigens in a cocktail immunization against PR8 revealed that the immune responses against NP and M2 had synergistic effects. The findings provide novel considerations for the future design of broadly acting IAV

vaccines. As currently licensed IAV vaccines are protecting insufficiently against heterologous IAVs, enhancing the breadth of the immune response is urgently needed to prepare for potential outbreaks of pandemic IAVs.

In the past, different approaches were used to achieve this enhancement, mainly by targeting conserved antibody domains like the stem region of HA (HA_{stem}) or the ectodomain of the M2 ion channel (M2e) (Impagliazzo et al. 2015; Neirynck et al. 1999), or by inducing cytotoxic T cell responses towards internal proteins like NP or M1 (Ulmer et al. 1993; Xie et al. 2009). Using VSV replicons to express the internal proteins NP and M1, we compared the humoral immunity towards those antigens with the immune response against widely used HA_{stem} and M2 antigens. Remarkably, in our experiments, NP induced even higher antibody titers than $H3_{stem}$ and M2. In the past, humoral immune responses against internal, conserved IAV proteins have been neglected, as they are not directly accessible for antibodies and thus are assumed to play only a minor role in protection compared to antibodies against surface antigens. However, it was shown that NP can be exposed on the surface of infected and dying cells, and that monoclonal antibodies against NP can protect against IAV pathogenicity and high viral lung titers in the mouse model when expressed *in vivo* or even after serum transfer (Virelizier et al. 1977; Carragher et al. 2008; Fujimoto et al. 2016; LaMere et al. 2011). The proposed mechanisms of action for non-neutralizing antibodies are based on FcγR effector functions and include ADCC, ADCP, and complement activation (Krammer 2019). We showed that immunization with NP, which partially protected from severe disease, induced the generation of IAV-specific total IgG levels, and especially IgG2b/c subclasses, which are known to confer antibody-dependent cell-mediated cytotoxicity. In fact, we demonstrated activation of FcγRIV by NP-specific antibodies, and also M2- and $H3_{stem}$-specific antibodies. Activation of FcγRIV by IgG2c and IgG2b can induce both ADCC and ADCP and may therefore represent a correlate of protection. However, the complex interplay between the different IgG subclasses is not fully understood and more insights are needed to reliably resolve the different, overlapping, or subsidiary functions of murine IgG. This is also stressed by a recent publication demonstrating that non-neutralizing IgG1 can suppress the protective efficacy of IgG2 by competitively binding to the virus and thereby reducing IgG2-effector functions (Shibuya et al. 2020).

Our findings underline the neglected potential of humoral immunity especially towards NP and reasons the inclusion of antibody epitopes from internal proteins to the concept of future IAV vaccine design.

5.1.1 VSV-based Replicons As a Vaccine Platform

We applied the VSV*ΔG replicon platform to investigate immune responses towards different IAV proteins. We showed via immunoblot and immunofluorescence analysis that insertion of different IAV genes into the VSV*ΔG replicon genome led to efficient expression of the respective proteins. Thus, the VSV platform serves as a versatile tool to express heterologous surface and internal antigens and to induce a broad range of immune responses against these antigens.

VSV was first investigated as a vaccine vector in 1998 (Roberts et al. 1998) and was since used for numerous preclinical and several clinical studies. In contrast to many other viral vectors discussed as vaccine candidates, like adenoviruses, poxviruses, or lentiviruses, VSV lacks a DNA intermediate in its replication cycle. This is a major safety advantage, as the risk of genome integration is avoided. Uncertainties about possible frequency and location of integration after administration of adenoviral vectors in the currently ongoing SARS-CoV-2 pandemic have fueled public discussion about their safety (Doerfler 2021; Mendonça et al. 2021). Regardless of the outcome of those discussions, doubts about safety of distinct vectors can lead to hesitation of populations in taking the vaccine, which is a critical factor for pandemic situations like SARS-CoV-2 or potentially upcoming IAVs. However, compared to most other viral vectors, VSV has a relatively small packaging capacity of approximately 6 kb, which is lower than for those mentioned above; poxviruses for example can package up to 30 kb (Lundstrom 2021). Another virus investigated as a potential vaccine vector is measles virus. Whereas measles virus does also not generate DNA during its replication cycle, it has the great disadvantage of neutralizing immunity present in most of the population, which raises discussions about its potential to be used as a vaccine vector. Similar concerns are appropriate for boosting the immune responses using two identical VSV vectors. Neutralizing antibodies against VSV-G generated after prime immunization may prevent transduction of cells and thereby protein expression after booster immunization. However, although we measured neutralizing antibodies directed against VSV-G after a first vaccination (data not shown), we can clearly demonstrate boosted

humoral responses after second vaccination in our mouse model. This indicates that existing immunity does not completely prevent efficient booster immunization.

Another main advantage of VSV as a vector is its ability to induce especially humoral, but also cellular immunity in many animal models (Humphreys and Sebastian 2018). However, VSV has to be attenuated to meet safety requirements, as non-attenuated VSV was shown to be neurovirulent (Johnson et al. 2007). We used a VSV vector lacking the VSV-G gene (VSVΔG), to generate single-round replicons. It was initially assumed that the attenuation-strategy may play an important role for its potential to induce immune responses towards encoded antigens, depicting VSV as an inflexible tool concerning its utilization as a vaccine vector. These assumptions were based on first clinical studies using a VSV-G-truncated vector against HIV gag protein (rVSVN4CT1-HIV-gag), which elicited modest CD4+ T cell responses and just low humoral immunity in many participants (Fuchs et al. 2015). In contrast to this, VSVΔG expressing the glycoprotein of Ebola resulted in strong antibody production, although also here, only low T cell responses were observed (Dahlke et al. 2017). These experiments paved the way for further optimization of VSV as a vaccine platform and resulted in the development of the first approved Ebola vaccine in 2019 (Ervebo) (Marzi et al. 2015; Banadyga and Marzi 2017). However, when comparing the above-mentioned platforms, it has to be taken into consideration that the choice of antigen as well determines strength and shape of the immune response. In fact, it was shown recently that VSV-G truncated vector expressing the glycoprotein of Ebola (rVSVN4CT1-EBOVGP), can not only protect non-human primates from lethal challenge (Matassov et al. 2015), but was also proven to be safe and highly immunogenic in a Phase I clinical trial, as 100% of participants in a high dose group developed neutralizing antibody titers (Clarke et al. 2020). This underlines the diverse possibilities of attenuating VSV and use it as a vaccine vector. Nevertheless, it has to be stressed that the glycoprotein of Ebola can facilitate infection of host cells in the context as rVSVN4CT1-EBOVGP, making this vector replication-competent.

VSV vectors have gained increasing attention during the currently ongoing SARS-CoV-2 pandemic as a promising platform to develop efficient vaccines. However, substituting VSV-G with heterologous viral surface proteins may lead to efficient replication and propagation of the viral vector (Case et al. 2020), which can have a substantial impact on tissue-tropism and induced pathogenicity by vaccine

candidates. In a recent publication, we reported on our approach to generate single-cycle VSV replicons as a vaccine vector against SARS-CoV-2 (Hennrich et al. 2021). These vectors were VSV-G deficient and encoded a chimeric protein of the receptor-binding domain (RBD) of SARS-CoV-2 spike protein and the transmembrane stem-anchor domain of the rabies virus glycoprotein (VSVΔG-minispike-eGFP). We demonstrated development of high titers of neutralizing antibodies in human ACE2-expressing transgenic mice after single immunization, which resulted in protection against several SARS-CoV-2 variants, including Wuhan (Hennrich et al. 2021), delta, and omicron (unpublished). Nevertheless, protection was diminished when animals were challenged with omicron variant, representing immune escape of the SARS-CoV-2 RBD. This shows that not only for IAV, but also for other viruses, broader immune responses are desirable and a bivalent VSV vector approach, as we used it in our cocktail immunizations against IAV, may be a promising tool to achieve that. We showed that the VSV replicons used in the project of this thesis are only capable of replication when VSV-G is provided *in trans*, even when the full-length HA of IAV is present. As it was found that IAV HA is very efficiently incorporated into VSV*ΔG replicons, lack of replication is most probably based on the lack of IAV NA (Kretzschmar et al. 1997).

5.1.2 Expression of $H3_{stem}$ Construct

Although modifications in the primary structure of antigens often rise concerns about the correct folding of secondary and tertiary structure, it has been demonstrated for $H3_{stem}$ that replacement of the head domain with a flexible linker consisting of four glycines does not disrupt the structure of the stem region, and that expression is comparable to full-length HA (Steel et al. 2010). The two cysteines flanking the substituted head domain are predicted *in silico* to build a stabilizing disulfide bond and were therefore used in previous studies to define the boundaries of N-terminus and C-terminus of the stem domain. We designed our $H3_{stem}$ construct based on the same concept, since these stabilizing residues were conserved in the HA derived from the A/Hong Kong/4801/2014(H3N2)-like IAV in our vaccine preparation. We were able to detect expression of our construct using HA-specific antibodies in an immunofluorescence microscopy assay, confirming that $H3_{stem}$ is efficiently expressed and presented on the surface of VSV*ΔG($H3_{stem}$) transduced cells.

HA can be categorized into two different groups, group 1 HA and group 2 HA, based on their phylogenetic similarities (Sutton et al. 2017). While H1 (PR8) belongs to group 1 HA, H3 (Hong Kong-like) and H7 (rSC35M) are classified in group 2 HA. This in in line with our amino acid homology analysis, showing a higher similarity between H3 and H7 (59.4%) than between H3 and H1 (46.8%) and stresses the challenge of HA_{stem}-based approaches, namely the broad protection against both groups of HA (Table 11). Interestingly, we found in our immunofluorescence analysis that H1 serum as well as H3 serum were capable of reacting with the $H3_{stem}$ construct, while full length PR8-derived HA only was recognized by H1 serum. Taken together, we did not only confirm efficient expression of our $H3_{stem}$ construct on the surface of VSV*ΔG($H3_{stem}$) transduced cells, but also showed that $H3_{stem}$ was bound by antibodies occurring after natural H1 or H3 IAV infection.

In our initial amplification strategy to obtain the LAIV-derived HA gene, we used primers potentially binding to H1 as well as H3, but nevertheless we only obtained H3 gene sequences. It would have been interesting to investigate the cross-reactivity of H1 and H3 sera against this $H1_{stem}$ construct and determine its protective potential during challenge experiments. Although these experiments have to be performed first, it can be hypothesized that $H1_{stem}$ more effectively protects against PR8 than rSC35M, which would be in line with our findings of $H3_{stem}$ and the above-described bias towards neutralization of HAs of the same group like the immunization antigen. Our results confirm the broader reactivity of HA_{stem}-directed antibodies via immunofluorescence and at the same time highlight restrictions of these approaches during antibody titrations.

5.1.3 Protection Against Heterologous IAV Challenge After VSV Replicon Immunization Correlates With Humoral Immune Responses Towards Internal Proteins

We show in our mouse model that VSV*ΔG(HA PR8) immunization resulted in complete immunity against the homologous PR8 virus, but no signs of protection in case of the heterologous rSC35M, emphasizing the limited protection of HA-based vaccines against heterologous strains. Although we observed some weight loss and development of symptoms in all groups of NP, M2, and $H3_{stem}$ vaccinated mice after challenge with PR8 or rSC35M, these antigens provided at least partial protection

against IAV-induced lethal infection, reducing overall disease scores, and improving survival rates of infected animals.

NP vaccinated animals exhibited reduced loss of weight and fast recovery, but immunization did not completely avoid disease. This phenotype is characteristic for non-sterile immunity, which is often contributed to cytotoxic T cells killing infected cells, in contrast to HA-based immunity which is mediated by antibodies directly neutralizing incoming virus particles. Because of this, we first hypothesized that the observed protection after VSV*ΔG(NP) immunization is based on T cells, especially $CD8^+$ T cell, which would be in line with previous publications. Different approaches using DNA-based vaccines (Ulmer et al. 1993; Laddy et al. 2008), viral vectors (Goodman et al. 2011; Hessel et al. 2014; Sipo et al. 2011), or recombinant protein (Li et al. 2021b; Del Campo et al. 2019) not only demonstrated that vaccination with NP can efficiently protect from lethal homologous as well as heterologous challenge, but also that this strongly correlates with $CD8^+$ T cell responses. Many of these studies detected measurable antibody titers, but experiments mainly focused on $IFN\gamma^+$ T cells. Although we found comparable or even superior protection after VSV*ΔG(NP) immunization, $IFN\gamma^+$ cellular immunity for any of the immunized groups was not found to be significantly elevated. A possible reason for these differences is the vector used, as it is well known that the elicited immune response highly depends on these and can vary strongly between different approaches. In line with this is an observation in a similar study using VSV replicons expressing IAV NA, where no significant $IFN\gamma^+$ T cell responses were reported (Walz et al. 2018). However, a comparable approach by Barefoot et al. in 2009 used a VSV vector expressing IAV NP and detected $CD8^+$ T cells directed against the immunodominant $NP_{366\text{-}374}$ in C57BL/6 mice, which express MHC class I H2-D^b (Barefoot et al. 2009). Notably, Barefoot et al. showed PR8-reactive $CD8^+$ T cells in mice after immunization with the homologous NP. In contrast, we used a heterologous NP derived from the LAIV for immunization, and the immunodominant peptide exhibits an amino acid substitution in this strain (366-ASNENMDTM-374) compared to both PR8 and rSC35M (366-ASNENMETM-374). This mutation may affect the ability of this epitope to efficiently generate PR8/rSC35M-reactive $CD8^+$ T cells.

In a different study, it was shown that BALB/c mice immunized intranasally with Fluenz® induced high numbers of NP-reactive $CD8^+$ T cells, but that this was not

sufficient to decrease viral lung titers or to avoid weight loss after heterologous PR8 challenge (Slütter et al. 2013). However, survival was increased and challenged mice recovered faster from the infection. When these mice were boosted with recombinant NP from PR8, protection was significantly increased in terms of viral load in the lung, survival, and weight loss. This indicates that NP-reactive $CD8^+$ T cells against heterologous viruses may be rather an advantage as a priming basis, which can then be broaden by appropriate boosting and that it not per se provides protection (Slütter et al. 2013). The striking difference here is that BALB/c mice express MHC-I H2-K^d, and the immunodominant epitope of NP is formed by amino acid residues 147-TYQRTRALV-155, which are absolutely conserved between the LAIV, PR8, and rSC35M strains. This shows how important it is to consider the MHC-I genotype when interpreting the protective effect of T cell epitopes. This in in line with observations from humans, where specificities of $CD8^+$ T cell responses after H1N1 infection were different from those measured after a previous H3N2 infection (Souquette and Thomas 2018). In our C57BL/6 model, potential $CD8^+$ T cells directed against Fluenz® NP may therefore not directly respond to PR8 or rSC35M infected cells to a measurable extent, while experiments performed in BALB/c mice may have led to the opposite result. To confirm whether peptide 366-374 of Fluenz® serves as a specific T cell epitope, experiments using Fluenz® infected stimulator cells would be necessary. Further experiments to get insights into potential T cell responses could also be addressed by stimulating splenocytes of vaccinated mice with heterologous, immunodominant epitopes like $NP_{366\text{-}374}$.

Although we did not observe strong $IFN\gamma^+$ T cell responses, high antibody titers after VSV*ΔG(NP) vaccination were produced. We therefore hypothesized that instead of $CD8^+$ T cells, $CD4^+$ T cells are generated, as these are essential for activation of B cells to form antibody-producing plasma cells. We chose IL-4 as a prominent $CD4^+$ T cell cytokine and determined its release in the supernatant of stimulated splenocytes. However, we did not observe significantly elevated IL-4 responses in any of the vaccinated groups, which indicates that in fact stimulation of splenocytes with infected cells is either too weak to induce a measurable response, or that Fluenz®-reactive T cells are not sufficiently reactivated by PR8- or rSC35M infected cells. The same considerations as for $CD8^+$ T cells may be applicable, as underlying $CD4^+$ T cells responses are not per se providing protection but can serve as a basis for subsequent broadening of immune reactions towards heterologous challenge virus.

We did not observe any beneficial effects after VSV*ΔG(M1) immunization against either virus, which is in line with other studies defining protection via M1 alone as negligible (Chen et al. 1998; Wiesener et al. 2011). As VSV*ΔG(M1) immunization did not provide any kind of protection during our challenge experiments, this is strong evidence that we did not fail to detect any existing T cell responses, and this is also an important consideration for the other VSV*ΔG(X) constructs. We concluded that in our model, the existing antibody responses were a stronger correlate of protection than cellular immunity via cytotoxic T cells. In our hands, VSV*ΔG(M1) failed to induce influenza-reactive antibodies. In contrast to NP, there is currently no strong data available suggesting surface presentation of M1 in infected or apoptotic/necrotic cells, and low levels of seroconversion after IAV infection in humans suggests suboptimal presentation of M1 to elicit humoral responses (Cretescu et al. 1978). In another study, immunization with M1 VLPs was able to reduce lung viral load after infection, but no IgG was detected (Moon et al. 2019). This strengthens the hypothesis that M1-mediated protection, if present at all, is not based on antibodies. It is also in line with previous studies where M1 vaccination utilizing recombinant vaccinia virus resulted in low humoral responses and absence of protection (Wang et al. 2015).

Investigations on $CD8^+$ T cell responses towards HA_{stem} or the complete HA protein are by far less often reported than NP or M1, presumably because the hemagglutinin of IAV is considered a target for antibodies and not cellular immunity. However, it was reported recently that immunization with different constructs of adjuvanted, chimeric HA can induce T cell responses dependent on the amino acid sequence of the HA_{stem} region (Liao et al. 2020). Although granzyme B production was measured and not IFNγ, this clearly indicates that $CD8^+$ T cell responses can be generated after HA immunization. Unfortunately, the exact peptides used for ELISpot stimulation are not stated, making it hard to determine whether these epitopes are conserved between the different strains of our study. Similar conclusions about M2 can be drawn. Although M2, especially the ectodomain M2e, are mainly considered to be antibody targets, different reports demonstrate that indeed T cell responses can be elicited against M2. This holds true for T cell responses in individuals after infection (Lee et al. 2008) as well as experimental vaccine approaches in mice (Herrera-Rodriguez et al. 2018). In summary, the generation of NP-, M2-, and $H3_{stem}$-specific antibodies suggests that T cells responses directed against the LAIV-derived antigens

exist, since these responses are required for efficient plasma cell and antibody generation. These T cell responses are likely directly activated by LAIV infection, which we unfortunately did not test. However, they are not directly activated by our challenge IAV strains PR8 and rSC35M, and therefore, T cell responses did likely not contribute to the protective effects observed in immunized mice.

The fact that we found non-neutralizing antibodies but did not detect T cell-meditated immunity against the challenge viruses in our model evokes the question how these antibodies could contribute to the partial protection in our challenge model. It was shown previously that IgG levels, as well as T cell immunity, are strong correlates for survival after vaccination with recombinant NP or M2e, independent of neutralizing activity of antibodies (Wang et al. 2012). In this regard, non-neutralizing antibody responses, especially FcγR effector functions like ADCC and ADCP, induce clearance of infected cells and can result in the observed protection. To investigate this possibility, we first examined the induced IgG subclass profiles after vaccination, as they are known to drive different effector functions. In a final step, we then determined if the antibodies can in fact activate ADCC/ADCP.

The modality (viral vector, adjuvanted protein, DNA, etc.) used to immunize mice is crucial for the shape of the IgG subclass expression (Hocart et al. 1989, 1988; Balkovic et al. 1987). These IgG subclasses bind to the FcγRs with different affinities and thereby trigger specific immune functions. Furthermore, they can affect each other, as recently shown by Shibuya et al, who demonstrated that high IgG1 titers inhibited IgG2-mediated FcγR functions. Our IgG subclass analysis revealed significant differences concerning the humoral immune response induced against the single IAV antigens, and most remarkably we found low IgG1 and high IgG2b/c titers in VSV*ΔG(NP) immunized animals when compared to the other groups. This is a phenomenon also observed in IAV infected mice (Balkovic et al. 1987; Ben-Ahmeida et al. 1994). As VSV*ΔG(NP) groups showed a lower level of weight loss and a faster recovery during PR8 challenge experiments, high titers of PR8-reactive IgG2b/c in combination with low titers of PR8-reactive IgG1 may have resulted in better protection. However, in case of rSC35M, no significant differences between rSC35M-reactive IgG1 and IgG2b/c subclasses were observed, and the immunization had a weaker beneficial effect in this challenge model. This suggests that in our model the exact IgG subclass profile plays an important role for the

protection against heterologous challenge and that IgG2b/c is a major driver of this. Another study showed that a fusion protein of IAV NP and M2e is more protective in animals when adjuvanted with aluminum hydroxide as compared to CpG 1826 (Wang et al. 2012). Aluminum hydroxide is known to induce a T_H1-primed immune response, in which IgG1 is the prominent IgG subclass, while the CpG 1826 adjuvant shows a reverted proportion with more IgG2 antibodies. These results are in contrast to our observations. However, it has to be taken into consideration that development of total humoral as well as cellular responses were remarkably higher in aluminum hydroxide adjuvanted animals and that protection cannot solely be attributed to IgG subclass profiles.

We then investigated if the non-neutralizing antibodies generated after NP-, M2-, or $H3_{stem}$ vaccination can confer effector functions by measuring mFcγRIV activation against PR8 and rSC35M. We chose to measure mFcγRIV activation as this receptor is known to not only induce ADCC and ADCP, but also to have a high affinity and selectivity for IgG2b and IgG2c subclasses (Bruhns and Jönsson 2015). We therefore hypothesized that this approach best translates the observed IgG2b/c subclass profiles into the Fc-mediated effector functions. One disadvantage on the other hand is that our experiments may not detect the full magnitude of ADCC/ADCP as potential effects through IgG1 are not detected. In fact, there are other approaches to measure ADCC/ADCP. Arunkumar et al. used reporter cells expressing the human FcγRIIa, which is known to cross react with all murine IgG subclasses except for IgG3, and found ADCC after immunization with a viral MVA vector expressing NP and M1 of IAV (Bruhns and Jönsson 2015; Asthagiri Arunkumar et al. 2019). Nevertheless, the approach of measuring murine IgG-induced Fc-mediated effects by human receptors is questioned by a recent publication finding relatively weak interaction between those (Temming et al. 2020). Finally, both experiments utilizing reporter cells expressing either human FcγRIIa or mFcγRIV showed that non-neutralizing antibodies directed against internal proteins of IAV can in fact induce Fc-mediated effector functions against heterologous viruses. Strikingly, when we tested the serum of a control animal infected with either PR8 or rSC35M, we only detected strain specific activation of murine FcγRIV, suggesting that the immune-dominance of HA during IAV infection outweigh other epitopes. Remarkably, against both viruses, M2-directed antibodies of all animals had a high capability to activate mFcγRIV. This in in line with current understanding of M2-directed

antibodies as they are not neutralizing but known to be protective in the murine model (Padilla-Quirarte et al. 2019). Lack of protection via M2e-specific antibodies in FcγR$^{-/-}$ mice highlights this necessity for Fc-mediated effector functions and that a dominant mechanism is ADCC by alveolar macrophages expressing mFcγRIV among others (Lee et al. 2014; El Bakkouri et al. 2011). Against both viruses, we found on average higher mFcγRIV activation in NP immunized animals when compared to the $H3_{stem}$ group, although generalization should be avoided due to limited sample numbers. However, besides neutralizing antibodies directed against the stem region of HA, which we did not detect for either virus, ADCC and complement activation through antibodies are considered to be major drivers of protection in the literature (Terajima et al. 2011; Jegaskanda et al. 2013). mFcγRIV activation in NP immunized animals against PR8 and rSC35M was comparable, which contradicts the concept of IgG2-based immunity supported by the different IgG subclass profiles. However, our findings underline the potential of NP and M2 to induce non-neutralizing, mFcγRIV-activating humoral responses against heterologous viruses after challenge. We chose a restrictive approach by utilizing mFcγRIV-expressing reporter cells. Future experiments using, for example, mFcγRIIB and mFcγRIII could evaluate if the Fc-mediated effector functions are indeed even stronger and to what extent IgG1 is important in this regard. This is especially important as many immune cells, for example NK cells, do express mFcγRIIB and mFcγRIII, which are strong drivers of ADCC (Bruhns and Jönsson 2015).

5.1.4 Combination of Most Promising Antigens Leads to Varying Outcomes Against PR8 and rSC35M Challenge

Although previous studies have demonstrated that single external, as well as internal, antigens can induce at least partial protection against IAV challenge in mice, it has become increasingly clear that future vaccines have to combine more than one IAV antigen. (Epstein et al. 2005; Tompkins et al. 2007; Vemula et al. 2017; Wraith et al. 1987) We therefore chose our most promising VSV replicons from initial challenge experiments and tested conferred protection via cocktail immunizations to examine the complementing protection and the influence of multiple antigens on the humoral immunity. We investigated a double cocktail containing VSV*ΔG(NP) and VSV*ΔG(M2) and a triple cocktail consisting of VSV*ΔG(NP), VSV*ΔG(M2), and

VSV*ΔG($H3_{stem}$). Interestingly, mice immunized with the double cocktail showed no weight loss and disease development after PR8 infection, and all mice consequently survived the infection, underlining the complementary principle of multiple antigens used in many approaches (Estrada and Schultz-Cherry 2019). A possible explanation for this may be that antibodies directed against NP and M2 activate different Fc-mediated effector functions, an explanation which is supported by different observations. Measurement of mFcγRIV activation revealed a very strong ADCC activity after VSV*ΔG(M2) immunization, although total antibody, as well as IgG subclass titers were found to be moderate. This shows that humoral immunity against M2 can induce strong Fc-mediated responses even at low titers. However, VSV*ΔG(NP) immunization elicited high antibody titers, for total antibodies as well as for IgG2b/c, but only inconsistent mFcγRIV activation, nevertheless, providing a high degree of protection. This indicates that antibodies against NP and M2 lead to protection via different mechanisms and can explain why antibodies against these proteins can complement each other. On the one hand, VSV*ΔG(M2) derived antibodies may recognize M2 expressed on living infected cell surfaces and support NK cell-mediated ADCC. On the other hand, a possible mechanism by which NP-directed antibodies can confer protection is ADCP, as they promote the internalization of dying cells by APCs and thereby increase the presentation of foreign antigens. In turn, this could lead to a more robust cell-mediated immune response driving protection. This is in line with the high expression of mFcγRIV on macrophages, the strong interaction of mFcγRIV activation with IgG2b/c, and the IgG2b/c-primed subclass profile after VSV*ΔG(NP) vaccination. Further experiments differentiating the exact interaction of elicited antibodies with the respective FcγRs could potentially provide a deeper mechanistic understanding of the complex interplay between the different FcγR effector functions.

In rSC35M infected animals, double-cocktail immunization had no striking effect and triple-cocktail immunization did not robustly protect mice from severe disease for both viruses. It has to be stressed, that total dose of replicons during all immunizations were 10^6 ffu/mouse. Animals vaccinated with double- or triple cocktail therefore only received a reduced dose of most protective VSV*ΔG(NP). As it is known for influenza vaccines to induce a more robust immune responses when administered in higher doses, a possible explanation may be that by diluting VSV*ΔG(NP) we undercut the threshold of antigen needed to elicit strong responses

(DiazGranados et al. 2013; Falsey et al. 2009). Our results from experiments using decreased doses (0.5 x and 0.3 x) of VSV*ΔG(NP) and VSV*ΔG(M2) before challenge revealed a trend towards lower antibody production and protection. Similar results were observed in experiments using a recombinant vaccinia virus expressing NP and M1 or in combination together with PB1, where combination of different antigens led to decreased total IgG, although here no difference in protection was observed (Wang et al. 2015). Studies in mice immunized with varying doses of IAV vaccines demonstrated the significant differences in produced total and subclass antibody titers (Hauge et al. 2007; Groves et al. 2018).

Taken together, when we compare undiluted, double- and triple cocktail immunization, we can observe the following pattern. For undiluted VSV*ΔG(X) vaccination, we see a correlation of total antibody titers and protection against PR8. Although humoral immune responses were decreased in double cocktail immunization, protection against PR8 was superior. As no T cells directly reactive to PR8 infection were detected even after undiluted VSV*ΔG(X) vaccination, we can assume that also in both cocktail approaches no cellular immunity is present. This indicates that the elicited antibodies found after double cocktail vaccination can in fact complement each other. However, when we further dilute the single antigens in a triple cocktail immunization approach, humoral immune responses as well as protection are inferior to both, undiluted as well as double cocktail immunization. A possible explanation for this could be that we undercut the threshold of single antigens to elicit protective antibody titers against the respective protein.

Overall, our studies demonstrated the strong potential of the internal IAV protein NP and M2 to induce humoral immune responses that correlate with protection after a potentially lethal challenge, while M1 failed to do so. We further showed that NP- and M2-specific antibodies can confer effector functions via FcγRIV-mediated ADCC or ADCP in a heterologous manner and that the reactivity was superior to $H3_{stem}$. Interestingly, these protective effects seem to be not solely dependent on T cells, as it was also previously reported for a recombinant NP vaccination strategy, where morbidity of IAV infection was reduced although only marginal T cell responses were detected (Carragher et al. 2008). The protection by NP could be further optimized by adding M2, which was also shown to be a promising target for mFcγRIV-activating IgGs and led to full protection against PR8. Taken together,

different mechanisms can be hypothesized, based on the presented data (Figure 38). While induced antibodies directed against NP or M2 were demonstrated to be not neutralizing, they clearly provide some degree of protection that can be leveraged through combination of both. Underlying mechanisms are, at least in part, conferred by mFcγRIV-mediated ADCC and ADCP, although it is highly probable that also other mFcγRs are activated. Innate immune cells, especially NK cells, but also macrophages and granulocytes, bind to antibodies recognizing infected cells and confer cell lysis by release of cytotoxic mediators like granzyme B and perforin (depicted in purple). Furthermore, APCs can resorb infected cells and their debris to clear infected cells and further improve infection-derived antigen presentation to lymphocytes (compare left side (yellow) and right side (blue)), leading to increased adaptive immune responses against the acute infection. Our work therefore stresses the promising potential of non-neutralizing antibodies in the protection against lethal IAV disease. It is advisable to implement internal proteins as a target for humoral immunity in the rational design of future IAV vaccines.

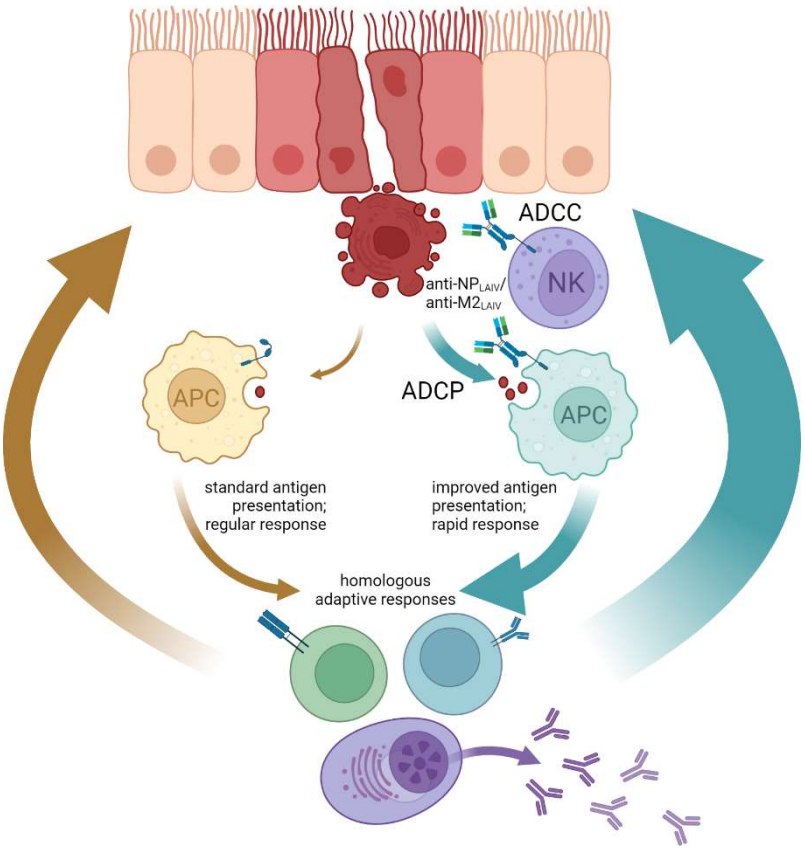

Figure 38: Possible mechanisms of ADCC and ADCP through heterologous antibodies.

IAV infected cells (red shades) can be recognized by heterologous antibodies through conserved epitopes in the internal proteins. While innate immune cells, for example NK cells (purple) can induce cell death via release of granzyme B and perforin, APCs use antibody-mediated uptake of infected cell debris to improve antigen presentation to lymphocytes (right, blue). This improved uptake and

presentation results in strong activation of adaptive immune responses and fast clearance. Without ADCP (left, yellow) uptake and presentation through APCs is suboptimal and viral clearance takes more time. Created using BioRender.

5.1.5 Further Considerations About Non-Neutralizing Antibodies

Neutralizing antibodies are the most reliable way of protecting from viral infection. However, many viruses, including IAV, can evade neutralizing antibodies, rending them inefficient. Therefore, many approaches were developed to target more conserved antigens, especially $CD8^+$ T cell epitopes, to induce a broad protection and support antibody responses in case of a humoral immune evasion. Many hurdles have to be taken when protective T cell responses are striven for. One obstacle is the population diversity of major histocompatibility complexes (MHC) (Barouch et al. 1995). The MHC is crucial for activating cellular immune responses by presenting pathogen-originated peptides and vaccines targeting conserved T cell epitopes may lead to varying responsiveness in different individuals, as it was shown in the mouse model (Bennink and Yewdell 1988). Furthermore, T cells need to be present in the lung tissue at the time of infection to take full effect against IAV infection (Wu et al. 2014). While this can be achieved shortly after vaccination, influenza-specific tissue-resident T cells wane over time, when no successive antigen is encountered. Another factor is the difficulty in measuring the correlation of protection after vaccination in the clinic, as T cell responses are commonly determined via peptide-specific $IFN\gamma^+$ ELISpot. In this respect, the magnitude of response is mainly determined by the exact peptide used for stimulation and can vary greatly as shown in mice (Wang et al. 2012). Taken together, although T cells can in fact provide supporting efficacy after vaccination, they still have to be considered an add-on, rather than the basis for protection. In contrast, non-neutralizing antibodies exhibit many advantages of neutralizing antibodies, but are not restricted to specific epitopes in the IAV HA. They can rather be directed against any antigen, as long as this is accessible during the course of infection and thereby provide protection by targeting genetically stable epitopes in internal proteins. Regarding the used LAIV proteins, it can be deliberated if targeted mutations of internal proteins can broaden the non-neutralizing antibody reactivity, thereby providing more protection against heterologous viruses after LAIV vaccination. However, it is important to consider that the cold-adapted and attenuated phenotype of the LAIV vaccine is based on these internal proteins, especially the polymerase proteins but also NP, and that further investigations are

needed to evaluate the benefit and risk of changing the amino acid sequence of these proteins to adapt them to different IAV strains.

5.1.6 Possible Limitations

We titrated the mouse-adapted PR8 and rSC35M virus to determine an infectious dose for following experiments with which we can induce a strong, potentially lethal IAV infection. Fast weight loss and early reaching of humane endpoints were obtained according to increasing doses of PR8 in these experiments, while rSC35M infection led to varying outcomes in the individual animals. One possible explanation is that PR8 and rSC35M have different tissue tropisms. While PR8 also infects the lining epithelial cells of the upper respiratory tract and spreads to the lung, rSC35M is mainly found in lung tissue and may be dependent on effective dissemination of viral solution to the lower respiratory tract (Gabriel et al. 2009; Gilbertson et al. 2017). However, the exact tissue-tropism of rSC35M in the respiratory tract remains elusive. Manifestation of disease may thus be varying in animals where the applied volume does not reach the deep lung. Separate LD_{50} titration experiments we performed using lower infection volumes also increased the variability of PR8 induced disease and highlight that dissemination of virus solution can greatly impact establishment of efficient infection.

Another possible limitation is the relatively low dose used for our challenge experiments. We chose infection titers of PR8 and rSC35M representing approximately the $3xLD_{50}$, respectively. This challenge dose did not cause 100% lethality in unvaccinated mice, but it reliably induced severe disease in these groups and at the same time was preventable by non-neutralizing antibodies generated by our vaccination strategy. In addition, a non-lethal infection model is close to the pathology of most influenza A virus strains in humans, which further justifies our experimental design. While repeating the shown experiments with higher doses causing 100% lethality in unvaccinated mice may provide more insights in the strength of the vaccine-induced immune responses and their potential to protect against highly pathogenic IAV infections, $3xLD_{50}$ are appropriate to draw conclusions on the potential of the chosen antigens to reduce disease outcome of mild and moderate infections with heterologous IAV strains.

Finally, possible limitations of IPMA-based antibody titrations have to be taken into consideration, as staining of infected cells and therefore read out of positive wells can differ between the used virus strains. We observed faster cell death rates after rSC35M infection when compared to PR8, and this affected the visualization of infected cells by IPMA. Massive amounts of necrotic cells can alter the overall presentation of internal proteins and caution should be taken when directly comparing rSC35M titers to PR8 titers. Furthermore, to titrate total IgG or subclasses we had to use different secondary antibodies specific for either subclass, which can result in varying intensities of IPMA staining.

5.2 ADAR1 Has Proviral Activity for Influenza A Virus

Although antiviral agents directed against the function of specific proteins of IAV have been developed in the past, the genetic variability of IAV can render these countermeasures ineffective by evolving resistance mutants. Targeting host factors that are necessary for viral replication are a promising way of developing broadly acting antivirals, as escape mutants are less probable to appear, since this would primarily depend on host genetics and less on the genetic flexibility of the virus. In this project, we examined the effect of ADAR1 on IAV replication as a possible target for antiviral therapy.

5.2.1 ADAR1p150 is a Proviral Factor in HeLa cells

It was demonstrated recently that ADAR1p150 can abolish innate immunity activation by IAV-derived dsRNA in A549 cells and that absence of ADAR1p150 results in increased RLR signaling and therefore increased viral replication (Vogel et al. 2020). Our results correlate with this, as HeLa cells lacking ADAR1p150 alone, or the ADAR1p150 and ADAR1p110 isoform (ADAR1^{KO}), showed decreased viral protein expression after infection with rSC35M. Interestingly, the effect on viral protein levels was more pronounced in the ADAR1p150-specific knockout than in the knockout affecting both isoforms. A possible explanation for the intermediate phenotype in infected HeLa-ADAR1^{KO} cells is that the simultaneous knock-out of the ADAR1p150 and ADAR1p110 isoforms compensate the individual opposing effects. This conclusion can be drawn from experiments investigating IAV replication in ADAR1p110^{KO} cells, as it was shown that ADAR1p110 has an antiviral effect (Vogel et al. 2020). However, the exact mechanism for this remains unknown. A possible explanation is that ADAR1p110 may edit some forms of viral RNA, which may result in hypermutated transcripts and translation of erroneous proteins (Cao et al. 2018). This can then lead to an antiviral effect of ADAR1p110 on IAV (Pfaller et al. 2021). Detection of ADAR-characteristic hypermutations in IAV genome preparations underline this hypothesis (Suspène et al. 2011). Interestingly, the immune-modulator NS1 also interacts with ADAR1p110 in the nucleus (Chassey et al. 2013). It is possible that this interaction of NS1 antagonizes ADAR1p110 and thereby inhibits its antiviral activity (Pfaller et al. 2021).

Vogel et al. demonstrated strong activation of IRF-3 and subsequent IFN-β expression and apoptosis in ADAR1p150^{KO} cells, which is a possible explanation for the impaired viral replication. In strong contrast to this, we detected no phosphorylation of IRF3 in HeLa cells, indicating that in our model different mechanisms are responsible for the decreased viral protein expression. One possible explanation is the difference in the experimental set-ups to investigate this. Vogel et al. used transfection of viral RNA as a substitute to characterize IFN-β expression in cells lacking ADAR1p150 on RLR signaling activation. In contrast, we examined these effects in the context of viral infection. While purified viral RNA induces innate immune responses in ADAR1p150-deficient cells, the situation in a real infection with IAV is more complex, since the virus has evolved additional mechanisms acting at the level or downstream of the recognition of viral dsRNA, preventing signal transduction. The NS1 protein is a well-known antagonist for IFN-β production and inhibits IRF3 activation (Samuel 2011b; Fensterl et al. 2015), which may explain our failure to observe strong IRF3 activation.

Furthermore, it was shown by Vogel et al. that indeed the binding property and not the catalytic activity of ADAR1p150 leads to decreased RIG-I activation. This suggests that ADAR1p150 may sequester viral RNA from innate immune receptors in an editing-independent manner rather than changing dsRNA secondary structures in an editing-dependent manner. In contrast, editing of MeV immuno-stimulatory RNA by ADAR1p150 was necessary for the full proviral effect, whereas a catalytically inactive ADAR1p150 only exhibited reduced capacity to counteract innate immunity activation by MeV (Pfaller et al. 2018). Future experiments examining

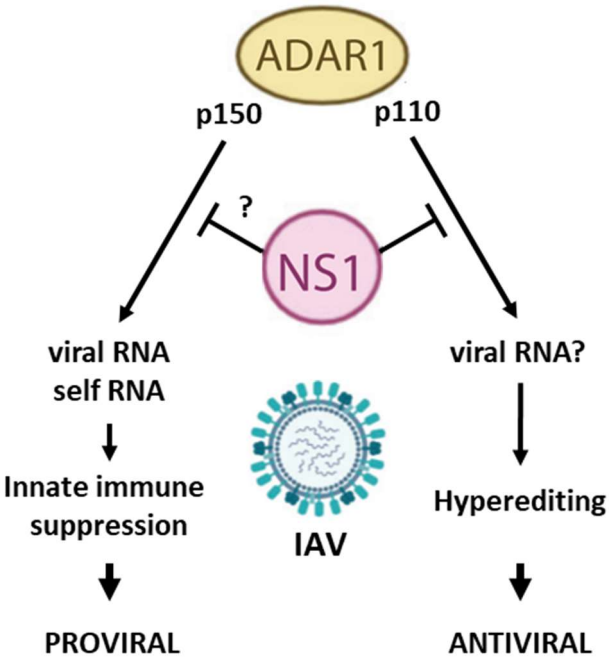

Figure 39: ADAR1 isoforms have different effects on IAV replication

ADAR1p150 binds to viral RNA, inhibiting sensing via innate immune receptors. This results in a proviral effect of ADAR1p150 during IAV replication. In contrast, ADAR1p110 binds viral RNA and potentially leads to hypermutations, and subsequent impaired viral protein expression. This results in an antiviral activity of ADAR1p110 on IAV replication. NS1 can counteract this by inhibiting ADAR1p110. Adapted from (Pfaller et al. 2021)

if ADAR1 isoforms differentially edit IAV RNA and how this affects viral gene expression and RIG-I signaling might provide important new insights into the complex interplay between IAV infection and ADAR1.

Taken together, it can be hypothesized that ADAR1p150 and ADAR1p110 have opposing functions during IAV replication (Figure 39). While ADAR1p150 masks viral RNA from detection via RLR and therefore has a proviral effect through suppression of innate immune activation, ADAR1p110 binds viral RNA and potentially hypermutates these, which leads to defective protein translation.

5.2.2 ADAR1 Isoforms Have a Proviral Effect on IAV in MDCK cells

To confirm the proviral effect of ADAR1, specifically of ADAR1p150, on IAV infection at the level of viral titers, we changed the cell model to MDCK cells, as HeLa cells do not support efficient release of infectious IAV particles, and thus are not suitable to determine the impact of ADAR1 on IAV infectivity. We used the CRISPR/Cas9n system to induce either an ADAR1p150 or an ADAR1 knock-out and infected the cells with PR8, which replicates to high titers in these cells. Remarkably, also by using a different cell line and IAV strain, we confirmed the proviral effect of ADAR1, and specifically of ADAR1p150, which further underlines the broad effect of ADAR1 on IAVs of different subtypes. We further focused on investigating the effect of ADAR1 on virus-induced apoptosis, Vogel et al. had reported increased PARP cleavage in the absence of ADAR1p150 in H1N1 infected A549 cells. However, we used an MTT assay in order to determine infection-induced cell death, since PARP-specific antibodies did not work in our hands to detect canine PARP in an immunoblot analysis. H1N1 infection at MOI of 1 induced PARP cleavage in ADAR1p150-deficient A549 cells, but not in wild type cells (Vogel et al. 2020). In contrast, we found that IAV infection at the same MOI induced strong CPE and led to cell death even in the wildtype MDCK cells, indicating that the induction of cell death in this cell line is independent of ADAR1p150. It has to be stressed that we did not distinguish between different mechanisms of cell death, such as apoptosis or necroptosis. It is reasonable to assume that this rate of cell death results from massive viral replication and release of particles, and thus marks an exhausted cell at the end of the viral life cycle. This is especially the case as we demonstrated before that virus replication and with this viral spread in the cell culture is diminished in MDCK ADAR1p150^{KO} cells. From this perspective, it is possible that the

ADAR1p150^{KO} indeed leads to higher rates of apoptosis in infected cells, but as fewer cells are infected over time, this effect is not visible with our MTT-based assay. This assumption is further supported by the finding that increasing the infection dose to MOI of 5 did even more increase the observed amount of dying cells. On the other hand, the low MOI of 0.1 did not induce substantial cell death at all. Future experiments comparing multiple MOIs between 0.1 and 1 can elucidate to what extent our MTT-based assay is suited to measure different rates of cell death. It has to be mentioned that we repeated the MTT-based assay with another MDCK ADAR1^{KO} clone we obtained in our initial knockout experiment. Interestingly, this clone showed contrary results, as we found a faster rate of infection-induced cell death when compared to MDCK wt cells. This indicates potential off-target effects of the CRISPR/Cas9 approach in these cell clones, and therefore we cannot make any definitive statements about the exact influence of ADAR1 on IAV-induced cell death and this issue has to be addressed in future experiments. Investigations examining specific apoptosis markers, like Annexin V staining, can contribute to the understanding of IAV-induced apoptosis in these cell lines.

In a recent study, MDCK and A549 cells were infected with a PR8 virus expressing different NS1 proteins and it was found that differences in viral growth are much more prominent in A549 cells as compared to MDCK cells. As NS1 interacts with ADAR1p110 and may reduce its antiviral activity, this again stresses the potentially different functions of ADAR1p110 in distinct cells (Nogales et al. 2019). Although this finding does not explain the observed phenotype, it again illustrates that ADAR1 can act upon the viral RNA, but also viral proteins can alternate ADAR1 functions, thereby potentially modifying its impact on the cell. In conclusion, to rule out interfering effects of NS1, the above-mentioned experiments can be repeated with an IAV depleted of NS1 (IAVΔNS1). This will shed further light on the potential interplay of IAV NS1 and ADAR1.

5.2.3 Future Considerations for ADAR1 as an Antiviral Target

Albeit these discrepancies raise questions concerning reproducibility of results in different setting, like cell culture systems or IAV strains used, the absence of innate immune activation observed in HeLa cells under ADAR1p150^{KO} may be advantageous in respect to targeting it with drugs during IAV infection. Severe pathogenicity and the subsequent death of affected individuals are results of an

exaggerated immune response, based on overt expression of pro-inflammatory cytokines (Iwasaki and Pillai 2014). A major driver of this are apoptotic and necrotic cells which are associated with IAV-induced ARDS (Korteweg and Gu 2008; Martin et al. 2005). On the one hand, activation of PRRs results in the expression and release of pro-inflammatory cytokines, especially type I IFN, IL-6 and TNF-α (Ampomah and Lim 2020). These cytokines can activate apoptosis of cells via the extrinsic pathways and ultimately lead to cell death (Locksley et al. 2001). In this respect, most approaches to protect from IAV-induced pathogenicity are not targeting the virus itself but try to reduce immune activation. For example, TGF-β, delivered via an adenoviral vector, TNF-blocking antibodies, or compounds prohibiting infiltration of neutrophils into the lung tissue have shown promising results in the mouse model (Carlson et al. 2010; Brandes et al. 2013; Hussell et al. 2001). Notably, ADAR1 is primarily an immunoregulatory enzyme, and its absence is associated with type-I interferonopathies in humans, such as Aicardi-Goutières-Syndrome (Rice et al. 2012). This would imply that blocking of ADAR1 activity during IAV infection would further boost inflammation and cytokine production and may enhance ARDS. It is therefore important to stress that absence of increased innate immune activation in ADAR1p150^{KO} cells upon infection with IAV may be advantageous by not further increasing the risk of ARDS. Using ADAR1p150 as a potential target for prophylactic treatment in a setting of highly-pathogenic and human-to-human transmissible IAV may have additional benefits over other classical approaches like therapeutic treatment with type-I IFN, which have proven to be inefficient in case of IAV infection (Calvaruso et al. 2011). ADAR1 modulates multiple innate immunity pathways beyond the classical IFN response, and, as our data suggest, also may directly impact IAV replication in an innate immunity-independent manner, and thus may build a broader protection against IAV. However, more research is needed to investigate the exact molecular mechanisms of the proviral effect of ADAR1, and also to assess the effects of ADAR1 inhibition *in vivo,* as cell culture systems may be misleading.

5.3 Conclusion

Extensive research in basic and applied sciences was performed for decades to develop strategies for subtype-independent approaches against IAV. This is foremost the development of a broadly protecting and long-lasting vaccine against IAV, but

also includes antiviral therapies to cope with extensive lung damage and the associated death in patients. This work provides insights in the potential of humoral immunity towards internal proteins of IAV and highlights the opportunity to deploy these in the design of future vaccines. Furthermore, the effect of ADAR1 on IAV replication and infection-induced cell death was further characterized and builds a promising basis for further research on this target for antiviral therapies.

6 SUMMARY

Influenza A virus (IAV) is a major burden for public health. Besides seasonal, human IAV, which circulates during the cold seasons and is responsible for hundreds of thousands of deaths each year, its potential to reassort with avian IAV fuels the fear of future pandemics. Currently licensed vaccines are standardized to elicit antibodies directed against the head domain of the hemagglutinin (HA) on the viral surface and binding of these can effectively neutralize virus particles. However, the antigenic plasticity of HA in consecutive IAV seasons and the above-mentioned potential for upcoming reassorted viruses make it necessary to update IAV vaccines on an annual basis and still, these vaccines cannot protect against outbreaks of zoonotic origin. It is therefore a major objective to develop new subtype-independent approaches against IAV via immunization as a first line of defense or via antiviral drugs.

This thesis is divided into two different projects. The first one investigates the protection against heterologous challenge after vaccination with single or combined IAV proteins and the underlying humoral immune response. The second project aims at characterizing the effect of ADAR1 (adenosine deaminase acting on RNA 1), a potential target for antiviral compounds, on IAV.

In the first project, the internal proteins NP and M1 derived from the live-attenuated influenza vaccine were investigated regarding their potential to elicit protective immunity against heterologous virus challenge and compared to currently used approaches based on the stem region of HA (HA_{stem}) or the membrane-integral M2 protein. Furthermore, underlying immune responses were characterized. We demonstrate that VSV-vectored immunization with the internal protein NP and M2, but also $H3_{stem}$ can remarkably reduce IAV-induced disease in a heterologous manner and that this effect is independent of detectable T cell responses. Analysis of humoral immunity revealed high IgG antibodies, distinct IgG subclass profiles against different viruses, and most importantly, activation of the murine FcγRIV, known to mediate antibody-dependent cell-mediated cytotoxicity and –phagocytosis via alveolar macrophages. Furthermore, we showed that the absence of humoral immunity after viral vector-based immunization with M1 correlated with the lack of protection against IAV challenge in mice, which suggests absence of protective, but undetected, T cell responses, and strengthens our assumption of antibody-mediated protection. Humoral immunity against internal proteins of IAV have first been

described decades ago but are often considered inferior to those directed against surface antigens. The main reason for this is the localization of internal proteins, as it raises questions about the capability to provide protection through humoral immune responses. Therefore, they were often neglected or ignored in the past. While these antibodies do not mediate neutralization, they can in fact activate Fc-mediated effector functions and protect from homologous as well as heterologous disease. Our results add further insights in these mechanisms and correlate with previously described capability of NP and M2 to induce protective antibodies. Our results therefore imply that these immune responses should not be ignored in the rational design of future IAV vaccines.

In the second project, we used two different cell culture systems to investigate the effect of different ADAR1 isoforms on the replication of IAV, in order to consider its potential as a target for antiviral therapies. We demonstrated that ADAR1p150 is a proviral factor for IAV infection and is required for efficient viral protein expression in HeLa cells, which is in line with previous publications describing this in other eukaryotic cell lines. This finding consolidates the concept of proviral ADAR1p150 for IAV, as it was described for other RNA viruses. Furthermore, we generated MDCK cells deficient for ADAR1p150 or complete ADAR1 using a CRISPR/Cas9n system and confirmed the proviral effect of ADAR1p150 on viral replication. We showed that absence of ADAR1 resulted in strikingly decreased IAV-induced cell death, which may be an essential factor for targeting it with antiviral compounds. Individuals passing away because of an IAV infection show severe damage of lung tissue, resulting from exaggerated innate immune responses, a pro-inflammatory milieu, and the subsequent collapse of the epithelial barrier in the lung. Our results in HeLa cells indicate that a potential knock-down or inhibition of ADAR1 does not necessarily lead to activated innate immunity pathways, as it could be expected from other RNA viruses, and in combination with the above-mentioned decreased cell death in infected MDCK ADAR1^{KO} cells builds a promising basis for the further investigation of ADAR1 as a target for anti-IAV treatment therapies.

7 ZUSAMMENFASSUNG

Influenza A Viren (IAVs) sind eine große Bedrohung für das Gesundheitssystem. Neben den saisonalen, auch „humanen“, IAVs, die jährlich Hundertausende Tote fordern, befeuert die Möglichkeit einer Reassortierung mit aviären IAVs die Sorge einer zukünftigen Pandemie. Momentan zugelassene Impfstoffe zielen darauf ab, Antikörper gegen die Kopfdomäne des Oberflächenproteins Hämagglutinin (HA) zu bilden, die das Virus effektiv neutralisieren können. Die stetige Veränderung des HA-Antigens von Saison zu Saison macht es jedoch unverzichtbar, dass die vorhandenen Impfstoffe jedes Jahr neu angepasst werden. Zusätzlich ist gegen möglichweise auftretende, zoonotische IAVs dadurch auch kein Schutz gewährleistet. Es ist demzufolge dringend notwendig, dass subtyp-unspezifische Ansätze gegen IAVs entwickelt werden, sei es als Impfstoff, um die initiale Ausbreitung zu stoppen und die Bevölkerung zu schützen, oder als antivirales Medikament, um schwere Krankheitsverläufe abzumildern.

In dieser Doktorarbeit wurden zwei unterschiedliche Projekte bearbeitet. Im ersten Projekt geht es darum, den Schutz gegen eine heterologe IAV Infektion nach einer vektor-basierten Immunisierung mit unterschiedlichen IAV Proteinen zu untersuchen und die zugrundeliegende Immunantwort zu charakterisieren. Das zweite Projekt zielt darauf ab den Effekt des zellulären Proteins ADAR1 (*adenosine deaminase acting on RNA 1*) auf die Replikation von IAV zu erforschen.

Im ersten Projekt wurden die internen Proteine NP und M1 bezüglich ihres Schutzpotentials gegen heterologe IAV Infektionen untersucht und mit den momentan weit verbreiteten Ansätzen einer Immunisierung gegen die Stammdomäne des HA (HA_{stem}) oder dem M2 Protein verglichen. Wir konnten zeigen, dass die Immunisierung mit NP und M2, aber auch $H3_{stem}$ mittels eines viralen Vektors die Schwere der Erkrankung einer heterologen IAV Infektion in Mäusen maßgeblich reduzieren kann und dass dies unabhängig von nachweisbaren T-Zell Antworten war. Eine Analyse der humoralen Immunantwort zeigt hohe IgG Titer, unterscheidbare IgG Subklassen-Profile gegen verschiedene IAVs und vor allem eine Aktivierung des murinen FcγRIV. Dieser ist dafür bekannt Antikörper-vermittelte zellbasierte Zytotoxizität und –Phagozytose durch alveoläre Makrophagen auszulösen. Außerdem konnte keine Schutzwirkung durch eine Immunisierung mit M1 beobachtet werden, was mit der Abwesenheit von

Antikörpern korreliert. Dieser Aspekt verdeutlicht erneut, dass die verabreichten Antigene keine T-Zell vermittelte Schutzfunktion ausübten, die in unseren Experimenten fälschlicherweise nicht detektiert worden wäre. Obwohl Antikörper gegen interne Proteine schon vor Jahrzenten beschrieben wurden, wurde ihnen bislang wenig Beachtung geschenkt. Der Hauptgrund dafür ist die Lokalisation der internen Proteine, da diese Fragen über den Schutzmechanismus durch humorale Immunantworten aufwerfen. Sie wurden daher in der Vergangenheit häufig vernachlässigt oder ignoriert. Obwohl keine Neutralisation der Viruspartikel stattfinden kann, können diese Antikörper jedoch Fc-vermittelten Schutz gegen homologe und auch heterologe Viren hervorrufen und so vor einem schweren Krankheitsverlauf schützen. Unsere Resultate bieten tiefere Einblicke in diese Mechanismen und korrelieren mit dem beschriebenen Potential von NP und M2 schützende Antikörperantworten auszulösen. Die vorliegenden Daten verdeutlicht daher, dass die beschriebenen Immunantworten bei der Entwicklung von zukünftigen IAV Impfstoffen nicht ignoriert werden sollten.

Im zweiten Projekt dieser Dissertation wurden zwei verschiedene Zellkultur-Systeme genutzt, um den Effekt von ADAR1 auf die virale Replikation des IAV zu untersuchen. Wir konnten einen proviralen Effekt der Isoform ADAR1p150 in HeLa Zellen nachweisen, was mit bereits publizierten Daten aus anderen Zellkultursystemen übereinstimmt und das Konzept des proviralen ADAR1p150 bezüglich IAV festigt. Außerdem haben wir den Effekt von verschiedenen ADAR1 Isoformen in IAV infizierten MDCK Zellen charakterisiert, die mittels CRISPR/Cas9n gentechnisch verändert wurden. Dabei haben wir eine signifikante Hemmung der viralen Replikation in Abwesenheit von ADAR1p150 gezeigt. Des Weiteren führte eine IAV-Infektion in ADAR1-defizienten MDCK Zellen zu einem reduzierten Zelltod, was ebenfalls für ADAR1 als ein vielversprechendes Ziel eines Medikaments spricht. Patienten, die an einer IAV Infektion versterben weisen eine starke Schädigung des Lungengewebes durch eine überschießende Immun- und Entzündungsreaktion auf, die zum Zusammenbruch der epithelialen Barrierefunktion der Lunge führt. Unsere Ergebnisse, dass eine Inhibition von ADAR1 nicht notwendigerweise zu einer angeborenen Immunaktivierung führt, in Kombination mit Hinweisen auf einen verringerten Zelltod, bilden eine vielversprechende Basis für die weiteren Untersuchungen von ADAR1 als Ziel antiviraler Therapeutika.

8 REFERENCES

Ampomah, Patrick B.; Lim, Lina H. K. (2020): Influenza A virus-induced apoptosis and virus propagation. In *Apoptosis : an international journal on programmed cell death* 25 (1-2), pp. 1–11. DOI: 10.1007/s10495-019-01575-3.

Asthagiri Arunkumar, Guha; McMahon, Meagan; Pavot, Vincent; Aramouni, Mario; Ioannou, Andriani; Lambe, Teresa et al. (2019): Vaccination with viral vectors expressing NP, M1 and chimeric hemagglutinin induces broad protection against influenza virus challenge in mice. In *Vaccine* 37 (37), pp. 5567–5577. DOI: 10.1016/j.vaccine.2019.07.095.

Balkovic, E. S.; Florack, J. A.; Six, H. R. (1987): Immunoglobulin G subclass antibody responses of mice to influenza virus antigens given in different forms. In *Antiviral research* 8 (3), pp. 151–160. DOI: 10.1016/0166-3542(87)90068-4.

Banadyga, Logan; Marzi, Andrea (2017): Closer than ever to an Ebola virus vaccine. In *Expert review of vaccines* 16 (5), pp. 401–402. DOI: 10.1080/14760584.2017.1309977.

Barefoot, Brice E.; Sample, Christopher J.; Ramsburg, Elizabeth A. (2009): Recombinant vesicular stomatitis virus expressing influenza nucleoprotein induces CD8 T-cell responses that enhance antibody-mediated protection after lethal challenge with influenza virus. In *Clin Vaccine Immunol* 16 (4), pp. 488–498. DOI: 10.1128/CVI.00451-08.

Barouch, D.; Friede, T.; Stevanović, S.; Tussey, L.; Smith, K.; Rowland-Jones, S. et al. (1995): HLA-A2 subtypes are functionally distinct in peptide binding and presentation. In *The Journal of experimental medicine* 182 (6), pp. 1847–1856. DOI: 10.1084/jem.182.6.1847.

Belshe, Robert B. (2005): The origins of pandemic influenza--lessons from the 1918 virus. In *The New England journal of medicine* 353 (21), pp. 2209–2211. DOI: 10.1056/NEJMp058281.

Ben-Ahmeida, E. T.; Potter, C. W.; Gregoriadis, G.; Adithan, C.; Jennings, R. (1994): IgG subclass response and protection against challenge following immunisation of mice with various influenza A vaccines. In *Journal of medical microbiology* 40 (4), pp. 261–269. DOI: 10.1099/00222615-40-4-261.

Bennink, J. R.; Yewdell, J. W. (1988): Murine cytotoxic T lymphocyte recognition of individual influenza virus proteins. High frequency of nonresponder MHC class I alleles. In *The Journal of experimental medicine* 168 (5), pp. 1935–1939. DOI: 10.1084/jem.168.5.1935.

Berger Rentsch, Marianne; Zimmer, Gert (2011): A vesicular stomatitis virus replicon-based bioassay for the rapid and sensitive determination of multi-species type I interferon. In *PLoS ONE* 6 (10), e25858. DOI: 10.1371/journal.pone.0025858.

Bergmann, M.; Garcia-Sastre, A.; Carnero, E.; Pehamberger, H.; Wolff, K.; Palese, P.; Muster, T. (2000): Influenza virus NS1 protein counteracts PKR-mediated inhibition of replication. In *Journal of virology* 74 (13), pp. 6203–6206. DOI: 10.1128/jvi.74.13.6203-6206.2000.

Blazejewska, Paulina; Koscinski, Lukasz; Viegas, Nuno; Anhlan, Darisuren; Ludwig, Stephan; Schughart, Klaus (2011): Pathogenicity of different PR8 influenza A virus variants in mice is determined by both viral and host factors. In *Virology* 412 (1), pp. 36–45. DOI: 10.1016/j.virol.2010.12.047.

Bodewes, Rogier; Geelhoed-Mieras, Martina M.; Wrammert, Jens; Ahmed, Rafi; Wilson, Patrick C.; Fouchier, Ron A. M. et al. (2013): In vitro assessment of the immunological significance of a human monoclonal antibody directed to the influenza a virus nucleoprotein. In *Clin Vaccine Immunol* 20 (8), pp. 1333–1337. DOI: 10.1128/CVI.00339-13.

Boer, G. F. de; Back, W.; Osterhaus, A. D. (1990): An ELISA for detection of antibodies against influenza A nucleoprotein in humans and various animal species. In *Archives of Virology* 115 (1-2), pp. 47–61. DOI: 10.1007/BF01310622.

Both, G. W.; Sleigh, M. J.; Cox, N. J.; Kendal, A. P. (1983): Antigenic drift in influenza virus H3 hemagglutinin from 1968 to 1980: multiple evolutionary pathways and sequential amino acid changes at key antigenic sites. In *Journal of virology* 48 (1), pp. 52–60. DOI: 10.1128/JVI.48.1.52-60.1983.

Brandes, Marlène; Klauschen, Frederick; Kuchen, Stefan; Germain, Ronald N. (2013): A systems analysis identifies a feedforward inflammatory circuit leading to lethal influenza infection. In *Cell* 154 (1), pp. 197–212. DOI: 10.1016/j.cell.2013.06.013.

Brody, J. A.; Fischer, G. F.; Peralta, P. H. (1967): Vesicular stomatitis virus in Panama. Human serologic patterns in a cattle raising area. In *American journal of epidemiology* 86 (1), pp. 158–161. DOI: 10.1093/oxfordjournals.aje.a120721.

Bruhns, Pierre; Jönsson, Friederike (2015): Mouse and human FcR effector functions. In *Immunological reviews* 268 (1), pp. 25–51. DOI: 10.1111/imr.12350.

Bui, M.; Whittaker, G.; Helenius, A. (1996): Effect of M1 protein and low pH on nuclear transport of influenza virus ribonucleoproteins. In *Journal of virology* 70 (12), pp. 8391–8401. DOI: 10.1128/JVI.70.12.8391-8401.1996.

Bullough, P. A.; Hughson, F. M.; Skehel, J. J.; Wiley, D. C. (1994): Structure of influenza haemagglutinin at the pH of membrane fusion. In *Nature* 371 (6492), pp. 37–43. DOI: 10.1038/371037a0.

Calvaruso, Vincenza; Mazza, Marta; Almasio, Piero L. (2011): Pegylated-interferon-α (2a) in clinical practice: how to manage patients suffering from side effects. In *Expert opinion on drug safety* 10 (3), pp. 429–435. DOI: 10.1517/14740338.2011.559161.

Cao, Yingying; Cao, Ruiyuan; Huang, Yaowei; Zhou, Hongxia; Liu, Yuanhua; Li, Xuan et al. (2018): A comprehensive study on cellular RNA editing activity in response to infections with different subtypes of influenza a viruses. In *BMC genomics* 19 (Suppl 1), p. 925. DOI: 10.1186/s12864-017-4330-1.

Carlson, Christina M.; Turpin, Elizabeth A.; Moser, Lindsey A.; O'Brien, Kevin B.; Cline, Troy D.; Jones, Jeremy C. et al. (2010): Transforming growth factor-β: activation by neuraminidase and role in highly pathogenic H5N1

influenza pathogenesis. In *PLoS pathogens* 6 (10), e1001136. DOI: 10.1371/journal.ppat.1001136.

Carragher, Damian M.; Kaminski, Denise A.; Moquin, Amy; Hartson, Louise; Randall, Troy D. (2008): A novel role for non-neutralizing antibodies against nucleoprotein in facilitating resistance to influenza virus. In *Journal of immunology (Baltimore, Md. : 1950)* 181 (6), pp. 4168–4176. DOI: 10.4049/jimmunol.181.6.4168.

Case, James Brett; Rothlauf, Paul W.; Chen, Rita E.; Kafai, Natasha M.; Fox, Julie M.; Smith, Brittany K. et al. (2020): Replication-Competent Vesicular Stomatitis Virus Vaccine Vector Protects against SARS-CoV-2-Mediated Pathogenesis in Mice. In *Cell host & microbe* 28 (3), 465-474.e4. DOI: 10.1016/j.chom.2020.07.018.

CDC (2019a): 1968 Pandemic (H3N2 virus). Edited by Center for Disease Control and Prevention. Center for Disease Control and Prevention. Available online at https://www.cdc.gov/flu/pandemic-resources/1968-pandemic.html, updated on 9/22/2021, checked on 9/22/2021.

CDC (2019b): 2009 H1N1 Pandemic. Available online at https://www.cdc.gov/flu/pandemic-resources/2009-h1n1-pandemic.html, updated on 8/11/2021, checked on 8/11/2021.

CDC (2021): Live Attenuated Influenza Vaccine [LAIV] (The Nasal Spray Flu Vaccine) | CDC. Available online at https://www.cdc.gov/flu/prevent/nasalspray.htm, updated on 10/28/2021, checked on 10/28/2021.

Chassey, Benoît de; Aublin-Gex, Anne; Ruggieri, Alessia; Meyniel-Schicklin, Laurène; Pradezynski, Fabrine; Davoust, Nathalie et al. (2013): The interactomes of influenza virus NS1 and NS2 proteins identify new host factors and provide insights for ADAR1 playing a supportive role in virus replication. In *PLoS pathogens* 9 (7), e1003440. DOI: 10.1371/journal.ppat.1003440.

Chen, Yao-Qing; Wohlbold, Teddy John; Zheng, Nai-Ying; Huang, Min; Huang, Yunping; Neu, Karlynn E. et al. (2018): Influenza Infection in Humans Induces Broadly Cross-Reactive and Protective Neuraminidase-Reactive Antibodies. In *Cell* 173 (2), 417-429.e10. DOI: 10.1016/j.cell.2018.03.030.

Chen, Z.; Sahashi, Y.; Matsuo, K.; Asanuma, H.; Takahashi, H.; Iwasaki, T. et al. (1998): Comparison of the ability of viral protein-expressing plasmid DNAs to protect against influenza. In *Vaccine* 16 (16), pp. 1544–1549. DOI: 10.1016/s0264-410x(98)00043-7.

Chung, Hachung; Calis, Jorg J. A.; Wu, Xianfang; Sun, Tony; Yu, Yingpu; Sarbanes, Stephanie L. et al. (2018): Human ADAR1 Prevents Endogenous RNA from Triggering Translational Shutdown. In *Cell* 172 (4), 811-824.e14. DOI: 10.1016/j.cell.2017.12.038.

Clarke, David K.; Xu, Rong; Matassov, Demetrius; Latham, Theresa E.; Ota-Setlik, Ayuko; Gerardi, Cheryl S. et al. (2020): Safety and immunogenicity of a highly attenuated rVSVN4CT1-EBOVGP1 Ebola virus vaccine: a randomised, double-blind, placebo-controlled, phase 1 clinical trial. In *The Lancet. Infectious diseases* 20 (4), pp. 455–466. DOI: 10.1016/S1473-3099(19)30614-0.

Collins, Andrew M. (2016): IgG subclass co-expression brings harmony to the quartet model of murine IgG function. In *Immunology and cell biology* 94 (10), pp. 949–954. DOI: 10.1038/icb.2016.65.

Collins, Andrew M.; Jackson, Katherine J. L. (2013): A Temporal Model of Human IgE and IgG Antibody Function. In *Front. Immunol.* 4, p. 235. DOI: 10.3389/fimmu.2013.00235.

Collins, Andrew M.; Wang, Yan; Roskin, Krishna M.; Marquis, Christopher P.; Jackson, Katherine J. L. (2015): The mouse antibody heavy chain repertoire is germline-focused and highly variable between inbred strains. In *Philosophical transactions of the Royal Society of London. Series B, Biological sciences* 370 (1676). DOI: 10.1098/rstb.2014.0236.

Corti, Davide; Suguitan, Amorsolo L.; Pinna, Debora; Silacci, Chiara; Fernandez-Rodriguez, Blanca M.; Vanzetta, Fabrizia et al. (2010): Heterosubtypic neutralizing antibodies are produced by individuals immunized with a seasonal influenza vaccine. In *The Journal of clinical investigation* 120 (5), pp. 1663–1673. DOI: 10.1172/JCI41902.

Couch, Robert B.; Atmar, Robert L.; Keitel, Wendy A.; Quarles, John M.; Wells, Janet; Arden, Nancy; Niño, Diane (2012): Randomized comparative study of the serum antihemagglutinin and antineuraminidase antibody responses to six licensed trivalent influenza vaccines. In *Vaccine* 31 (1), pp. 190–195. DOI: 10.1016/j.vaccine.2012.10.065.

Cox, N. J.; Kitame, F.; Kendal, A. P.; Maassab, H. F.; Naeve, C. (1988): Identification of sequence changes in the cold-adapted, live attenuated influenza vaccine strain, A/Ann Arbor/6/60 (H2N2). In *Virology* 167 (2), pp. 554–567.

Cox, N. J.; Subbarao, K. (2000): Global epidemiology of influenza: past and present. In *Annual review of medicine* 51, pp. 407–421. DOI: 10.1146/annurev.med.51.1.407.

Cox, R. J.; Brokstad, K. A. (1999): The postvaccination antibody response to influenza virus proteins. In *APMIS : acta pathologica, microbiologica, et immunologica Scandinavica* 107 (3), pp. 289–296. DOI: 10.1111/j.1699-0463.1999.tb01556.x.

Cretescu, L.; Beare, A. S.; Schild, G. C. (1978): Formation of antibody to matrix protein in experimental human influenza A virus infections. In *Infection and immunity* 22 (2), pp. 322–327. DOI: 10.1128/iai.22.2.322-327.1978.

Cureton, David K.; Massol, Ramiro H.; Whelan, Sean P. J.; Kirchhausen, Tomas (2010): The length of vesicular stomatitis virus particles dictates a need for actin assembly during clathrin-dependent endocytosis. In *PLoS pathogens* 6 (9), e1001127. DOI: 10.1371/journal.ppat.1001127.

Dahlke, Christine; Kasonta, Rahel; Lunemann, Sebastian; Krähling, Verena; Zinser, Madeleine E.; Biedenkopf, Nadine et al. (2017): Dose-dependent T-cell Dynamics and Cytokine Cascade Following rVSV-ZEBOV Immunization. In *EBioMedicine* 19, pp. 107–118. DOI: 10.1016/j.ebiom.2017.03.045.

Davenport, F. M.; Hennessy, A. V.; Maassab, H. F.; Minuse, E.; Clark, L. C.; Abrams, G. D.; Mitchell, J. R. (1977): Pilot studies on recombinant cold-

adapted live type A and B influenza virus vaccines. In *J INFECT DIS* 136 (1), pp. 17–25. DOI: 10.1093/infdis/136.1.17.

Deenick, E. K.; Hasbold, J.; Hodgkin, P. D. (1999): Switching to IgG3, IgG2b, and IgA is division linked and independent, revealing a stochastic framework for describing differentiation. In *Journal of immunology (Baltimore, Md. : 1950)* 163 (9), pp. 4707–4714.

Del Campo, Judith; Pizzorno, Andres; Djebali, Sophia; Bouley, Julien; Haller, Marjorie; Pérez-Vargas, Jimena et al. (2019): OVX836 a recombinant nucleoprotein vaccine inducing cellular responses and protective efficacy against multiple influenza A subtypes. In *NPJ vaccines* 4, p. 4. DOI: 10.1038/s41541-019-0098-4.

Deng, Lei; Cho, Ki Joon; Fiers, Walter; Saelens, Xavier (2015): M2e-Based Universal Influenza A Vaccines. In *Vaccines* 3 (1), pp. 105–136. DOI: 10.3390/vaccines3010105.

DiazGranados, Carlos A.; Dunning, Andrew J.; Jordanov, Emilia; Landolfi, Victoria; Denis, Martine; Talbot, H. Keipp (2013): High-dose trivalent influenza vaccine compared to standard dose vaccine in elderly adults: safety, immunogenicity and relative efficacy during the 2009-2010 season. In *Vaccine* 31 (6), pp. 861–866. DOI: 10.1016/j.vaccine.2012.12.013.

Doerfler, Walter (2021): Adenoviral Vector DNA- and SARS-CoV-2 mRNA-Based Covid-19 Vaccines: Possible Integration into the Human Genome - Are Adenoviral Genes Expressed in Vector-based Vaccines? In *Virus research* 302, p. 198466. DOI: 10.1016/j.virusres.2021.198466.

Dou, Dan; Revol, Rebecca; Östbye, Henrik; Wang, Hao; Daniels, Robert (2018): Influenza A Virus Cell Entry, Replication, Virion Assembly and Movement. In *Front. Immunol.* 9, p. 1581. DOI: 10.3389/fimmu.2018.01581.

Doyle, Joshua D.; Chung, Jessie R.; Kim, Sara S.; Gaglani, Manjusha; Raiyani, Chandni; Zimmerman, Richard K. et al. (2019): Interim Estimates of 2018-19 Seasonal Influenza Vaccine Effectiveness - United States, February 2019. In *MMWR. Morbidity and mortality weekly report* 68 (6), pp. 135–139. DOI: 10.15585/mmwr.mm6806a2.

Drake, J. W. (1993): Rates of spontaneous mutation among RNA viruses. In *Proceedings of the National Academy of Sciences* 90 (9), pp. 4171–4175. DOI: 10.1073/pnas.90.9.4171.

Dreyfus, Cyrille; Laursen, Nick S.; Kwaks, Ted; Zuijdgeest, David; Khayat, Reza; Ekiert, Damian C. et al. (2012): Highly conserved protective epitopes on influenza B viruses. In *Science (New York, N.Y.)* 337 (6100), pp. 1343–1348. DOI: 10.1126/science.1222908.

Dricu, Anica (Ed.) (2012): Methylation - From DNA, RNA and Histones to Diseases and Treatment: InTech.

Ekiert, Damian C.; Bhabha, Gira; Elsliger, Marc-André; Friesen, Robert H. E.; Jongeneelen, Mandy; Throsby, Mark et al. (2009): Antibody recognition of a highly conserved influenza virus epitope. In *Science (New York, N.Y.)* 324 (5924), pp. 246–251. DOI: 10.1126/science.1171491.

El Bakkouri, Karim; Descamps, Francis; Filette, Marina de; Smet, Anouk; Festjens, Els; Birkett, Ashley et al. (2011): Universal vaccine based on ectodomain of

matrix protein 2 of influenza A: Fc receptors and alveolar macrophages mediate protection. In *Journal of immunology (Baltimore, Md. : 1950)* 186 (2), pp. 1022–1031. DOI: 10.4049/jimmunol.0902147.

EMA (2021): Fluenz Tetra | European Medicines Agency. Available online at https://www.ema.europa.eu/en/medicines/human/EPAR/fluenz-tetra, updated on 10/28/2021, checked on 10/28/2021.

Epstein, Suzanne L.; Kong, Wing-pui; Misplon, Julia A.; Lo, Chia-Yun; Tumpey, Terrence M.; Xu, Ling; Nabel, Gary J. (2005): Protection against multiple influenza A subtypes by vaccination with highly conserved nucleoprotein. In *Vaccine* 23 (46-47), pp. 5404–5410. DOI: 10.1016/j.vaccine.2005.04.047.

Estrada, Leonardo D.; Schultz-Cherry, Stacey (2019): Development of a Universal Influenza Vaccine. In *Journal of immunology (Baltimore, Md. : 1950)* 202 (2), pp. 392–398. DOI: 10.4049/jimmunol.1801054.

Falsey, Ann R.; Treanor, John J.; Tornieporth, Nadia; Capellan, Jose; Gorse, Geoffrey J. (2009): Randomized, double-blind controlled phase 3 trial comparing the immunogenicity of high-dose and standard-dose influenza vaccine in adults 65 years of age and older. In *J INFECT DIS* 200 (2), pp. 172–180. DOI: 10.1086/599790.

FDA (2012): FDA approves first seasonal influenza vaccine manufactured using cell culture technology. Available online at https://web.archive.org/web/20130106013450/http://www.fda.gov/newsevents/newsroom/pressannouncements/ucm328982.htm, updated on 10/28/2021, checked on 10/28/2021.

Fedson, D. S. (1998): Measuring protection: efficacy versus effectiveness. In *Developments in biological standardization* 95, pp. 195–201.

Fensterl, Volker; Chattopadhyay, Saurabh; Sen, Ganes C. (2015): No Love Lost Between Viruses and Interferons. In *Annual review of virology* 2 (1), pp. 549–572. DOI: 10.1146/annurev-virology-100114-055249.

Fields, Bernard N.; Knipe, David Mahan; Howley, Peter M. (2015): Fields Virology. Philadelphia: Wolters Kluwer. Available online at http://gbv.eblib.com/patron/FullRecord.aspx?p=3418302.

Finkelshtein, Danit; Werman, Ariel; Novick, Daniela; Barak, Sara; Rubinstein, Menachem (2013): LDL receptor and its family members serve as the cellular receptors for vesicular stomatitis virus. In *Proceedings of the National Academy of Sciences* 110 (18), pp. 7306–7311. DOI: 10.1073/pnas.1214441110.

Fouchier, Ron A. M.; Schneeberger, Peter M.; Rozendaal, Frans W.; Broekman, Jan M.; Kemink, Stiena A. G.; Munster, Vincent et al. (2004): Avian influenza A virus (H7N7) associated with human conjunctivitis and a fatal case of acute respiratory distress syndrome. In *Proceedings of the National Academy of Sciences* 101 (5), pp. 1356–1361. DOI: 10.1073/pnas.0308352100.

Francis, T. (1937): Epidemiological Studies in Influenza. In *American journal of public health and the nation's health* 27 (3), pp. 211–225. DOI: 10.2105/ajph.27.3.211.

Fuchs, Jonathan D.; Frank, Ian; Elizaga, Marnie L.; Allen, Mary; Frahm, Nicole; Kochar, Nidhi et al. (2015): First-in-Human Evaluation of the Safety and Immunogenicity of a Recombinant Vesicular Stomatitis Virus Human

Immunodeficiency Virus-1 gag Vaccine (HVTN 090). In *Open forum infectious diseases* 2 (3), ofv082. DOI: 10.1093/ofid/ofv082.

Fujii, Yutaka; Goto, Hideo; Watanabe, Tokiko; Yoshida, Tetsuya; Kawaoka, Yoshihiro (2003): Selective incorporation of influenza virus RNA segments into virions. In *Proceedings of the National Academy of Sciences* 100 (4), pp. 2002–2007. DOI: 10.1073/pnas.0437772100.

Fujimoto, Yoshikazu; Tomioka, Yukiko; Takakuwa, Hiroki; Uechi, Gen-Ichiro; Yabuta, Toshiyo; Ozaki, Kinuyo et al. (2016): Cross-protective potential of anti-nucleoprotein human monoclonal antibodies against lethal influenza A virus infection. In *The Journal of general virology* 97 (9), pp. 2104–2116. DOI: 10.1099/jgv.0.000518.

Furuyama, Wakako; Reynolds, Pierce; Haddock, Elaine; Meade-White, Kimberly; Quynh Le, Mai; Kawaoka, Yoshihiro et al. (2020): A single dose of a vesicular stomatitis virus-based influenza vaccine confers rapid protection against H5 viruses from different clades. In *NPJ vaccines* 5 (1), p. 4. DOI: 10.1038/s41541-019-0155-z.

Gabriel, Gülsah; Klingel, Karin; Planz, Oliver; Bier, Katja; Herwig, Astrid; Sauter, Martina; Klenk, Hans-Dieter (2009): Spread of infection and lymphocyte depletion in mice depends on polymerase of influenza virus. In *The American journal of pathology* 175 (3), pp. 1178–1186. DOI: 10.2353/ajpath.2009.090339.

Geraci, J. R.; St Aubin, D. J.; Barker, I. K.; Webster, R. G.; Hinshaw, V. S.; Bean, W. J. et al. (1982): Mass mortality of harbor seals: pneumonia associated with influenza A virus. In *Science (New York, N.Y.)* 215 (4536), pp. 1129–1131. DOI: 10.1126/science.7063847.

Gerdil, Catherine (2003): The annual production cycle for influenza vaccine. In *Vaccine* 21 (16), pp. 1776–1779. DOI: 10.1016/s0264-410x(03)00071-9.

Gilbertson, Brad; Ng, Wy Ching; Crawford, Simon; McKimm-Breschkin, Jenny L.; Brown, Lorena E. (2017): Mouse Saliva Inhibits Transit of Influenza Virus to the Lower Respiratory Tract by Efficiently Blocking Influenza Virus Neuraminidase Activity. In *Journal of virology* 91 (14). DOI: 10.1128/JVI.00145-17.

Global Influenza Surveillance and Response System (GISRS) (2021). Available online at https://www.who.int/initiatives/global-influenza-surveillance-and-response-system, updated on 8/19/2021, checked on 8/19/2021.

Gog, Julia R.; Afonso, Emmanuel Dos Santos; Dalton, Rosa M.; Leclercq, India; Tiley, Laurence; Elton, Debra et al. (2007): Codon conservation in the influenza A virus genome defines RNA packaging signals. In *Nucleic acids research* 35 (6), pp. 1897–1907. DOI: 10.1093/nar/gkm087.

Goodman, Alan G.; Heinen, Paul P.; Guerra, Susana; Vijayan, Aneesh; Sorzano, Carlos Oscar S.; Gomez, Carmen E.; Esteban, Mariano (2011): A human multi-epitope recombinant vaccinia virus as a universal T cell vaccine candidate against influenza virus. In *PLoS ONE* 6 (10), e25938. DOI: 10.1371/journal.pone.0025938.

Grant, Emma; Wu, Chao; Chan, Kok-Fei; Eckle, Sidonia; Bharadwaj, Mandvi; Zou, Quan Ming et al. (2013): Nucleoprotein of influenza A virus is a major target

of immunodominant CD8+ T-cell responses. In *Immunology and cell biology* 91 (2), pp. 184–194. DOI: 10.1038/icb.2012.78.

Graves, P. N.; Schulman, J. L.; Young, J. F.; Palese, P. (1983): Preparation of influenza virus subviral particles lacking the HA1 subunit of hemagglutinin: unmasking of cross-reactive HA2 determinants. In *Virology* 126 (1), pp. 106–116. DOI: 10.1016/0042-6822(83)90465-8.

Groves, Helen T.; McDonald, Jacqueline U.; Langat, Pinky; Kinnear, Ekaterina; Kellam, Paul; McCauley, John et al. (2018): Mouse Models of Influenza Infection with Circulating Strains to Test Seasonal Vaccine Efficacy. In *Front. Immunol.* 9, p. 126. DOI: 10.3389/fimmu.2018.00126.

Guilliams, Martin; Bruhns, Pierre; Saeys, Yvan; Hammad, Hamida; Lambrecht, Bart N. (2014): The function of Fcγ receptors in dendritic cells and macrophages. In *Nat Rev Immunol* 14 (2), pp. 94–108. DOI: 10.1038/nri3582.

Guo, Fucheng; Yang, Jinjin; Pan, Junbin; Liang, Xianghui; Shen, Xuejuan; Irwin, David M. et al. (2020): Origin and Evolution of H1N1/pdm2009: A Codon Usage Perspective. In *Frontiers in microbiology* 11, p. 1615. DOI: 10.3389/fmicb.2020.01615.

Hai, Rong; Krammer, Florian; Tan, Gene S.; Pica, Natalie; Eggink, Dirk; Maamary, Jad et al. (2012): Influenza viruses expressing chimeric hemagglutinins: globular head and stalk domains derived from different subtypes. In *Journal of virology* 86 (10), pp. 5774–5781. DOI: 10.1128/JVI.00137-12.

Halbherr, Stefan J.; Brostoff, Terza; Tippenhauer, Merve; Locher, Samira; Berger Rentsch, Marianne; Zimmer, Gert (2013): Vaccination with recombinant RNA replicon particles protects chickens from H5N1 highly pathogenic avian influenza virus. In *PLoS ONE* 8 (6), e66059. DOI: 10.1371/journal.pone.0066059.

Hashem, Anwar M. (2015): Prospects of HA-based universal influenza vaccine. In *BioMed research international* 2015, p. 414637. DOI: 10.1155/2015/414637.

Hashemi, Hamidreza; Pouyanfard, Somayeh; Bandehpour, Mojgan; Noroozbabaei, Zahra; Kazemi, Bahram; Saelens, Xavier; Mokhtari-Azad, Talat (2012): Immunization with M2e-displaying T7 bacteriophage nanoparticles protects against influenza A virus challenge. In *PLoS ONE* 7 (9), e45765. DOI: 10.1371/journal.pone.0045765.

Hauge, Solveig; Madhun, Abdullah; Cox, Rebecca Jane; Haaheim, Lars Reinhardt (2007): Quality and kinetics of the antibody response in mice after three different low-dose influenza virus vaccination strategies. In *Clin Vaccine Immunol* 14 (8), pp. 978–983. DOI: 10.1128/CVI.00033-07#R13.

He, Xiao-Song; Holmes, Tyson H.; Zhang, Caiqiu; Mahmood, Kutubuddin; Kemble, George W.; Lewis, David B. et al. (2006): Cellular immune responses in children and adults receiving inactivated or live attenuated influenza vaccines. In *Journal of virology* 80 (23), pp. 11756–11766. DOI: 10.1128/JVI.01460-06.

Hennrich, Alexandru A.; Sawatsky, Bevan; Santos-Mandujano, Rosalía; Banda, Dominic H.; Oberhuber, Martina; Schopf, Anika et al. (2021): Safe and effective two-in-one replicon-and-VLP minispike vaccine for COVID-19:

Protection of mice after a single immunization. In *PLoS pathogens* 17 (4), e1009064. DOI: 10.1371/journal.ppat.1009064.

Hensley, Scott E.; Das, Suman R.; Bailey, Adam L.; Schmidt, Loren M.; Hickman, Heather D.; Jayaraman, Akila et al. (2009): Hemagglutinin receptor binding avidity drives influenza A virus antigenic drift. In *Science (New York, N.Y.)* 326 (5953), pp. 734–736. DOI: 10.1126/science.1178258.

Herold, Susanne; Becker, Christin; Ridge, Karen M.; Budinger, G. R. Scott (2015): Influenza virus-induced lung injury: pathogenesis and implications for treatment. In *The European respiratory journal* 45 (5), pp. 1463–1478. DOI: 10.1183/09031936.00186214.

Herrera-Rodriguez, José; Meijerhof, Tjarko; Niesters, Hubert G.; Stjernholm, Grete; Hovden, Arnt-Ove; Sørensen, Birger et al. (2018): A novel peptide-based vaccine candidate with protective efficacy against influenza A in a mouse model. In *Virology* 515, pp. 21–28. DOI: 10.1016/j.virol.2017.11.018.

Hessel, Annett; Savidis-Dacho, Helga; Coulibaly, Sogue; Portsmouth, Daniel; Kreil, Thomas R.; Crowe, Brian A. et al. (2014): MVA vectors expressing conserved influenza proteins protect mice against lethal challenge with H5N1, H9N2 and H7N1 viruses. In *PLoS ONE* 9 (2), e88340. DOI: 10.1371/journal.pone.0088340.

Hocart, M. J.; Mackenzie, J. S.; Stewart, G. A. (1988): The IgG subclass responses induced by wild-type, cold-adapted and purified haemagglutinin from influenza virus A/Queensland/6/72 in CBA/CaH mice. In *The Journal of general virology* 69 (Pt 8), pp. 1873–1882. DOI: 10.1099/0022-1317-69-8-1873.

Hocart, M. J.; Mackenzie, J. S.; Stewart, G. A. (1989): The IgG subclass responses to influenza virus haemagglutinin in the mouse: effect of route of inoculation. In *The Journal of general virology* 70 (Pt 4), pp. 809–818. DOI: 10.1099/0022-1317-70-4-809.

Hoffmann, E.; Stech, J.; Guan, Y.; Webster, R. G.; Perez, D. R. (2001): Universal primer set for the full-length amplification of all influenza A viruses. In *Archives of Virology* 146 (12), pp. 2275–2289. DOI: 10.1007/s007050170002.

Horimoto, Taisuke; Kawaoka, Yoshihiro (2005): Influenza: lessons from past pandemics, warnings from current incidents. In *Nature reviews. Microbiology* 3 (8), pp. 591–600. DOI: 10.1038/nrmicro1208.

Hovanessian, A. G. (1989): The double stranded RNA-activated protein kinase induced by interferon: dsRNA-PK. In *Journal of interferon research* 9 (6), pp. 641–647. DOI: 10.1089/jir.1989.9.641.

Humphreys, Ian R.; Sebastian, Sarah (2018): Novel viral vectors in infectious diseases. In *Immunology* 153 (1), pp. 1–9. DOI: 10.1111/imm.12829.

Hussell, T.; Pennycook, A.; Openshaw, P. J. (2001): Inhibition of tumor necrosis factor reduces the severity of virus-specific lung immunopathology. In *European journal of immunology* 31 (9), pp. 2566–2573. DOI: 10.1002/1521-4141(200109)31:9<2566::aid-immu2566>3.0.co;2-l.

Ibricevic, Aida; Pekosz, Andrew; Walter, Michael J.; Newby, Celeste; Battaile, John T.; Brown, Earl G. et al. (2006): Influenza virus receptor specificity and cell tropism in mouse and human airway epithelial cells. In *Journal of virology* 80 (15), pp. 7469–7480. DOI: 10.1128/JVI.02677-05.

ICTV (2021): Virus Taxonomy: 2020 Release. Negative Sense RNA Viruses. Edited by International Committee on Taxonomy of Viruses. International Committee on Taxonomy of Viruses. Available online at https://talk.ictvonline.org/ictv-reports/ictv_9th_report/negative-sense-rna-viruses-2011/w/negrna_viruses/209/orthomyxoviridae, updated on 8/11/2021, checked on 8/11/2021.

Impagliazzo, Antonietta; Milder, Fin; Kuipers, Harmjan; Wagner, Michelle V.; Zhu, Xueyong; Hoffman, Ryan M. B. et al. (2015): A stable trimeric influenza hemagglutinin stem as a broadly protective immunogen. In *Science (New York, N.Y.)* 349 (6254), pp. 1301–1306. DOI: 10.1126/science.aac7263.

Iwasaki, Akiko; Pillai, Padmini S. (2014): Innate immunity to influenza virus infection. In *Nat Rev Immunol* 14 (5), pp. 315–328. DOI: 10.1038/nri3665.

Jackson, Claire (2009): History lessons: the Asian flu pandemic. In *The British journal of general practice : the journal of the Royal College of General Practitioners* 59 (565), pp. 622–623. DOI: 10.3399/bjgp09X453882.

Jackson, Michael L.; Chung, Jessie R.; Jackson, Lisa A.; Phillips, C. Hallie; Benoit, Joyce; Monto, Arnold S. et al. (2017): Influenza Vaccine Effectiveness in the United States during the 2015-2016 Season. In *The New England journal of medicine* 377 (6), pp. 534–543. DOI: 10.1056/NEJMoa1700153.

Jazayeri, Seyed Davoud; Poh, Chit Laa (2019): Development of Universal Influenza Vaccines Targeting Conserved Viral Proteins. In *Vaccines* 7 (4), p. 169. DOI: 10.3390/vaccines7040169.

Jegaskanda, Sinthujan; Co, Mary Dawn T.; Cruz, John; Subbarao, Kanta; Ennis, Francis A.; Terajima, Masanori (2017): Induction of H7N9-Cross-Reactive Antibody-Dependent Cellular Cytotoxicity Antibodies by Human Seasonal Influenza A Viruses that are Directed Toward the Nucleoprotein. In *J INFECT DIS* 215 (5), pp. 818–823. DOI: 10.1093/infdis/jiw629.

Jegaskanda, Sinthujan; Job, Emma R.; Kramski, Marit; Laurie, Karen; Isitman, Gamze; Rose, Robert de et al. (2013): Cross-reactive influenza-specific antibody-dependent cellular cytotoxicity antibodies in the absence of neutralizing antibodies. In *Journal of immunology (Baltimore, Md. : 1950)* 190 (4), pp. 1837–1848. DOI: 10.4049/jimmunol.1201574.

Jiao, Huipeng; Wachsmuth, Laurens; Kumari, Snehlata; Schwarzer, Robin; Lin, Juan; Eren, Remzi Onur et al. (2020): Z-nucleic-acid sensing triggers ZBP1-dependent necroptosis and inflammation. In *Nature* 580 (7803), pp. 391–395. DOI: 10.1038/s41586-020-2129-8.

Johnson, J. Erik; Nasar, Farooq; Coleman, John W.; Price, Roger E.; Javadian, Ali; Draper, Kenneth et al. (2007): Neurovirulence properties of recombinant vesicular stomatitis virus vectors in non-human primates. In *Virology* 360 (1), pp. 36–49. DOI: 10.1016/j.virol.2006.10.026.

Johnson, Niall P. A. S.; Mueller, Juergen (2002): Updating the accounts: global mortality of the 1918-1920 "Spanish" influenza pandemic. In *Bulletin of the history of medicine* 76 (1), pp. 105–115. DOI: 10.1353/bhm.2002.0022.

Johnson, P. R.; Feldman, S.; Thompson, J. M.; Mahoney, J. D.; Wright, P. F. (1985): Comparison of long-term systemic and secretory antibody responses

in children given live, attenuated, or inactivated influenza A vaccine. In *Journal of medical virology* 17 (4), pp. 325–335. DOI: 10.1002/jmv.1890170405.

Jones, Steven M.; Feldmann, Heinz; Ströher, Ute; Geisbert, Joan B.; Fernando, Lisa; Grolla, Allen et al. (2005): Live attenuated recombinant vaccine protects nonhuman primates against Ebola and Marburg viruses. In *Nature medicine* 11 (7), pp. 786–790. DOI: 10.1038/nm1258.

Joseph, Udayan; Su, Yvonne C. F.; Vijaykrishna, Dhanasekaran; Smith, Gavin J. D. (2017): The ecology and adaptive evolution of influenza A interspecies transmission. In *Influenza and other respiratory viruses* 11 (1), pp. 74–84. DOI: 10.1111/irv.12412.

Kalhoro, Nazeer H.; Veits, Jutta; Rautenschlein, Silke; Zimmer, Gert (2009): A recombinant vesicular stomatitis virus replicon vaccine protects chickens from highly pathogenic avian influenza virus (H7N1). In *Vaccine* 27 (8), pp. 1174–1183. DOI: 10.1016/j.vaccine.2008.12.019.

Kalil, Andre C.; Thomas, Paul G. (2019): Influenza virus-related critical illness: pathophysiology and epidemiology. In *Critical care (London, England)* 23 (1), p. 258. DOI: 10.1186/s13054-019-2539-x.

Kapadia, Sagar U.; Simon, Ian D.; Rose, John K. (2008): SARS vaccine based on a replication-defective recombinant vesicular stomatitis virus is more potent than one based on a replication-competent vector. In *Virology* 376 (1), pp. 165–172. DOI: 10.1016/j.virol.2008.03.002.

Kärber, G. (1931): Beitrag zur kollektiven Behandlung pharmakologischer Reihenversuche. In *Archiv f. experiment. Pathol. u. Pharmakol* 162 (4), pp. 480–483. DOI: 10.1007/BF01863914.

Kendal, Alan P.; Maassab, Hunein F.; Alexandrova, Galina I.; Ghendon, Yuri Z. (1982): Development of cold-adapted recombinant live, attenuated influenza A vaccines in the U.S.A. and U.S.S.R. In *Antiviral research* 1 (6), pp. 339–365. DOI: 10.1016/0166-3542(82)90034-1.

Kilbourne, E. D.; Schulman, J. L.; Schild, G. C.; Schloer, G.; Swanson, J.; Bucher, D. (1971): Related studies of a recombinant influenza-virus vaccine. I. Derivation and characterization of virus and vaccine. In *J INFECT DIS* 124 (5), pp. 449–462. DOI: 10.1093/infdis/124.5.449.

Kim, Se Mi; Kim, Young-Il; Pascua, Philippe Noriel Q.; Choi, Young Ki (2016): Avian Influenza A Viruses: Evolution and Zoonotic Infection. In *Seminars in respiratory and critical care medicine* 37 (4), pp. 501–511. DOI: 10.1055/s-0036-1584953.

Klenk, H. D.; Rott, R.; Orlich, M.; Blödorn, J. (1975): Activation of influenza A viruses by trypsin treatment. In *Virology* 68 (2), pp. 426–439. DOI: 10.1016/0042-6822(75)90284-6.

Klenk, Hans D.; Garten, Wolfgang; Matrosovich, Mikhail (2011): Molecular mechanisms of interspecies transmission and pathogenicity of influenza viruses: Lessons from the 2009 pandemic. In *BioEssays : news and reviews in molecular, cellular and developmental biology* 33 (3), pp. 180–188. DOI: 10.1002/bies.201000118.

Korteweg, Christine; Gu, Jiang (2008): Pathology, molecular biology, and pathogenesis of avian influenza A (H5N1) infection in humans. In *The*

American journal of pathology 172 (5), pp. 1155–1170. DOI: 10.2353/ajpath.2008.070791.

Krammer, Florian (2019): The human antibody response to influenza A virus infection and vaccination. In *Nat Rev Immunol* 19 (6), pp. 383–397. DOI: 10.1038/s41577-019-0143-6.

Krammer, Florian; Palese, Peter (2013): Influenza virus hemagglutinin stalk-based antibodies and vaccines. In *Current opinion in virology* 3 (5), pp. 521–530. DOI: 10.1016/j.coviro.2013.07.007.

Krammer, Florian; Smith, Gavin J. D.; Fouchier, Ron A. M.; Peiris, Malik; Kedzierska, Katherine; Doherty, Peter C. et al. (2018): Influenza. In *Nature reviews. Disease primers* 4 (1), p. 3. DOI: 10.1038/s41572-018-0002-y.

Kretzschmar, E.; Buonocore, L.; Schnell, M. J.; Rose, J. K. (1997): High-efficiency incorporation of functional influenza virus glycoproteins into recombinant vesicular stomatitis viruses. In *Journal of virology* 71 (8), pp. 5982–5989. DOI: 10.1128/JVI.71.8.5982-5989.1997.

Laddy, Dominick J.; Yan, Jian; Kutzler, Michele; Kobasa, Darwyn; Kobinger, Gary P.; Khan, Amir S. et al. (2008): Heterosubtypic protection against pathogenic human and avian influenza viruses via in vivo electroporation of synthetic consensus DNA antigens. In *PLoS ONE* 3 (6), e2517. DOI: 10.1371/journal.pone.0002517.

Laghlali, Gabriel; Lawlor, Kate E.; Tate, Michelle D. (2020): Die Another Way: Interplay between Influenza A Virus, Inflammation and Cell Death. In *Viruses* 12 (4). DOI: 10.3390/v12040401.

LaMere, Mark W.; Lam, Ho-Tak; Moquin, Amy; Haynes, Laura; Lund, Frances E.; Randall, Troy D.; Kaminski, Denise A. (2011): Contributions of antinucleoprotein IgG to heterosubtypic immunity against influenza virus. In *Journal of immunology (Baltimore, Md. : 1950)* 186 (7), pp. 4331–4339. DOI: 10.4049/jimmunol.1003057.

Lawson, N. D.; Stillman, E. A.; Whitt, M. A.; Rose, J. K. (1995): Recombinant vesicular stomatitis viruses from DNA. In *Proceedings of the National Academy of Sciences* 92 (10), pp. 4477–4481. DOI: 10.1073/pnas.92.10.4477.

Lazarowitz, Sondra G.; Choppin, Purnell W. (1975): Enhancement of the infectivity of influenza A and B viruses by proteolytic cleavage of the hemagglutinin polypeptide. In *Virology* 68 (2), pp. 440–454. DOI: 10.1016/0042-6822(75)90285-8.

Lee, Laurel Yong-Hwa; Ha, Do Lien Anh; Simmons, Cameron; Jong, Menno D. de; van Chau, Nguyen Vinh; Schumacher, Reto et al. (2008): Memory T cells established by seasonal human influenza A infection cross-react with avian influenza A (H5N1) in healthy individuals. In *The Journal of clinical investigation* 118 (10), pp. 3478–3490. DOI: 10.1172/JCI32460.

Lee, Yu-Na; Lee, Young-Tae; Kim, Min-Chul; Hwang, Hye Suk; Lee, Jong Seok; Kim, Ki-Hye; Kang, Sang-Moo (2014): Fc receptor is not required for inducing antibodies but plays a critical role in conferring protection after influenza M2 vaccination. In *Immunology* 143 (2), pp. 300–309. DOI: 10.1111/imm.12310.

Li, S. Q.; Orlich, M.; Rott, R. (1990): Generation of seal influenza virus variants pathogenic for chickens, because of hemagglutinin cleavage site changes. In *Journal of virology* 64 (7), pp. 3297–3303. DOI: 10.1128/JVI.64.7.3297-3303.1990.

Li, Tian; Li, Zhenyu; Deans, Erin E.; Mittler, Eva; Liu, Meisui; Chandran, Kartik; Ivanovic, Tijana (2021a): The shape of pleomorphic virions determines resistance to cell-entry pressure. In *Nat Microbiol* 6 (5), pp. 617–629. DOI: 10.1038/s41564-021-00877-0.

Li, Yansheng; Xu, Mingkai; Li, Yongqiang; Gu, Wu; Halimu, Gulinare; Li, Yuqi et al. (2021b): A recombinant protein containing influenza viral conserved epitopes and superantigen induces broad-spectrum protection. In *eLife* 10. DOI: 10.7554/eLife.71725.

Li, Yize; Banerjee, Shuvojit; Goldstein, Stephen A.; Dong, Beihua; Gaughan, Christina; Rath, Sneha et al. (2017): Ribonuclease L mediates the cell-lethal phenotype of double-stranded RNA editing enzyme ADAR1 deficiency in a human cell line. In *eLife* 6. DOI: 10.7554/elife.25687.

Liao, Hsin-Yu; Wang, Shih-Chi; Ko, Yi-An; Lin, Kuo-I; Ma, Che; Cheng, Ting-Jen Rachel; Wong, Chi-Huey (2020): Chimeric hemagglutinin vaccine elicits broadly protective CD4 and CD8 T cell responses against multiple influenza strains and subtypes. In *Proceedings of the National Academy of Sciences* 117 (30), pp. 17757–17763. DOI: 10.1073/pnas.2004783117.

Liddicoat, Brian J.; Piskol, Robert; Chalk, Alistair M.; Ramaswami, Gokul; Higuchi, Miyoko; Hartner, Jochen C. et al. (2015): RNA editing by ADAR1 prevents MDA5 sensing of endogenous dsRNA as nonself. In *Science (New York, N.Y.)* 349 (6252), pp. 1115–1120. DOI: 10.1126/science.aac7049.

Liu, C.; Eichelberger, M. C.; Compans, R. W.; Air, G. M. (1995): Influenza type A virus neuraminidase does not play a role in viral entry, replication, assembly, or budding. In *Journal of virology* 69 (2), pp. 1099–1106. DOI: 10.1128/JVI.69.2.1099-1106.1995.

Livingston, John H.; Lin, Jean-Pierre; Dale, Russell C.; Gill, Deepak; Brogan, Paul; Munnich, Arnold et al. (2014): A type I interferon signature identifies bilateral striatal necrosis due to mutations in ADAR1. In *Journal of medical genetics* 51 (2), pp. 76–82. DOI: 10.1136/jmedgenet-2013-102038.

Locksley, R. M.; Killeen, N.; Lenardo, M. J. (2001): The TNF and TNF receptor superfamilies: integrating mammalian biology. In *Cell* 104 (4), pp. 487–501. DOI: 10.1016/s0092-8674(01)00237-9.

Long, Jason S.; Mistry, Bhakti; Haslam, Stuart M.; Barclay, Wendy S. (2019): Host and viral determinants of influenza A virus species specificity. In *Nature reviews. Microbiology* 17 (2), pp. 67–81. DOI: 10.1038/s41579-018-0115-z.

Loo, Yueh-Ming; Fornek, Jamie; Crochet, Nanette; Bajwa, Gagan; Perwitasari, Olivia; Martinez-Sobrido, Luis et al. (2008): Distinct RIG-I and MDA5 signaling by RNA viruses in innate immunity. In *Journal of virology* 82 (1), pp. 335–345. DOI: 10.1128/JVI.01080-07.

Lundstrom, Kenneth (2021): Viral Vectors for COVID-19 Vaccine Development. In *Viruses* 13 (2). DOI: 10.3390/v13020317.

Ma, Wenjun; Kahn, Robert E.; Richt, Juergen A. (2008): The pig as a mixing vessel for influenza viruses: Human and veterinary implications. In *Journal of molecular and genetic medicine : an international journal of biomedical research* 3 (1), pp. 158–166.

Maassab, H. F. (1967): Adaptation and growth characteristics of influenza virus at 25 degrees c. In *Nature* 213 (5076), pp. 612–614. DOI: 10.1038/213612a0.

Maassab, H. F.; Kendal, A. P.; Abrams, G. D.; Monto, A. S. (1982): Evaluation of a cold-recombinant influenza virus vaccine in ferrets. In *J INFECT DIS* 146 (6), pp. 780–790. DOI: 10.1093/infdis/146.6.780.

Maassab, H. F.; Kendal, A. P.; Davenport, F. M. (1972): Hybrid formation of influenza virus at 25. In *Proceedings of the Society for Experimental Biology and Medicine. Society for Experimental Biology and Medicine (New York, N.Y.)* 139 (3), pp. 768–773. DOI: 10.3181/00379727-139-35234.

Margine, Irina; Hai, Rong; Albrecht, Randy A.; Obermoser, Gerlinde; Harrod, A. Carson; Banchereau, Jacques et al. (2013): H3N2 influenza virus infection induces broadly reactive hemagglutinin stalk antibodies in humans and mice. In *Journal of virology* 87 (8), pp. 4728–4737. DOI: 10.1128/JVI.03509-12.

Martin, Matthew D.; Badovinac, Vladimir P. (2018): Defining Memory CD8 T Cell. In *Front. Immunol.* 9, p. 2692. DOI: 10.3389/fimmu.2018.02692.

Martin, Thomas R.; Hagimoto, Naoki; Nakamura, Morio; Matute-Bello, Gustavo (2005): Apoptosis and epithelial injury in the lungs. In *Proceedings of the American Thoracic Society* 2 (3), pp. 214–220. DOI: 10.1513/pats.200504-031AC.

Marzi, Andrea; Robertson, Shelly J.; Haddock, Elaine; Feldmann, Friederike; Hanley, Patrick W.; Scott, Dana P. et al. (2015): EBOLA VACCINE. VSV-EBOV rapidly protects macaques against infection with the 2014/15 Ebola virus outbreak strain. In *Science (New York, N.Y.)* 349 (6249), pp. 739–742. DOI: 10.1126/science.aab3920.

Matassov, Demetrius; Marzi, Andrea; Latham, Terri; Xu, Rong; Ota-Setlik, Ayuko; Feldmann, Friederike et al. (2015): Vaccination With a Highly Attenuated Recombinant Vesicular Stomatitis Virus Vector Protects Against Challenge With a Lethal Dose of Ebola Virus. In *J INFECT DIS* 212 Suppl 2, S443-51. DOI: 10.1093/infdis/jiv316.

Matsuoka, Yumiko; Lamirande, Elaine W.; Subbarao, Kanta (2009): The mouse model for influenza. In *Current protocols in microbiology* Chapter 15, Unit 15G.3. DOI: 10.1002/9780471729259.mc15g03s13.

Melville, M. W.; Tan, S. L.; Wambach, M.; Song, J.; Morimoto, R. I.; Katze, M. G. (1999): The cellular inhibitor of the PKR protein kinase, P58(IPK), is an influenza virus-activated co-chaperone that modulates heat shock protein 70 activity. In *The Journal of biological chemistry* 274 (6), pp. 3797–3803. DOI: 10.1074/jbc.274.6.3797.

Mendonça, Samir Andrade; Lorincz, Reka; Boucher, Paul; Curiel, David T. (2021): Adenoviral vector vaccine platforms in the SARS-CoV-2 pandemic. In *NPJ vaccines* 6 (1), p. 97. DOI: 10.1038/s41541-021-00356-x.

Monto, Arnold S.; Petrie, Joshua G.; Cross, Rachel T.; Johnson, Emileigh; Liu, Merry; Zhong, Weimin et al. (2015): Antibody to Influenza Virus

Neuraminidase: An Independent Correlate of Protection. In *J INFECT DIS* 212 (8), pp. 1191–1199. DOI: 10.1093/infdis/jiv195.

Moody, M. Anthony; Zhang, Ruijun; Walter, Emmanuel B.; Woods, Christopher W.; Ginsburg, Geoffrey S.; McClain, Micah T. et al. (2011): H3N2 influenza infection elicits more cross-reactive and less clonally expanded anti-hemagglutinin antibodies than influenza vaccination. In *PLoS ONE* 6 (10), e25797. DOI: 10.1371/journal.pone.0025797.

Moon, Eun-Kyung; Kang, Hae-Ji; Chu, Ki-Back; Lee, Su-Hwa; Lee, Dong-Hun; Soh, Yunsoo; Quan, Fu-Shi (2019): Immune Correlates of Protection Induced by Virus-Like Particles Containing 2009 H1N1 Pandemic Influenza HA, NA or M1 Proteins. In *Immunological investigations* 48 (4), pp. 355–366. DOI: 10.1080/08820139.2018.1544640.

Moreira, Étori Aguiar; Weber, Anna; Bolte, Hardin; Kolesnikova, Larissa; Giese, Sebastian; Lakdawala, Seema et al. (2016): A conserved influenza A virus nucleoprotein code controls specific viral genome packaging. In *Nat Commun* 7, p. 12861. DOI: 10.1038/ncomms12861.

Mostafa, Ahmed; Abdelwhab, Elsayed M.; Mettenleiter, Thomas C.; Pleschka, Stephan (2018): Zoonotic Potential of Influenza A Viruses: A Comprehensive Overview. In *Viruses* 10 (9). DOI: 10.3390/v10090497.

Munis, Altar M.; Bentley, Emma M.; Takeuchi, Yasuhiro (2020): A tool with many applications: vesicular stomatitis virus in research and medicine. In *Expert opinion on biological therapy* 20 (10), pp. 1187–1201. DOI: 10.1080/14712598.2020.1787981.

Murphy, B. R.; Holley, H. P.; Berquist, E. J.; Levine, M. M.; Spring, S. B.; Maassab, H. F. et al. (1979): Cold-adapted variants of influenza A virus: evaluation in adult seronegative volunteers of A/Scotland/840/74 and A/Victoria/3/75 cold-adapted recombinants derived from the cold-adapted A/Ann Arbor/6/60 strain. In *Infection and immunity* 23 (2), pp. 253–259. DOI: 10.1128/iai.23.2.253-259.1979.

Murphy, B. R.; Rennels, M. B.; Douglas, R. G.; Betts, R. F.; Couch, R. B.; Cate, T. R. et al. (1980): Evaluation of influenza A/Hong Kong/123/77 (H1N1) ts-1A2 and cold-adapted recombinant viruses in seronegative adult volunteers. In *Infection and immunity* 29 (2), pp. 348–355. DOI: 10.1128/iai.29.2.348-355.1980.

Murphy, Kenneth; Weaver, Casey (2018): Janeway Immunologie. 9. Aufl. 2018. Berlin, Heidelberg: Springer Berlin Heidelberg. Available online at http://nbn-resolving.org/urn:nbn:de:bsz:31-epflicht-1584460.

Neirynck, S.; Deroo, T.; Saelens, X.; Vanlandschoot, P.; Jou, W. M.; Fiers, W. (1999): A universal influenza A vaccine based on the extracellular domain of the M2 protein. In *Nature medicine* 5 (10), pp. 1157–1163. DOI: 10.1038/13484.

Noda, Takeshi (2011): Native morphology of influenza virions. In *Frontiers in microbiology* 2, p. 269. DOI: 10.3389/fmicb.2011.00269.

Nogales, Aitor; Aydillo, Teresa; Ávila-Pérez, Gines; Escalera, Alba; Chiem, Kevin; Cadagan, Richard et al. (2019): Functional Characterization and Direct

Comparison of Influenza A, B, C, and D NS1 Proteins in vitro and in vivo. In *Frontiers in microbiology* 10, p. 2862. DOI: 10.3389/fmicb.2019.02862.

Pabis, Anna; Rawle, Robert J.; Kasson, Peter M. (2020): Influenza hemagglutinin drives viral entry via two sequential intramembrane mechanisms. In *Proceedings of the National Academy of Sciences of the United States of America* 117 (13), pp. 7200–7207. DOI: 10.1073/pnas.1914188117.

Padilla-Quirarte, Herbey O.; Lopez-Guerrero, Delia V.; Gutierrez-Xicotencatl, Lourdes; Esquivel-Guadarrama, Fernando (2019): Protective Antibodies Against Influenza Proteins. In *Front. Immunol.* 10, p. 1677. DOI: 10.3389/fimmu.2019.01677.

Palese, Peter; Shaw, Megan L. (2007): Orthomyxoviridae: The Viruses and Their Replication. In Bernard N. Fields, David Mahan Knipe, Peter M. Howley (Eds.): Fields' virology. 5th ed. Philadelphia: Wolters Kluwer Health/Lippincott Williams & Wilkins.

Palese, Peter; Tobita, Kiyotake; Ueda, Masahiro; Compans, Richard W. (1974): Characterization of temperature sensitive influenza virus mutants defective in neuraminidase. In *Virology* 61 (2), pp. 397–410. DOI: 10.1016/0042-6822(74)90276-1.

Pan, Weiqi; Dong, Zhenyuan; Li, Feng; Meng, Weixu; Feng, Liqiang; Niu, Xuefeng et al. (2013): Visualizing influenza virus infection in living mice. In *Nat Commun* 4 (1), p. 2369. DOI: 10.1038/ncomms3369.

Peiris, M.; Yuen, K. Y.; Leung, C. W.; Chan, K. H.; Ip, P. L.; Lai, R. W. et al. (1999): Human infection with influenza H9N2. In *The Lancet* 354 (9182), pp. 916–917. DOI: 10.1016/s0140-6736(99)03311-5.

Pfaller, Christian K.; Donohue, Ryan C.; Nersisyan, Stepan; Brodsky, Leonid; Cattaneo, Roberto (2018): Extensive editing of cellular and viral double-stranded RNA structures accounts for innate immunity suppression and the proviral activity of ADAR1p150. In *PLoS biology* 16 (11), e2006577. DOI: 10.1371/journal.pbio.2006577.

Pfaller, Christian K.; George, Cyril X.; Samuel, Charles E. (2021): Adenosine Deaminases Acting on RNA (ADARs) and Viral Infections. In *Annual review of virology*. DOI: 10.1146/annurev-virology-091919-065320.

Pica, Natalie; Hai, Rong; Krammer, Florian; Wang, Taia T.; Maamary, Jad; Eggink, Dirk et al. (2012): Hemagglutinin stalk antibodies elicited by the 2009 pandemic influenza virus as a mechanism for the extinction of seasonal H1N1 viruses. In *Proceedings of the National Academy of Sciences* 109 (7), pp. 2573–2578. DOI: 10.1073/pnas.1200039109.

Pinto, L. H.; Holsinger, L. J.; Lamb, R. A. (1992): Influenza virus M2 protein has ion channel activity. In *Cell* 69 (3), pp. 517–528. DOI: 10.1016/0092-8674(92)90452-i.

Placido, Diana; Brown, Bernard A.; Lowenhaupt, Ky; Rich, Alexander; Athanasiadis, Alekos (2007): A left-handed RNA double helix bound by the Z alpha domain of the RNA-editing enzyme ADAR1. In *Structure (London, England : 1993)* 15 (4), pp. 395–404. DOI: 10.1016/j.str.2007.03.001.

Plotkin, Stanley (2014): History of vaccination. In *Proceedings of the National Academy of Sciences* 111 (34), pp. 12283–12287. DOI: 10.1073/pnas.1400472111.

Potter, C. W.; Oxford, J. S. (1979): Determinants of immunity to influenza infection in man. In *British medical bulletin* 35 (1), pp. 69–75. DOI: 10.1093/oxfordjournals.bmb.a071545.

Rajão, Daniela S.; Pérez, Daniel R. (2018): Universal Vaccines and Vaccine Platforms to Protect against Influenza Viruses in Humans and Agriculture. In *Frontiers in microbiology* 9, p. 123. DOI: 10.3389/fmicb.2018.00123.

Ran, F. Ann; Hsu, Patrick D.; Lin, Chie-Yu; Gootenberg, Jonathan S.; Konermann, Silvana; Trevino, Alexandro E. et al. (2013): Double nicking by RNA-guided CRISPR Cas9 for enhanced genome editing specificity. In *Cell* 154 (6), pp. 1380–1389. DOI: 10.1016/j.cell.2013.08.021.

Rice, Gillian I.; Kasher, Paul R.; Forte, Gabriella M. A.; Mannion, Niamh M.; Greenwood, Sam M.; Szynkiewicz, Marcin et al. (2012): Mutations in ADAR1 cause Aicardi-Goutières syndrome associated with a type I interferon signature. In *Nature genetics* 44 (11), pp. 1243–1248. DOI: 10.1038/ng.2414.

Roberts, A.; Buonocore, L.; Price, R.; Forman, J.; Rose, J. K. (1999): Attenuated vesicular stomatitis viruses as vaccine vectors. In *Journal of virology* 73 (5), pp. 3723–3732. DOI: 10.1128/JVI.73.5.3723-3732.1999.

Roberts, A.; Kretzschmar, E.; Perkins, A. S.; Forman, J.; Price, R.; Buonocore, L. et al. (1998): Vaccination with a recombinant vesicular stomatitis virus expressing an influenza virus hemagglutinin provides complete protection from influenza virus challenge. In *Journal of virology* 72 (6), pp. 4704–4711. DOI: 10.1128/JVI.72.6.4704-4711.1998.

Roy, A. M.; Parker, J. S.; Parrish, C. R.; Whittaker, G. R. (2000): Early stages of influenza virus entry into Mv-1 lung cells: involvement of dynamin. In *Virology* 267 (1), pp. 17–28. DOI: 10.1006/viro.1999.0109.

Rust, Michael J.; Lakadamyali, Melike; Zhang, Feng; Zhuang, Xiaowei (2004): Assembly of endocytic machinery around individual influenza viruses during viral entry. In *Nature structural & molecular biology* 11 (6), pp. 567–573. DOI: 10.1038/nsmb769.

Ryder, Alex B.; Nachbagauer, Raffael; Buonocore, Linda; Palese, Peter; Krammer, Florian; Rose, John K. (2015): Vaccination with Vesicular Stomatitis Virus-Vectored Chimeric Hemagglutinins Protects Mice against Divergent Influenza Virus Challenge Strains. In *Journal of virology* 90 (5), pp. 2544–2550. DOI: 10.1128/JVI.02598-15.

Saelens, Xavier (2019): The Role of Matrix Protein 2 Ectodomain in the Development of Universal Influenza Vaccines. In *J INFECT DIS* 219 (Suppl_1), S68-S74. DOI: 10.1093/infdis/jiz003.

Samuel, Charles E. (2011a): Adenosine deaminases acting on RNA (ADARs) and A-to-I editing. Berlin: Springer (Current topics in microbiology and immunology, 353).

Samuel, Charles E. (2011b): Adenosine deaminases acting on RNA (ADARs) are both antiviral and proviral. In *Virology* 411 (2), pp. 180–193. DOI: 10.1016/j.virol.2010.12.004.

Sandbulte, Matthew R.; Spickler, Anna R.; Zaabel, Pamela K.; Roth, James A. (2015): Optimal Use of Vaccines for Control of Influenza A Virus in Swine. In *Vaccines* 3 (1), pp. 22–73. DOI: 10.3390/vaccines3010022.

Sauter, N. K.; Hanson, J. E.; Glick, G. D.; Brown, J. H.; Crowther, R. L.; Park, S. J. et al. (1992): Binding of influenza virus hemagglutinin to analogs of its cell-surface receptor, sialic acid: analysis by proton nuclear magnetic resonance spectroscopy and X-ray crystallography. In *Biochemistry* 31 (40), pp. 9609–9621. DOI: 10.1021/bi00155a013.

Scheiblauer, H.; Kendal, A. P.; Rott, R. (1995): Pathogenicity of influenza A/Seal/Mass/1/80 virus mutants for mammalian species. In *Archives of Virology* 140 (2), pp. 341–348. DOI: 10.1007/BF01309867.

Schotsaert, M.; Ysenbaert, T.; Neyt, K.; Ibañez, L. I.; Bogaert, P.; Schepens, B. et al. (2013): Natural and long-lasting cellular immune responses against influenza in the M2e-immune host. In *Mucosal immunology* 6 (2), pp. 276–287. DOI: 10.1038/mi.2012.69.

Schwartz, T.; Behlke, J.; Lowenhaupt, K.; Heinemann, U.; Rich, A. (2001): Structure of the DLM-1-Z-DNA complex reveals a conserved family of Z-DNA-binding proteins. In *Nature structural biology* 8 (9), pp. 761–765. DOI: 10.1038/nsb0901-761.

Sealy, Robert; Surman, Sherri; Hurwitz, Julia L.; Coleclough, Christopher (2003): Antibody response to influenza infection of mice: different patterns for glycoprotein and nucleocapsid antigens. In *Immunology* 108 (4), pp. 431–439. DOI: 10.1046/j.1365-2567.2003.01615.x.

Shibuya, Meito; Aoshi, Taiki; Kuroda, Etsushi; Yoshioka, Yasuo (2020): Murine Cross-Reactive Nonneutralizing Polyclonal IgG1 Antibodies Induced by Influenza Vaccine Inhibit the Cross-Protective Effect of IgG2 against Heterologous Virus in Mice. In *Journal of virology* 94 (12). DOI: 10.1128/JVI.00323-20.

Siddiqui, Mohammad Adnan; Mukherjee, Sushovita; Manivannan, Praveen; Malathi, Krishnamurthy (2015): RNase L Cleavage Products Promote Switch from Autophagy to Apoptosis by Caspase-Mediated Cleavage of Beclin-1. In *International journal of molecular sciences* 16 (8), pp. 17611–17636. DOI: 10.3390/ijms160817611.

Sieczkarski, Sara B.; Whittaker, Gary R. (2002): Influenza virus can enter and infect cells in the absence of clathrin-mediated endocytosis. In *Journal of virology* 76 (20), pp. 10455–10464. DOI: 10.1128/jvi.76.20.10455-10464.2002.

Sipo, Isaac; Knauf, Mathias; Fechner, Henry; Poller, Wolfgang; Planz, Oliver; Kurth, Reinhard; Norley, Stephen (2011): Vaccine protection against lethal homologous and heterologous challenge using recombinant AAV vectors expressing codon-optimized genes from pandemic swine origin influenza virus (SOIV). In *Vaccine* 29 (8), pp. 1690–1699. DOI: 10.1016/j.vaccine.2010.12.037.

Slütter, Bram; Pewe, Lecia L.; Lauer, Peter; Harty, John T. (2013): Cutting edge: rapid boosting of cross-reactive memory CD8 T cells broadens the protective capacity of the Flumist vaccine. In *Journal of immunology (Baltimore, Md. : 1950)* 190 (8), pp. 3854–3858. DOI: 10.4049/jimmunol.1202790.

Smith, Wilson; Andrewes, C. H.; Laidlaw, P. P. (1933): A VIRUS OBTAINED FROM INFLUENZA PATIENTS. In *The Lancet* 222 (5732), pp. 66–68. DOI: 10.1016/S0140-6736(00)78541-2.

Smith-Garvin, Jennifer E.; Koretzky, Gary A.; Jordan, Martha S. (2009): T cell activation. In *Annual review of immunology* 27, pp. 591–619. DOI: 10.1146/annurev.immunol.021908.132706.

Snapper, C. M.; Mond, J. J. (1993): Towards a comprehensive view of immunoglobulin class switching. In *Immunology today* 14 (1), pp. 15–17. DOI: 10.1016/0167-5699(93)90318-F.

Souquette, Aisha; Thomas, Paul G. (2018): Past Life and Future Effects-How Heterologous Infections Alter Immunity to Influenza Viruses. In *Front. Immunol.* 9, p. 1071. DOI: 10.3389/fimmu.2018.01071.

Spearman, C. (1908): The method of 'right and wrong cases' ('constant stimuli') without Gauss's formulae. In *British Journal of Psychology, 1904-1920* 2 (3), pp. 227–242. DOI: 10.1111/j.2044-8295.1908.tb00176.x.

Spreeuwenberg, Peter; Kroneman, Madelon; Paget, John (2018): Reassessing the Global Mortality Burden of the 1918 Influenza Pandemic. In *American journal of epidemiology* 187 (12), pp. 2561–2567. DOI: 10.1093/aje/kwy191.

Steel, John; Lowen, Anice C.; Wang, Taia T.; Yondola, Mark; Gao, Qinshan; Haye, Kester et al. (2010): Influenza virus vaccine based on the conserved hemagglutinin stalk domain. In *mBio* 1 (1). DOI: 10.1128/mBio.00018-10.

Su, Shuo; Fu, Xinliang; Li, Gairu; Kerlin, Fiona; Veit, Michael (2017): Novel Influenza D virus: Epidemiology, pathology, evolution and biological characteristics. In *Virulence* 8 (8), pp. 1580–1591. DOI: 10.1080/21505594.2017.1365216.

Subbarao, Kanta (2019): The Critical Interspecies Transmission Barrier at the Animal–Human Interface. In *Tropical medicine and infectious disease* 4 (2). DOI: 10.3390/tropicalmed4020072.

Subbarao, Kanta; Joseph, Tomy (2007): Scientific barriers to developing vaccines against avian influenza viruses. In *Nat Rev Immunol* 7 (4), pp. 267–278. DOI: 10.1038/nri2054.

Sui, Zhiwei; Chen, Quanjiao; Fang, Fang; Zheng, Mei; Chen, Ze (2010): Cross-protection against influenza virus infection by intranasal administration of M1-based vaccine with chitosan as an adjuvant. In *Vaccine* 28 (48), pp. 7690–7698. DOI: 10.1016/j.vaccine.2010.09.019.

Suspène, Rodolphe; Petit, Vincent; Puyraimond-Zemmour, David; Aynaud, Marie-Ming; Henry, Michel; Guétard, Denise et al. (2011): Double-stranded RNA adenosine deaminase ADAR-1-induced hypermutated genomes among inactivated seasonal influenza and live attenuated measles virus vaccines. In *Journal of virology* 85 (5), pp. 2458–2462. DOI: 10.1128/JVI.02138-10.

Sutter, G.; Ohlmann, M.; Erfle, V. (1995): Non-replicating vaccinia vector efficiently expresses bacteriophage T7 RNA polymerase. In *FEBS letters* 371 (1), pp. 9–12. DOI: 10.1016/0014-5793(95)00843-x.

Sutton, Troy C.; Chakraborty, Saborni; Mallajosyula, Vamsee V. A.; Lamirande, Elaine W.; Ganti, Ketaki; Bock, Kevin W. et al. (2017): Protective efficacy of influenza group 2 hemagglutinin stem-fragment immunogen vaccines. In *NPJ vaccines* 2, p. 35. DOI: 10.1038/s41541-017-0036-2.

Taubenberger, Jeffery K.; Morens, David M. (2006): 1918 Influenza: the mother of all pandemics. In *Emerging infectious diseases* 12 (1), pp. 15–22. DOI: 10.3201/eid1201.050979.

Taubenberger, Jeffery K.; Morens, David M. (2008): The pathology of influenza virus infections. In *Annual review of pathology* 3, pp. 499–522. DOI: 10.1146/annurev.pathmechdis.3.121806.154316.

Taylor, P. M.; Askonas, B. A. (1986): Influenza nucleoprotein-specific cytotoxic T-cell clones are protective in vivo. In *Immunology* 58 (3), pp. 417–420.

Temming, A. Robin; Bentlage, Arthur E. H.; Taeye, Steven W. de; Bosman, Gerlof P.; Lissenberg-Thunnissen, Suzanne N.; Derksen, Ninotska I. L. et al. (2020): Cross-reactivity of mouse IgG subclasses to human Fc gamma receptors: Antibody deglycosylation only eliminates IgG2b binding. In *Molecular immunology* 127, pp. 79–86. DOI: 10.1016/j.molimm.2020.08.015.

Terajima, Masanori; Cruz, John; Co, Mary Dawn T.; Lee, Jane-Hwei; Kaur, Kaval; Wrammert, Jens et al. (2011): Complement-dependent lysis of influenza a virus-infected cells by broadly cross-reactive human monoclonal antibodies. In *Journal of virology* 85 (24), pp. 13463–13467. DOI: 10.1128/JVI.05193-11.

Thakur, Aneesh; Pedersen, Lasse E.; Jungersen, Gregers (2012): Immune markers and correlates of protection for vaccine induced immune responses. In *Vaccine* 30 (33), pp. 4907–4920. DOI: 10.1016/j.vaccine.2012.05.049.

Tompkins, Stephen Mark; Zhao, Zi-Shan; Lo, Chia-Yun; Misplon, Julia A.; Liu, Teresa; Ye, Zhiping et al. (2007): Matrix protein 2 vaccination and protection against influenza viruses, including subtype H5N1. In *Emerging infectious diseases* 13 (3), pp. 426–435. DOI: 10.3201/eid1303.061125.

Tong, Suxiang; Li, Yan; Rivailler, Pierre; Conrardy, Christina; Castillo, Danilo A. Alvarez; Chen, Li-Mei et al. (2012): A distinct lineage of influenza A virus from bats. In *Proceedings of the National Academy of Sciences of the United States of America* 109 (11), pp. 4269–4274. DOI: 10.1073/pnas.1116200109.

Tong, Suxiang; Zhu, Xueyong; Li, Yan; Shi, Mang; Zhang, Jing; Bourgeois, Melissa et al. (2013): New world bats harbor diverse influenza A viruses. In *PLoS pathogens* 9 (10), e1003657. DOI: 10.1371/journal.ppat.1003657.

Ullman-Culleré, M. H.; Foltz, C. J. (1999): Body condition scoring: a rapid and accurate method for assessing health status in mice. In *Laboratory animal science* 49 (3), pp. 319–323.

Ulmer, J. B.; Donnelly, J. J.; Parker, S. E.; Rhodes, G. H.; Felgner, P. L.; Dwarki, V. J. et al. (1993): Heterologous protection against influenza by injection of DNA encoding a viral protein. In *Science (New York, N.Y.)* 259 (5102), pp. 1745–1749. DOI: 10.1126/science.8456302.

Vanderven, Hillary A.; Ana-Sosa-Batiz, Fernanda; Jegaskanda, Sinthujan; Rockman, Steven; Laurie, Karen; Barr, Ian et al. (2016): What Lies Beneath: Antibody Dependent Natural Killer Cell Activation by Antibodies to Internal Influenza Virus Proteins. In *EBioMedicine* 8, pp. 277–290. DOI: 10.1016/j.ebiom.2016.04.029.

Vemula, Sai V.; Sayedahmed, Ekramy E.; Sambhara, Suryaprakash; Mittal, Suresh K. (2017): Vaccine approaches conferring cross-protection against influenza

viruses. In *Expert review of vaccines* 16 (11), pp. 1141–1154. DOI: 10.1080/14760584.2017.1379396.

Virelizier, J. L.; Allison, A. C.; Oxford, J. S.; Schild, G. C. (1977): Early presence of ribonucleoprotein antigen on surface of influenza virus-infected cells. In *Nature* 266 (5597), pp. 52–54. DOI: 10.1038/266052a0.

Vogel, Olivia A.; Han, Julianna; Liang, Chieh-Yu; Manicassamy, Santhakumar; Perez, Jasmine T.; Manicassamy, Balaji (2020): The p150 Isoform of ADAR1 Blocks Sustained RLR signaling and Apoptosis during Influenza Virus Infection. In *PLoS pathogens* 16 (9), e1008842. DOI: 10.1371/journal.ppat.1008842.

Walz, Lisa; Kays, Sarah-Katharina; Zimmer, Gert; Messling, Veronika von (2018): Neuraminidase-Inhibiting Antibody Titers Correlate with Protection from Heterologous Influenza Virus Strains of the Same Neuraminidase Subtype. In *Journal of virology* 92 (17). DOI: 10.1128/JVI.01006-18.

Wang, Taia T.; Tan, Gene S.; Hai, Rong; Pica, Natalie; Petersen, Erin; Moran, Thomas M.; Palese, Peter (2010): Broadly protective monoclonal antibodies against H3 influenza viruses following sequential immunization with different hemagglutinins. In *PLoS pathogens* 6 (2), e1000796. DOI: 10.1371/journal.ppat.1000796.

Wang, Wenling; Huang, Baoying; Jiang, Tao; Wang, Xiuping; Qi, Xiangrong; Gao, Yingying et al. (2012): Robust immunity and heterologous protection against influenza in mice elicited by a novel recombinant NP-M2e fusion protein expressed in E. coli. In *PLoS ONE* 7 (12), e52488. DOI: 10.1371/journal.pone.0052488.

Wang, Wenling; Huang, Baoying; Jiang, Tao; Wang, Xiuping; Qi, Xiangrong; Tan, Wenjie; Ruan, Li (2014): Maximal immune response and cross protection by influenza virus nucleoprotein derived from E. coli using an optimized formulation. In *Virology* 468-470, pp. 265–273. DOI: 10.1016/j.virol.2014.08.008.

Wang, Wenling; Li, Renqing; Deng, Yao; Lu, Ning; Chen, Hong; Meng, Xin et al. (2015): Protective Efficacy of the Conserved NP, PB1, and M1 Proteins as Immunogens in DNA- and Vaccinia Virus-Based Universal Influenza A Virus Vaccines in Mice. In *Clin Vaccine Immunol* 22 (6), pp. 618–630. DOI: 10.1128/CVI.00091-15.

Webster, R. G.; Hinshaw, V. S.; Bean, W. J.; van Wyke, K. L.; Geraci, J. R.; St Aubin, D. J.; Petursson, G. (1981): Characterization of an influenza A virus from seals. In *Virology* 113 (2), pp. 712–724. DOI: 10.1016/0042-6822(81)90200-2.

Wei, Chih-Jen; Crank, Michelle C.; Shiver, John; Graham, Barney S.; Mascola, John R.; Nabel, Gary J. (2020): Next-generation influenza vaccines: opportunities and challenges. In *Nature reviews. Drug discovery* 19 (4), pp. 239–252. DOI: 10.1038/s41573-019-0056-x.

WHO (2017): Up to 650 000 people die of respiratory diseases linked to seasonal flu each year. Edited by World Health Organization. World Health Organization. Available online at https://www.who.int/news/item/13-12-2017-up-to-650-000-people-die-of-respiratory-diseases-linked-to-seasonal-flu-each-year, updated on 8/4/2021, checked on 8/11/2021.

WHO manual on animal influenza diagnosis and surveillance (2002). Available online at https://apps.who.int/iris/bitstream/handle/10665/68026/who_cds?sequence=1.

Wiesener, Nadine; Schütze, Tatjana; Lapp, Sara; Lehmann, Melissa; Jarasch-Althof, Nadine; Wutzler, Peter; Henke, Andreas (2011): Analysis of different DNA vaccines for protection of experimental influenza A virus infection. In *Viral immunology* 24 (4), pp. 321–330. DOI: 10.1089/vim.2011.0001.

Wolf, Amaya I.; Mozdzanowska, Krystyna; Williams, Katie L.; Singer, David; Richter, Monique; Hoffmann, Ralf et al. (2011): Vaccination with M2e-based multiple antigenic peptides: characterization of the B cell response and protection efficacy in inbred and outbred mice. In *PLoS ONE* 6 (12), e28445. DOI: 10.1371/journal.pone.0028445.

Wood, J. M.; Levandowski, R. A. (2003): The influenza vaccine licensing process. In *Vaccine* 21 (16), pp. 1786–1788. DOI: 10.1016/s0264-410x(03)00073-2.

Wraith, D. C.; Vessey, A. E.; Askonas, B. A. (1987): Purified influenza virus nucleoprotein protects mice from lethal infection. In *The Journal of general virology* 68 (Pt 2), pp. 433–440. DOI: 10.1099/0022-1317-68-2-433.

Wrammert, Jens; Koutsonanos, Dimitrios; Li, Gui-Mei; Edupuganti, Srilatha; Sui, Jianhua; Morrissey, Michael et al. (2011): Broadly cross-reactive antibodies dominate the human B cell response against 2009 pandemic H1N1 influenza virus infection. In *The Journal of experimental medicine* 208 (1), pp. 181–193. DOI: 10.1084/jem.20101352.

Wright, P. F.; Okabe, N.; McKee, K. T.; Maassab, H. F.; Karzon, D. T. (1982): Cold-adapted recombinant influenza A virus vaccines in seronegative young children. In *J INFECT DIS* 146 (1), pp. 71–79. DOI: 10.1093/infdis/146.1.71.

Wright, Peter F.; Neumann, Gabriele; Kawaoka, Y. (2007): Orthomyxoviruses. In Bernard N. Fields, David Mahan Knipe, Peter M. Howley (Eds.): Fields' virology. 5th ed. Philadelphia: Wolters Kluwer Health/Lippincott Williams & Wilkins.

Wu, Tao; Hu, Yinghong; Lee, Young-Tae; Bouchard, Keith R.; Benechet, Alexandre; Khanna, Kamal; Cauley, Linda S. (2014): Lung-resident memory CD8 T cells (TRM) are indispensable for optimal cross-protection against pulmonary virus infection. In *Journal of leukocyte biology* 95 (2), pp. 215–224. DOI: 10.1189/jlb.0313180.

Xie, Hang; Liu, Teresa M.; Lu, Xiuhua; Wu, Zhengqi; Belser, Jessica A.; Katz, Jacqueline M. et al. (2009): A live attenuated H1N1 M1 mutant provides broad cross-protection against influenza A viruses, including highly pathogenic A/Vietnam/1203/2004, in mice. In *J INFECT DIS* 200 (12), pp. 1874–1883. DOI: 10.1086/648405.

Yuen, K. Y.; Chan, P. K.; Peiris, M.; Tsang, D. N.; Que, T. L.; Shortridge, K. F. et al. (1998): Clinical features and rapid viral diagnosis of human disease associated with avian influenza A H5N1 virus. In *The Lancet* 351 (9101), pp. 467–471. DOI: 10.1016/s0140-6736(98)01182-9.

Zebedee, S. L.; Lamb, R. A. (1988): Influenza A virus M2 protein: monoclonal antibody restriction of virus growth and detection of M2 in virions. In *Journal of virology* 62 (8), pp. 2762–2772. DOI: 10.1128/jvi.62.8.2762-2772.1988.

Zhang, Ting; Yin, Chaoran; Boyd, David F.; Quarato, Giovanni; Ingram, Justin P.; Shubina, Maria et al. (2020): Influenza Virus Z-RNAs Induce ZBP1-Mediated Necroptosis. In *Cell* 180 (6), 1115-1129.e13. DOI: 10.1016/j.cell.2020.02.050.

Zheng, M.; Luo, J.; Chen, Z. (2014): Development of universal influenza vaccines based on influenza virus M and NP genes. In *Infection* 42 (2), pp. 251–262. DOI: 10.1007/s15010-013-0546-4.

Zhong, Weimin; Reed, Carrie; Blair, Patrick J.; Katz, Jacqueline M.; Hancock, Kathy (2014): Serum antibody response to matrix protein 2 following natural infection with 2009 pandemic influenza A(H1N1) virus in humans. In *J INFECT DIS* 209 (7), pp. 986–994. DOI: 10.1093/infdis/jit811.

Zimmer, Gert (2010): RNA replicons - a new approach for influenza virus immunoprophylaxis. In *Viruses* 2 (2), pp. 413–434. DOI: 10.3390/v2020413.

Zimmer, Gert; Locher, Samira; Berger Rentsch, Marianne; Halbherr, Stefan J. (2014): Pseudotyping of vesicular stomatitis virus with the envelope glycoproteins of highly pathogenic avian influenza viruses. In *The Journal of general virology* 95 (Pt 8), pp. 1634–1639. DOI: 10.1099/vir.0.065201-0.

Zimmerman, Richard K.; Nowalk, Mary Patricia; Chung, Jessie; Jackson, Michael L.; Jackson, Lisa A.; Petrie, Joshua G. et al. (2016): 2014-2015 Influenza Vaccine Effectiveness in the United States by Vaccine Type. In *Clinical Infectious Diseases* 63 (12), pp. 1564–1573. DOI: 10.1093/cid/ciw635.

Der Anhang 9.1 (CURRICULUM VITAE) enthält persönliche Daten. Er ist deshalb nicht Bestandteil der Online-Veröffentlichung.

9.1.1 PUBLICATION LIST

Wittwer K, Anderson DE, Pfeffermann K, Cox RM, Wolf JD, Santibanez S, Mankertz A, Plesker R, Sticher ZM, Kolkykhalov AA, Natchus MG, Pfaller CK, Plemper RK, von Messling V. Small-molecule polymerase inhibitor protects non-human primates from measles and reduces shedding. *Nat Commun*. 2021 Sep 2;12(1):5233. doi: 10.1038/s41467-021-25497-4. PMID: 34475387; PMCID: PMC8413292.

Wittwer K, Zimmer G, Sawatsky B, Rezincuic S, Rommel MGE, von Messling V, Pfaller CK. Non-Neutralizing Antibody Responses after Vesicular stomatitis virus-vectored Influenza A Virus Vaccine Correlate With Protection. *In preparation*

Tan CW, **Wittwer K**, Lim XF, Uehara A, Mani S, Wang LF, Anderson DE. Serological evidence and experimental infection of cynomolgus macaques with pteropine orthoreovirus reveal monkeys as potential hosts for transmission to humans. *Emerg Microbes Infect*. 2019;8(1):787-795. doi: 10.1080/22221751.2019.1621668. PMID: 31132935; PMCID: PMC6542153.

Hennrich AA, Sawatsky B, Santos-Mandujano R, Banda DH, Oberhuber M, Schopf A, Pfaffinger V, **Wittwer K**, Riedel C, Pfaller CK, Conzelmann KK. Safe and effective two-in-one replicon-and-VLP minispike vaccine for COVID-19: Protection of mice after a single immunization. *PLoS Pathog*. 2021 Apr 21;17(4):e1009064. doi: 10.1371/journal.ppat.1009064. PMID: 33882114; PMCID: PMC8092985.

Rommel MGE, Walz L, Kohlscheen S, Schenk F, Miskey C, Botezatu L, **Wittwer K**, Krebs Y, Ivics Z, Pfaller CK, von Messling V, Modlich U. Influenza A Virus Infection Instructs Hematopoiesis to Megakaryocyte-lineage Output. *Under submission in Cell Reports*

Hauptstein N, Pouyan P, **Wittwer K**, Dirauf M, Cinar G, Raschig M, Licha K, Scherf-Clavel O, Lühmann T, Nischang I, Schubert US, Pfaller CK, Haag R, Meinel L. Polymer selection impacts the pharmaceutical profile of site-specifically conjugated Interferon-α2a. ChemRxiv. 2022; doi: 10.26434/chemrxiv-2022-j85br; *Under review in Biomacromolecules.*

Hauptstein N, Dirauf M, **Wittwer K**, Cinar G, Siering O, Raschig M, Lühmann T, Scherf-Clavel O, Sawatsky B, Nischang I, Schubert US, Pfaller CK, Meinel L. PEtOxylated Interferon- α2a bioconjugates addressing H1N1 influenza A virus infection. *Under review in Journal of Controlled Release*

Siering O, Doerr M, Herrmann M, **Wittwer K**, von Messling V, Sawatsky B, Pfaller CK. Natural canine distemper virus diversity confers rapid adaptation to new carnivore host. *Under review in mBio*

9.2 VERZEICHNIS DER AKADEMISCHEN LEHRER

Dr. Andreas Kaufmann
Dr. Brandon Greene
Dr. Christian Pfaller
Dr. Christian Wrocklage
Dr. Danielle Anderson
Dr. Dominique Brandt
Dr. Dorothea Strauer
Dr. Markus Eickmann
Dr. Matthias Conrad
Dr. Michael Schween
Dr. Mikhail Matrosovich
Dr. Nina Timmesfeld
Dr. Philipp Reiß
Dr. Philipp Yu
Dr. Ralf Wagner
Dr. Sabrina Höbenreich
Dr. Thomas Strecker
Dr. Ulrich Mühlenhoff
PD Dr. Gert Zimmer
PD Dr. Ingrid Böhm
PD Dr. Olga Dolnik
PD Dr. Reiner Westermann
Prof. Dr. Alexander Brehm
Prof. Dr. Alexander Visekruna
Prof. Dr. Andrea Maisner
Prof. Dr. Bernd Schmeck
Prof. Dr. Dominik Oliver
Prof. Dr. Dr. Johannes T. Heverhagen
Prof. Dr. Dr. Jürgen Daut
Prof. Dr. Eva Friebertshäuser
Prof. Dr. Friedemann Weber
Prof. Dr. Guntram Suske
Prof. Dr. Hans-Peter Elsässer
Prof. Dr. Heinz Jänsch
Prof. Dr. Johannes Oberwinkler
Prof. Dr. Magdalena Huber
Prof. Dr. Markus Schnare
Prof. Dr. Ralf Jacob
Prof. Dr. Roland Lill
Prof. Dr. Rolf Müller
Prof. Dr. Stefan Bauer
Prof. Dr. Stephan Becker
Prof. Dr. Thorsten Stiewe
Prof. Dr. Timothy D. Plant
Prof. Dr. Ulrich Steinhoff
Prof. Dr. Uta-Maria Bauer
Prof. Dr. Veronika von Messling
Prof. Dr. Wolfgang Garten

Der Anhang 9.3 (ACKNOWLEDGEMENTS) enthält persönliche Daten. Er ist deshalb nicht Bestandteil der Online-Veröffentlichung.

9.4 EHRENWÖRTLICHE ERKLÄRUNG

Ich erkläre ehrenwörtlich, dass ich die dem Fachbereich Medizin Marburg zur Promotionsprüfung eingereichte Arbeit mit dem Titel „Targeting Subtype-Independent Immune Responses Against Influenza A Virus“ im Institut für Virologie unter Leitung von Prof. Dr. Stephan Becker mit Unterstützung durch das Paul-Ehrlich-Institut ohne sonstige Hilfe selbst durchgeführt und bei der Abfassung der Arbeit keine anderen als die in der Dissertation aufgeführten Hilfsmittel benutzt habe. Ich habe bisher an keinem in- oder ausländischen Medizinischen Fachbereich ein Gesuch um Zulassung zur Promotion eingereicht, noch die vorliegende oder eine andere Arbeit als Dissertation vorgelegt.

Ich versichere, dass ich sämtliche wörtlichen oder sinngemäßen Übernahmen und Zitate kenntlich gemacht habe.

Mit dem Einsatz von Software zur Erkennung von Plagiaten bin ich einverstanden.

Ort, Datum, Unterschrift Doktorandin/Doktorand

Die Hinweise zur Erkennung von Plagiaten habe ich zur Kenntnis genommen

Ort, Datum, Unterschrift Referentin/Referent